

Design and Synthesis of Low Toxicity Biodegradable Ionic Liquids and their Applications in Materials Science

By Hannah Prydderch MSci (Hons)

Under the supervision of Dr Andreas Heise and
Prof. Nicholas Gathergood
(Tallinn University of Technology, Estonia)

School of Chemical Sciences
Dublin City University

For the award of PhD

August 2016

Declaration

I hereby certify that this material, which I now submit for assessment on the programme of study leading to the award of PhD is entirely my own work, and that I have exercised reasonable care to ensure that the work is original, and does not to the best of my knowledge breach any law of copyright, and has not been taken from the work of others save and to the extent that such work has been cited and acknowledged within the text of my work.

Signed:

Hannah Prydderch

ID No: 12211400

Date:

**To Andrew,
your unwavering support
and guidance made this possible.**

Acknowledgements

I would like to thank my supervisors Prof. Nicholas Gathergood and Dr Andreas Heise for the chance to carry out this PhD in DCU and for the opportunities afforded to me as a student on the REFINE project. I am very grateful for funding received from the European Union's Seventh Framework Programme for research, technological development and demonstration under grant agreement N° 289253.

I wish to thank those I have collaborated with on this project including Dr Marcel Špulák (Charles University, Czech Republic), Dr Klaus Kümmerer (Leuphana University Lüneburg, Germany), Dr Derek Irvine (The University of Nottingham, UK), Prof. Theo Tervoort (ETH, Zurich) and Dr Brid Quilty (DCU). I also wish to acknowledge Dr Florence McCathy (UCC) for HRMS analysis. I am especially grateful for Gagik Ghazaryan's constant advice, support and guidance both during and after my secondment in ETH Zürich. My most sincere thanks go to the technical staff at DCU for making the university such a great place to work; in particular Veronica, Catherine, Ambrose, Damien, John and Vinny.

I will be forever grateful for the Gathergood Group members past and present who helped me become the chemist I am today. Thank you Rohit and Mukund for your invaluable advice and training during the early days of my PhD. To Adam, Dong, Natasha and also Alan (I am in constant awe of your encyclopaedic knowledge of organic chemistry). Lastly to Andrew, I owe you everything. You are my cushiony rock.

I am particularly thankful for all the friends I made at DCU, namely Aoife, Orla, Brian, Rachel, Nicky, Seán, Leeanne, Laura, Sarah, Declan, Nicola, Kae, Andrew M and Kerri. Thank you for accepting me despite my Britishness. Without you, life at DCU would not have been the same. Also, my sincere thanks go to the students of the REFINE project who made this PhD a very memorable experience; Jaco, Gagik, Amy, Marina, Silvio, Liliana, Chunliang, Alessandro, Antonino, Stefan, Susana, Livia, Simona, Onar and Christina. In particular, my memories of Hong Kong are some of my fondest. Good luck to those that are still on the long road to finishing up.

Finally, I wish to thank my family; Laura, Thomas, Mum and Dad, who gave me all the support I ever needed and more. You made me believe I could do it.

Table of Contents

Declaration	ii
Dedication	iii
Acknowledgements	iv
List of Abbreviations.....	viii
List of Figures	xii
List of Schemes	xvi
List of Tables.....	xvii
List of Equations	xix
List of Appendices	xx
Abstract	xxii
1.0 Literature Review	1
1.1 Introduction	1
1.2 Ionic Liquids.....	2
1.3 Green Chemistry.....	3
1.3.1 The 12 Principles of Green Chemistry.....	4
1.3.2 Green Chemistry Metrics	5
1.4 Toxicity and Biodegradation of ILs	5
1.4.1 Toxicity of ILs.....	9
1.4.2 Biodegradation of ILs	19
1.5 Conclusion.....	23
1.6 Thesis Aims and Objectives	24
1.7 Acknowledgements	26
1.8 References	27
2.0 Mandelic Acid ILs – Synthesis, Toxicity and Biodegradation	34
2.1 Introduction	34
2.2 Synthesis.....	39
2.2.1 Synthesis of Mandelic Acid Esters	42
2.2.2 Synthesis of Mandelic Acid Amides.....	44
2.2.3 Synthesis of Mandelic Acid Alkylating Regents	47
2.2.4 Synthesis of Mandelic Acid ILs	49
2.2.5 Critique on the ‘Greenness’ of the Synthesis.....	59
2.3 Antimicrobial Activity	62
2.3.1 Antibacterial Activity – High Concentrations.....	62
2.3.2 Antibacterial Activity – Low Concentrations	65
2.3.3 Antifungal Activity	68
2.4 Biodegradation	70
2.4.1 Proposed Biodegradation Metabolites	74

2.5	Conclusion.....	76
2.6	Future Work	77
2.7	References	78
3.0	Plasticisation of Poly(L-lactic acid) with 1-Methylimidazolium Ester ILs.....	83
3.1	Introduction	83
3.1.1	Properties of PLA.....	84
3.1.2	Mechanical Properties of Materials	85
3.1.3	Modification of PLA	88
3.1.4	ILs as Plasticisers	89
3.1.5	Physical ageing of PLA.....	90
3.1.6	Selection of ILs for Plasticisation	90
3.2	Synthesis of ILs for Plasticisation	92
3.2.1	Synthesis of Bromoester Alkylating Reagents.....	93
3.2.2	Synthesis of 1-Methylimidazolium Ester ILs	96
3.3	Thermogravimetric Analysis of ILs	101
3.4	Plasticisation of PLLA with ILs	105
3.4.1	PLLA and PLLA/IL Film Formation.....	105
3.4.2	Mechanical Properties	107
3.4.3	Physical Ageing Study	113
3.4.4	Differential Scanning Calorimetry Analysis of PLLA/IL Films.....	116
3.4.5	Thermal Stability of PLLA/IL Films	118
3.5	Conclusions	120
3.6	Future Work	121
3.7	References	122
4.0	The Dielectric Properties of ILs	125
4.1	Introduction	125
4.1.1	Dielectric Measurement Techniques.....	129
4.1.2	Static Dielectric Constants of ILs	132
4.1.3	Selection of ILs for Dielectric Property Measurements.....	133
4.2	Results and Discussion	134
4.2.1	Mandelic Acid ILs.....	134
4.2.2	1-Methylimidazolium Ester ILs	136
4.2.3	High Temperature Experiments	138
4.3	Conclusion.....	147
4.4	Future Work	148
4.5	References	149
5.0	Conclusion and Future Work	151
5.1	Conclusion.....	151
5.2	Future Work	153

5.3	References	156
6.0	Experimental	157
6.1	Introduction	157
6.1.1	Chemicals	157
6.1.2	NMR Analysis.....	157
6.1.3	IR Analysis.....	158
6.1.4	Melting Points	158
6.1.5	Mass Spectrometry.....	158
6.1.6	Thermogravimetric Analysis.....	158
6.1.7	Melt Extrusion.....	158
6.1.8	Film Casting	159
6.1.9	Tensile Testing	159
6.1.10	Differential Scanning Calorimetry	159
6.1.11	Cavity Perturbation Apparatus	159
6.2	Experimental Preparations for Mandelate ILs.....	160
6.2.1	Mandelate Esters	160
6.2.2	Mandelate Amide	161
6.2.3	Mandelate Alkylating Reagents	162
6.2.4	Mandelate Bromide ILs.....	164
6.3	Experimental Preparations for 1-Methylimidazolium Ester ILs	172
6.3.1	Alkylating Regents.....	172
6.3.2	Bromide ILs	173
6.3.3	Bistriflimide ILs	175
6.3.4	Octyl Sulfate ILs	178
6.4	Experimental Preparations for PLLA and PLLA/IL Films	180
6.5	Antimicrobial Screening Test Procedures	180
6.5.1	Antibacterial Activity – DCU	180
6.5.2	Antibacterial Activity – Charles University.....	181
6.5.3	Antifungal Activity – Charles University	182
6.6	Closed Bottle Biodegradation Test Procedure	183
6.7	References	184
	Appendices.....	A-1
	Appendix A – HMBC Spectra	A-1
	Appendix B – Antimicrobial Screening Data	B-5
	Appendix C – TGA Curves.....	C-1
	Appendix D – Tensile Testing Graphs.....	D-1
	Appendix E – DSC Traces	E-7
	Appendix F – High Temperature Dielectric Data	F-10

List of Abbreviations

A

[AOEMIM] – 1-Acetoxyethyl-3-methylimidazolium

AcCl – Acetyl chloride

AChE – Acetylcholinesterase

ACS – American Chemical Society

ATCC – American Type Culture Collection

ATR – Attenuated total reflectance

B

[BZMIM] – 1-Benzyl-3-methylimidazolium

BOD – Biochemical oxygen demand

Bu – Butyl

C

CBT – Closed bottle test

COSY – Correlation spectroscopy

D

[DECMIM] – 1-Decyl-3-methylimidazolium

[DODECPY] – 1-Dodecylpyridinium

DAST – Diethylaminosulfur trifluoride

DCA – Dicyanamide

DCM – Dichloromethane

DCU – Dublin City University

DES – Deep eutectic solvents

DMAP – 4-Dimethylaminopyridine

DMSO-d₆ – Deuterated dimethylsulfoxide

DSC – Differential scanning calorimetry

E

ε' – Dielectric constant

ε'' – Dielectric loss factor

E factor – Environmental factor

EC – Effective concentration
EDC – 1-Ethyl-3-(3-dimethylaminopropyl)carbodiimide
EPA – Environmental Protection Agency
eq. – Equivalents
ESI – Electrospray ionisation
Et – Ethyl
EtOAc – Ethyl acetate

F

FESEM – Field emission scanning electron microscopy

G

GCI – Green Chemistry Institute
GSK – GlaxoSmithKline

H

[HEXMIM] – 1-Hexyl-3-methylimidazolium
HMBC- Heteronuclear multiple-bond correlation
HMQC – Heteronuclear multiple-quantum correlation
HOSu – *N*-Hydroxysuccinimide
HPLC – High performance liquid chromatography
HRMS – High resolution mass spectrometry

I

IC – Inhibitory concentration
IL – Ionic liquid
IR – Infrared

L

LC – Lethal concentration

M

[MMIM] – 1-Methyl-3-methylimidazolium
[MPI] – 1-Methyl-3-pentylimidazolium
[MPY] – 1-Methylpyridinium

2-MeTHF – 2-Methyltetrahydrofuran

Me – Methyl

MH – Mueller-Hinton

MIC – Minimum inhibitory concentration

mp – Melting point

MW – Molecular weight

N

NaOctSO₄ – Sodium octyl sulfate

NBS – *N*-Bromosuccinimide

NMR – Nuclear magnetic resonance

NTf₂ – Bistriflimide

O

[OCTPY] – 1-Octylpyridinium

[OctSO₄] – Octyl sulfate

[OMIM] – 1-Octyl-3-methylimidazolium

OECD – Organisation for Economic Co-operation and Development

P

PD – Polydispersity

PDLA – Poly(D-lactic acid)

PDLLA – Poly(D,L-lactic acid)

Pebax® – Polyether-polyamide block copolymer

PEG – Poly(ethylene glycol)

PET – Poly(ethylene terephthalate)

PLA – Poly(lactic acid)

PLLA – Poly(L-lactic acid)

PMMA – Poly(methyl methacrylate)

Pr – Propyl

PVC – Poly(vinyl chloride)

PVDF – Poly(vinylidene fluoride)

Q

QSAR – Qualitative structure activity relationship

R

REACH – Registration, Evaluation, Authorisation and Restriction of Chemicals

ROP – Ring opening polymerisation

rt – Room temperature

RTIL – Room temperature ionic liquid

S

[SbF₆] – Hexafluoroantimonate

ScCO₂ – Supercritical carbon dioxide

SulI – Sulfonamide resistance gene

T

tan δ – Dielectric loss tangent

T_c – Temperature of crystallisation

TEA – Triethylamine

T_g – Glass transition temperature

TGA – Thermogravimetric analysis

THF – Tetrahydrofuran

TLC – Thin layer chromatography

T_m – Melting temperature

TMS – Tetramethylsilane

T_{onset} – Onset temperature of decomposition

TSIL – Task specific ionic liquid

T_{start} – Start temperature of decomposition

U

UCC – University College Cork

V

VNA – Vector network analyser

VOC – Volatile organic compound

W

WHO – World Health Organisation

List of Figures

Figure 1.1 Comparison of the ionic nature of an IL (right) and NaCl (left) at room temperature (rt).....	2
Figure 1.2 Most commonly used cations and anions in ILs.....	3
Figure 1.3 5-Dimensional risk comparison of [BMIM][BF ₄] with acetone. Very high risk = 4 and very low risk = 1. R = Release, S = Spatiotemporal Range, B = Bioaccumulation, A = Biological activity, U = Uncertainty. ²⁸ Adapted from Ref. 28 with permission from the Royal Society of Chemistry.....	6
Figure 1.4 Design strategy for a ‘green’ IL.....	9
Figure 1.5 Properties of an ‘ideal’ IL.....	9
Figure 1.6 Features of ILs for toxicity towards <i>E. electricus</i> derived using discernment, regression and docking analysis carried out by Das <i>et al.</i> ⁹⁸ Reprinted with permission from R. N. Das and K. Roy, <i>Ind. Eng. Chem. Res.</i> , 2014, 53 , 1020. Copyright 2014 American Chemical Society.....	18
Figure 2.1 Renewable resource mandelic acid (1).	34
Figure 2.2 Previously published mandelic acid derived ILs from the Gathergood group (8–15). ¹⁸	37
Figure 2.3 Target mandelate and mandelamide ILs (16–25).	38
Figure 2.4 Percentage yields for mandelic acid methyl (26), ethyl (27) and butyl (28) esters synthesised from mandelic acid (1).	42
Figure 2.5 ¹ H NMR of mandelic acid methyl ester (26) in CDCl ₃ showing the doublets for proton H4 at the stereogenic centre (left) and the alcohol proton H5 (right).	43
Figure 2.6 ¹ H NMR of mandelic acid ethyl ester (27) in CDCl ₃ showing the two doublets of quartets of the H6 protons (H6’ and H6’’).....	44
Figure 2.7 ¹ H NMR of butyl amide of mandelic acid (29) in CDCl ₃ with the NH (H10) and OH (H5) peaks clearly visible at 6.1 and 3.8 ppm respectively.....	46
Figure 2.8 Percentage yields for mandelic acid α-bromoester and α-bromoamide alkylating reagents (30–33), synthesised from mandelic acid esters 26–28 and amide 29.	48
Figure 2.9 N-Heterocycles used for synthesis of ILs 16–25: 1-methylimidazole, pyridine, 3-methoxypyridine and ethyl nicotinate.	50
Figure 2.10 Percentage yields for mandelate and mandelamide bromide ILs (16–25)..	51
Figure 2.11 N-Heterocyclic region of the ¹ H NMR for 3-methoxypyridinium IL (22) (top) and 3-(ethoxycarbonyl)pyridinium IL (23) (bottom) in CDCl ₃	53

Figure 2.12 Target monofluoro mandelate IL (34).	54
Figure 2.13 Percentage yields for the monofluoro intermediates (35 and 36), and the monofluoro mandelate IL (37).	55
Figure 2.14 ^1H NMR of α -fluoroester of mandelic acid (35) in CDCl_3	56
Figure 2.15 NMR doublets observed for the coupling of fluorine to carbon C7 in 35 , as observed in the ^{13}C NMR (left) and the ^{19}F NMR (right) in CDCl_3	57
Figure 2.16 ^1H NMR of the α -bromo- α -fluoroester of mandelic acid (36) in CDCl_3	58
Figure 2.17 ^{19}F NMR of the α -bromo- α -fluoroester of mandelic acid (36) in CDCl_3 . ..	58
Figure 2.18 ^1H NMR of the monofluoro mandelate IL (37) in $\text{DMSO}-d_6$	59
Figure 2.19 Previously published mandelic acid derived ILs (8–11). ¹⁸	65
Figure 2.20 Proposed metabolites for ILs 16–25 (38–41).	74
Figure 3.1 D-lactic acid (44) and L-lactic acid (45); the building blocks for poly(D-lactic acid) and poly(L-lactic acid) respectively.	83
Figure 3.2 DSC trace of PLLA showing the glass transition temperature (T_g), the crystallisation temperature (T_c) and the melting temperature (T_m).	84
Figure 3.3 Typical stress-strain diagram for various polymer types. ¹⁵	87
Figure 3.4 Percentage yields for bromoester alkylating reagents (58–61), synthesised from bromoacetyl bromide. Percentage yield for 61 reported from previous synthesis. ⁴⁴	94
Figure 3.5 ^1H NMR of alkylating reagent 58 in CDCl_3	95
Figure 3.6 ^1H NMR of 1-methylimidazolium ester bromide IL 46 in CDCl_3	97
Figure 3.7 ^1H NMR of 1-methylimidazolium ester bistriflimide IL 50 in CDCl_3	99
Figure 3.8 ^{13}C NMR of 1-methylimidazolium ester bistriflimide IL 50 , showing the quartet formed by C-F coupling of the CF_3 groups in the NTf_2 anion in CDCl_3	99
Figure 3.9 ^1H NMR of 1-methylimidazolium ester octyl sulfate IL 54 in CDCl_3	101
Figure 3.10 TGA curve for IL 53 showing how the start (T_{start}) and onset (T_{onset}) decomposition temperatures were detected.	102
Figure 3.11 Laboratory scale co-rotating twin-screw extruder used for mixing of PLLA and ILs 50–56	105
Figure 3.12 Dumbbell-shaped specimen used for tensile testing of the PLLA/IL films, with a gauge length of 12.7 mm.	107
Figure 3.13 Stress-strain curves of neat PLLA (4 days aged) and PLLA/IL 50 with 10 wt% IL (last of four samples tested).	109
Figure 3.14 Stress-strain curves for PLLA/IL 50 with 20 and 30 wt% IL.	112
Figure 3.15 TGA curves of neat PLLA and PLLA/IL 52 with 30 wt% IL.	119

Figure 4.1 Mechanisms of polarisation in an applied electric field (E); a) electronic; b) atomic; c) ionic; d) orientational (dipolar).	126
Figure 4.2 Frequency response of dielectric mechanisms as shown by the dielectric resonance spectra for the real (ϵ') and imaginary (ϵ'') parts of permittivity, where dielectric relaxation occurs up to 10^{10} Hz. ¹³ Figure adapted by author from M. Huang, PhD Thesis, Ruhr University Bochum, 2011.	128
Figure 4.3 Schematic representation of the loss tangent ($\tan \delta$).	129
Figure 4.4 Schematic of the cavity perturbation apparatus. ¹⁸ Reprinted with permission from A. D. Smith, E. H. Lester, K. J. Thurecht, S. W. Kingman, J. El Harfi, G. Dimitrakis, J. P. Robinson and D. J. Irvine, <i>Ind. Eng. Chem. Res.</i> , 2010, 49 , 3011. Copyright 2010 American Chemical Society.	130
Figure 4.5 2-Hydroxyethyl ammonium lactate with static dielectric constant $\epsilon = 85.6$, as determined using the coaxial probe method. ¹⁹	132
Figure 4.6 Mandelic acid ILs 18–20 and 22–25 selected to investigate the dielectric properties of ILs using the cavity perturbation technique.	133
Figure 4.7 1-Methylimidazolium ILs 49–51 selected to investigate the dielectric properties of ILs using the cavity perturbation technique.	134
Figure 4.8 Mandelic acid ILs 20 and 23 and 1-methylimidazolium IL 50 utilised in the high temperature studies on the dielectric properties of ILs.	138
Figure 4.9 Variation in ϵ' of IL 20 at 910 and 2470 MHz over the temperature range 20–120 °C using the cavity perturbation technique.	139
Figure 4.10 Variation in ϵ'' of IL 20 at 910 and 2470 MHz over the temperature range 20–120 °C using the cavity perturbation technique.	140
Figure 4.11 Variation in $\tan \delta$ of IL 20 at 910 and 2470 MHz over the temperature range 20–120 °C using the cavity perturbation technique.	141
Figure 4.12 Variation in ϵ' of IL 23 at 910 and 2470 MHz over the temperature range 20–105 °C using the cavity perturbation technique.	142
Figure 4.13 Variation in ϵ'' of IL 23 at 910 and 2470 MHz over the temperature range 20–105 °C using the cavity perturbation technique.	143
Figure 4.14 Variation in $\tan \delta$ of IL 23 at 910 and 2470 MHz over the temperature range 20–105 °C using the cavity perturbation technique.	144
Figure 4.15 Variation in ϵ' of IL 50 at 910 and 2470 MHz over the temperature range 20–120 °C using the cavity perturbation technique.	145
Figure 4.16 Variation in ϵ'' of IL 50 at 910 and 2470 MHz over the temperature range 20–120 °C using the cavity perturbation technique.	146

Figure 4.17 Variation in $\tan \delta$ of IL 50 at 910 and 2470 MHz over the temperature range 20–120 °C using the cavity perturbation technique.	147
Figure 5.1 Suggested mandelic acid ILs (63–66) with DCA and OctSO ₄ anions for further investigation into the dielectric properties of ILs.....	155

List of Schemes

Scheme 2.1 Microbial metabolic pathway for the degradation of mandelic acid (1). Enzymes: a) mandelate dehydrogenase; b) phenylglyoxylate decarboxylase; c) benzaldehyde dehydrogenase; d) benzoate oxidase; e) benzoate 4-hydroxylase; f) 4-hydroxybenzoate 3-hydroxylase. The β -ketoadipate pathway: g) catechol branch; h) protocatechuate branch.....	35
Scheme 2.2 General synthesis of mandelate ILs (16–23) with percentage yields.....	40
Scheme 2.3 General synthesis of mandelamide ILs (24 and 25) with percentage yields.	41
Scheme 2.4 Generation of 2 eq. of HCl <i>in situ</i> from the reaction of thionyl chloride with alcohol.....	42
Scheme 2.5 <i>tert</i> -Butoxide assisted amidation of ethyl esters alkanoates with amines. ²²	45
Scheme 2.6 <i>tert</i> -Butoxide assisted amidation of methyl ester of mandelic acid (27) with <i>n</i> -butylamine.	45
Scheme 2.7 Reaction mechanism of α -bromoester and α -bromoamide formation.	49
Scheme 2.8 General synthesis route to monofluoro mandelate bromide IL (34).	55
Scheme 2.9 Proposed biodegradation pathway for IL 23	76
Scheme 3.1 General synthesis route to 1-methylimidazolium ester ILs (46–57).	93

List of Tables

Table 2.1 Comparison of the coupling and acetyl chloride methods used to synthesise the butyl amide of mandelic acid (29).....	47
Table 2.2 Physical appearance and melting points of mandelate and mandelamide bromide ILs (16–25).	52
Table 2.3 Antibacterial screening results for ILs 16–25 (IC ₅₀).	63
Table 2.4 Aqueous solubility of ILs 16–25 up to a maximum concentration of 2 M. ...	63
Table 2.5 Antibacterial screening results for ILs 8–11 (IC ₅₀). ¹⁸	65
Table 2.6 Antibacterial screening results for ILs 16–25 (MIC, IC ₉₅).	66
Table 2.7 Antifungal screening results for ILs 16–25 (MIC, IC ₈₀ or IC ₅₀).	69
Table 2.8 Percentage biodegradation for ILs 16–25 in the CBT after 28 days.	71
Table 2.9 Calculation of theoretical ester/amide biodegradation for ILs 16–25 with a comparison to the experimental results obtained in the CBT after 28 days.....	73
Table 2.10 Proposed metabolites for ILs 16–25 (38–41).	75
Table 3.1 Comparison of the mechanical properties of the thermoplastics PLLA and PET. ¹⁶	88
Table 3.2 1-Methylimidazolium ester ILs (46–57) with various alkyl/ether chain lengths and different anions.....	92
Table 3.3 Percentage yields for bromoester alkylating reagents (58–61).	95
Table 3.4 Percentage yields and melting points for 1-methylimidazolium ester bromide ILs (46–49).....	96
Table 3.5 Percentage yields and melting points for 1-methylimidazolium ester NTf ₂ ILs (50–53).	98
Table 3.6 Percentage yields and melting points for 1-methylimidazolium ester OctSO ₄ ILs (54–57).....	100
Table 3.7 TGA data for ILs 46–57, where T _{start} is the start temperature of decomposition and T _{onset} is the onset temperature of decomposition.	103
Table 3.8 Key to the structures of the 1-methylimidazolium ester ILs (50–56) used for the synthesis of the corresponding PLLA/IL films (PLLA/IL50–56).	106
Table 3.9 Visual appearance of PLLA/IL films with 10, 20 and 30 wt% IL.	107
Table 3.10 Effect of physical aging on the mechanical properties of neat PLLA films.	108
Table 3.11 Elongation at break for PLLA/IL50–56 plasticised with 10 wt% NTf ₂ and OctSO ₄ ILs on day 0, for four consecutively tested samples.	109

Table 3.12 Tensile testing results for neat PLLA, aged for 4 days, and PLLA/IL 50–53 with 10, 20 and 30 wt% NTf ₂ IL.....	110
Table 3.13 Tensile testing results for 4 day aged PLLA and PLLA/IL 50–53 with 10, 20 and 30 wt% OctSO ₄ IL.....	113
Table 3.14 Effect of physical aging on the elongation at break of PLLA/IL 51–53 with 20 and 30 wt% NTf ₂ IL.....	114
Table 3.15 Effect of physical aging on the Young's modulus of PLLA/IL 51–53 with 20 and 30 wt% NTf ₂ IL.....	115
Table 3.16 Effect of physical aging on the tensile strength of PLLA/IL 51–53 with 20 and 30 wt% NTf ₂ IL.....	116
Table 3.17 Effect of plasticisation with 10, 20 and 30 wt% NTf ₂ IL 50–53 on the thermal properties and degree of crystallinity of PLLA.	117
Table 3.18 TGA data for PLLA and PLLA/IL 52 with 30 wt% IL.	119
Table 4.1 Dielectric properties of mandelic acid ILs 18–20 and 22–25 measured at room temperature and 910 MHz, where ϵ' is the dielectric constant, ϵ'' is the dielectric loss and $\tan \delta$ is the loss tangent.	135
Table 4.2 Dielectric properties of mandelic acid ILs 18–20 and 22–25 measured at room temperature and 2470 MHz, where ϵ' is the dielectric constant, ϵ'' is the dielectric loss and $\tan \delta$ is the loss tangent.	136
Table 4.3 Dielectric properties of 1-methylimidazolium ester ILs 49–51 measured at room temperature and 910 MHz, where ϵ' is the dielectric constant, ϵ'' is the dielectric loss and $\tan \delta$ is the loss tangent.	137
Table 4.4 Dielectric properties of 1-methylimidazolium ester ILs 49–51 measured at room temperature and 2470 MHz, where ϵ' is the dielectric constant, ϵ'' is the dielectric loss and $\tan \delta$ is the loss tangent.	137
Table 6.1 Mass of IL and PLLA used to synthesis PLLA/IL films with 0, 10, 20 and 30 wt% IL.....	180

List of Equations

Equation 3.1 The degree of crystallinity (χ_c) of a polymer calculated from the DSC trace, where ΔH_m is the heat of fusion, ΔH_c is the enthalpy of cold-crystallisation and ΔH_m^0 is the enthalpy of fusion for a 100 % crystalline polymer. ΔH_m^0 is 93.1 J g ⁻¹ for 100 % crystalline PLLA. ¹	85
Equation 3.2 Axial stress (σ) of test specimen, where P is the axial load and A is the cross sectional sample area.	86
Equation 3.3 Axial strain (ε) of test specimen, where δ is the measured elongation and L is the gauge length.	86
Equation 3.4 Percentage elongation at break, where L_1 is the gauge length at fracture and L_0 the original gauge length.	87
Equation 3.5 Young's modulus (E) of test specimen, where σ is the axial stress and ε is the axial strain.	87
Equation 4.1 Absolute permittivity (ε) of a material, where ε_r is the relative permittivity and ε_0 is the permittivity of free space (8.854×10^{-12} F m ⁻¹). ¹⁶	126
Equation 4.2 Relative permittivity (ε_r) of a material expressed as a ratio of absolute complex permittivity (ε) to the permittivity of free space (ε_0) (8.854×10^{-12} F m ⁻¹). ..	126
Equation 4.3 Relative permittivity (ε_r) of a material expressed in terms of the dielectric constant (ε') and the dielectric loss factor (ε''), where j is an imaginary unit. ¹⁶	127
Equation 4.4 Dielectric loss tangent ($\tan \delta$), where ε' is the dielectric constant and ε'' is the dielectric loss factor of the material. ¹⁶	128
Equation 4.5 Quality factor of the empty cavity (Q_C), where f_C is the resonant frequency of the empty cavity and Δf_C is the bandwidth at half power of the empty cavity. ²¹	131
Equation 4.6 Quality factor of the cavity containing the sample (Q_S), where f_S is the resonant frequency of the cavity containing the sample and Δf_S is the bandwidth at half power of the cavity containing the sample. ²¹	131
Equation 4.7 Dielectric constant (ε'), where V_C is the volume of the empty cavity, V_S is the volume of the sample, f_C is the resonant frequency of the empty cavity and f_S is the resonant frequency of the cavity containing the sample. ²¹	131
Equation 4.8 Dielectric loss factor (ε''), where V_C is the volume of the empty cavity, V_S is the volume of the sample, Q_S is the quality factor of the cavity containing the sample and Q_C is the quality factor of the empty cavity. ²¹	131

List of Appendices

A1 HMBC spectrum of IL 22 in CDCl ₃ showing the presence of the multiple bond correlation between H10 to C4, and the absence of the correlation between H12 and C4.	A-1
A2 Full HMBC spectrum of IL 22 in CDCl ₃	A-2
A3 HMBC spectrum of IL 23 in CDCl ₃ showing the presence of the multiple bond correlation between H10 to C4, and the absence of the correlation between H12 and C4.	A-3
A4 Full HMBC spectrum of IL 23 in CDCl ₃	A-4
B1 Antibacterial screening results for ILs 8–11 (MIC, IC ₉₅). ^{1,2}	B-5
B2 Antifungal screening results for ILs 8–11 (MIC, IC ₈₀ or IC ₅₀). ^{1,2}	B-6
C1 TGA curve for IL 46	C-1
C2 TGA curve for IL 47	C-1
C3 TGA curve for IL 48	C-2
C4 TGA curve for IL 49	C-2
C5 TGA curve for IL 50	C-3
C6 TGA curve for IL 51	C-3
C7 TGA curve for IL 52	C-4
C8 TGA curve for IL 53	C-4
C9 TGA curve for IL 54	C-5
C10 TGA curve for IL 55	C-5
C11 TGA curve for IL 56	C-6
C12 TGA curve for IL 57	C-6
C13 TGA curve for PLLA.	C-7
C14 TGA curve for PLLA/IL 52 with 20 wt% IL.	C-7
D1 Elongation at break for PLLA/IL 50 with 20 and 30 wt% IL.	D-1
D2 Elongation at break for PLLA/IL 51 with 20 and 30 wt% IL.	D-1
D3 Elongation at break for PLLA/IL 52 with 20 and 30 wt% IL.	D-2
D4 Elongation at break for PLLA/IL 53 with 20 and 30 wt% IL.	D-2
D5 Young's modulus for PLLA/IL 50 with 20 and 30 wt% IL.	D-3
D6 Young's modulus for PLLA/IL 51 with 20 and 30 wt% IL.	D-3
D7 Young's modulus for PLLA/IL 52 with 20 and 30 wt% IL.	D-4
D8 Young's modulus for PLLA/IL 53 with 20 and 30 wt% IL.	D-4
D9 Tensile strength for PLLA/IL 50 with 20 and 30 wt% IL.	D-5

D10 Tensile strength for PLLA/IL 51 with 20 and 30 wt% IL.....	D-5
D11 Tensile strength for PLLA/IL 52 with 20 and 30 wt% IL.....	D-6
D12 Tensile strength for PLLA/IL 53 with 20 and 30 wt% IL.....	D-6
E1 DSC trace for PLLA.....	E-7
E2 DSC trace for PLLA/IL 50	E-7
E3 DSC trace for PLLA/IL 51	E-8
E4 DSC trace for PLLA/IL 52	E-8
E5 DSC trace for PLLA/IL 53	E-9
F1 Dielectric properties of mandelic acid IL 20 measured at 20–120 °C and 910 MHz, where ϵ' is the dielectric constant, ϵ'' is the dielectric loss and $\tan \delta$ is the loss tangent.	F-10
F2 Dielectric properties of mandelic acid IL 20 measured at 20–120 °C and 2470 MHz, where ϵ' is the dielectric constant, ϵ'' is the dielectric loss and $\tan \delta$ is the loss tangent.	F-11
F3 Dielectric properties of mandelic acid IL 23 measured at 20–105 °C and 910 MHz, where ϵ' is the dielectric constant, ϵ'' is the dielectric loss and $\tan \delta$ is the loss tangent.	F-12
F4 Dielectric properties of mandelic acid IL 23 measured at 20–105 °C and 2470 MHz, where ϵ' is the dielectric constant, ϵ'' is the dielectric loss and $\tan \delta$ is the loss tangent.	F-13
F5 Dielectric properties of mandelic acid IL 50 measured at 20–120 °C and 910 MHz, where ϵ' is the dielectric constant, ϵ'' is the dielectric loss and $\tan \delta$ is the loss tangent.	F-14
F6 Dielectric properties of mandelic acid IL 50 measured at 20–120 °C and 2470 MHz, where ϵ' is the dielectric constant, ϵ'' is the dielectric loss and $\tan \delta$ is the loss tangent.	F-15

Abstract

Design and Synthesis of Low Toxicity Biodegradable Ionic Liquids and their Applications in Materials Science

Hannah Prydderch

A series of ten ionic liquids (ILs) was synthesised from the renewable resource mandelic acid. Low antimicrobial activity was demonstrated towards thirteen bacterial and twelve fungi strains, with a general trend of increasing bacterial toxicity in the order methyl ester < ethyl ester < butyl ester/amide. IL biodegradability was evaluated using the Closed Bottle Test (OECD 301D) and increased in the order of increasing alkyl chain length for the ester ILs (methyl < ethyl < butyl). Despite none of the ILs presenting as readily biodegradable, a series of biodegradation metabolites has been proposed.

A series of twelve 1-methylimidazolium ester ILs was synthesised with bromide, bistriflimide (NTf₂) and octyl sulfate (OctSO₄) anions. Eight ILs suitable for plasticisation with poly(L-lactic acid) (PLLA) were melt extruded with PLLA at 10, 20 and 30 wt% IL. The tensile strength, Young's modulus and elongation at break of the PLLA/IL films were measured. All four NTf₂ ILs successfully plasticised PLLA (confirmed by depression of the T_g in DSC). Plasticisation was most successful at 20 wt% NTf₂ IL, with the OctSO₄ ILs demonstrating poor compatibility with PLLA. The effects of plasticisation were retained after 100 days for the NTf₂ PLLA/IL films, with only minimal ageing observed.

The dielectric properties of seven mandelic acid ILs and three 1-methylimidazolium ester ILs were measured using microwave dielectric spectroscopy. An insight into the polarity of the ILs was gained by using a cavity perturbation technique to obtain the IL dielectric constant, dielectric loss factor and loss tangent. The effect of the IL physical state on the dielectric properties was also investigated by taking measurements for three ILs above their melting points. These preliminary results allow the IL structures to be related to their dielectric properties, enabling the design of ILs with increased polarity.

1.0 Literature Review

1.1 Introduction

The physical properties that the majority of ionic liquids (ILs) possess make them an attractive candidate as a 'green' alternative to volatile organic compounds (VOCs) widely used in the chemical industry. These properties include, but are not limited to, low vapour pressure, low flammability and high thermostability. Despite research showing that not all ILs possess these properties,^{1,2} an even bigger factor needs to be addressed when evaluating the 'greenness' of an IL. These factors are the environmental properties of ILs.

Even with care taken to prevent the release of an IL utilised in an industrial setting into the environment, the possible outcome that some of the IL will reach the environment should be considered. Potential causes for this could be product contamination, release via wastewater streams or through solvent disposal. Even small amounts of released IL will interact with the environment; therefore, it is highly necessary to study and understand how each individual IL will interact with the environment, and the potential impact on the ecosystems affected. Thus, for an IL to be classified as a 'green' alternative to VOCs, environmental factors such as biocompatibility, bioaccumulation, toxicity and biodegradability need to be taken into account.³ It is also pertinent to evaluate the biodegradation pathways that an IL follows during breakdown.⁴⁻⁷ Metabolites generated in the biodegradation process may be more toxic and bioaccumulate to a greater extent in the environment than the parent IL.⁸ Thus, an assessment of metabolite formation, toxicity and stability is highly recommended.⁹⁻¹¹

This introduction will focus on the toxicity and biodegradation of ILs by providing an overview of the current research in the area of IL toxicity and biodegradability. It is important to understand how to design an IL for increased biodegradability and low toxicity, and this is discussed from a structure activity perspective. IL toxicity towards enzymes has also been reviewed using the acetylcholinesterase (AChE) assay, providing an insight into how IL structures influence toxicity towards enzymes.

1.2 Ionic Liquids

Ionic liquids (ILs) are defined as pure compounds that consist of a cation (often organic) and an anion, often with a melting point at or below 100 °C.¹² They are distinct from molten salts which have high melting points (e.g. 800 °C for NaCl),¹³ are highly viscous and corrosive.¹² ILs that are liquid at room temperature are often referred to as room temperature ionic liquids (RTILs). At the COIL-6 conference in South Korea in 2015, Professor Kenneth Seddon proposed that the arbitrary use of 100 °C as a melting point cut-off for the definition of an IL was inflexible and constraining and should no longer be used as a prerequisite for classification as an IL.¹⁴ Thus, the terminology of IL is used throughout this thesis despite a number of the ILs described possessing melting points >100 °C.

An IL typically consists of a bulky organic cation associated with an organic or inorganic anion.¹⁵ The ions are unsymmetrical and thus poorly coordinated, resulting in a destabilisation of the crystal lattice and a low melting point liquid (Figure 1.1). In a molten salt, such as NaCl, both ions are small and of similar shape so they can tightly pack together (Figure 1.1). A large amount of energy is needed to overcome the ionic bonding of the lattice and melt the salt; consequently, they have high melting points.

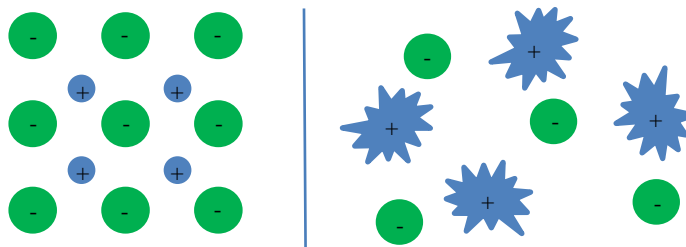


Figure 1.1 Comparison of the ionic nature of an IL (right) and NaCl (left) at room temperature (rt).

ILs are highly solvating, non-flammable, highly thermally stable, of low vapour pressure and possess a large liquid range.¹⁶ The physical properties of an IL can be altered by modifying the IL cation or anion. Properties that can be changed include melting point, viscosity, solvation ability, refractive index and surface tension. Consequently, a myriad of ILs with different properties have been synthesised, with applications in many areas such as electrochemistry, synthetic chemistry, engineering and analytical chemistry.¹⁷ The ability to tune an IL to a particular process has led to

them being described in the literature as ‘designer solvents’. The most commonly utilised cations (imidazolium, pyridinium, phosphonium, ammonium and sulfonium) and anions (acetate, dicyanamide, bistriflimide, bromide, iodide, hexafluorophosphate, tetrafluoroborate, octyl sulfate and methyl sulfate) in ILs are depicted in Figure 1.2.

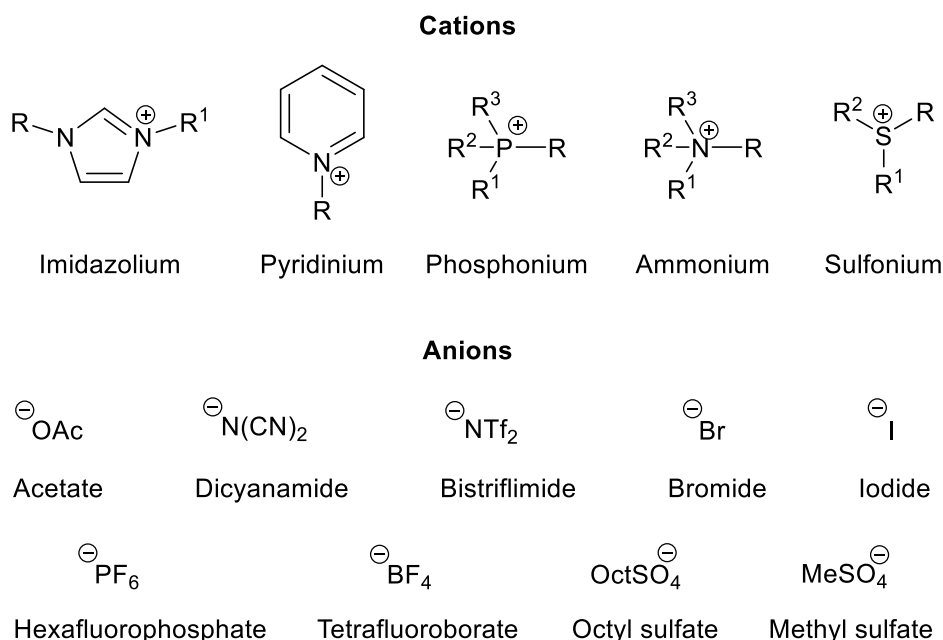


Figure 1.2 Most commonly used cations and anions in ILs.

The properties of low vapour pressure and non-flammability of ILs has also made them very attractive for use in the area of green chemistry.

1.3 Green Chemistry

Green chemistry is used in the evaluation, design and implementation of sustainable and environmentally friendly chemical processes. The idea of green chemistry was first conceptualised by Trevor Kletz in 1978, who published a pioneering article on the use of safer raw materials as replacements for the hazardous chemicals used in chemical processes and industrial plants.¹⁸ His idea to use safer raw materials at lower temperatures and pressures, to avoid problems rather than solving them at a later date, is a key concept of green chemistry. However, the introduction of the term green chemistry only began in the early 1990's when it was coined by Paul Anastas of the US Environmental Protection Agency (EPA).

1.3.1 The 12 Principles of Green Chemistry

Anastas and Warner published a pioneering book on the topic of green chemistry in 1998 where they introduced the 12 principles of green chemistry.¹⁹ These principles still serve as a guideline for those who practice green chemistry research both in industry and academia today. These principles are as follows:

1. Prevention

Preventing the formation of waste is better than treating or cleaning up waste.

2. Atom Economy

Design synthetic methods to maximise incorporation of all materials used in the process into the final product.

3. Less Hazardous Chemical Syntheses

Design synthetic methods to utilise and generate substances with little or no toxicity to human health and the environment.

4. Designing Safer Chemicals

Design chemical products suitable for their desired function whilst minimising toxicity.

5. Safer Solvents and Auxiliaries

No unnecessary use of auxiliary substances and replace with safer alternatives when used.

6. Design for Energy Efficiency

The environmental and economic impact of energy used in chemical processes should be recognised and minimised. Synthetic methods should be carried out at ambient temperature and pressure where possible.

7. Use of Renewable Feedstocks

Renewable feedstocks should be used instead of finite resources wherever possible.

8. Reduce Derivatives

Minimise or avoid use of unnecessary derivatisation to prevent the use of additional reagents and additional generation of waste.

9. Catalysis

Preferentially use catalysts over stoichiometric reagents.

10. Design for Degradation

Design chemical products to break down into innocuous, non-persistent degradation products at the end of their use.

11. Real-time analysis for Pollution Prevention

Develop analytical methodologies to allow for real-time, in-process monitoring and control prior to hazardous substance formation.

12. Inherently Safer Chemistry for Accident Prevention

Minimise the potential for chemical accidents (spills, explosions, fires) by selecting the appropriate substances with the appropriate form.

1.3.2 Green Chemistry Metrics

The ‘greenness’ of a chemical process can be evaluated using green chemistry metrics.²⁰ These metrics allow chemists to directly compare the ‘greenness’ of different processes and to determine which is ‘greener’. They also help to identify where a particular process needs to be improved to make it ‘greener’. These metrics are quantitative and examples include effective mass yield,²¹ environmental factor (E-factor),^{22,23} atom economy,²⁴ reaction mass efficiency,^{25,26} carbon efficiency²⁵ and mass intensity.²⁵

1.4 Toxicity and Biodegradation of ILs²⁷

Initial publications in the field of ILs focused on their suitability for a wide range of applications, and promoted how their esoteric physical properties made them ‘green’ alternatives to VOCs. It was not until the early 2000’s that the environmental impact of ILs was investigated, with the first toxicity tests being carried out by Jastorff *et al.* in 2002.²⁸ In this work, the environmental risk potential of ILs was evaluated and theoretical toxicity evaluations of the commonly used C₄ and C₁₀ [BF₄] ILs were made. A high ‘uncertainty’ factor was identified in the multidimensional risk analysis carried out, due to the lack of information available on the IL decomposition residues, bioaccumulation, biodegradation and biological activity (Figure 1.3). This highlighted not only the potential overlooked toxicity of the second generation of ILs (*vide infra*), but also the crucial need for the evaluation of IL toxicity and biodegradation. This work

was also able to demonstrate the use of quantitative structure–activity relationships (QSAR) as a methodology for predicting IL toxicity.

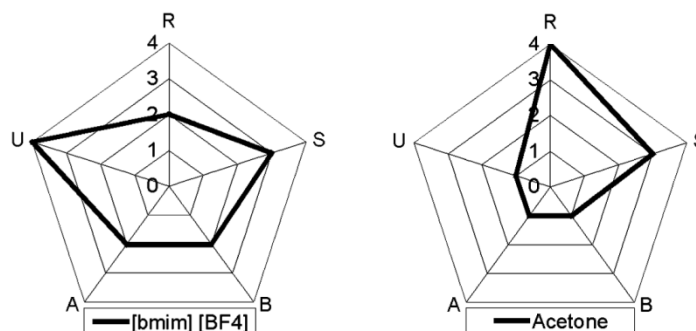


Figure 1.3 5-Dimensional risk comparison of [BMIM][BF₄] with acetone. Very high risk = 4 and very low risk = 1. R = Release, S = Spatiotemporal Range, B = Bioaccumulation, A = Biological activity, U = Uncertainty.²⁸ Adapted from Ref. 28 with permission from the Royal Society of Chemistry.

Since this work, numerous toxicity and biodegradation studies have been carried out on the second generation of ILs, highlighting the need for the redesign of ILs for lower toxicity and increased biodegradation.^{29–33} It is now also known that the widely employed anions [BF₄] and [PF₆] readily hydrolyse to highly corrosive hydrogen fluoride (HF), especially in the presence of water and heat.^{31,32} [PF₆] has also been shown to additionally release the toxic and corrosive hydrolysis products HPO₂F₂, H₂PO₃F and POF₃.^{34,35} Consequently, there has been speculation that some of the early results of [BF₄] and [PF₆] IL catalysis may have been no more than catalysis by HF produced from IL breakdown.¹⁶ However, the main problem highlighted here is that the additional toxic and corrosive hydrolysis products generated from these ILs, which are often overlooked, clearly present a barrier to their widespread application in industrial processes.

The series of ILs that have found the most applications to date are often referred to as the second generation of ILs.³⁶ These ILs are oxygen and water stable with weakly coordinating anions such as [BF₄], [PF₆] or halides ([Cl], [Br] and [I]). The most common cations found in the second generation of ILs are imidazolium, pyridinium, ammonium and phosphonium. These ILs are designed to remain inert and are also the most studied and applied in the field of biocatalysts.³⁷ Modifications to the structure of the second generation of ILs resulted in the production of a third generation of task

specific ILs (TSILs). These were designed with an anion or cation that would actively take part in chemical reactions. An example is the imidazolium ILs synthesised and utilised by Myles *et al.* that act as Brønsted acidic catalysts in the presence of protic additives.^{38,39}

However, research into the biodegradability and toxicity of the second generation ILs placed uncertainty over their ‘greenness’. Progress has been made towards increasing the biodegradability of the second generation of ILs, by introducing functionalities such as ester groups and ether linkages into the cation side chain, and by replacing the common halogenated anions with the biodegradable low toxicity counterion octyl sulfate.⁴⁰⁻⁴² IL toxicity has also been reduced by the addition of ether linkages and the avoidance of long alkyl chains ($> C_6$).⁴³ However, the imidazolium ring has been shown to be highly resistant to biodegradation and therefore inappropriate for designing biodegradable ILs.⁴⁴

There has been a recent introduction of a fourth generation of ILs, based on more biodegradable, readily available, renewable and less toxic cations and/or anions. More hydrophobic stable anions prepared from sugars, amino acids, organic acids, and the cation choline have thus been employed. However, despite the introduction of these types of moieties into ILs, results still show that ILs designed in this way are not always readily biodegradable ($> 60\%$ biodegradation over 28 days).^{45,46} It appears that incorporating both high biodegradation and low toxicity into an IL is still a challenge today and is an area that would clearly benefit from further research.

A class of solvents with similar properties to ILs are the deep eutectic solvents (DES). These are mixtures of salts (e.g. choline chloride) and uncharged hydrogen bond donors (e.g. urea and glycerol).⁴⁷ They have also been proposed as green alternatives to the second and third generations of ILs due to the non-toxic, renewable and biodegradable nature of their synthesis materials. They are also likely to be less expensive than previous generations of ILs with no purification required after the formation of the DES.⁴⁸ Examples of low toxicity readily biodegradable DES have been identified in the literature.^{49,50} However, current research suggests that further work is still required to assess the full ecotoxicological profile and biodegradability of DES before they can be classed as ‘greener’ alternatives to the early generations of ILs.^{51,52} In addition, a study

on the identification of DES biodegradation breakdown products, and an evaluation of their toxicity, is currently not available in the literature.

Toxicity and biodegradation tests on ILs are often carried out independently, yet it is important not to consider results from these tests as two unrelated datasets.⁵³ IL toxicity can have a significant influence on the biodegradation test results, as the IL being tested may be toxic to the microorganisms necessary for biodegradation.^{54,55} If so, the microorganisms will not have the opportunity to biodegrade the IL. A low level of biodegradation will be observed in the test, even if the IL has many accessible breakdown pathways. To prevent erroneous biodegradation results, IL concentrations should not exceed, if possible, levels that are toxic to the microorganisms used in the test. Thus, to promote IL breakdown in the environment, the avoidance of high toxicity needs to be considered when designing an IL for enhanced biodegradability.

A compound that breaks down too readily will not be useful for a wide range of applications with various conditions, such as high temperatures and a wide range of pH values. When investigating biological process in IL media, it is critical to establish that the IL will not be broken down by the reaction conditions or the enzymes used in the process. The resulting degradation products of the IL may hinder the reaction, react in a way that damages the process, or contaminate the final product.⁵⁶ The IL would also no longer be able to be recycled in the process and additional costs for separation of contaminants from the product, purchasing of fresh IL and the disposal of the unusable degraded IL, would be incurred as a result.⁵⁷ Thus, although counterintuitive, it is possible to design a compound that is potentially ‘too biodegradable’.

The research groups directly related to the synthesis and study of ‘green’ ILs will likely have a different design approach to those synthesising task specific ILs, where ‘green’ properties of the ILs may be secondary to the IL application. The approach of a green chemist would be to design for biodegradation and low toxicity first, and to select an appropriate application afterwards. If no suitable application can be found the toxicity and biodegradation data can be fed back into the design of the next class of ‘green’ ILs (Figure 1.4). This is where one has to think about ‘greenness’ vs application, and which is more important and should be considered first during the IL design. Preferably fulfilling all three criteria of biodegradable, low toxicity and task specific would lead to an improved, potentially ‘ideal’, IL (Figure 1.5).

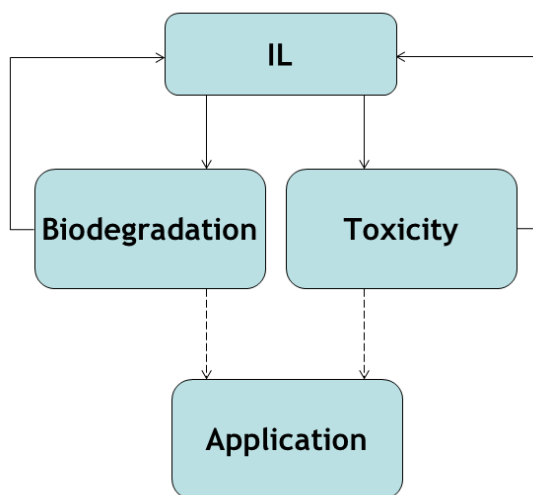


Figure 1.4 Design strategy for a ‘green’ IL.

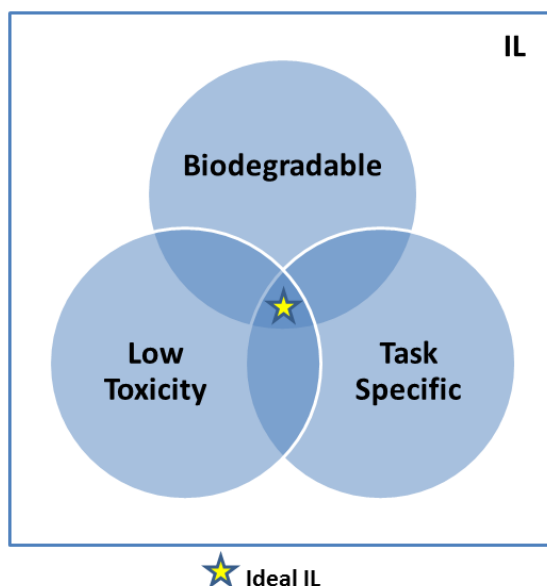


Figure 1.5 Properties of an ‘ideal’ IL.

1.4.1 Toxicity of ILs

IL toxicity has been studied using bacteria,⁵⁸⁻⁶¹ fungi,⁵⁸ algae,⁶²⁻⁶⁸ enzymes,⁶⁹⁻⁷¹ and multicellular organisms including *Daphnia magna*,⁷² *Danio rerio*,⁷³ soil invertebrates,⁵⁹ mammals,⁷⁴ mammalian cells^{59,60,75-77} and fish cells.⁷⁸ A generalised overview of the current data available on the assessment of the second generation ILs (e.g. ILs with [BMIM], [MMIM] and [MPY] cations) shows they have toxicity in some cases, equal to or even one hundred to ten thousand times higher than conventional organic solvents such as benzene, methanol, dimethylformamide or propan-2-ol.^{31,62,68,72} The results are dependent on the structure of the IL (cation and anion pair) and the test system selected.

The toxicity of ILs is known to be much more affected by the structure of the cation than the anion.^{77,79} The cation alkyl chain length has been shown to be very important, with the longer alkyl chains (i.e. decyl vs ethyl) resulting in higher toxicity.⁷⁹ This is directly related to the longer alkyl chains increasing the hydrophobicity of the IL, and thus lipophilicity. The increased lipophilicity increases the likelihood of an interaction with the phospholipid bilayers of cell membranes, and membrane protein hydrophobic domains. This interaction causes the cell membranes to rupture, leading ultimately to cell death.³¹ Polar groups, such as ether groups, introduced on the cation side chain have also been shown to reduce the toxicity of ILs.^{43,75}

In the following sections individual test systems and areas of IL toxicity are discussed. These include aquatic toxicity (1.4.1.1), bacterial and fungal toxicity (1.4.1.2), cytotoxicity (1.4.1.3), antimicrobial resistance (1.4.1.4) and acetylcholinesterase toxicity (1.4.1.5).

1.4.1.1 Aquatic Toxicity

When the environmental effects of ILs were initially considered around 2005 the aquatic toxicity of ILs was the first area to be investigated.⁶⁷ This can be rationalised by the fact that if ILs were ever accidentally released into the environment, it is likely that their first point of contact would be with the aquatic ecosystem. The majority of ILs have high water solubility and thus they are likely to move rapidly through the environment, interacting with a large range of aquatic organisms.

Algae are primary producers of organic matter necessary to sustain the lives of many species in the freshwater food chain. They also have short life cycles, so they respond quickly to environmental change.³⁰ Both these factors have led to the use of algae to assess the aquatic toxicity of ILs. In 2005, Latała *et al.* studied the effect of [EMIM][BF₄], [BMIM][BF₄], [HEXMIM][BF₄], and [BZMIM][BF₄] ILs on the growth inhibition of the green alga *Oocystis submarina* and the diatom *Cyclotella meneghiniana* from the southern Baltic Sea.⁶⁷ The responses of both species were markedly different. *O. submarina* appeared to acclimatise to the lower IL concentrations and recovered their growing ability after ca five days. In contrast, the growth of *C. meneghiniana* was inhibited for the duration of the test at all IL concentrations. [BMIM][BF₄] and [BZMIM][BF₄] were shown to have a lower toxic effect on *O. submarina* at higher water salinity, which is an interesting result as the salinity of the

Baltic Sea varies greatly. At higher water salinity the likelihood of the IL cations pairing with the chloride ions, instead of the hydroxyl groups (green algae) or silanol groups (diatom) in algae cell wall functionalities, increases. This in turn reduces the permeability of the IL cations through the algal cell walls. The outcome is that the IL is less toxic to the algae.

Since 2005, algae assays have been widely used to evaluate the aquatic toxicity of ILs. Further work has been conducted by Latała *et al.*, studying the toxicity of 1-alkyl-3-methylimidazolium ILs towards planktonic green algae (*Chlorella vulgaris* and *O. submarina*), diatoms (*C. meneghiniana*, *Skeletonema marinoi* and *Bacillaria paxillifer*), and blue-green algae (*Geitlerinema amphibium*).⁶⁴⁻⁶⁶ A pronounced alkyl chain effect was observed with all organisms studied and indicated that sensitivity towards ILs decreases in the order blue-green algae > diatoms > green algae. The main reason for this observed trend is the difference in cell wall structures. Blue-green algae have peptidoglycan cell walls, diatoms have silica based cell walls and green algae have cellulose based cell walls. [BF₄] and [CF₃SO₃] anions were shown to increase IL toxicity due to either HF formation from [BF₄] hydrolysis, or increased cell wall penetration with highly lipophilic [CF₃SO₃]. Cell size is also significant in determining the level of toxicity with a 10 times difference in cell size leading to a 100 % more sensitive reaction to ILs in green algae and diatoms.⁶⁵ 1-Alkyl-3-methylimidazolium chloride ILs also showed the same previously observed trend of lower toxicity at higher water salinities.⁶⁴

Additional studies on algae toxicity all followed the same observed alkyl chain trend of increasing IL toxicity with increasing chain length.^{59,63,80} Kulacki and Lamberti also stated that the EC₅₀ values they reported suggested that the ILs tested were more, or just as toxic to the algae as many of the solvents they are intended to replace.⁶³ Cho and Pham *et al.* also showed that imidazolium ILs comprising the anion [SbF₆] were the most toxic of anions tested and found pyridinium ILs were more toxic than their imidazolium counterparts.^{62,68}

D. magna are a species of cladoceran freshwater water flea. They are widely used in the laboratory environment to examine the toxic effect a compound has on reproduction and life expectancy. The first IL toxicity studies on *D. magna*, undertaken in 2005 by Bernot *et al.*, investigated the acute and chronic toxic effects of imidazolium ILs with various

anions such as [Cl], [Br], [BF₄] and [PF₆].⁷² Median lethal toxicity (LC₅₀) values were more than an order of magnitude higher than the corresponding sodium salts, showing that the IL toxicity was related to the imidazolium cation and not the anion. Toxicity was comparable to that of common industrial solvents of the time, such as phenol and ammonia; however, they were two to three orders of magnitude more toxic than methanol or acetonitrile.⁷² Since this work, numerous studies on the toxicity of ILs towards *D. magna* have been undertaken.^{55,81,82} The overriding conclusion from this work is that imidazolium, pyridinium and quaternary ammonium ILs with increasing alkyl chain length have an increased toxicity towards *D. magna*. Again, the nature of the anion had a smaller effect on IL toxicity than the cation. Couling *et al.* used QSAR modelling to help identify the specific part of the IL responsible for the toxic effects towards *D. magna*.⁸² It was determined that ILs with longer alkyl residues attached to aromatic nitrogen atoms, and a higher number of aromatic nitrogen atoms, had increased toxicity. Addition of a methyl group on the aromatic carbons was shown to reduce the IL toxicity.

The model vertebrate Zebrafish (*Danio rerio*) was used by Pretti *et al.* in 2006 to study the toxic effect of ammonium, imidazolium, pyridinium and pyrrolidinium ILs.⁷³ The imidazolium, pyridinium and pyrrolidinium ILs gave LC₅₀ values > 100 mg L⁻¹ and were thus regarded as non-highly lethal towards zebrafish. In stark contrast, the ammonium ILs AMMOENGTM 100 and 130 were much more toxic, with LC₅₀ values of 5.9 and 5.2 mg L⁻¹ respectively. These LC₅₀ values were remarkably lower than those for common organic solvents and tertiary amines. It was thus concluded that ILs may have a different effect on fish related to the IL chemical structure. However, it is important to note that the ammonium ILs used in the study were AMMOENGTM 100, 110, 112 and 130. These acyclic ammonium salts are used industrially as cationic surfactants and contain poly(ethylene glycol) (PEG) and alkyl chains of various lengths on the cation.⁸³ These PEG and alkyl chains are much longer than the ethyl and butyl chains on the imidazolium and pyridinium ILs used in the study. Long alkyl chain length has been shown to increase IL toxicity, and this should be taken into account when concluding that ammonium ILs were more toxic to fish than the imidazolium and pyridinium ILs.

1.4.1.2 Bacterial and Fungal Toxicity

The short generation times of bacteria make them an ideal starting point for toxicity studies. Preliminary toxicity studies showed that compounds containing quaternary ammonium and pyridinium moieties have clinical inhibitory effects on a variety of bacteria and fungi.³⁰

Pernak *et al.* published a paper in 2003 on the anti-microbial properties of 3-alkoxymethyl-1-methylimidazolium ILs with [Cl], [BF₄] and [PF₆] anions.⁷⁹ Here they showed an increase in alkyl chain length increased the toxicity towards rods, cocci and fungi. ILs with 10, 11, 12 and 14 carbon atoms in the alkyl chain were shown to have the highest toxicity towards the screened bacteria. Additional work by Pernak *et al.* corroborated this trend with pyridinium salts.^{84,85} Pernak *et al.* also found that the stereochemistry of the anion in lactate ILs affected their toxicity towards bacteria. In general the L-lactate ILs gave lower minimum inhibitory concentration (MIC) values than the racemates.⁸⁴

In 2005, Docherty and Kulpa examined the antimicrobial effects of various alkyl chain length imidazolium and pyridinium ILs, at a concentration of 1000 ppm, on the growth of a *Escherichia coli*, *Staphylococcus aureus*, *Bacillus subtilis*, *Pseudomonas fluorescens* and *Saccharomyces cerevisiae*.⁵⁸ Increased antimicrobial activity was observed at increased alkyl chain lengths. Imidazolium and pyridinium bromide ILs with hexyl and octyl chains showed considerable antimicrobial activity towards pure cultures of the microorganisms, with ILs [OMIM][Br], [OPY][Br] and [HEXMIM][Br] having log EC₅₀ values 0.07, 0.25 and 0.81 respectively.

In general, studies on the microbial toxicity of imidazolium ILs have shown that the anion has a slight effect on activity.^{58,79,81,84} Whereas for alkyltrihexyl phosphonium ILs, both the anion type and cation structure have been shown to have a significant effect on the IL microbial toxicity.⁸⁵

The rod-shaped bacterium *Vibrio fischeri* is often used to measure IL toxicity using the acute bioluminescence assay (DIN EN ISO 11348).^{59,80,82} Gathergood *et al.* also used *photobacterium phosphoreum* for the same purpose.⁸¹ For both bacteria increasing alkyl chain length was again shown to increase the toxicity of the ILs. With *V. fischeri* the

same trend was observed by Docherty *et al.* for imidazolium and pyridinium IL using the Microtox assay.⁵⁸ Ranke *et al.* showed IL toxicity was mainly due to the cationic portion of the IL; however, ILs containing the anion [PF₆] were slightly more toxic. At concentrations below the ILs inhibitory concentration, slight hormesis was observed.⁶⁰ Couling *et al.* found that the same trend of increasing alkyl chain length leading to increased IL toxicity was apparent for the toxicity of ILs towards *D. magna*, with quaternary ammonium ILs being the least toxic of those studied.⁸² The same QSAR model and trends found for the toxicity of the ILs towards *V. fischeri* also applied to *D. magna*.

Stolte *et al.* studied the effect of headgroups and side chains on the aquatic toxicity of ILs, and showed that short functionalised side chains reduce the lipophilicity and thus toxicity (by six to seven orders of magnitude).⁸⁰ The morpholinium headgroup was recommended for use and the 4-dimethylaminopyridinium (DMAP) recommended for avoidance due to its effect on the aquatic organisms in the study. It was found that the halide anions ([Cl] and [Br]) did not exhibit an intrinsic toxic effect; however, ILs containing the [NTf₂] anion were more toxic to *V. fischeri*. This is in contrast to the work by Matzke *et al.* where [NTf₂] showed no intrinsic toxicity to *V. fischeri*.⁵⁹

In 2006, Docherty *et al.* carried out the Ames test with *Salmonella typhimurium* strains TA98 and TA100 to assess the mutagenicity of ten ILs containing imidazolium, pyridinium and quaternary ammonium cations.⁸⁶ The level that the ILs caused mutation in the bacteria was measured and related to higher organism carcinogenicity. None of the ILs tested fell under the US EPA classification for mutagenicity.⁸⁷ However, imidazolium ILs [BMIM][Br] and [OMIM][Br] indicated the potential for mutagenicity at high doses (20 mg plate⁻¹ for [BMIM][Br] and 1.0 mg plate⁻¹ for [OMIM][Br]), suggesting that further testing is required before the mutagenic potential of ILs is fully understood. Based on this study alone, designing ILs based on pyridinium and quaternary ammonium cations instead of imidazolium cations is encouraged to reduce the potential for mutagenicity.

1.4.1.3 Cytotoxicity

Stolte *et al.* studied the cytotoxicity of ILs on the IPC-81 rat leukaemia cell line using the WST-1 cell viability assay.^{75,88} 100 ILs containing various anions, cations and side chains were tested, and showed a low cytotoxicity compared to previous ILs tested.

Low cytotoxicity was linked to the polar ether, hydroxyl and nitrile functional groups in the IL side chains decreasing the IL lipophilicity and consequently cell uptake.⁷⁵ The headgroup was shown to have little effect on cytotoxicity with the [NTf₂] anion having a marked effect on cytotoxicity. The correlation between IL cation lipophilicity and cytotoxicity was also confirmed using a HPLC derived lipophilicity parameter. Further work by Ranke *et al.* on 74 ILs with comparatively small anions [Cl], [Br], [BF₄] and [PF₆] demonstrated that the IL side chain has a greater influence on IL cytotoxicity than the IL headgroup or the anion, reinforcing the link between increased lipophilicity and increased IL cytotoxicity.⁷⁷

1.4.1.4 Antimicrobial Resistance

It is important to consider what happens to ILs if they are released into the environment, where they are likely to come into contact with a plethora of different microorganisms. A major problem that has recently been highlighted in the media is that of antimicrobial resistance. This is described by the World Health Organisation (WHO) as an increasingly serious threat to global public health that requires action across all government sectors and society.⁸⁹

In 2014, Luo *et al.* investigated the ability of the IL [BMIM][PF₆] to promote the proliferation and dissemination of antibiotic resistance genes in environmental bacteria.⁹⁰ [BMIM][PF₆] was found to increase the abundance of *sulI* (sulfonamide resistance gene) in freshwater microcosms by 500 times, when compared to untreated controls. The IL also significantly increased the abundance of class I integrons, which are particularly adapted to transfer and disseminate antibiotic resistance through horizontal gene transfer between different bacterial strains. Cell membranes in bacteria are hugely significant in preventing horizontal gene transfer. Results suggested that *sulI* propagation mediated by class I integrons was up to 88 times higher in the presence of the IL. This was concluded to be due to the presence of the IL causing an increase in cell membrane permeability. Flow cytometry results showed that in the presence of just 0.5 g L⁻¹ of the IL the bacterial cell membrane permeability increased by over 230 % when compared to untreated cells.

This work by Luo *et al.* is the first to report that ILs can facilitate the proliferation of antibiotic resistant genes in environmental bacteria, and highlights ILs as a potential public health risk. Despite the clear merits of this work, it should be highlighted that

only one IL has been evaluated in this study. The IL [BMIM][PF₆] is also a second generation IL, and various preceding work has already shown this IL has high levels of toxicity to certain bacteria and aquatic organisms. This IL also presents a high usage and release hazard, especially through the formation of degradation products. Thus a wider range of ILs needs to be evaluated, including non-toxic and biodegradable ILs, before a clear picture can be built up as to how concerned we should be over the ability of ILs to promote antimicrobial resistance.

1.4.1.5 Acetylcholinesterase Inhibition

A widely used test to study the molecular toxicity of ILs is the acetylcholinesterase (AChE) assay, where the purified enzyme from the electric eel (*Electrophorus electricus*) is most often used. This enzyme has a vital role in the nervous system of almost all higher organisms, including humans, as a neurotransmitter. Inhibition of AChE has been linked to various conditions such as muscular weakness, fatigue and heart disease.⁷⁰

Stock *et al.*, in 2004, were the first to use the AChE assay to evaluate the toxicity of ILs.⁶⁹ They give many reasons for their selection of the AChE assay, including that the active site of AChE has been widely studied and was the main target during extensive research into the design of insecticides based on phosphoric acid esters and carbamates.⁹¹⁻⁹³ This work would help to facilitate a detailed quantitative structural activity relationship (QSAR) study linking IL structural features to enzyme inhibition. Previous work on pharmaceuticals showed that AChE inhibition was linked to a positively charged nitrogen, an electron deficient aromatic system, and a certain lipophilicity, all common features of ILs.⁹⁴ The AChE active site has also been shown to be comparable between organisms, thus any QSAR conclusions drawn would be applicable to organisms other than those tested.⁶⁹

Imidazolium, pyridinium and phosphonium ILs were chosen for AChE inhibition assays in particular because the chemical structures of the IL cations and acetylcholine (substrate for acetylcholinesterase enzyme) are similar.⁶⁹ Both are cationic and the positive charge is masked by the lipophilic residues.⁹⁵ Inhibition was shown to be dependent on the cationic structure and alkyl side chain with 1-butyl-2-methylpyridinium, [OMIM] and [DECMIM] ILs all showing pronounced AChE inhibition only 3–10 times weaker than a potent inhibiting insecticide Aldicarb.³⁵ ILs

with short alkyl chains gave less inhibition correlating to results in *V. fischeri* and leukaemia cells. When considering only AChE inhibition phosphonium < pyridinium < imidazolium thus phosphonium IL use is preferred.⁶⁹ The influence of the anion was shown to not dominate the toxicity of the IL.

A further study by Arning *et al.* in 2007 identified a positively charged nitrogen atom, a widely delocalised aromatic system and the lipophilicity of the cation alkyl chain as key structural elements of IL binding to the AChE active site.⁷⁰ The DMAP, quinolinium and pyridinium headgroups were listed as having a very strong inhibitory potential, whereas the polar and non-aromatic morpholinium headgroup was only weakly inhibiting. The inhibitory potential was shown to be lowered when ether, nitrile or polar hydroxyl groups were introduced to the alkyl side chain. A wide range of commonly used anions were tested with most showing no inhibitory potential. Only fluorine and fluoride containing anions which readily undergo hydrolytic cleavage showed any inhibitory potential. The 'side chain' effect was observed in this study with increased lipophilicity of the cation alkyl side chain increasing enzyme inhibition.

A review in 2007 by Ranke *et al.* listed the AChE inhibition (log EC₅₀) values for 292 compounds, including a large number of ILs and closely related salts.³⁵ The review compiled into one table the largest selection of ILs tested in a single biological test to date. The AChE inhibitory concentrations spanned more than three orders of magnitude and followed the trends of potent IL AChE inhibitors having a positively charged nitrogen centre, a broadly delocalised aromatic ring system and a certain lipophilicity.

The results obtained in the aforementioned AChE inhibition studies were often rationalised using QSAR.^{69,70} QSAR analysis aims to relate the chemical structures of molecules to their biological activity, thus enabling a prediction about the toxicity of novel molecules to be made. QSAR modelling is currently being used more readily in the area of predicting IL toxicity, although it is still rare for the prediction of AChE inhibition.^{96,97} Recently, work has been published by Das *et al.* on the *in silico* modelling of ILs towards inhibition of AChE.⁹⁸ In this study the chemical attributes of a broad range of 292 ILs were investigated using predictive regression and classification-based quantitative mathematical models. Topological features and electronic parameters of the ILs were considered in the model. The results showed that the main contributors to IL toxicity were positively charged nitrogen species, branching, hydrophobicity and

hydrophilicity as summarised in Figure 1.6. These conclusions were additionally supported by molecular docking studies, carried out for the first time in this area, which investigated the structural features responsible for IL binding to the AChE enzyme cavity.

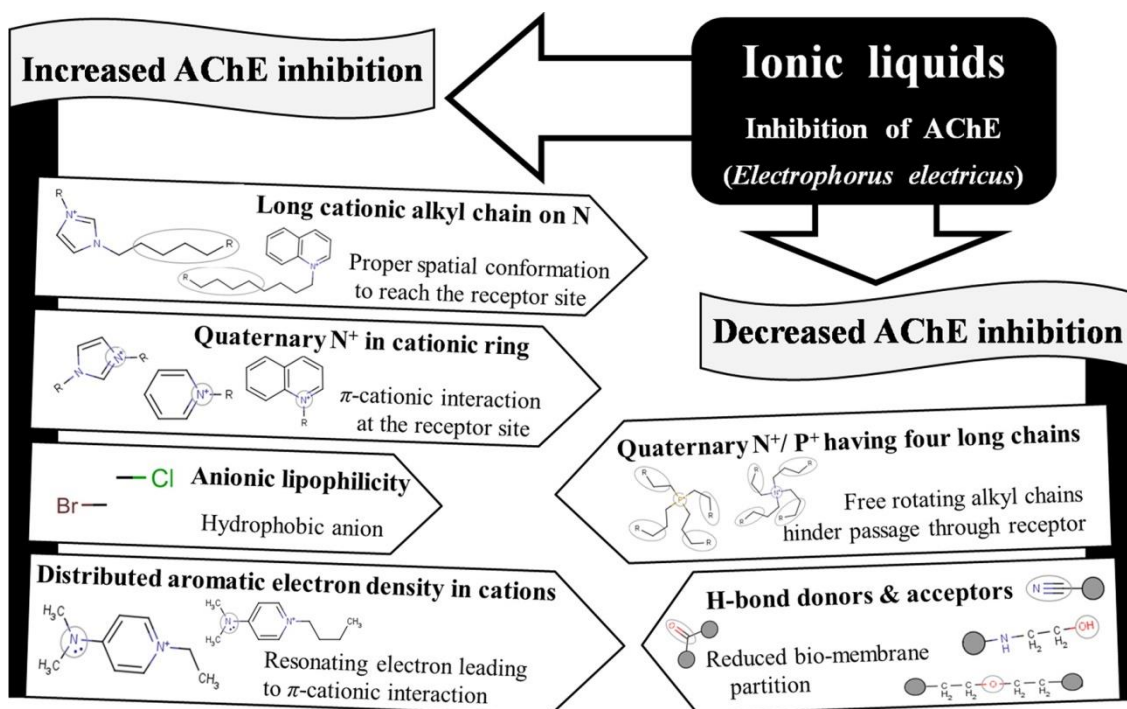


Figure 1.6 Features of ILs for toxicity towards *E. electricus* derived using discernment, regression and docking analysis carried out by Das *et al.*⁹⁸ Reprinted with permission from R. N. Das and K. Roy, *Ind. Eng. Chem. Res.*, 2014, **53**, 1020. Copyright 2014 American Chemical Society.

A paper in 2013 by Hou *et al.* evaluated a series of cholinium amino acid ILs, composed entirely of renewable biomaterials, for acetylcholinesterase inhibition.⁹⁹ The cholinium ILs had much lower toxicity towards AChE with inhibitory potentials approximately an order of magnitude lower than [BMIM][BF₄]. They also displayed low toxicity towards the bacteria tested against. For several ILs lengthening the amino acid side chain increased the AChE inhibition. This is due to an increased anion lipophilicity resulting in stronger hydrophobic interactions with the lipophilic amino acid residues in the AChE enzyme cavity. However, for amino acids with hydrophobic aliphatic side chains, increasing the size of the side chain beyond valine (-CH(CH₃)₂) resulted in lower AChE inhibition. This is likely due to steric hindrance preventing the amino acid entering the active site of the enzyme. The introduction of hydrophilic groups such as hydroxyl, carboxyl and amino into the amino acid generally decreased

the IL AChE inhibition. Aromatic systems introduced into the cation side chains also led to greater AChE inhibition.

1.4.2 Biodegradation of ILs

Biodegradation is classified as the breakdown of a compound by microorganisms via enzymatic processes. This breakdown pathway is preferred over chemical degradation, especially if the release of the compound into the environment is a possibility. The ultimate biodegradation of a compound (total breakdown of the test compound by microorganisms) can be studied by several methods. The most widely used today are those carried out following OECD Guidelines for chemical testing and include the dissolved oxygen content (DOC) die-away test (OECD 301 A),¹⁰⁰ the CO₂ evolution/modified Sturm test (OECD 301 B),¹⁰⁰ the closed bottle test (OECD 301 D),¹⁰⁰ the manometric respirometry test (OECD 301 F),¹⁰⁰ and the CO₂ headspace test (OECD 310/ISO 14593).^{101,102}

There are many classifications for evaluating the level of biodegradation of a compound. The term readily biodegradable is most often used when evaluating the ultimate biodegradation of an IL. If an IL passes a specified level of degradation in a certain amount of time, as determined by the particular ultimate biodegradation test used, the IL can be classed as readily biodegradable. For the OECD tests 301 A, B, D and F a removal of at least 70 % dissolved organic carbon or a production of 60 % theoretical oxygen demand/theoretical carbon dioxide, during the 28 day test period, classifies a compound as readily biodegradable.¹⁰⁰ There is also a 10-day window for biodegradation following attainment of 10 % biodegradation, in which the compound must biodegrade to the specified level to be classified as readily biodegradable. For the CO₂ headspace test (OECD 310) production of > 60 % theoretical inorganic carbon within the 10-day window demonstrates that the test substance is readily biodegradable under aerobic conditions.¹⁰¹

The biodegradation of ILs was first reviewed by Coleman and Gathergood⁷ in 2010 and subsequently by Stolte *et al.*²⁷ in 2011. Most recently the biodegradation of ILs has been critically reviewed by Jordan and Gathergood in 2015.³³ All three reviews provide a detailed explanation of IL biodegradation assays, and the links found between IL structure and biodegradation are discussed. In this section, an overview as to how to

best design a biodegradable IL, based on the research contained in the reviews, will be presented. Recent examples of interest in the literature will be highlighted.

1.4.2.1 Designing for Biodegradation

Gathergood and Scammells were the first to study the biodegradation of ILs in 2002.¹⁰³ They introduced functional groups susceptible to enzymatic hydrolysis to increase IL biodegradation. Incorporating ester groups into the IL side chain significantly improved IL biodegradation; however, ILs with additional amide groups were poorly biodegradable.⁴⁰ Further work by Gathergood *et al.* focused on the effect of the anion on IL biodegradation, leading to a series of results where imidazolium ester ILs combined with octyl sulfate anions (first used in ILs by Wasserscheid *et al.*)⁴² showed high levels of biodegradation.⁸¹ Readily biodegradable ILs of this type were identified using the CO₂ headspace test.⁴¹ ILs prepared from pyridine or nicotinic acid with an ester side chain moiety by Harjani *et al.* in 2009 also showed high levels of biodegradation in the CO₂ headspace test and were classed as readily biodegradable.¹⁰⁴ In 2009 Morrissey *et al.* incorporated ether and poly ether side chains into imidazolium ester ILs.⁴³ Six of the ILs were classed as readily biodegradable by the CO₂ headspace test, all containing the octyl sulfate anion, with amide ILs again shown to be less biodegradable than ester ILs. The introduction of ether and poly ether side chains was also shown to reduce IL bacterial toxicity compared to long alkyl chain derivatives.

Further research in the area of biodegradable ILs led to investigating the biodegradation pathways of ILs and the resulting metabolites.⁷ It is of paramount importance to identify the resultant metabolites of IL biodegradation, especially if a compound is not ultimately biodegradable. HPLC-MS is widely utilised by research groups to determine the structure of metabolites. It is vital to know which metabolites are recalcitrant, so further generations of ILs can be designed which only form biodegradable metabolites during biodegradation. Analysis of the toxicity of metabolites is also recommended. A concern is that metabolites, especially persistent metabolites, may be more toxic than the IL.

Recent work on the biodegradation of ILs has included the evaluation of cholinium amino acid ILs based on renewable resources.⁹⁹ The choline cation was paired with 18 different amino acids as anions and each IL was evaluated for aerobic biodegradability via the closed bottle and CO₂ headspace test. The ILs were compared to choline acetate

and the reference sodium benzoate. Biodegradability was > 60 % after 28 days for all ILs in both tests, so all can be classed as readily biodegradable. The high level of biodegradation for the cholinium amino acid ILs was attributed to the cholinium cation, and the presence of the carboxyl and primary amino groups in the anion. The addition of branched side chains decreased the levels of biodegradation, and the addition of hydroxyl groups increased IL biodegradation. The ILs with carboxylic acid and primary amide groups gave very high levels of biodegradability (> 86 %). Particularly interesting to note from this work is that previous problems with designing ILs for both low toxicity and biodegradation were not present in this study. With relatively few exceptions, the cholinium amino acid ILs with lower toxicity had a higher level of biodegradability.

The toxicity of an IL can have an effect on biodegradation test results. Recent work by Markiewicz *et al.* showed this to be the case for ILs with highly hydrophobic cations and anions.⁵⁴ It was recommended that for such ILs lower than normal IL test concentrations should be used to avoid false negative biodegradation results. This work also showed that the type of inoculum used in the biodegradation test had a strong influence on the test result. However, when considering toxicity, no significant differences in sensitivity/tolerance of the activated sludge could be determined.

Neumann *et al.* recently published a paper on the biodegradability of 27 pyrrolidinium, morpholinium, piperidinium, imidazolium and pyridinium IL cations under aerobic conditions.⁴⁴ The ILs contained different alkyl chains and halide counterions and were assessed for ultimate biodegradability using the manometric respirometry test (OECD 301 F). ILs classed as readily biodegradable were assessed for full mineralisation through BOD measurements. For all five headgroups ILs that were readily or inherently (20–70 %) biodegradable were identified, with biodegradation being solely attributed to the cation. The headgroup influenced the biodegradation level with pyrrolidinium and pyridinium cations having higher levels of biodegradation than piperidinium and morpholinium cations. The imidazolium cation was classified as the least biodegradable headgroup, and as in previous work presented as recalcitrant. Side chain type also influenced biodegradation levels with hydroxyl substitution and longer chain length both increasing biodegradation. This work also corroborated previous work stating that the level of biodegradation was dependent on the inoculum used and the conditions of the test.

When analysing the structural attributes of an IL that influence biodegradability, increased biodegradability has been observed in pyridinium, imidazolium and DMAP ILs with elongated alkyl side chains.⁷ However, this design strategy is directly opposed to creating a low toxicity IL, where long alkyl side chains have been shown to increase IL toxicity. It has also been shown that introducing ester groups into the IL side chains can increase IL biodegradation.

ILs with pyridinium headgroups generally have a higher degree of biodegradation than imidazolium and DMAP ILs. The literature reports many examples of readily biodegradable pyridinium ILs, even when linked to short alkyl chains and when tested under stringent readily biodegradable analysis conditions. For imidazolium ILs, only the alkyl side chain has been shown to degrade under the same readily biodegradable test conditions, with the imidazolium core remaining resistant to biodegradation. However, the use of industrial inocula has indicated that degradation of the imidazolium core is possible under certain conditions.⁷

Anions that have been used to increase the biodegradation of ILs include alkyl sulfates (such as methyl sulfate or octyl sulfate), linear alkyl sulfonates (such as methyl sulfonate), linear alkylbenzyl sulfonates (such as *p*-toluenesulfonate) and carboxylates (such as acetate or lactate). These anions are also recommended for use when designing low toxicity ILs. Fluorine containing anions (such as [NTf₂] and [(C₂F₅)₃PF₃]) should be avoided as they are likely to be recalcitrant in the environment, and accumulate in the tissues of living organisms due to their high hydrophobicity.

Modelling and predicting the biodegradation of ILs is important. It can be costly and time consuming to substitute an IL at a late stage of project. This would be advisable if the IL was determined to be unsuitable for use due to unacceptably high toxicity and poor biodegradation. Thus, it would be a major benefit to have QSAR models that were used widely and highly reliable for the prediction of an ILs biodegradation. Unfortunately, we are not there yet and a review from 2012 by Rücker and Kümmerer details some of the reasons why.¹⁰⁵ A particular problem highlighted was the slow progress of QSAR model development due to the poor reproducibility of experimental data. However, a large part of this is unavoidable due to the variation in bacterial populations. Also noted was the dearth of high quality experimental data which often remains confidential in industry, and the need for it to be made publicly available. The

conclusion was that models need to be published in detail, including all the data a model is built on and any corresponding software, to facilitate the wider use and enhancement of such models for predicting biodegradation.

1.5 Conclusion

It can be concluded from reviewing the literature that there is a long way to go before the design of low toxicity and biodegradable ILs is a priority for researchers synthesising and using ILs for specific applications. Certain features have been identified with the potential to increase IL toxicity, such as long lipophilic alkyl chains on the cation, positively charged nitrogen atoms and a widely delocalised aromatic system, and would best be avoided when designing ILs for low toxicity. The IL cation has been found to have a more marked effect on toxicity than the anion, with phosphonium, ammonium and morpholinium in many cases preferred over imidazolium, pyridinium and DMAP cations. The stereochemistry of the cation has also been noted to affect IL toxicity. Anions containing fluorine atoms, particularly those prone to hydrolysis such as $[\text{BF}_4]$ and $[\text{PF}_6]$, are also best avoided when designing low toxicity ILs, and also for biodegradability. The introduction of ether, hydroxyl and nitrile groups to alkyl side chains have also been shown to be promising in reducing IL toxicity.

Increasing the alkyl chain lengths in IL cations has been shown to increase IL biodegradability, but also to increase IL toxicity. This increase in toxicity was reduced by the introduction of ether groups to the alkyl chains. ILs with hydroxyl groups and hydrolysable ester groups in the alkyl chains showed higher levels of biodegradability. Branching of alkyl chains, amides moieties and imidazolium headgroups were all shown to reduce IL biodegradability. The use of alkyl sulfate and alkyl sulfonate groups has been employed successfully to increase the overall biodegradation of ILs. ILs with pyrrolidinium, pyridinium and nicotinic acid headgroups were often more biodegradable than those containing imidazolium and morpholinium headgroups.

Each IL will have a new distinct environmental profile. With numerous cation and anion pairs available, it is not possible to evaluate the toxicity and biodegradation of each and every IL before its use. Thus the use of QSAR models for the prediction of IL toxicity for future generations of ILs is recommended, and they have so far proved to be very promising in predicting the toxicity of various IL classes. However, as previously

mentioned, the use of QSAR for predicting IL biodegradation is an area that needs further work if the future generations of ILs can be assessed in this way. The implementation of a highly applicable QSAR model is most likely being held back by the fact that biodegradation assays are highly dependent on the type of inoculum used and the test conditions employed.

Incorporating functional groups known to promote biodegradation into IL and pairing cations with biodegradable anions can yield ILs which are classed as readily biodegradable. However, uncertainty exists about whether these readily biodegradable ILs are ultimately biodegradable ILs. If the breakdown products of the parent IL are not biodegradable they will persist in the environment unable to further biodegrade. Thus, we should be using the information gathered from the studies discussed herein to help design ultimately biodegradable IL from the ground up. In this way, we can prevent the build-up of recalcitrant IL components in the environment should their release ever occur.

It is envisaged that by carrying out IL toxicity and biodegradation analysis in tandem with performance analysis, we can promote the use of 'greener' IL alternatives. The appeal of ILs to industry has often been in their ability to solve complex problems due to their multifaceted properties, with the 'greenness' of the ILs often considered to a lesser extent. However, if given the choice of two ILs with identical performance capabilities but different toxicological profiles, the 'greener' IL would likely be chosen. Thus, by collecting IL toxicity and biodegradation data alongside performance data, the use of green ILs in industry may indeed become a reality. We need to be sensitive to industry requirements whilst still promoting the Gathergood group's philosophy that the 'greenest' possible solution to these problems should be targeted.

1.6 Thesis Aims and Objectives

The first aim of this thesis (chapter 2) was targeted towards the synthesis of a new class of low toxicity readily biodegradable ILs, utilising the design strategy discussed in the preceding sections. This body of work builds on a previous study undertaken in the Gathergood group where a series of low toxicity mandelic acid ILs were synthesised.¹⁰⁶ There was a significant opportunity to expand on this work by synthesising a new series of mandelic acid IL directly from the renewable resource in a shorter and more efficient synthesis. In addition, by carrying out toxicity screening under identical conditions to

the previously published work a direct comparison of IL toxicity between the two series would be possible. An insight into the effect of the new IL structures on IL toxicity would be gained. This work also expands on the previous study by aiming to provide an evaluation of the biodegradability of the newly synthesised ILs.

As discussed in the introduction to this thesis, it is highly important to facilitate the introduction of ‘green’ ILs into industry. If ILs with performance capabilities comparable to the current state of the art can be identified, the goal of introducing green ILs into industry could indeed become a reality. One area where ‘green’ ILs could be commercially applied is as replacements to the current chemicals used as plasticisers. Plasticisers are often required for a variety of materials, most notably plastics, where they are introduced to increase material ductility and softness¹⁰⁷ and in turn widen the applicability of the material. Currently the most highly used phthalate plasticisers are coming under increasingly stringent regulation (i.e. REACH)¹⁰⁸ due to concerns about their toxicity,¹⁰⁹⁻¹¹¹ thus replacing them with more environmentally friendly alternatives is highly industrially relevant. In this thesis (chapter 3) the use of a series of 1-methylimidazolium ester ILs as plasticisers for poly(L-lactic acid) (PLLA) is proposed. These ILs have been previously evaluated for their toxicity and biodegradability, with low toxicity readily biodegradable examples identified.⁴³ A significant aim of this work was to utilise the ‘green’ ILs as PLLA plasticisers to overcome a number of the limitations of current PLLA plasticisers such as low thermal stability, poor biocompatibility, plasticiser leaching and the requirement for increased ductility and material performance.¹¹² Preventing the physical aging of PLLA through IL plasticisation was also an important goal (see chapter 3, section 3.1.5). In this chapter the mechanical properties of the IL plasticised PLLA films were evaluated along with a thermal analysis study to investigate both plasticiser efficiency and the thermal stability of the materials. This work was designed as a proof of concept study where a number of prototype materials were synthesised. It is envisaged that this work will be further progressed in the future by utilising functionalised and task specific ILs as plasticisers, with the aim of creating plasticised materials targeted to specific applications.

The importance of evaluating the ‘greenness’ of ILs alongside performance analysis was previously discussed in section 1.5. In chapter 4 of this thesis the dielectric properties of a number of the mandelic acid and 1-methylimidazolium ester ILs, designed for low toxicity and high biodegradability, were evaluated with the aim of

facilitating the utilisation of these ILs in an industrial setting. Highly polar materials can be heated by microwaves based on their dielectric constants.¹¹³ Thus, evaluating the dielectric constant of ILs provides an insight into their polarity and their applicability as solvents and as electrolytes,¹¹⁴ where increased polarity is a desirable feature. In this work the dielectric constants of the ILs were evaluated using microwave dielectric spectroscopy (see chapter 4). It was desired that this study will help to facilitate the utilisation of ‘green’ ILs with microwaves in industry, so reactions with safer solvents (replacement of VOCs with ‘green’ ILs) and increased energy efficiency (shorter reaction times, and lower temperatures) can be employed, fulfilling the 5th and 6th principles of green chemistry respectively. It is expected that the ILs studied in this work will possess a wide range of dielectric constants, due to the impact of the differing nature of the cations and anions and physical state of the ILs.¹¹⁵ It is also widely known that dielectric constants are affected by both frequency and temperature;¹¹⁶ thus, it was desired to study both the impact of temperature and frequency on the dielectric properties of the ILs.

The work in this thesis aims to fulfil the 4th, 7th and 10th principles of green chemistry (outlined in section 1.3.1); designing safer chemicals, the use of renewable feedstocks and designing for degradation (respectively). The use of renewable feedstocks is addressed by the synthesis of a novel series of ILs directly from the renewable resource mandelic acid. The IL backbone of mandelic acid was chosen with the aim of increasing IL degradation (see chapter 2, section 2.1), without significantly increasing IL toxicity compared to the previous class of mandelic acid ILs. The overarching theme of designing low toxicity biodegradable ILs also directly addresses the 4th principle of green chemistry (designing safer chemicals). The ILs utilised in chapter 3 for the plasticisation of PLLA were also chosen because they were originally designed for low toxicity and high biodegradability, again meeting the 4th green chemistry principle of designing safer chemicals.

1.7 Acknowledgements

Section 1.4 is reproduced from Ref. 27 with permission from the Royal Society of Chemistry.

1.8 References

1. P. Wasserscheid, *Nature*, 2006, **439**, 797.
2. M. Smiglak, W. M. Reichert, J. D. Holbrey, J. S. Wilkes, L. Y. Sun, J. S. Thrasher, K. Kirichenko, S. Singh, A. R. Katritzky and R. D. Rogers, *Chem. Commun.*, 2006, 2554.
3. N. Sun, H. Rodriguez, M. Rahman and R. D. Rogers, *Chem. Commun.*, 2011, **47**, 1405.
4. K. M. Docherty, J. K. Dixon and C. F. Kulpa, *Biodegradation*, 2007, **18**, 481.
5. S. Stolte, S. Abdulkarim, J. Arning, A. K. Blomeyer-Nienstedt, U. Bottin-Weber, M. Matzke, J. Ranke, B. Jastorff and J. Thoming, *Green Chem.*, 2008, **10**, 214.
6. T. P. T. Pham, C. W. Cho, C. O. Jeon, Y. J. Chung, M. W. Lee and Y. S. Yun, *Environ. Sci. Technol.*, 2009, **43**, 516.
7. S. Stolte, S. Steudte, A. Igartua and P. Stepnowski, *Curr. Org. Chem.*, 2011, **15**, 1946.
8. A. B. A. Boxall, C. J. Sinclair, K. Fenner, D. Kolpin and S. J. Maud, *Environ. Sci. Technol.*, 2004, **38**, 368a.
9. K. Kummerer, *Green Chem.*, 2007, **9**, 899.
10. H. Sutterlin, R. Alexy, A. Coker and K. Kummerer, *Chemosphere*, 2008, **72**, 479.
11. K. M. Docherty, M. V. Joyce, K. J. Kulacki and C. F. Kulpa, *Green Chem.*, 2010, **12**, 701.
12. P. Wasserscheid and W. Keim, *Angew. Chem., Int. Ed.*, 2000, **39**, 3772.
13. J. S. Wilkes, *Green Chem.*, 2002, **4**, 73.
14. K. R. Seddon, unpublished work.
15. H. M. Yau, S. J. Chan, S. George, J. Hook, A. Croft and J. Harper, *Molecules*, 2009, **14**, 2521.
16. S. Sowmiah, V. Srinivasadesikan, M. C. Tseng and Y. H. Chu, *Molecules*, 2009, **14**, 3780.
17. N. V. Plechkova and K. R. Seddon, *Chem. Soc. Rev.*, 2008, **37**, 123.
18. T. A. Kletz, *Chemistry and Industry*, 1978, **6**, 30.
19. P. T. Anastas and J. C. Warner, *Green Chemistry: Theory and Practice*, Oxford University Press, New York, 1998.

20. D. J. C. Constable, A. D. Curzons and V. L. Cunningham, *Green Chem.*, 2002, **4**, 521.
21. T. Hudlicky, D. A. Frey, L. Koroniak, C. D. Claeboe and L. E. Brammer Jr, *Green Chem.*, 1999, **1**, 57.
22. R. A. Sheldon, *Chem. Ind. (London, U. K.)*, 1992, 903.
23. R. A. Sheldon, *Green Chem.*, 2007, **9**, 1273.
24. B. M. Trost, *Science*, 1991, **254**, 1471.
25. A. D. Curzons, D. J. C. Constable, D. N. Mortimer and V. L. Cunningham, *Green Chem.*, 2001, **3**, 1.
26. J. Andraos, *Org. Process Res. Dev.*, 2006, **10**, 212.
27. H. Prydderch, A. Heise and N. Gathergood, in *Ionic Liquids in the Biorefinery Concept: Challenges and Perspectives*, ed. R. Bogel-Lukasik, The Royal Society of Chemistry, Cambridge, 2016, ch. 6, pp. 168-201.
28. B. Jastorff, R. Stormann, J. Ranke, K. Molter, F. Stock, B. Oberheitmann, W. Hoffmann, J. Hoffmann, M. Nuchter, B. Ondruschka and J. Filser, *Green Chem.*, 2003, **5**, 136.
29. D. Coleman and N. Gathergood, *Chem. Soc. Rev.*, 2010, **39**, 600.
30. T. P. T. Pham, C.-W. Cho and Y.-S. Yun, *Water Res.*, 2010, **44**, 352.
31. M. C. Bubalo, K. Radosevic, I. R. Redovnikovic, J. Halambek and V. G. Srcek, *Ecotoxicol. Environ. Saf.*, 2014, **99**, 1.
32. M. Petkovic, K. R. Seddon, L. P. N. Rebelo and C. S. Pereira, *Chem. Soc. Rev.*, 2011, **40**, 1383.
33. A. Jordan and N. Gathergood, *Chem. Soc. Rev.*, 2015.
34. R. P. Swatloski, J. D. Holbrey and R. D. Rogers, *Green Chem.*, 2003, **5**, 361.
35. J. Ranke, S. Stolte, R. Stormann, J. Arning and B. Jastorff, *Chem. Rev.*, 2007, **107**, 2183.
36. A. Pathak, N. Jangid, R. Ameta and P. B. Punjabi, in *Green Chemistry: Fundamentals and Application*, ed. S. C. Ameta and R. Ameta, Apple Academic Press, Inc., Canada, 2013, ch. 5, pp. 109-136.
37. P. Domínguez de María, in *Ionic Liquids in Biotransformations and Organocatalysis: Solvents and Beyond*, ed. P. Domínguez de María, John Wiley & Sons, Inc., New Jersey, 2012, ch. 1, pp. 1-14.
38. L. Myles, R. G. Gore, M. Spulak, I. Beadham, T. M. Garcia, S. J. Connon and N. Gathergood, *Green Chem.*, 2013, **15**, 2747.

39. L. Myles, R. Gore, M. Spulak, N. Gathergood and S. J. Connon, *Green Chem.*, 2010, **12**, 1157.
40. N. Gathergood, M. T. Garcia and P. J. Scammells, *Green Chem.*, 2004, **6**, 166.
41. N. Gathergood, P. J. Scammells and M. T. Garcia, *Green Chem.*, 2006, **8**, 156.
42. P. Wasserscheid, R. v. Hal and A. Bosmann, *Green Chem.*, 2002, **4**, 400.
43. S. Morrissey, B. Pegot, D. Coleman, M. T. Garcia, D. Ferguson, B. Quilty and N. Gathergood, *Green Chem.*, 2009, **11**, 475.
44. J. Neumann, S. Steudte, C. W. Cho, J. Thoming and S. Stolte, *Green Chem.*, 2014, **16**, 2174.
45. N. Ferlin, M. Courty, A. N. V. Nhien, S. Gatard, M. Pour, B. Quilty, M. Ghavre, A. Haiss, K. Kummerer, N. Gathergood and S. Bouquillon, *RSC Adv.*, 2013, **3**, 26241.
46. N. Ferlin, M. Courty, S. Gatard, M. Spulak, B. Quilty, I. Beadham, M. Ghavre, A. Haiss, K. Kummerer, N. Gathergood and S. Bouquillon, *Tetrahedron*, 2013, **69**, 6150.
47. J. Gorke, F. Srienc and R. Kazlauskas, *Biotechnol. Bioprocess Eng.*, 2010, **15**, 40.
48. Q. Zhang, K. De Oliveira Vigier, S. Royer and F. Jerome, *Chem. Soc. Rev.*, 2012, **41**, 7108.
49. K. Radosevic, M. C. Bubalo, V. G. Sreck, D. Grgas, T. L. Dragicevic and I. R. Redovnikovic, *Ecotoxicol. Environ. Saf.*, 2015, **112**, 46.
50. I. Juneidi, M. Hayyan and M. A. Hashim, *RSC Adv.*, 2015, **5**, 83636.
51. P. de Moraes, F. Gonçalves, J. A. P. Coutinho and S. P. M. Ventura, *ACS Sustain. Chem. Eng.*, 2015, **3**, 3398.
52. Q. Wen, J. X. Chen, Y. L. Tang, J. Wang and Z. Yang, *Chemosphere*, 2015, **132**, 63.
53. R. Alexy, T. Kumpel and K. Kummerer, *Chemosphere*, 2004, **57**, 505.
54. M. Markiewicz, M. Piszora, N. Caicedo, C. Jungnickel and S. Stolte, *Water Res.*, 2013, **47**, 2921.
55. A. S. Wells and V. T. Coombe, *Org. Process Res. Dev.*, 2006, **10**, 794.
56. G. Chatel and D. R. MacFarlane, *Chem. Soc. Rev.*, 2014, **43**, 8132.
57. S. I. Abu-Eishah, in *Ionic Liquids Recycling for Reuse, Ionic Liquids – Classes and Properties*, ed. S. Handy, InTech, Croatia, 2011, ch. 11, pp. 239-241.
58. K. M. Docherty and C. F. Kulpa, *Green Chem.*, 2005, **7**, 185.

59. M. Matzke, S. Stolte, K. Thiele, T. Juffernholz, J. Arning, J. Ranke, U. Welz-Biermann and B. Jastorff, *Green Chem.*, 2007, **9**, 1198.
60. J. Ranke, K. Molter, F. Stock, U. Bottin-Weber, J. Poczobutt, J. Hoffmann, B. Ondruschka, J. Filser and B. Jastorff, *Ecotoxicol. Environ. Saf.*, 2004, **58**, 396.
61. S. P. M. Ventura, C. S. Marques, A. A. Rosatella, C. A. M. Afonso, F. Goncalves and J. A. P. Coutinho, *Ecotoxicol. Environ. Saf.*, 2012, **76**, 162.
62. C. W. Cho, T. P. T. Pham, Y. C. Jeon and Y. S. Yun, *Green Chem.*, 2008, **10**, 67.
63. K. J. Kulacki and G. A. Lamberti, *Green Chem.*, 2008, **10**, 104.
64. A. Latala, M. Nedzi and P. Stepnowski, *Green Chem.*, 2010, **12**, 60.
65. A. Latala, M. Nedzi and P. Stepnowski, *Green Chem.*, 2009, **11**, 580.
66. A. Latala, M. Nedzi and P. Stepnowski, *Green Chem.*, 2009, **11**, 1371.
67. A. Latala, P. Stepnowski, M. Nedzi and W. Mroziak, *Aquat. Toxicol.*, 2005, **73**, 91.
68. T. P. T. Pham, C. W. Cho, J. Min and Y. S. Yun, *J. Biosci. Bioeng.*, 2008, **105**, 425.
69. F. Stock, J. Hoffmann, J. Ranke, R. Stormann, B. Ondruschka and B. Jastorff, *Green Chem.*, 2004, **6**, 286.
70. J. Arning, S. Stolte, A. Boschen, F. Stock, W. R. Pitner, U. Welz-Biermann, B. Jastorff and J. Ranke, *Green Chem.*, 2008, **10**, 47.
71. A. C. Skladanowski, P. Stepnowski, K. Kleszczynski and B. Dmochowska, *Environ. Toxicol. Pharmacol.*, 2005, **19**, 291.
72. R. J. Bernot, M. A. Brueseke, M. A. Evans-White and G. A. Lamberti, *Environ. Toxicol. Chem.*, 2005, **24**, 87.
73. C. Pretti, C. Chiappe, D. Pieraccini, M. Gregori, F. Abramo, G. Monni and L. Intorre, *Green Chem.*, 2006, **8**, 238.
74. M. Yu, S. M. Li, X. Y. Li, B. J. Zhang and J. J. Wang, *Ecotoxicol. Environ. Saf.*, 2008, **71**, 903.
75. S. Stolte, J. Arning, U. Bottin-Weber, A. Muller, W. R. Pitner, U. Welz-Biermann, B. Jastorff and J. Ranke, *Green Chem.*, 2007, **9**, 760.
76. X. F. Wang, C. A. Ohlin, Q. H. Lu, Z. F. Fei, J. Hu and P. J. Dyson, *Green Chem.*, 2007, **9**, 1191.
77. J. Ranke, A. Muller, U. Bottin-Weber, F. Stock, S. Stolte, J. Arning, R. Stormann and B. Jastorff, *Ecotoxicol. Environ. Saf.*, 2007, **67**, 430.

78. K. Radosevic, M. Cvjetko, N. Kopjar, R. Novak, J. Dumic and V. G. Srcek, *Ecotoxicol. Environ. Saf.*, 2013, **92**, 112.
79. J. Pernak, K. Sobaszekiewicz and I. Mirska, *Green Chem.*, 2003, **5**, 52.
80. S. Stolte, M. Matzke, J. Arning, A. Boschen, W. R. Pitner, U. Welz-Biermann, B. Jastorff and J. Ranke, *Green Chem.*, 2007, **9**, 1170.
81. M. T. Garcia, N. Gathergood and P. J. Scammells, *Green Chem.*, 2005, **7**, 9.
82. D. J. Couling, R. J. Bernot, K. M. Docherty, J. K. Dixon and E. J. Maginn, *Green Chem.*, 2006, **8**, 82.
83. B. Weyershausen and K. Lehmann, *Green Chem.*, 2005, **7**, 15.
84. J. Pernak, I. Goc and I. Mirska, *Green Chem.*, 2004, **6**, 323.
85. A. Cieniecka-Roslonkiewicz, J. Pernak, J. Kubis-Feder, A. Ramani, A. J. Robertson and K. R. Seddon, *Green Chem.*, 2005, **7**, 855.
86. K. M. Docherty, S. Z. Hebbeler and C. F. Kulpa, *Green Chem.*, 2006, **8**, 560.
87. W. J. Stang, *Microbial Bioassay for Toxic and Hazardous Materials (Ames Test for mutagenicity)*, National Enforcement Investigations Center, United States Environmental Protection Agency, Office of Enforcement, EPA-330/9-80-002, August 1980.
88. S. Stolte, J. Arning, U. Bottin-Weber, M. Matzke, F. Stock, K. Thiele, M. Uerdingen, U. Welz-Biermann, B. Jastorff and J. Ranke, *Green Chem.*, 2006, **8**, 621.
89. W. H. Organisation, Antimicrobial resistance: global report on surveillance, <http://www.who.int/mediacentre/factsheets/fs194/en/>, Accessed September 2014.
90. Y. Luo, Q. Wang, Q. Lu, Q. Mu and D. Mao, *Environ. Sci. Technol. Lett.*, 2014, **1**, 266.
91. P. H. Axelsen, M. Harel, I. Silman and J. L. Sussman, *Protein Sci.*, 1994, **3**, 188.
92. M. A. Sogorb and E. Vilanova, *Toxicol. Lett.*, 2002, **128**, 215.
93. J. Massoulie, L. Pezzementi, S. Bon, E. Krejci and F. M. Vallette, *Prog. Neurobiol.*, 1993, **41**, 31.
94. J. Kaur and M. Q. Zhang, *Curr. Med. Chem.*, 2000, **7**, 273.
95. B. Jastorff, K. Molter, P. Behrend, U. Bottin-Weber, J. Filser, A. Heimers, B. Ondruschka, J. Ranke, M. Schaefer, H. Schroder, A. Stark, P. Stepnowski, F. Stock, R. Stormann, S. Stolte, U. Welz-Biermann, S. Ziegert and J. Thoming, *Green Chem.*, 2005, **7**, 362.

96. F. Y. Yan, S. Q. Xia, Q. Wang and P. S. Ma, *J. Chem. Eng. Data*, 2012, **57**, 2252.
97. J. S. Torrecilla, J. Garcia, E. Rojo and F. Rodriguez, *J. Hazard. Mater.*, 2009, **164**, 182.
98. R. N. Das and K. Roy, *Ind. Eng. Chem. Res.*, 2014, **53**, 1020.
99. X. D. Hou, Q. P. Liu, T. J. Smith, N. Li and M. H. Zong, *PLoS One*, 2013, **8**, e59145.
100. Organization for Economic Cooperation and Development (OECD), *OECD Guideline for Testing of Chemicals; Ready Biodegradability*, Paris, July 1992.
101. Organization for Economic Cooperation and Development (OECD), *OECD Guidelines for the Testing of Chemicals; Ready Biodegradability - CO₂ in sealed vessels (Headspace Test)*, Paris, March 2006.
102. International Organization for Standardization (ISO), *ISO Standard 14593; Water quality — Evaluation of ultimate aerobic biodegradability of organic compounds in aqueous medium — Method by analysis of inorganic carbon in sealed vessels (CO₂ headspace test)*, Geneva, March 1999.
103. N. Gathergood and P. J. Scammells, *Aust. J. Chem.*, 2002, **55**, 557.
104. J. R. Harjani, R. D. Singer, M. T. Garciac and P. J. Scammells, *Green Chem.*, 2009, **11**, 83.
105. C. Rucker and K. Kummerer, *Green Chem.*, 2012, **14**, 875.
106. S. P. M. Ventura, M. Gurbisz, M. Ghavre, F. M. M. Ferreira, F. Goncalves, I. Beadham, B. Quilty, J. A. P. Coutinho and N. Gathergood, *ACS Sustain. Chem. Eng.*, 2013, **1**, 393.
107. L. Xiao, B. Wang, G. Yang and M. Gauthier, in *Biomedical Science, Engineering and Technology*, ed. D. N. Ghista, InTech, Croatia, 2012, ch. 11, pp. 255-256.
108. J. Rank, *TES*, 2005, **4**, 1.
109. G. Latini, M. Ferri and F. Chiellini, *Curr. Med. Chem.*, 2010, **17**, 2979.
110. M. Rahman and C. S. Brazel, *Polym. Degrad. Stab.*, 2006, **91**, 3371.
111. D. Y. Bang, M. Kyung, M. J. Kim, B. Y. Jung, M. C. Cho, S. M. Choi, Y. W. Kim, S. K. Lim, D. S. Lim, A. J. Won, S. J. Kwack, Y. Lee, H. S. Kim and B. M. Lee, *Compr. Rev. Food Sci. Food Saf.*, 2012, **11**, 453.
112. T. Mekonnen, P. Mussone, H. Khalil and D. Bressler, *J. Mater. Chem. A*, 2013, **1**, 13379.
113. A. Baiano, *Molecules*, 2014, **19**, 14821.

- 114. D. Rochefort, in *Functional Materials: For Energy, Sustainable Development and Biomedical Sciences*, eds. M. Leclerc and R. Gauvin, Walter de Gruyter GmbH, 2014, ch. 9, pp. 189–206, DOI: 10.1515/9783110307825.189
- 115. M. Huang, PhD Thesis, Ruhr University Bochum, 2011.
- 116. M. T. Jilani, M. Z. u. Rehman, A. M. Khan, M. T. Khan and S. M. Ali, *Int. J. Inf. Technol. Electr. Eng.*, 2012, **1**, 1.

2.0 Mandelic Acid ILs – Synthesis, Toxicity and Biodegradation

2.1 Introduction

The necessity to use renewable feedstocks to design chemicals for use in today's society, and to promote low toxicity and high biodegradation in chemical design, was discussed in depth in the literature review in chapter 1. This section of work is intended to outline and discuss the synthesis of ILs from the renewable feedstock mandelic acid (**1**) (Figure 2.1). The ILs were designed to optimise biodegradation properties and to exhibit low antimicrobial and antifungal activity.

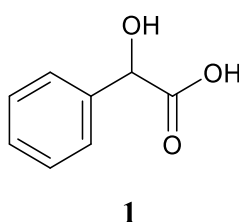


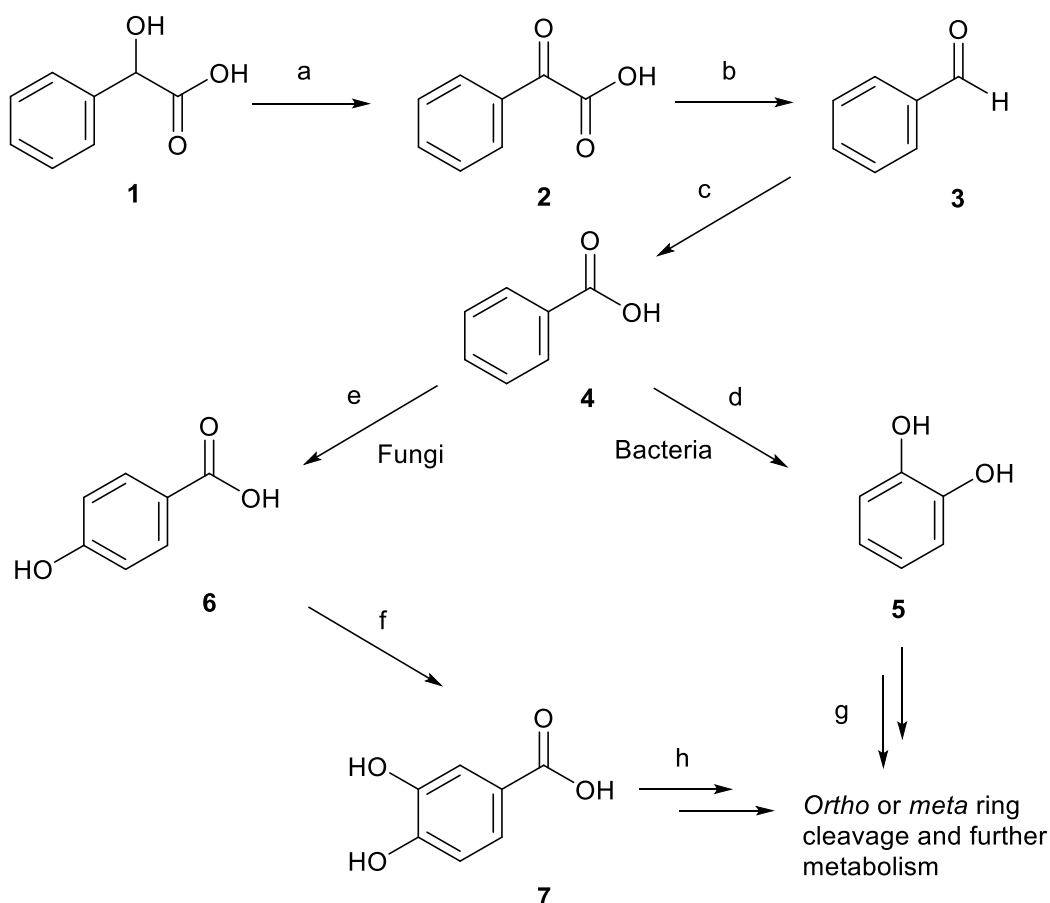
Figure 2.1 Renewable resource mandelic acid (**1**).

Mandelic acid is an aromatic α -hydroxy acid that is found naturally in small quantities in plant tissues such as wheat leaves and grapes.¹ A wide range of organisms (e.g. *Penicillium chrysogenum*² and phytoplankton³) can convert the naturally occurring compounds L-phenylalanine and phenyl acetic acid into mandelic acid.¹ Mandelic acid can be obtained by heating the glycoside amygdalin with concentrated hydrochloric acid.⁴ Amygdalin can be isolated from the seeds of the bitter almond tree^{5,6} and is also found in apricots^{6,7} and peach pits.¹ In industry mandelic acid is made from the acid or enzyme catalysed hydrolysis of mandelonitrile.⁸ Optically pure (*R*)- and (*S*)-mandelic acid has also been produced from the renewable feedstock glucose using a genetically modified strain of *E. Coli*.⁹

Two routes that mandelic acid can enter the environment are through excretion in the urine, where it is detected due to its use to treat urinary tract infections,¹⁰ and as a key metabolite of the widely used polymer precursor styrene, which is known to enter the bodies of plastic industry workers through inhalation.^{11,12} Despite its release into the environment, there have been no reports of its concentration in soil.¹ This, coupled with the fact that numerous metabolic breakdown pathways of mandelic acid by

microorganisms have been described over the years,^{1,13} suggests that it is rapidly metabolised in the environment.¹

The most widely accepted degradation pathway of mandelic acid (**1**) is via benzoylformic acid (**2**) and benzaldehyde (**3**) to benzoic acid (**4**) (Scheme 2.1).¹⁴ Further degradation occurs by bacteria (e.g. *Pseudomonas putida*)¹⁵ to catechol (**5**), which is further metabolised via the catechol branch of the β -ketoadipate pathway.¹⁶ Alternatively, degradation of (**4**) occurs by fungi (e.g. *Aspergillus niger*)¹⁷ to 4-hydroxybenzoic acid (**6**) and 3,4-dihydroxybenzoic acid (**7**), which is further metabolised via the protocatechuate branch of the β -ketoadipate pathway.¹⁶



Scheme 2.1 Microbial metabolic pathway for the degradation of mandelic acid (**1**). Enzymes: a) mandelate dehydrogenase; b) phenylglyoxylate decarboxylase; c) benzaldehyde dehydrogenase; d) benzoate oxidase; e) benzoate 4-hydroxylase; f) 4-hydroxybenzoate 3-hydroxylase. The β -ketoadipate pathway: g) catechol branch; h) protocatechuate branch.

A series of ILs based on mandelic acid (**8–15**) (Figure 2.2) was previously described in the literature and evaluated for their bacterial and algal toxicity.¹⁸ The majority of the ILs were derived from 3,4-methylenedioxymandelic acid (**8–11** and **13–15**), with the exception of IL **12** which was derived from 3,4-dimethoxymandelic acid. IL **12** was included in this study as it was envisaged that the group would be more stable to a wider set of conditions (less susceptible to nucleophilic attack), thus leading to a greater scope of applications. All the ILs (**8–15**) incorporated a high oxygen content (e.g. ether, phenol and catechol groups are present), and had low toxicity to the bacterial (e.g. IL **9**, IC_{50} = 100–200 mM against *P. putida*) and algae (e.g. IL **9**, EC_{50} = 1670 μ M against *C. vulgaris*) strains they were screened against.

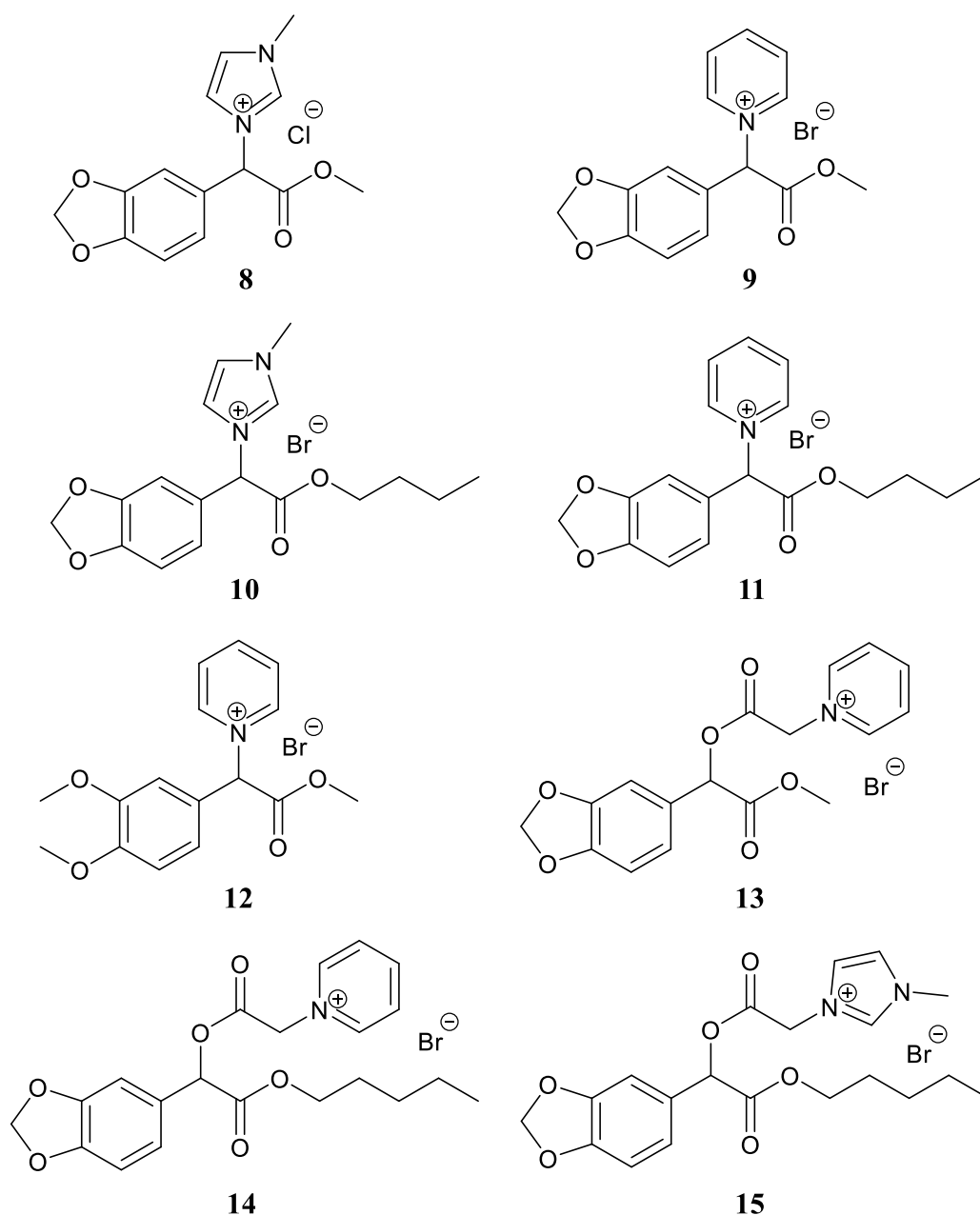


Figure 2.2 Previously published mandelic acid derived ILs from the Gathergood group (8–15).¹⁸

The low antimicrobial activity of the previous class of compounds (8–15) was postulated to be due to the aromatic ring of the IL backbone, in contrast to a linear alkyl chain, and also the oxygen atoms present on the aromatic ring. However, the importance of the aromatic ring oxygen atoms towards the resultant low toxicity was not established in the previous work. To evaluate the impact of the aromatic ring oxygen atoms on IL toxicity, a target series of ten mandelic acid ILs (16–25) (Figure 2.3) was proposed. These ILs were designed to include and exclude specific structural motifs to allow for the investigation of their effect on IL toxicity and biodegradation. These structural features included:

- Three alkyl chain lengths – butyl, ethyl and methyl
- Phenyl ring – C₆H₅
- Ester or amide functional groups
- Halide anion – bromide
- Four *N*-heterocyclic cation headgroups – 1-methylimidazolium, pyridinium, 3-methoxypyridinium and 3-(ethoxycarbonyl)pyridinium

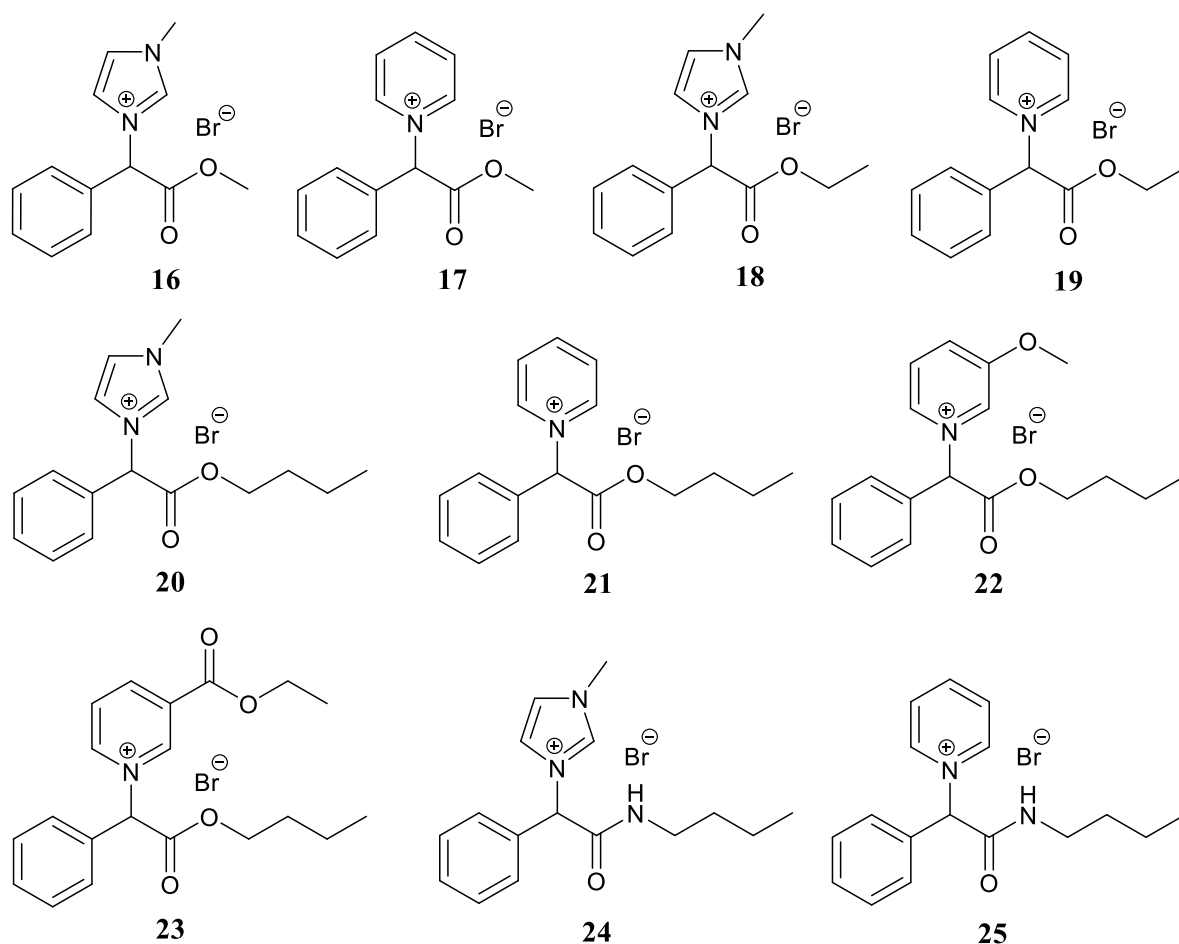


Figure 2.3 Target mandelate and mandelamide ILs (**16–25**).

The toxicity of the new series of ILs (**16–25**) was anticipated to increase on removal of the aromatic ring oxygen atoms. However, as ILs (**8–15**) from the previous study had very low antimicrobial activity,¹⁹ synthesis and evaluation of this new class of ILs was considered worthwhile. The previous ILs (**8–15**) were synthesised from mandelic acid derivatives, with an additional synthetic step required to make the derivative.¹⁸ Thus, the synthesis of the ILs described herein satisfies the 8th principle of green chemistry by reducing the number of derivatives in the synthesis from the previously published work.¹⁸ The new target series of ILs (**16–25**) were designed with a synthesis route directly from mandelic acid; therefore, they have a shorter synthesis directly from the

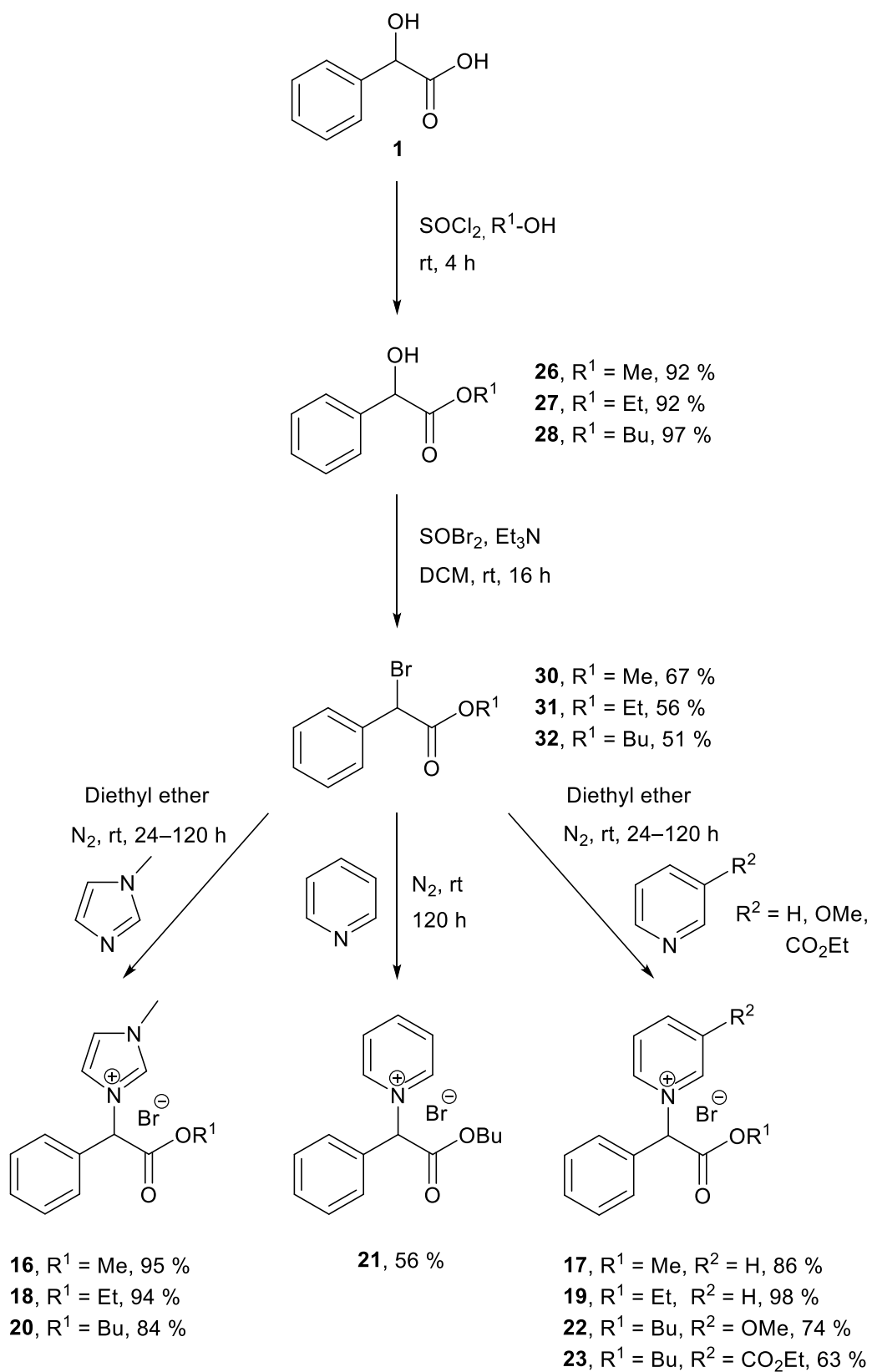
renewable resource. This satisfies the 3rd principle of green chemistry where a less hazardous chemical synthesis to the previous published work was utilised.¹⁸ This work also goes further than the previously published work by providing a biodegradation evaluation of the newly synthesised ILs. Overall, this section of work aims to satisfy the 4th, 7th and 10th principles of green chemistry (outlined in section 1.3.1); designing safer chemicals, the use of renewable feedstocks and designing for degradation (respectively).

2.2 Synthesis

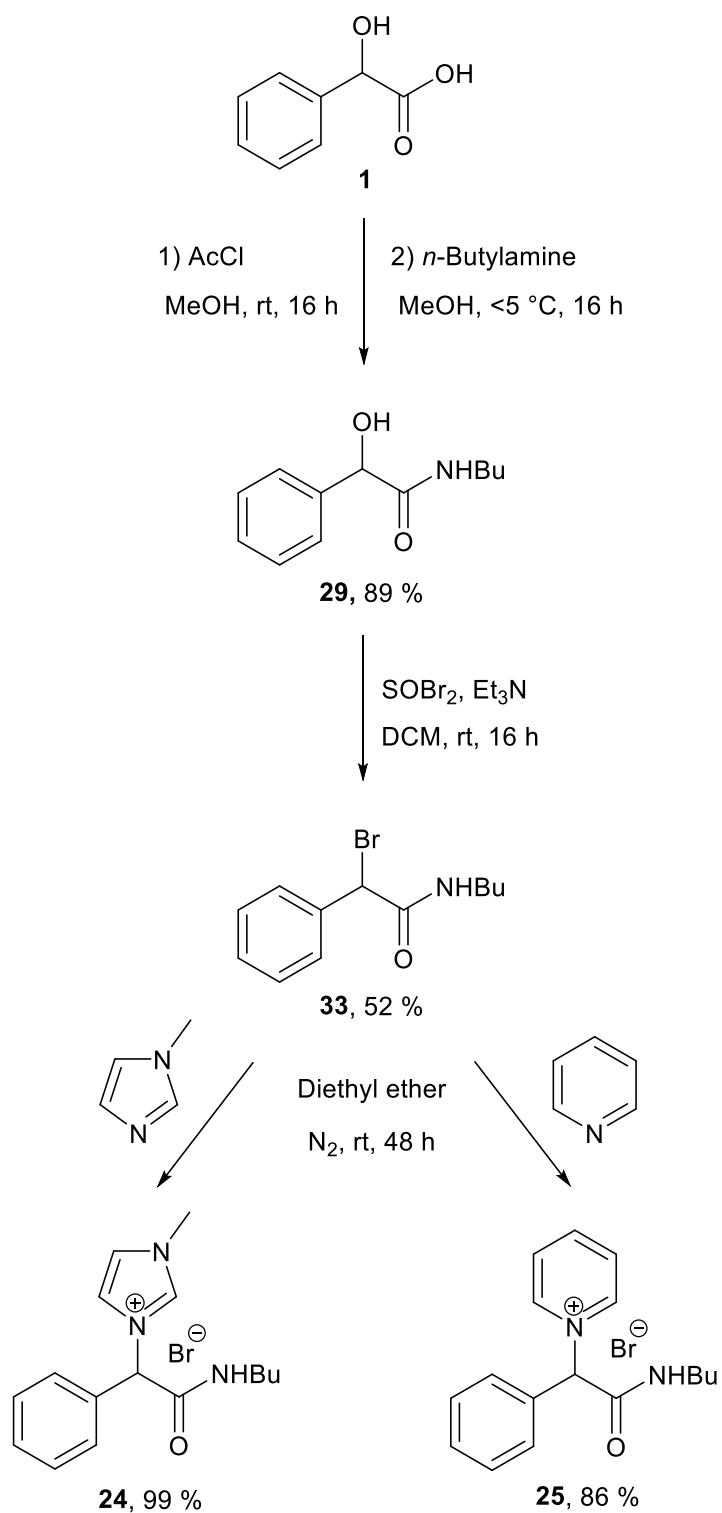
The ten target mandelic acid ILs (**16–25**) (Figure 2.3) were all synthesised from the starting material (*R,S*)-mandelic acid. Although both the (*R*)- and (*S*)-isomers are known to occur in nature,¹⁴ the racemate was selected as the starting material due to the expected loss of defined stereochemistry during the proposed synthesis. The synthesis of the ILs consisted of three parts (Scheme 2.2 and 2.3):

1. Esterification or amidation of mandelic acid
2. Halogenation of the α -position of the ester/amide with thionyl bromide
3. Nucleophilic substitution reaction of the α -halo ester with aromatic *N*-heterocycle

Full procedural detail for the preparation of the mandelic acid ILs is provided in the experimental section of this work (chapter 6, section 6.2).



Scheme 2.2 General synthesis of mandelate ILs (**16–23**) with percentage yields.



Scheme 2.3 General synthesis of mandelamide ILs (**24** and **25**) with percentage yields.

2.2.1 Synthesis of Mandelic Acid Esters

Esterification of mandelic acid (**1**) was carried out by the well-known Fischer-Speier method²⁰ to produce the methyl (**26**), ethyl (**27**) and butyl (**28**) mandelic acid esters (Figure 2.4).

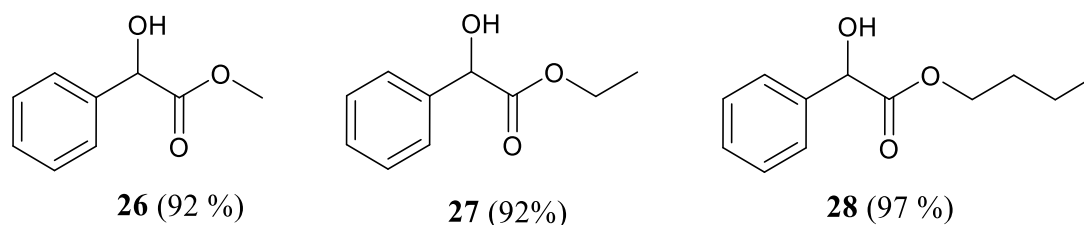
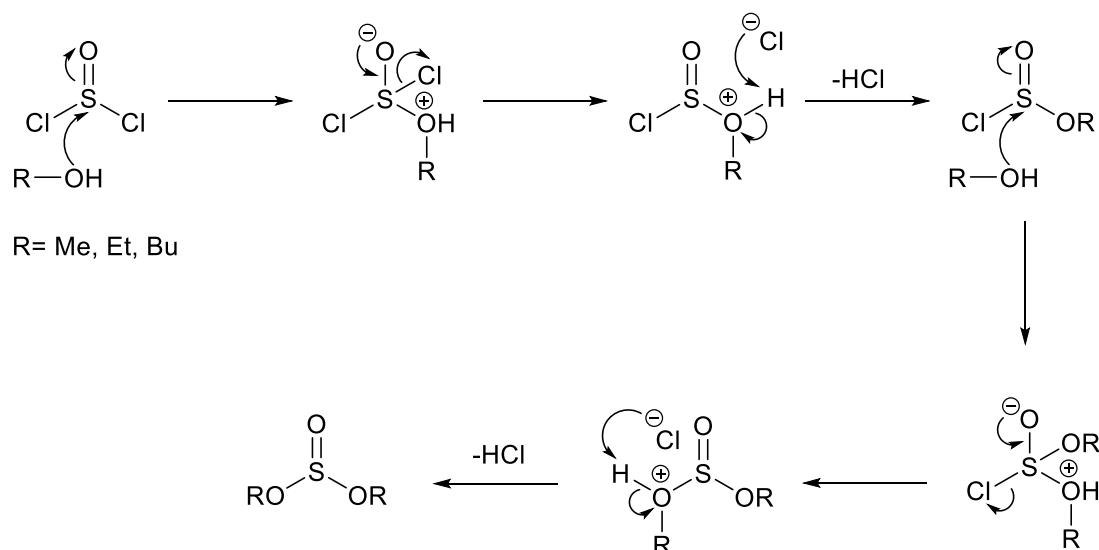


Figure 2.4 Percentage yields for mandelic acid methyl (**26**), ethyl (**27**) and butyl (**28**) esters synthesised from mandelic acid (**1**).

The esterification of mandelic acid was carried out with thionyl chloride (SOCl_2) in the solvent alcohol of the required alkyl chain length. The SOCl_2 reacts with the alcohol releasing 2 eq. of HCl for every 1 eq. of SOCl_2 , which promotes the reaction (Scheme 2.4). Mandelic acid was dissolved in an excess of alcohol and SOCl_2 (0.5 eq.) was added dropwise at 0°C . The reaction was stirred at rt for 4 h and reaction completion was confirmed by TLC. After reaction work-up no further purification was required to give esters **26–28** in excellent yields (92–97 %) (Figure 2.4).



Scheme 2.4 Generation of 2 eq. of HCl *in situ* from the reaction of thionyl chloride with alcohol.

In the ^1H NMR of the mandelic acid methyl ester (**26**) in CDCl_3 the proton at the α -position to the carbonyl group (H4) forms a doublet at 5.18 ppm by coupling to the alcohol proton (OH) with $J = 5.1$ Hz (Figure 2.6). The alcohol proton on the mandelic acid ester (H5) thus gives a doublet in the ^1H NMR at 3.44 ppm, when the spectra is highly resolved, due to coupling to the proton on the α -position with $J = 5.1$ Hz (Figure 2.5).

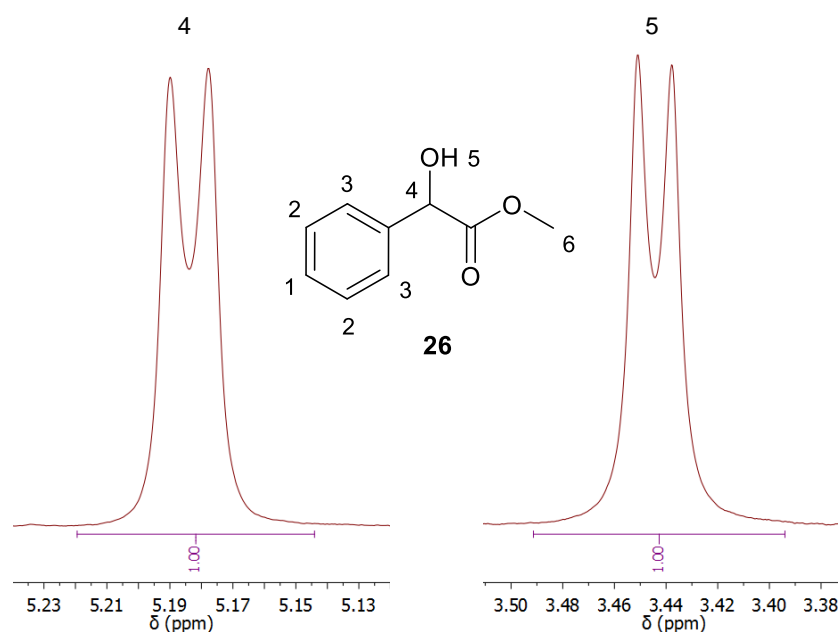


Figure 2.5 ^1H NMR of mandelic acid methyl ester (**26**) in CDCl_3 showing the doublets for proton H4 at the stereogenic centre (left) and the alcohol proton H5 (right).

In the ^1H NMR of the mandelic acid ethyl ester (**27**) in CDCl_3 the two protons of the CH_2 group attached to the ester oxygen (H6) are diastereotopic and thus couple. They also couple to the adjacent CH_3 protons (H7). This forms two separate doublets of quartets at 4.27 and 4.17 ppm, each with eight peaks and coupling constants $J = 10.8$ and 7.1 Hz (Figure 2.6).

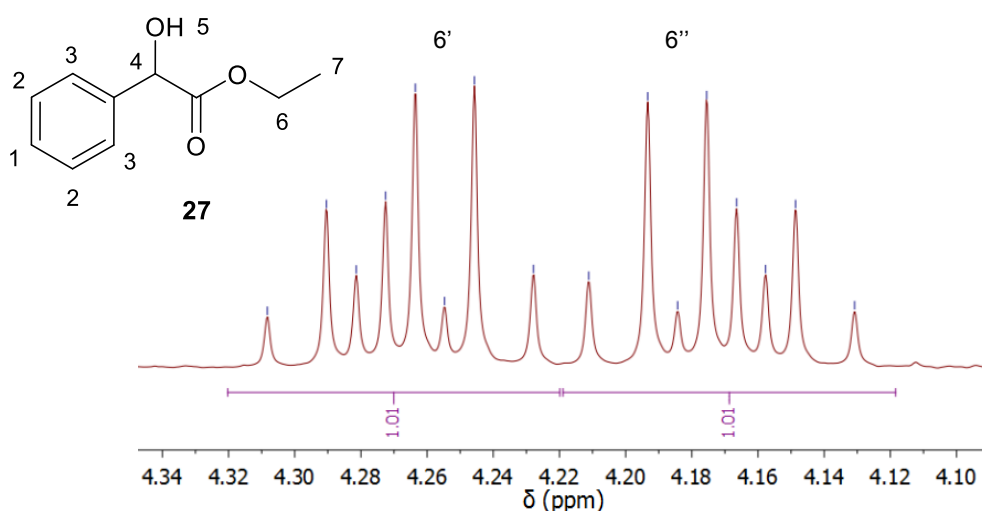
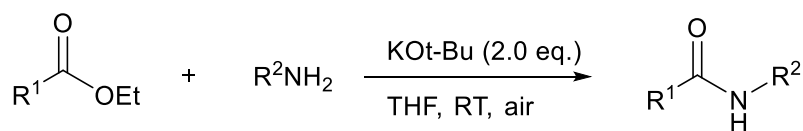


Figure 2.6 ^1H NMR of mandelic acid ethyl ester (**27**) in CDCl_3 showing the two doublets of quartets of the H6 protons (H6' and H6'').

2.2.2 Synthesis of Mandelic Acid Amides

Two procedures with green reaction conditions were initially selected to synthesise a mandelic acid amide. The first was a thermal amidation procedure which required no solvent, was waste minimal, and good yields were reported for a variety of carboxylic acid substrates.²¹ A reaction was carried out with mandelic acid (**1**), *n*-butylamine (1.0 eq.) and 3 Å molecular sieves at reflux under an N_2 atmosphere. After 24 h the TLC showed no remaining mandelic acid, but three spots on the plate with a 94 % crude yield. Product purification by recrystallisation was unsuccessful, and column chromatography also proved problematic yielding only 9 % of the desired product.

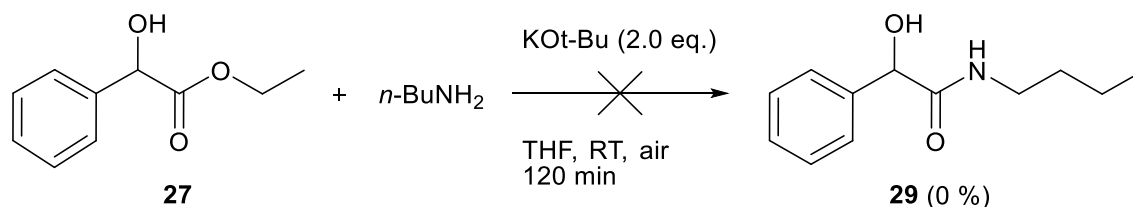
The second procedure was a *tert*-butoxide assisted amidation of esters carried out under mild conditions, reported to be a rapid (≤ 60 min) and versatile reaction (Scheme 2.5).²² Mandelic acid ethyl ester (**27**) was reacted with *n*-butylamine (1.0 eq.) in the presence of potassium *tert*-butoxide (2.0 eq.) in THF at rt in air to synthesise the target butyl ester of mandelic acid (**29**) (Scheme 2.6). After 2 h TLC confirmed no unreacted ester or amine remained. However, after work-up only a very small amount of material was recovered (2 %), which ^1H NMR confirmed was not the desired product. Further inspection of the literature showed that a substrate similar to mandelic acid, with a hydroxyl group at the carbon α to the ester group, gave a very poor yield with this procedure (4 %) (Scheme 2.5).²²



$R^1 = C_6H_5$, $R^2 = n\text{-BuNH}_4$, (60 min, 79 %)

$R^1 = CH(OH)CH_3$, $R^2 = C_6H_5NH_2$, (30 min, 4 %)

Scheme 2.5 *tert*-Butoxide assisted amidation of ethyl esters alkananoates with amines.²²



Scheme 2.6 *tert*-Butoxide assisted amidation of methyl ester of mandelic acid (**27**) with *n*-butylamine.

Coupling reagents are widely employed in synthetic chemistry to activate carboxylic acids and facilitate the formation of an amide bonds.^{23,24} A coupling reaction was undertaken to obtain the butyl amide of mandelic acid (**29**) using 1-ethyl-3-(3-dimethylaminopropyl)carbodiimide (EDC) (1.1 eq.), *N*-hydroxysuccinimide (HOSu) (1.1 eq.) and *n*-butylamine (1.0 eq.). After 2 days of stirring at rt no unreacted mandelic acid was detected by TLC. The crude product was purified by column chromatography to give **29** as a white crystalline solid in moderate yield (45 %).

Alongside the coupling method, a reaction to produce amide **29** was undertaken with acetyl chloride according to a modified version of a the literature procedure (Scheme 2.3).²⁵ Mandelic acid (**1**) was dissolved in methanol and acetyl chloride (1.02 eq.) was added dropwise at 0 °C. The reaction was stirred overnight at rt and a complete reaction of mandelic acid was confirmed by TLC. The reaction was cooled to 0 °C and *n*-butylamine (4.0 eq.) was added and the reaction was placed in the fridge (< 5 °C) overnight. TLC confirmed reaction completion and **29** was isolated as a white crystalline solid in excellent yield (89 %). The ¹H NMR of the **29** in CDCl₃ clearly shows the presence of both the NH (H10) and OH (H5) protons as broad singlets at 6.12 and 3.77 ppm respectively (Figure 2.7). A D₂O shake was carried out on the NMR sample and led to a disappearance of the NH and OH peaks from the subsequent ¹H NMR spectra, further confirming the identity of these peaks.

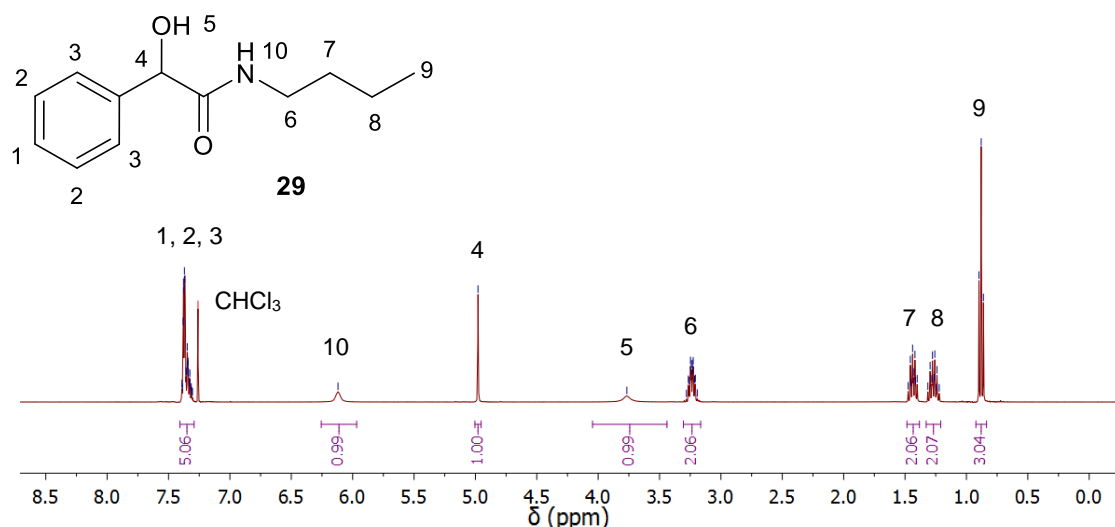
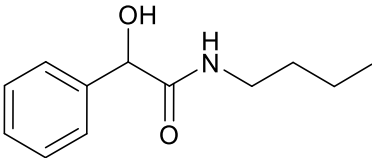


Figure 2.7 ^1H NMR of butyl amide of mandelic acid (**29**) in CDCl_3 with the NH (H10) and OH (H5) peaks clearly visible at 6.1 and 3.8 ppm respectively.

To deduce the mechanism of the acetyl chloride reaction, a sample was removed on completion of the reaction between mandelic acid (**1**) and acetyl chloride, confirmed by TLC, before the addition of *n*-butylamine. Analysis of the sample by ^1H and ^{13}C NMR showed that the intermediate produced in the reaction was the methyl ester of mandelic acid. The ^1H NMR spectra was identical to the previously prepared mandelic acid methyl ester **26**. This confirmed that the mechanism of the reaction was by HCl generation through the reaction of acetyl chloride with methanol, followed by acid catalysed Fischer-Speier esterification of mandelic acid. In the second stage of the reaction, a nucleophilic substitution reaction of *n*-butylamine with the methyl ester produced amide **29**.

There are several benefits to the acetyl chloride procedure over the coupling procedure to produce amide **39**. The procedure with acetyl chloride does not require column chromatography to be undertaken and is a much higher yielding procedure than the coupling reaction (89 and 45 % respectively) (Table 2.1).

Table 2.1 Comparison of the coupling and acetyl chloride methods used to synthesise the butyl amide of mandelic acid (**29**).

Compound	Structure	Synthesis method	Yield (%)	Column purification
29		EDC coupling	45	Yes
		Acetyl chloride	89	No

The overall duration of each reaction method is the same two-day length. However, the reaction with acetyl chloride is carried out with a large excess of *n*-butylamine (4 eq.), which is necessary to force the reaction to completion. Some *n*-butylamine is also used to neutralise any HCl remaining from the esterification step. Knowing that the reaction mechanism proceeds through the methyl ester of mandelic acid (**26**), a reaction was carried out directly between **26** and *n*-butylamine in methanol to see if amide **27** could be synthesised using less *n*-butylamine. Despite requiring a lower amount of *n*-butylamine (1.55 eq.) and giving a good yield (78 %), the reaction took 6 days to reach completion, including 3 days at reflux. Due to this long reaction time and the requirement to initially synthesise **26** to undertake the reaction, the acetyl chloride procedure was preferred for the synthesis of amide **27**.

2.2.3 Synthesis of Mandelic Acid Alkylating Regents

The synthesis of α -bromoester and α -bromoamide alkylating reagents **30–33** (Figure 2.8) was carried out by the addition of thionyl bromide (SOBr₂) to the mandelic acid esters **26–28** and amide **29**. The reaction occurs via a *meso* substitution of the alcohol by bromine (Scheme 2.6).

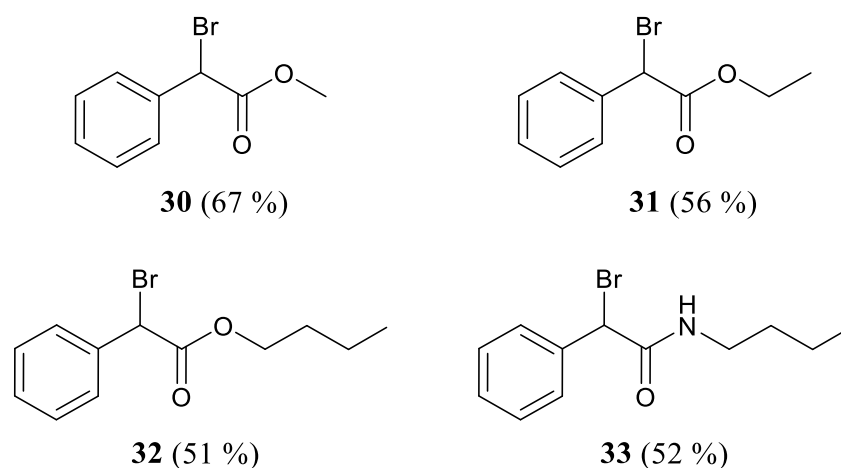
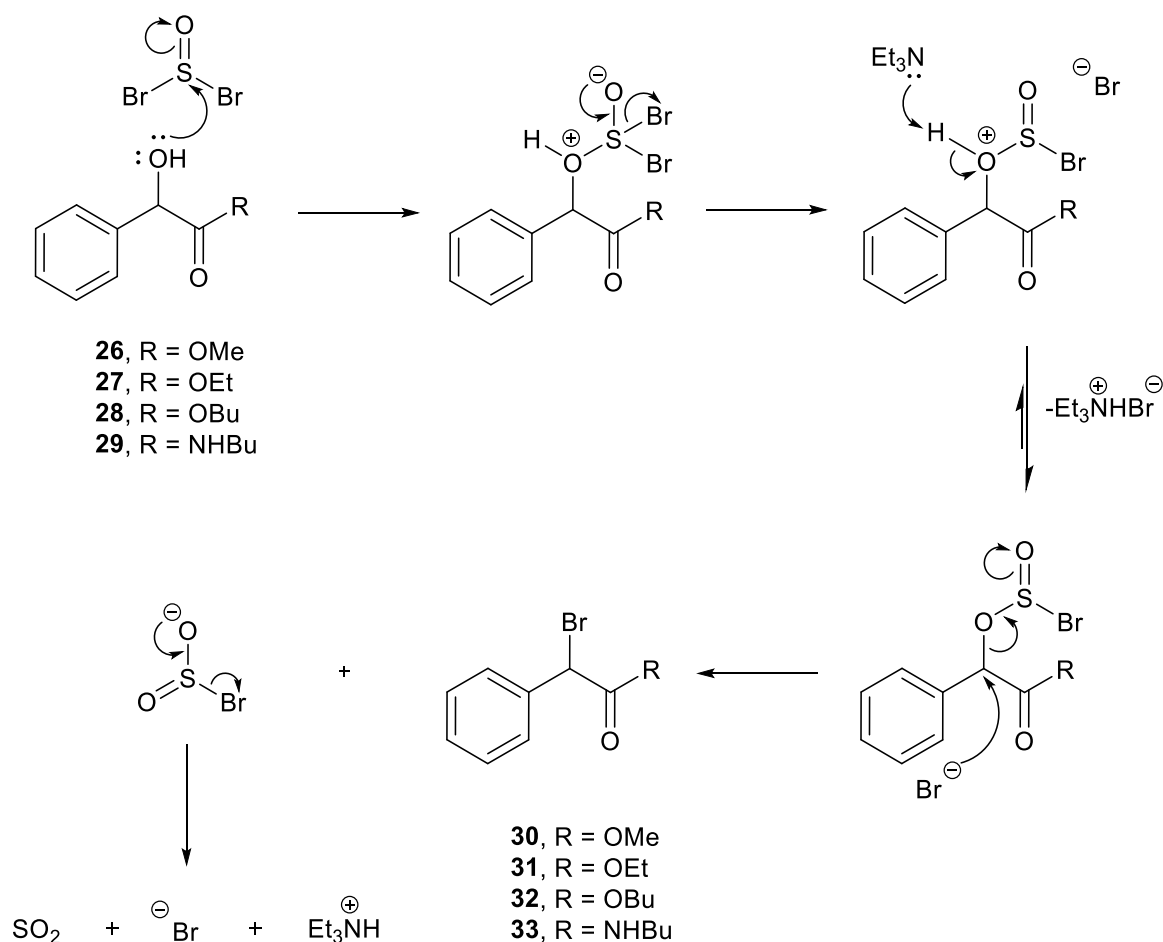


Figure 2.8 Percentage yields for mandelic acid α -bromoester and α -bromoamide alkylating reagents (**30–33**), synthesised from mandelic acid esters **26–28** and amide **29**.

In a typical reaction, the mandelic acid ester/amide was dissolved in dry dichloromethane (DCM) with triethylamine (TEA) (1.5 eq.) under N_2 . $SOBr_2$ (1.2 eq.) was added dropwise at 0 °C and the reaction was stirred at rt for 4 h. The crude product was purified by column chromatography (SiO_2 , EtOAc:hexane) to give **30–33** in moderate yields (51–67 %).

The mechanism of the reaction occurs through the alcohol of mandelic acid, which acts as a nucleophile towards $SOBr_2$ on its addition. This reaction converts the alcohol into a good leaving group, and subsequent reaction of the resultant bromide at the benzylic position on the mandelic acid results in the removal of SO_2 and the formation of either the desired α -bromoester or α -bromoamide product (Scheme 2.7).



Scheme 2.7 Reaction mechanism of α -bromoester and α -bromoamide formation.

2.2.4 Synthesis of Mandelic Acid ILs

Ten mandelate and mandelamide bromide ILs (**16–25**) were synthesised via a nucleophilic substitution reaction between an *N*-heterocycle and the α -bromoester or α -bromoamide of mandelic acid (**30–31**), as previously described in the literature (Scheme 2.2 and 2.3).²⁶ This type of reaction is more specifically called a Menshutkin reaction, with the reaction mechanism being either a bimolecular S_N2 process or a unimolecular S_N1 process, dependent on the nature of both the solvent and the reactants.^{27,28} However, extensive mechanistic studies of the reactions between benzylic systems and aromatic tertiary amines have shown that the reactions occur simultaneously through independent S_N1 and S_N2 mechanisms,^{29–32} with the rate of the reaction dependent on the reaction conditions.³³ The *N*-heterocycles selected for the IL synthesis of ILs (**16–25**) were 1-methylimidazole, pyridine, 3-methoxypyridine and ethyl nicotinate (Figure 2.9). When using ethyl nicotinate as the *N*-heterocycle the resultant IL was the 3-(ethoxycarbonyl)pyridinium IL, which can also be described as a nicotinic acid derived IL.

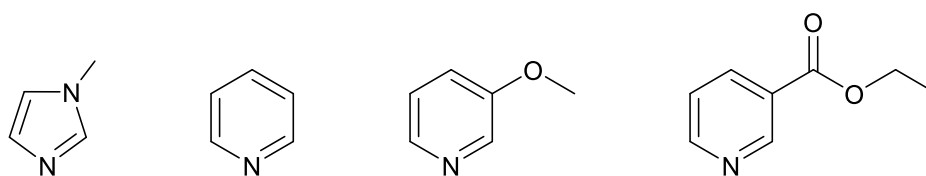


Figure 2.9 *N*-Heterocycles used for synthesis of ILs **16–25**: 1-methylimidazole, pyridine, 3-methoxypyridine and ethyl nicotinate.

In addition to the research carried out on this particular class of compounds directly preceding this work, and previously discussed in section 2.1,¹⁸ there have been several mentions of this class of compounds in the literature.^{34–36} However, the only exact compound match for this new series that could be found in the literature was for the pyridinium butyl ester IL (**19**), where compound characterisation could be found, but not biodegradation and toxicity analysis.³⁷

ILs **16–18** and **20–25** were synthesised by the addition of the *N*-heterocycle to the appropriate α -bromoester or α -bromoamide (1.02–1.05 eq.) dissolved in diethyl ether. The reaction was stirred for 2 days and completion was confirmed by TLC. Trituration was carried out with diethyl ether before removal of the solvent to give the desired ILs as solids in good to excellent yields (56–99 %). IL **19** was synthesised by the addition of the *N*-heterocycle (0.98 eq.) directly to the neat α -bromoester, as the reaction was found to proceed very slowly in diethyl ether (> 2 weeks to reach 95 % yield). Trituration was carried out with diethyl ether before removal of the solvent to obtain the IL as white solid in excellent yield (98 %).

Seven of the ILs were produced in excellent yields (**16–20**, **24** and **25**) (84–99 %) with the three butyl esters with pyridinium (**21**), 3-methoxypyridinium (**22**) and 3-(ethoxycarbonyl)pyridinium (**23**) headgroups produced in moderate yields (56, 74 and 63 % respectively) (Figure 2.10). For the methyl ester (**16** and **17**), butyl ester (**20** and **21**) and butyl amide (**24** and **25**) ILs, higher percentage yields were obtained for the ILs with a 1-methylimidazolium headgroup (e.g. **16** at 95 % vs **17** at 86 %). The opposite was observed for the ethyl ester ILs (**18** and **19**) with both 1-methylimidazolium and pyridinium IL having similar percentage yields (94 and 98 % respectively). For the butyl esters (**13–16**) the percentage yields were in the order, pyridinium < 3-(ethoxycarbonyl)pyridinium < methoxypyridinium < 1-methylimidazolium. It is clear that substitution on the pyridine ring influenced the reaction rate.

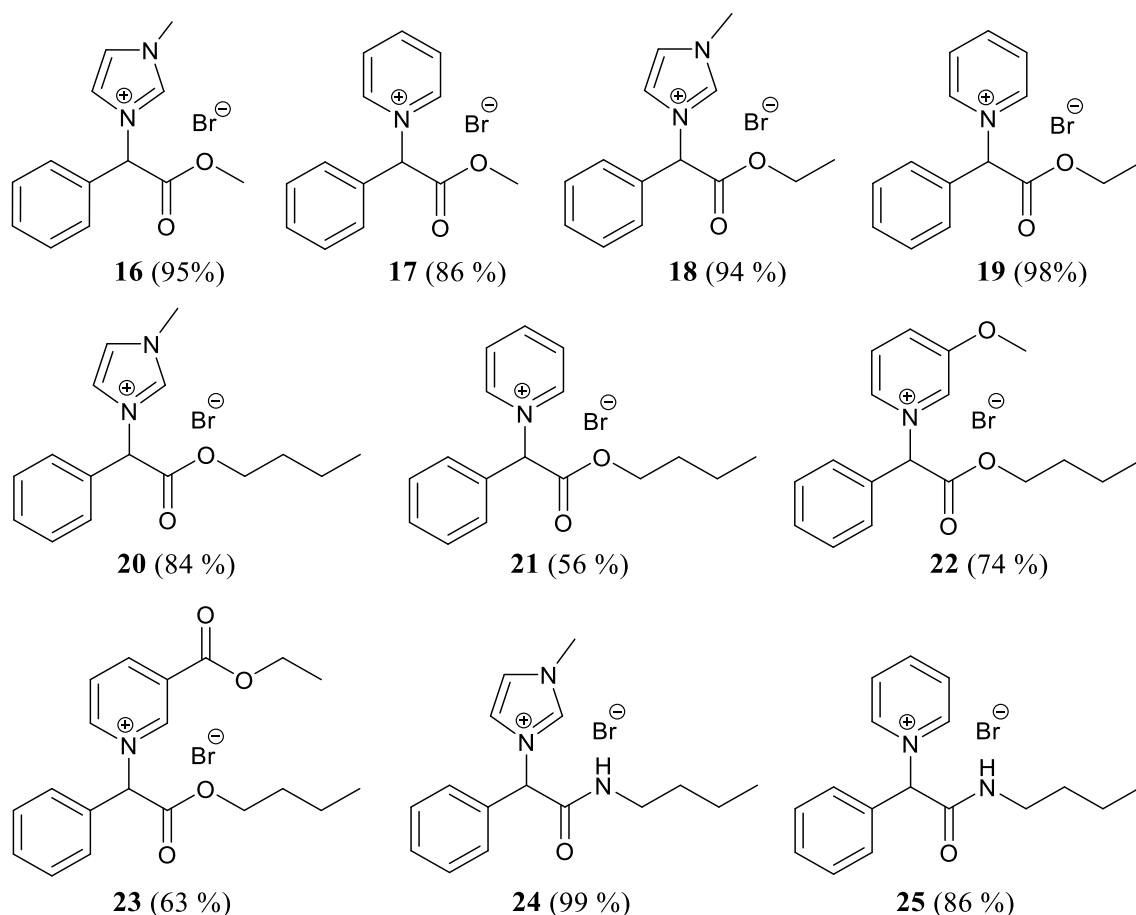


Figure 2.10 Percentage yields for mandelate and mandelamide bromide ILs (**16–25**).

All ten ILs were obtained as crystalline solids with a wide range of melting points observed (48–169 °C) (Table 2.2). It is anticipated that these ILs will be used in applications above their melting points, exploiting the potential solvent properties of the ILs. ILs **16** and **21** had the lowest melting points (61–63 and 48–50 °C respectively) despite any similar structural features. The highest melting points were observed for the pyridinium ILs **19** and **25** (161–162 and 167–169 °C respectively). ILs **17** and **24** had melting points around 140 °C (140–142 and 143–145 °C respectively), again with no similar structural features. ILs **18** and **20** had moderately high melting points (101–102 and 99–101 °C respectively), both with 1-methylimidazolium headgroups. ILs **22** and **23** had moderately high melting points (127–128 and 112–113 °C respectively), both butyl esters with 3-methoxypyridinium (**22**) and 3-(ethoxycarbonyl)pyridinium (**23**) headgroups. In conclusion, the headgroup has a more marked effect on the IL melting points than the alkyl chain length. In all but one case the pyridinium ILs had higher melting points than the 1-methylimidazolium ILs with the same ester/amide alkyl chain, with this trend only reversed for the butyl ester ILs **20** and **21**. The butyl amides ILs **24**

and **25** had higher melting points than the butyl ester ILs, which can be expected due to their high hydrogen bonding ability.

Table 2.2 Physical appearance and melting points of mandelate and mandelamide bromide ILs (**16–25**).

IL	Appearance	mp (°C)
16	White solid	61–63
17	White solid	140–142
18	White solid	101–102
19	White solid	161–162
20	White solid	99–101
21	Brown solid	48–50
22	White solid	127–128
23	Light pink solid	112–113
24	White solid	143–145
25	White solid	167–169

The ^1H NMR spectra of the 3-methoxypyridinium (**22**) and 3-(ethoxycarbonyl)pyridinium (**23**) ILs in CDCl_3 give distinct coupling patterns with characteristic J values of *ortho* and *meta* coupling for the *N*-heterocyclic rings (Figure 2.11). *Ortho* and *meta* coupling constants in pyridines are typically 6–9 and 1–3 Hz respectively.³⁸ The 3-methoxypyridinium IL (**22**) H9 proton gives a doublet of doublets (dd) at 9.81 ppm with $J = 2.6$ and 1.3 Hz due to coupling to protons H12 and H10 respectively, which are *meta* to H9. The H10 proton gives a doublet of doublet of doublets (ddd) at 8.63 ppm with $J = 6.0$, 1.3 and 1.1 Hz due to coupling to proton H11 which is *ortho* to H10, and to protons H9 and H12 respectively, which are *meta* to H10. A ddd is also observed at 7.99 ppm for the H12 proton with $J = 8.8$, 2.6 and 1.1 Hz due to coupling to proton H11 which is *ortho* to H12, and to protons H9 and H10 respectively, which are *meta* to H12. Finally, the H11 proton gives a dd at 7.87 ppm with $J = 8.8$ and 6.0 Hz due to coupling to protons H12 and H10 respectively, which are *ortho* to H11.

Two-dimensional NMR was also used to facilitate the assignment of protons H10 and H12 in IL **22**. Heteronuclear multiple-bond correlation (HMBC) spectroscopy can be

used to detect heteronuclear through-bond correlation over 2–3 bonds.³⁹ The HMBC spectrum of IL **22** shows that proton H10 correlates to C4 (3 bonds away), whereas proton H12 does not correlate to C4 (5 bonds away) (Appendix A1). This information allows for the unambiguous assignment of protons H10 and H12. The full HMBC spectrum of IL **22** is provided in Appendix A2.

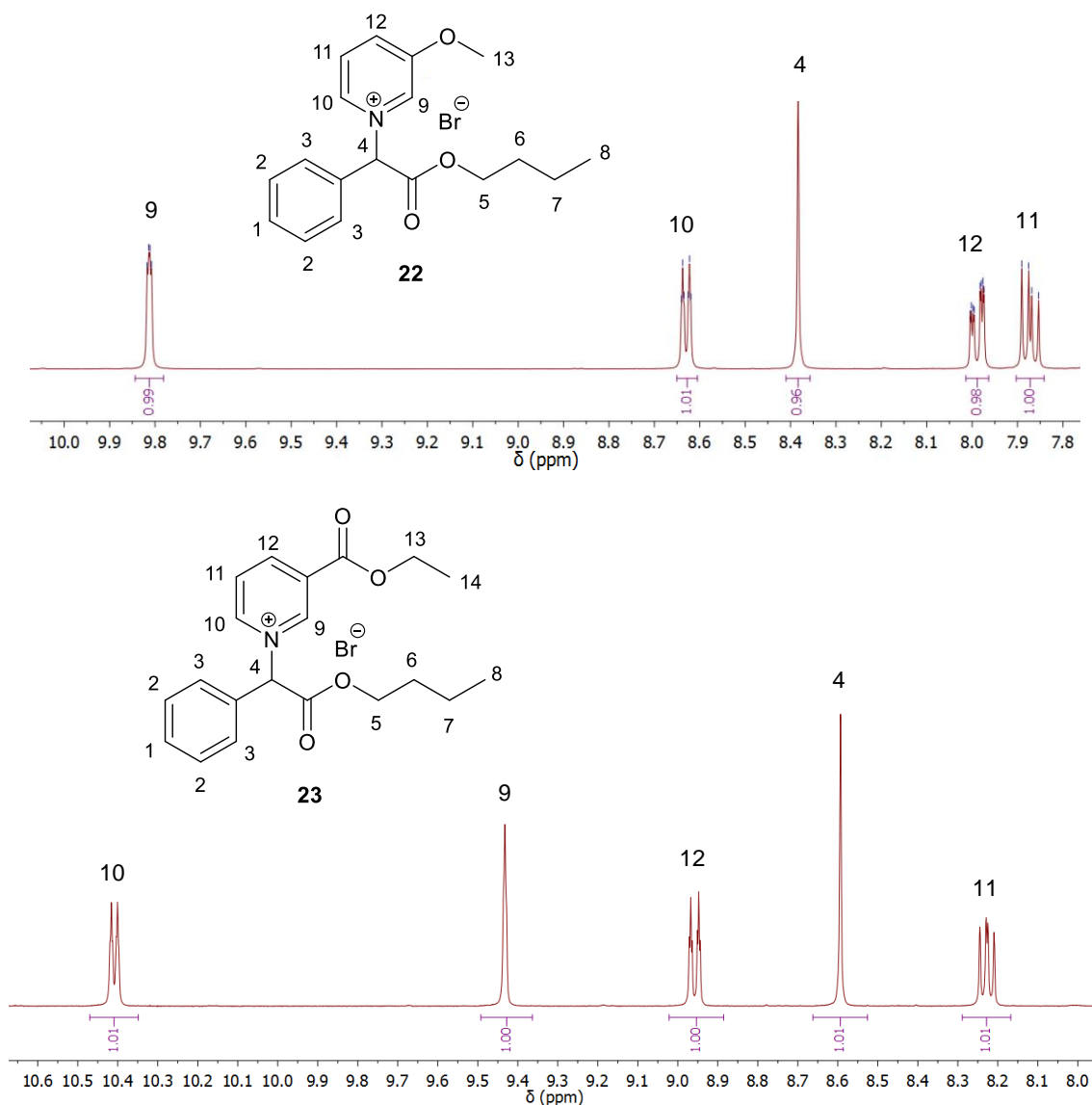


Figure 2.11 *N*-Heterocyclic region of the ¹H NMR for 3-methoxypyridinium IL (**22**) (top) and 3-(ethoxycarbonyl)pyridinium IL (**23**) (bottom) in CDCl₃.

The 3-(ethoxycarbonyl)pyridinium IL (**23**) H10 proton gives a ddd at 10.41 ppm with $J = 6.3, 1.4$ and 1.4 Hz due to coupling to proton H11 which is ortho to H10, and to protons H9 and H12 which are *meta* to H10. The H9 proton gives a broad singlet at 9.43 ppm. A ddd is observed at 8.96 ppm for the H12 proton with $J = 8.0, 1.4$ and

1.4 Hz due to coupling to proton H11 which is *ortho* to H12, and to protons H9 and H10 which are *meta* to H12. Finally, the H11 proton gives a dd at 8.23 ppm with $J = 8.0$ and 6.3 Hz due to coupling to protons H12 and H10 which are *ortho* to H11. HMBC spectroscopy was again used to facilitate the unambiguous assignment of protons H10 and H12. The HMBC spectrum of IL **23** shows that proton H10 correlates to C4 (3 bonds away), whereas proton H12 does not correlate to C4 (5 bonds away) (Appendix A3). The full HMBC spectrum of IL **23** is provided in Appendix A4.

2.2.4.1 Synthesis of Monofluoro Mandelic Acid ILs

In certain applications where the mandelic acid ILs will find use, it is possible that they may be exposed to harsh reaction conditions such as acidic, basic or photochemical reactions. Under basic conditions it is possible for α -protons to be abstracted, as was observed in the case of acetate ILs ($pK_a = 4.76$),¹⁹ therefore it is possible that the α -proton in the mandelic acid ILs may be abstracted under basic conditions. This may lead to breakdown of the IL, rendering it unsuitable for its given application.

To increase the chemical stability of the mandelate bromide ILs, and in turn widen their applicability, replacement of the α -proton in the ILs with a fluorine atom was proposed (Figure 2.12). Fluorine is often found in IL structures, most commonly in BF_4 , PF_6 and NTf_2 anions, but also as alkyl fluorides, such as in the highly fluorinate phosphonium ILs.⁴⁰ Whilst the use of BF_4 and PF_6 is best avoided due to hydrolysis to toxic HF,⁴¹ the incorporation of fluorine atoms into the alkyl structure of ILs is still widely employed.⁴²⁻⁴⁵ In this work, the introduction of only one fluorine atom into the structure of the mandelic acid ILs, to give target IL **34** (Figure 2.12), was proposed. Biodegradation and antimicrobial activity analysis of any new fluorine ILs synthesised would ideally be carried out in line with the project aim of designing low toxicity biodegradable ILs.

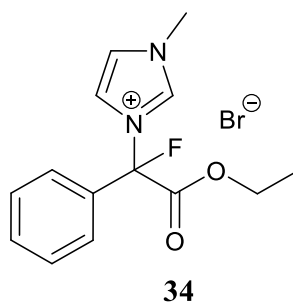
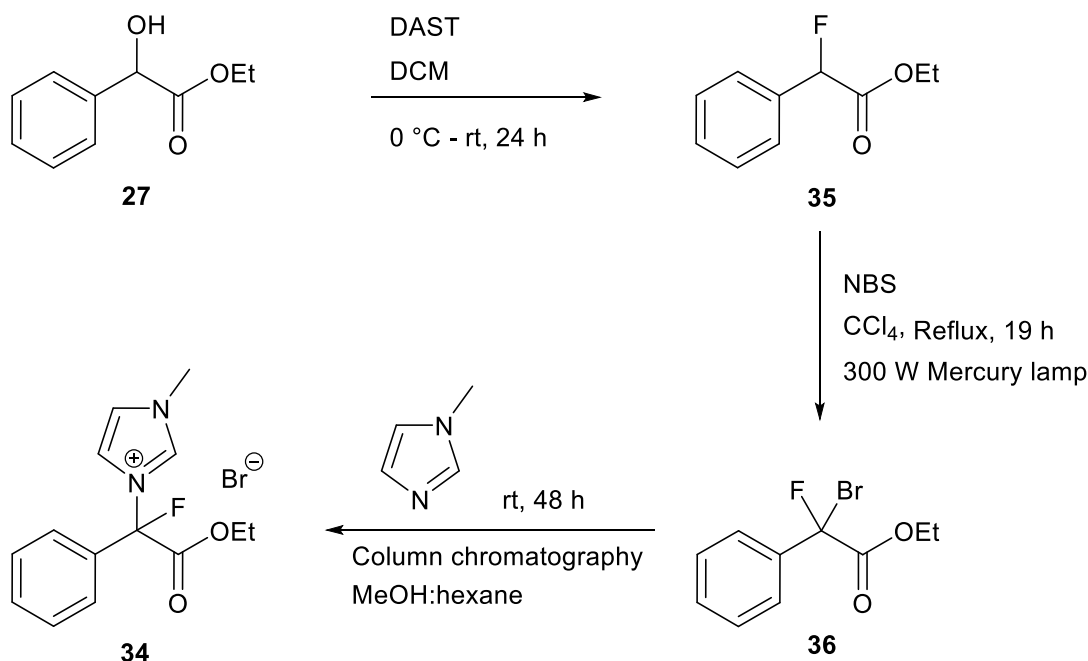


Figure 2.12 Target monofluoro mandelate IL (**34**).

The general route to synthesise the monofluoro mandelate bromide IL (**34**) consisted of three parts (Scheme 2.8).



Scheme 2.8 General synthesis route to monofluoro mandelate bromide IL (**34**).

Compound **35** (Figure 2.13) was synthesised by reacting mandelic acid ethyl ester (**27**) and diethylaminosulfur trifluoride (DAST) according to the literature procedure.⁴⁶ DAST (1.8 eq.) was added dropwise to **27** in DCM at 0 °C and the reaction was stirred for 1 day at rt. After quenching, work-up and subsequent column chromatography (SiO₂, EtOAc:hexane) the α -fluoroester **35** was obtained as a yellow oil in 64 % yield.

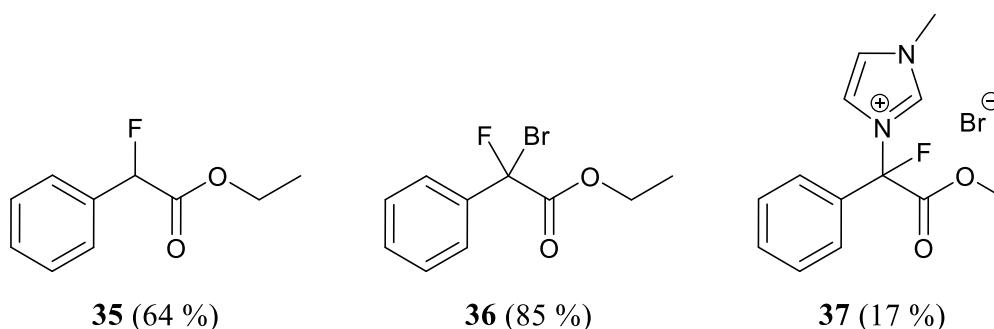


Figure 2.13 Percentage yields for the monofluoro intermediates (**35** and **36**), and the monofluoro mandelate IL (**37**).

The reaction of **27** with DAST is a nucleophilic *meso* substitution reaction where fluoride acts as a nucleophile. The ^1H NMR spectrum of **35** in CDCl_3 shows a doublet at 5.78 ppm for H4 with $J_{\text{H-F}} = 47.8$, due to coupling to the fluorine atom (Figure 2.14).

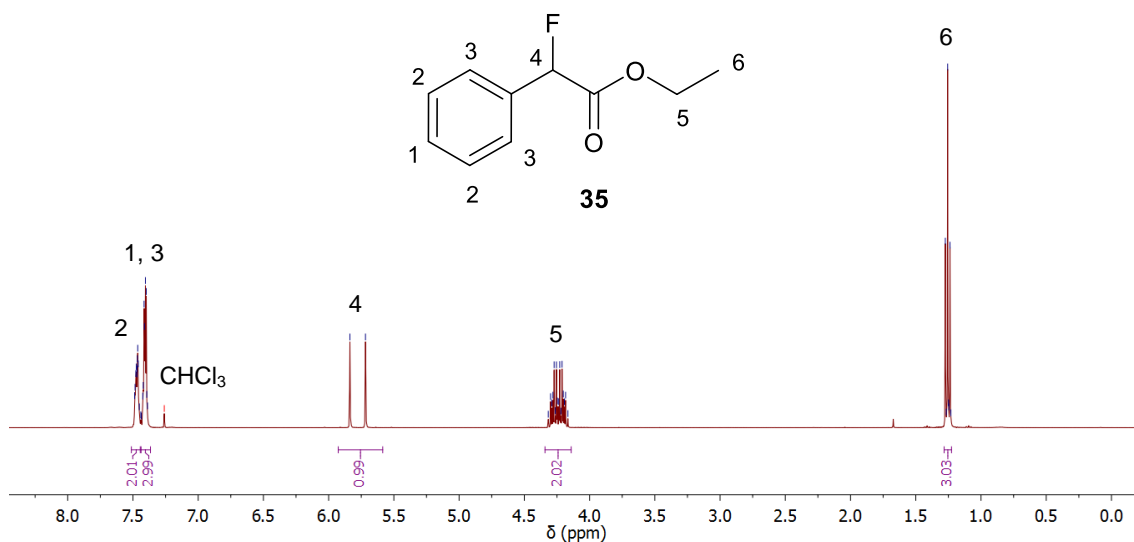


Figure 2.14 ^1H NMR of α -fluoroester of mandelic acid (**35**) in CDCl_3 .

In the ^{13}C NMR spectrum of **35** in CDCl_3 coupling of the fluorine atom to the adjacent carbon atom (C7) gives a doublet at 89.45 ppm with $J = 185.3$ Hz (Figure 2.15). This is a typical coupling constant for one bond C-F coupling in ester containing mono-fluoro compounds.⁴⁷ Coupling of the C7, C8, C3 and C1 carbons to the fluorine atom is also observed with $J = 27.4$, 20.4, 6.0 and 2.3 Hz respectively. Such long range coupling (≥ 4 , 5 and 6 bonds) is frequently observed in the NMR of fluorinated compounds.⁴⁸ In the ^{19}F NMR spectrum of **35** in CDCl_3 a doublet is observed at -179.77 ppm due to two bond coupling of the fluorine atom to proton H4 with $J = 47.9$ Hz (Figure 2.14).

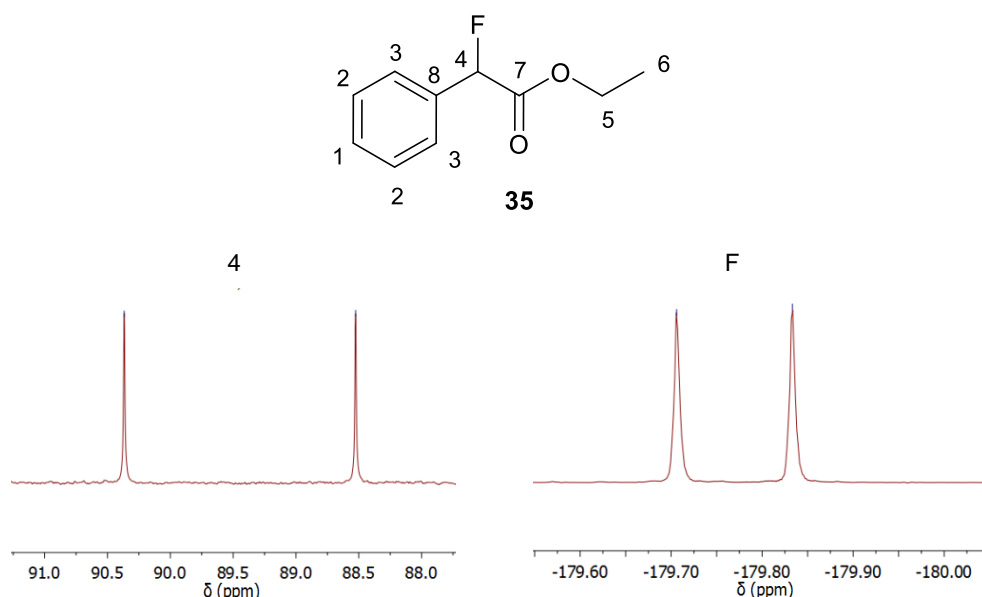


Figure 2.15 NMR doublets observed for the coupling of fluorine to carbon C7 in **35**, as observed in the ^{13}C NMR (left) and the ^{19}F NMR (right) in CDCl_3 .

Compound **36** (Figure 2.13) was synthesised by a photochemical reaction of **35** with *N*-bromosuccinimide (NBS) in CCl_4 at reflux. The literature describes α -bromination of α -fluoro ketones to give *gem*-bromohalo analogues by irradiation with a 300 W tungsten lamp in the presence of NBS.⁴⁹ In DCU a tungsten lamp was not available; however, a mercury lamp was accessible and was tested as an alternative lamp source. A solution of **35** and NBS (1.8 eq.) was irradiated with a 300 W mercury lamp at reflux for 19 h. On reaction completion, confirmed by TLC, the solvent was removed and the crude product was purified by column chromatography (SiO_2 , EtOAc:hexane) to give the α -bromo- α -fluoroester **36** as a colourless viscous liquid in 85 % yield. Thus, in our labs the literature procedure was successfully applied to give compound **36** using a mercury lamp.

The ^1H NMR spectrum of **36** in CDCl_3 shows the disappearance of the doublet observed at 5.7 ppm for the proton at the stereogenic centre in compound **35** (Figure 2.16), confirming successful bromination at the α -position. The ^{19}F NMR of compound **36** in CDCl_3 shows a large downfield shift of the fluorine doublet from -179.77 to -144.41 ppm (Figure 2.17). This further confirms α -bromination as the downfield shift is caused by a deshielding of the fluorine nucleus by the bromine atom.⁴⁷ A doublet is observed for this peak due to four bond coupling of the fluorine atom to proton H3 with $^4J_{\text{F-H}} = 8.2$ Hz.

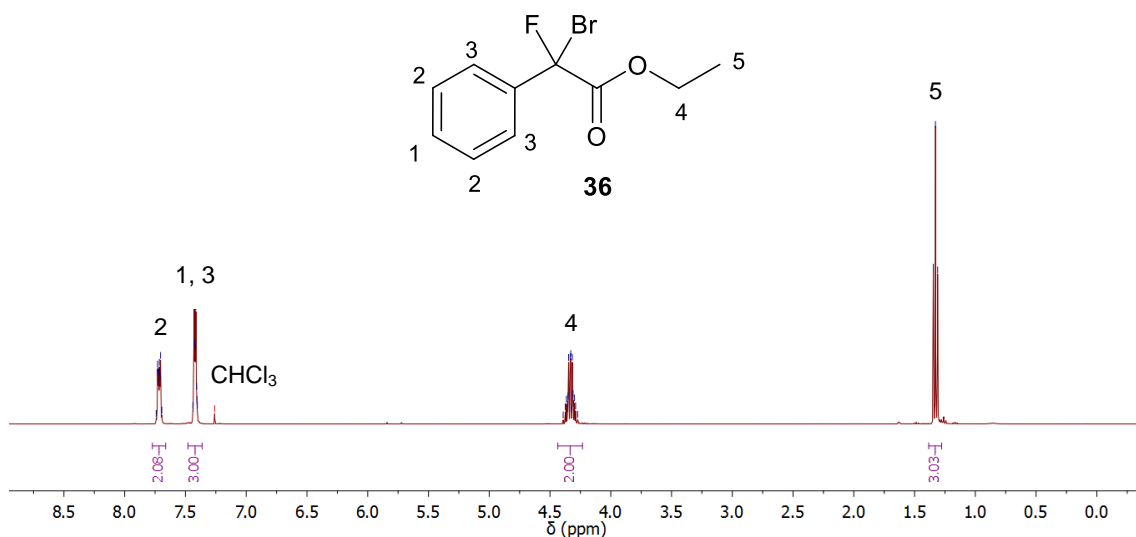


Figure 2.16 ^1H NMR of the α -bromo- α -fluoroester of mandelic acid (**36**) in CDCl_3 .

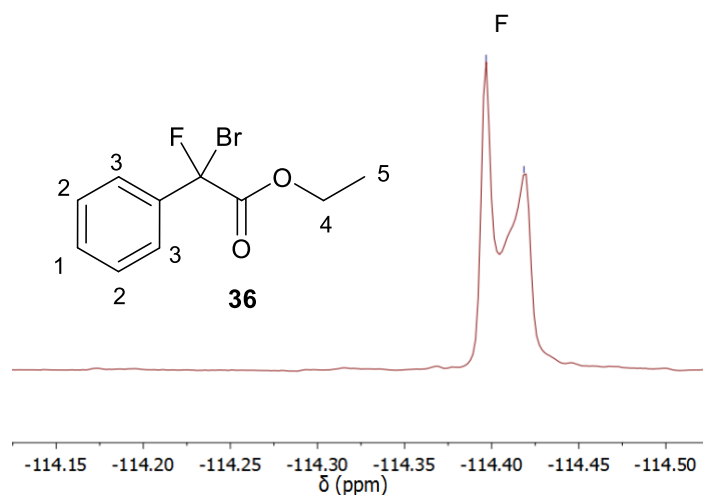


Figure 2.17 ^{19}F NMR of the α -bromo- α -fluoroester of mandelic acid (**36**) in CDCl_3 .

Compound **37** (Figure 2.13) was synthesised by a nucleophilic substitution reaction between 1-methylimidazole and compound **36**. 1-Methylimidazole was added dropwise to compound **36** (1.0 eq.) and the reaction was stirred for 2 days. Completion was confirmed by TLC. Trituration was carried out with diethyl ether, the solvent removed, and the crude product was purified by column chromatography (SiO_2 , MeOH/DCM), where transesterification to the methyl ester occurred to give compound **37** as an off-white solid in 17 % yield. The target compound for the nucleophilic substitution reaction of 1-methylimidazole with compound **36** was IL **34** (the ethyl ester derivative of compound **37**), as shown in Figure 2.12 and in the general synthesis route to monofluoro mandelate bromide ILs (Scheme 2.8). However, the ^1H NMR in $\text{DMSO}-d_6$ obtained after column purification of the crude reaction product clearly shows that a methyl ester (**37**) was isolated, with the CH_3 protons (H4) for the methyl ester seen

clearly as a singlet at 3.35 ppm (Figure 2.18). The reason for isolation of the methyl ester is likely due to transesterification of the ethyl ester crude product on the silica column, caused by the use of methanol in the column solvent and the fact that the silica gel (silicon dioxide) has weakly acidic sites.⁵⁰ Purification on the column was difficult (low yield of 17 %) despite a solvent gradient of 5–10 % MeOH:DCM being employed to increase the separation of the product and the impurities. However, the use of a solvent gradient increased the time that the compound remained on the column, likely facilitating the transesterification. Thus, purification of the IL would be reconsidered if the reaction were repeated. A shorter column time and the use of ethanol instead of methanol to prevent transesterification are recommended. Unfortunately, there was not enough time to investigate this work in more detail as success in other areas of the project moved the focus and dedication of time away from this area of work.

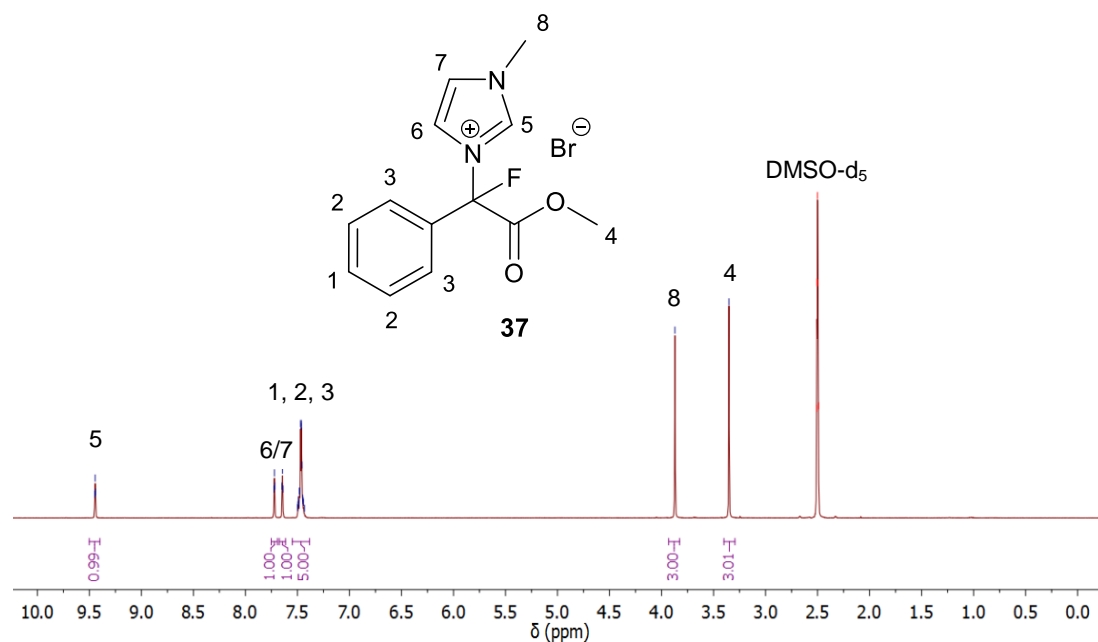


Figure 2.18 ^1H NMR of the monofluoro mandelate IL (**37**) in DMSO-d_6 .

2.2.5 Critique on the ‘Greenness’ of the Synthesis

The aim of this section of work was to synthesise a series of ‘green’ ILs from the renewable resource mandelic acid. Thus, it is necessary to evaluate the ‘greenness’ of all stages of the synthesis of the mandelic acid ILs (scheme 2.2). Herein a preliminary critique of the ‘greenness’ of the synthetic methodologies is presented.

Firstly, the synthesis of the mandelic acid esters (**26–28**) employs the use of the reagent SOCl_2 . SOCl_2 has been classified as a reagent with ‘some issues’ in a publication by

GlaxoSmithKline (GSK), which presents a reagent guide and discusses reagent selection based on sustainability.⁵¹ SOCl₂ is also a lachrymator.⁵¹ Alternative reagents that could be employed for this synthesis include acetyl chloride, sulfuric acid or hydrochloric acid. However, SOCl₂ is required at lower equivalents than HCl as it releases 2 eq. of HCl for every 1 eq. of SOCl₂. HCl is used only as a catalyst in the reaction, thus it is highly probable that the equivalents of SOCl₂ necessary for successful reaction completion could be further reduced if investigated. Utilising the alcohol of the required alkyl chain length as both the solvent and reagent in the reaction enhances the 'greenness' of this synthesis, with no extra unnecessary solvents required (5th principle of green chemistry). The reaction is also carried out at room temperature for only 4 h which is an energy efficient process (6th principle of green chemistry).

The synthesis of the mandelic acid amide (**29**) employed acetyl chloride and *n*-butylamine (4 eq.) in the reaction. Two 'green' methods were trialled for this reaction but they were unsuccessful (see section 2.2.2).^{21,22} Despite the fact that a high equivalence of *n*-butylamine was required to reach reaction completion (see section 2.2.2), the alternative EDC coupling method that was investigated is far less desirable from a green chemistry perspective. Coupling reactions with carbodiimides are known to produce a lot of waste and have very poor atom economy (contravening the 3rd principle of green chemistry).⁵² Recently, the American Chemical Society Green Chemistry Institute (ACS GCI) Pharmaceutical Roundtable identified direct amide formation avoiding poor atom economy a research area of high priority for sustainable synthetic method development.⁵² The coupling reaction also required column purification. Alternative reagents that could be proposed for this synthesis include enzymes (satisfying the 9th principle of green chemistry), *N,N'*-Carbonyldiimidazole (side products of CO₂ and imidazole are relatively innocuous)⁵³ and isobutyl chloroformate (side products of isobutanol and CO₂ are relatively harmless)⁵⁴.

The synthesis of the mandelic acid α -bromoester and α -bromoamide alkylating reagents (**30–33**) employs the use of SOBr₂, DCM and TEA. DCM poses significant human and environmental toxicity issues.⁵⁵ Thus, the reactions would be improved by the replacement of the chlorinated solvent DCM, which could be facilitated by using the GSK solvent sustainability guides.^{56,57} 2-Methyltetrahydrofuran (2-MeTHF) could be investigated for use as an alternative to DCM and can be produced from renewable resources such as furfural or levulinic acid (addressing the 7th principle of green

chemistry).⁵⁸ Compounds **30–33** were all purified by column chromatography, an additional step in the synthesis that further increased the use of solvents and auxiliaries (SiO₂). However, it is important to note that the solvent system used to purify **30–33**, EtOAc:hexane, is a much ‘greener’ choice than a solvent system using DCM.⁵⁵ The use of SOBr₂ is also undesired from a green chemistry perspective as the reaction produces the toxic gases SO₂ and HBr. However, the use of TEA prevents the gaseous release of HBr from the reaction. An alternative to SOBr₂ may be the use of HBr and a bromide IL, as a similar process for the chlorination of alcohols using HCl and a chloride IL (without the formation of by-products) has been commercialised by BASF.⁵⁹

Synthesis of the mandelic acid ILs **16–18** and **20–25** was carried out in diethyl ether via a nucleophilic substitution reaction. Diethyl ether is highly undesired as a reaction solvent in industry as it has a low boiling point, high volatility, high flammability and presents an explosion risk.⁵⁷ A more sustainable and safer solvent for the synthesis, such as 2-MeTHF, could be selected by consulting the GSK solvent sustainability guides^{56,57} Mandelic acid IL **21** was synthesised in a solventless synthesis, satisfying the 5th principle of green chemistry (no unnecessary use of auxiliary substances). Therefore, an investigation into the solventless synthesis of ILs **16–20** and **22–25** may result in a reduction of the amount of diethyl ether necessary for successful reaction completion.

There are several areas that could be addressed in the synthesis of the target monofluoro mandelic acid ester IL (**34**) to increase the ‘greenness’. The α -fluoroester (**35**) was synthesised using the reagents DAST and DCM. As previously discussed, replacement of the chlorinated solvent DCM is advisable. In addition, DAST is known to be converted to extremely toxic and corrosive SF₄ and explosive bis(diethylamino)sulfur difluoride when heated.⁶⁰ Aminodifluorosulfonium salts have been shown to be a safer alternative to DAST (increased thermal stability, more easily handled, do not generate highly toxic and corrosive HF) and could be considered for the synthesis of **35**.⁶⁰ The synthesis of the α -bromo- α -fluoroester (**36**) was carried out with NBS and CCl₄ in a photochemical reaction. CCl₄ has a relatively high toxicity, is carcinogenic and its use is restricted under the Montreal Protocol due to its ozone depleting effects.⁶¹ Consequently, replacement of CCl₄ is highly recommended. (Trifluoromethyl)-benzene has been shown to be a suitable alternative to CCl₄ in photochemical reactions with NBS, and its inertness and low toxicity make it a much ‘greener’ replacement.⁶² The use of NBS is undesired as the reaction has poor atom economy; however, it is a much safer

and more easily handled alternative to Br₂ which is corrosive and fumes at room temperature releasing toxic bromine gas.⁶³ A solvent free reaction was carried out to produce IL **34** from **36**, yet purification by column chromatography was required (MeOH:DCM). The use of a greener solvent system, without DCM, could potentially be investigated for the purification.

The environmental impact of solvents can be reduced in two ways; by identifying and replacing with greener solvents and by minimising solvent use.⁶⁴ However, the only way to truly find the best solvent for the synthesis is by carrying out a full life cycle analysis on the solvent in a specific application.⁶⁴

2.3 Antimicrobial Activity

The antimicrobial activity of the ten mandelate and mandelamide bromide ILs (**16–25**) was evaluated in three separate toxicity tests.

2.3.1 Antibacterial Activity – High Concentrations

The antibacterial activities of ILs **16–25** (Table 2.3) were evaluated against one Gram-positive bacterial strain: *Bacillus subtilis* (*B. subtilis*; DSMZ 10), and four Gram-negative bacterial strains: *Escherichia coli* (*E. coli*; DSMZ 498), *Pseudomonas fluorescens* (*P. fluorescens*; DSMZ 50090), *Pseudomonas putida* (*P. putida*; CP1), and *P. putida* (KT 2440). The bacterial toxicity of the ILs was determined by a 24 h bacterial growth inhibition assay and are expressed as IC₅₀ values. Stock solutions of the ILs were prepared in deionised water to a maximum concentration of 2 M. The concentration of each stock solution was determined by the maximum aqueous solubility of each IL up to 2 M (Table 2.4). ILs **17**, **19**, **22** and **24** had a solubility limit lower than the maximum stock solution concentration of 2 M. The maximum test concentration of the IL was a factor of 10 dilution of the IL stock solution (see chapter 6, section 6.5.1). This work was carried out in collaboration with Dr Brid Quilty from the School of Biotechnology in DCU.

Table 2.3 Antibacterial screening results for ILs **16–25** (IC₅₀).

IL	IC ₅₀ (mM)				
	<i>E. coli</i>	<i>B. subtilis</i>	<i>P. fluorescens</i>	<i>P. putida</i> (CP1)	<i>P. putida</i> (KT 2440)
16	50–100	50–100	50–100	50–100	100–200
17	25–50	25–50	25–50	25–50	50–100
18	25–50	50–100	25–50	25–50	50–100
19	25–50	50–100	50–100	50–100	> 100 ^a
20	6.25–12.5	12.5–25	12.5–25	6.25–12.5	12.5–25
21	12.5–25	25–50	25–50	12.5–25	25–50
22	12.5–25	12.5–25	12.5–25	12.5–25	25–50
23	12.5–25	25–50	25–50	12.5–25	25–50
24	6.25–12.5	12.5–25	12.5–25	12.5–25	25–50
25	6.25–12.5	12.5–25	6.25–12.5	12.5–25	12.5–25

^aSolubility limit; IC₅₀ value greater than solubility in media.

Table 2.4 Aqueous solubility of ILs **16–25** up to a maximum concentration of 2 M.

IL	Solubility (M)
16	2.00
17	0.89
18	2.00
19	1.00
20	2.00
21	2.00
22	0.89
23	2.00
24	1.00
25	2.00

The majority of the ILs had low toxicity towards the bacterial strains they were screened against, with the lowest toxicity observed for the pyridinium ethyl ester IL (**19**) against *P. putida* (KT 2440) (IC₅₀ > 100 mM) (Table 2.3). The highest levels of inhibition were observed for the 1-methylimidazolium butyl ester IL (**20**) which inhibited *E. coli* and *P.*

putida (CP1) with IC_{50} values of 6.25–12.5 mM, the butyl amide pyridinium IL (**25**) which inhibited *E. coli* and *P. fluorescens* with IC_{50} values of 6.25–12.5 mM, and the 1-methylimidazolium butyl amide (**24**) which inhibited *E. coli* with IC_{50} values of 6.25–12.5 mM. A general trend of increasing IL toxicity with increasing alkyl chain length was observed across all bacterial strains in the order methyl ester < ethyl ester < butyl ester/amide. In general, the methyl ester ILs **16** and **17** had lower toxicity (IC_{50} = 25–200 mM) than the ethyl ester ILs **18** and **19** (IC_{50} = 25–100 mM), which in turn had lower toxicity than the butyl ester/amide ILs **20–25** (IC_{50} = 6.25–50 mM). This observed trend is expected as the literature shows that ILs with longer alkyl chain lengths have increased levels of toxicity.⁶⁵ The ILs with longer alkyl chains have a higher lipophilicity, which increases their ability to permeate through the cell membrane and disrupt it, leading ultimately to cell death.⁶⁶ There was no observed trend for the level of bacterial inhibition between 1-methylimidazolium ILs and pyridinium ILs across the various alkyl chain lengths. When comparing the IC_{50} values of the butyl ester ILs with pyridinium (**21**), 3-methoxypyridinium (**22**) and 3-(ethoxycarbonyl)pyridinium (**23**) headgroups, a difference in inhibition was only observed for IL **22** which showed the same increase in inhibition towards *B. subtilis* and *P. fluorescens* (IC_{50} = 12.5–25 mM). When comparing the inhibition of the Gram-positive bacteria *E. coli* with the Gram-negative bacteria *B. subtilis*, seven ILs (**18–21** and **23–25**) inhibited *E. coli* to a greater extent than *B. subtilis*. The remaining ILs (**9**, **10** and **15**) inhibited both *E. coli* and *B. subtilis* to the same extent.

It is necessary to compare the IC_{50} values of the 1-methylimidazolium and pyridinium methyl and butyl ester ILs (**16**, **17**, **20** and **21**) (Table 2.3) to the previously published mandelic acid derived ILs with the same ester alkyl chain length and headgroup (**8–11**) (Figure 2.19 and Table 2.5).¹⁸ IL **8** has been included here for comparison purposes despite containing a chloride anion, as the halide anions bromide and chloride have previously been reported to have similar toxic effects in imidazolium IL.⁶⁷ In all cases the previous class of ILs (**8–11**) had lower levels of inhibition for every bacterial strain that was screened against. Despite the maximum inhibition for the previous class of ILs being lower than the new class (maximum IC_{50} = 25–50 mM for IL **11** across all bacterial strains), the new class of ILs do not represent a large increase in the level of inhibition (maximum IC_{50} = 6.25–12.5 mM for IL **20**, **24** and **25** to several bacterial strains). A lower level of inhibition is expected for the previous ILs (**8–11**) due to the presence of the oxygen functionality on the aromatic ring. The increased oxygen content

decreases the lipophilicity of the ILs and increases their hydrophilicity, in turn decreasing the toxicity of the ILs towards the bacterial strains for reasons previously described (see chapter 1, section 1.4.1).⁶⁶

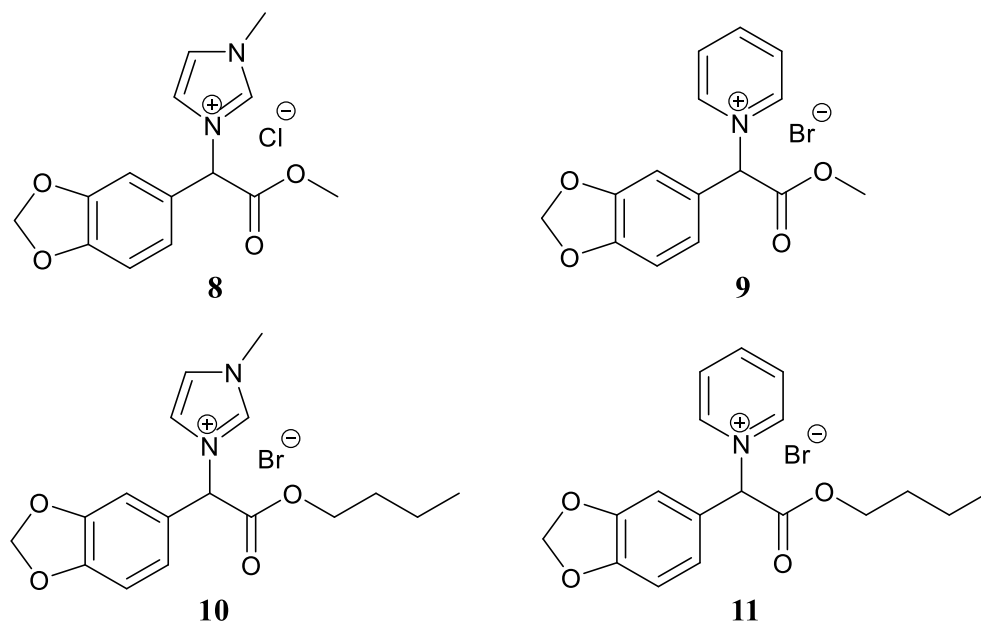


Figure 2.19 Previously published mandelic acid derived ILs (**8–11**).¹⁸

Table 2.5 Antibacterial screening results for ILs **8–11** (IC₅₀).¹⁸

IL	IC ₅₀ (mM)				
	<i>E. coli</i>	<i>B. subtilis</i>	<i>P. fluorescens</i>	<i>P. putida</i> (CP1)	<i>P. putida</i> (KT 2440)
8	50–100	50–100	100–200	100–200	100–200
9	100–200	50–100	100–200	100–200	100–200
10	50–100	50–100	100–200	100–200	100–200
11	25–50	25–50	25–50	25–50	25–50

2.3.2 Antibacterial Activity – Low Concentrations

The *in vitro* antibacterial activities of ILs **16–25** (Table 2.5) were evaluated against three ATCC strains: *Staphylococcus aureus* (**SA**; ATCC 6538), *Escherichia coli* (**EC**; ATCC 8739), *Pseudomonas aeruginosa* (**PA**; ATCC 9027) and five clinical isolates: *Staphylococcus aureus* MRSA (**MRSA**; HK5996/08), *Staphylococcus epidermidis* (**SE**; HK6966/08), *Enterococcus sp.* (**EF**; HK14365/08), *Klebsiella pneumoniae* (**KP**; HK11750/08) and *Klebsiella pneumoniae* ESBL (**KP-E**; HK14368/08). The ATCC strains were also used as the quality control strains. MIC values were calculated after 24

and 48 h. The MICs were defined as 95 % inhibition (IC₉₅) of the control growth. The maximum test concentration of the IL was dependent on the IL aqueous solubility, with the highest IL concentration in the test being 2000 µM. All the isolates were maintained on Mueller-Hinton dextrose agar prior to being tested. This work was carried out in collaboration with Dr Marcel Špulák from the Department of Organic and Inorganic Chemistry in the Faculty of Pharmacy at Charles University in Hradec Králové, Czech Republic.

Table 2.6 Antibacterial screening results for ILs **16–25** (MIC, IC₉₅).

Strain	Time (h)	IL MIC (µM)							
		16	17, 23	18	19, 22	20	21	24	25
SA	24h	2000	>2000	500	>1000	2000	500	>2000	2000
	48h	2000	>2000	500	>1000	>2000	2000	>2000	2000
MRSA	24h	>2000	>2000	500	>1000	>2000	2000	>2000	>2000
	48h	>2000	>2000	500	>1000	>2000	>2000	>2000	>2000
SE	24h	2000	2000	250	>1000	2000	500	>2000	2000
	48h	2000	2000	250	>1000	>2000	1000	>2000	2000
EF	24h	>2000	>2000	500	>1000	>2000	>2000	>2000	>2000
	48h	>2000	>2000	500	>1000	>2000	>2000	>2000	>2000
EC	24h	>2000	>2000	2000	>1000	>2000	>2000	>2000	>2000
	48h	>2000	>2000	2000	>1000	>2000	>2000	>2000	>2000
KP	24h	>2000	>2000	2000	>1000	>2000	>2000	>2000	>2000
	48h	>2000	>2000	2000	>1000	>2000	>2000	>2000	>2000
KP-E	24h	2000	>2000	1000	>1000	1000	>2000	>2000	>2000
	48h	2000	>2000	1000	>1000	>2000	>2000	>2000	>2000
PA	24h	>2000	>2000	>2000	>1000	>2000	>2000	>2000	>2000
	48h	>2000	>2000	>2000	>1000	>2000	>2000	>2000	>2000

The majority of the ILs did not have high toxicity towards the bacterial strains they were screened against. The pyridinium ethyl ester IL (**19**) and the 3-methoxypyridinium butyl ester (**22**) did not have high toxicity, up to the maximum IL concentration limit, with IC₉₅ values > 1000 µM. The 1-methylimidazolium butyl amide IL (**24**) also did not have high toxicity with IC₉₅ values > 2000 µM. The 1-methylimidazolium and pyridinium methyl ester ILs (**16** and **17**), the 3-methoxypyridinium butyl ester IL (**16**) and the pyridinium butyl amide IL (**25**) all inhibited *S. epidermidis* at a concentration of

2000 μM , with IL **25** additionally inhibiting *S. aureus* at 2000 μM and IL **16** additionally inhibiting *S. aureus* and *K. pneumoniae* ESBL at 2000 μM . The 1-methylimidazolium butyl ester IL (**20**) inhibited *S. aureus* and *S. epidermidis* at 2000 μM and *K. pneumoniae* ESBL at 1000 μM after 24 h, but after 48 h no longer inhibited *S. aureus*, *S. epidermidis* and *K. pneumoniae* ESBL up to the test concentration of 2000 μM , suggesting that the bacterial strains were able to overcome the initial observed inhibition after 24 h and recover. The pyridinium butyl ester IL (**21**) inhibited *S. aureus* MRSA at 2000 μM after 24 h, but after 48 h no longer inhibited *S. aureus* MRSA up to the test concentration of 2000 μM . IL **21** also inhibited *S. aureus* and *S. epidermidis* at 500 μM after 24 h, which reduced to inhibition at 2000 μM to *S. aureus* and 1000 μM to *S. epidermidis* after 48 h. The 1-methylimidazolium ethyl ester IL (**18**) showed the greatest level of inhibition to the bacterial strains across the board with the highest level of inhibition observed against *S. epidermidis* ($\text{IC}_{95} = 250 \mu\text{M}$) and against *S. aureus*, *S. aureus* MRSA and *Enterococcus* sp. ($\text{IC}_{95} = 500 \mu\text{M}$). ILs **18** and **21** generally showed greater inhibition towards the Gram-positive bacterial strains (*S. aureus*, *S. aureus* MRSA, *S. epidermidis* and *Enterococcus* sp.) than towards the Gram-negative bacterial strains (*E. coli*, *K. pneumoniae*, *K. pneumoniae* ESBL and *P. aeruginosa*). This observation was most pronounced for IL **18** where the greatest level of inhibition towards a Gram-negative bacterial strain was observed against *K. pneumoniae* ESBL ($\text{IC}_{95} = 500 \mu\text{M}$), and the greatest level of inhibition towards a Gram-positive bacterial strain was observed against *S. epidermidis* ($\text{IC}_{95} = 250 \mu\text{M}$). IL **18** did not present the same inhibition towards *E. coli* as observed in the previous high concentration bacterial toxicity screening (Table 2.4), and this is attributed to the use of two different strains of *E. coli*. The overall findings are that none of the ILs demonstrated high toxicity to the various bacterial strains screened against, with moderate toxicity observed for IL **18** against several of the bacterial strains.

It is again necessary to compare the IC_{95} values of the 1-methylimidazolium and pyridinium methyl and butyl ester ILs (**16**, **17**, **20** and **21**) (Table 2.6) to the previously published mandelic acid derived ILs with the same ester alkyl chain length and headgroup (**8–11**)¹⁸ (Figure 2.20, Appendix B1). In all cases the previous class of ILs (**8–11**) had lower levels of inhibition for every bacterial strain that was screened against, with no high toxicity observed up to the maximum IL concentration limit ($\text{IC}_{95} > 2000 \mu\text{M}$).^{19,68} Again a lower level of inhibition is expected for the previous ILs (**8–**

11) due to the presence of the oxygen functionality on the aromatic ring, which increases IL hydrophilicity and in turn decreases IL toxicity. Despite a higher toxicity observed for the new ILs (**16**, **17**, **20** and **21**) the results herein do not represent a large increase in the level of inhibition. The greatest increase in inhibition was observed for IL **14** which inhibited *S. aureus* and *S. epidermidis* at 500 μM after 24 h, which reduced to inhibition at 2000 μM to *S. aureus* and 1000 μM to *S. epidermidis* after 48 h.

2.3.3 Antifungal Activity

The *in vitro* antifungal activities of ILs **9–18** (Table 2.7) were evaluated against four ATCC strains: *Candida albicans* (**CA1**; ATCC 44859), *Candida albicans* (**CA2**; ATCC 90028), *Candida parapsilosis* (**CP**; ATCC 22019), *Candida krusei* (**CK1**; ATCC 6258) and eight clinical isolates of fungi: five yeasts; *Candida krusei* (**CK2**; E28), *Candida tropicalis* (**CT**; 156), *Candida glabrata* (**CG**; 20/I), *Candida lusitanae* (**CL**; 2446/I), *Trichosporon asahii* (**TA**; 1188) and three filamentous fungi; *Aspergillus fumigatus* (**AF**; 231), *Absidia corymbifera* (**AC**; 272), *Trichophyton mentagrophytes* (**TM**; 445). The CA1, CP and CK1 ATCC strains were also used as the quality control strains. All the isolates were maintained on Sabouraud dextrose agar prior to being tested. MICs were determined using a modified CLSI standard of the microdilution format of the M27-A3 and M38-A2 documents, for yeasts and filamentous fungi respectively.^{69,70} MIC values were calculated after 72 and 120 h for TM, and for all other strains MIC values were calculated after 24 and 48 h. The MICs were defined as 50 % inhibition (IC_{50}) of the control growth for yeasts or 80 % inhibition (IC_{80}) of the control growth for filamentous fungi. The maximum test concentration of the IL was dependent on the IL aqueous solubility, with the highest IL concentration in the test being 2000 μM . This work was carried out in collaboration with Dr Marcel Špulák from the Department of Organic and Inorganic Chemistry in the Faculty of Pharmacy at Charles University in Hradec Králové, Czech Republic.

Table 2.7 Antifungal screening results for ILs **16–25** (MIC, IC₈₀ or IC₅₀).

Strain	Time (h)	IL MIC (μM) ^a			
		16, 23 24, 25	17, 19, 22	18	20, 21
CA1	24h	>2000	>1000	>2000	>2000
	48h	>2000	>1000	>2000	>2000
CA2	24h	>2000	>1000	>2000	>2000
	48h	>2000	>1000	>2000	>2000
CP	24h	>2000	>1000	>2000	>2000
	48h	>2000	>1000	>2000	>2000
CK1	24h	>2000	>1000	500	>2000
	48h	>2000	>1000	500	>2000
CK2	24h	>2000	>1000	1000	>2000
	48h	>2000	>1000	1000	>2000
CT	24h	>2000	>1000	>2000	2000
	48h	>2000	>1000	>2000	>2000
CG	24h	>2000	>1000	>2000	>2000
	48h	>2000	>1000	>2000	>2000
CL	24h	>2000	>1000	>2000	>2000
	48h	>2000	>1000	>2000	>2000
TA	24h	>2000	>1000	>2000	>2000
	48h	>2000	>1000	>2000	>2000
AF	24h	>2000	>1000	>2000	>2000
	48h	>2000	>1000	>2000	>2000
AC	24h	>2000	>1000	>2000	>2000
	48h	>2000	>1000	>2000	>2000
TM	72h	>2000	>1000	>2000	>2000
	120h	>2000	>1000	>2000	>2000

^aIC₅₀ values were assessed for AF, AC and TM and IC₈₀ for all other strains.

The 1-methylimidazolium methyl ester IL (**16**), the 3-(ethoxycarbonyl)pyridinium butyl ester IL (**23**) and the 1-methylimidazolium and pyridinium butyl amide ILs (**24** and **25**) did not have high toxicity up to the maximum IL concentration limit, with IC₅₀/IC₈₀ values > 2000 μM (Table 2.7). The pyridinium methyl and ethyl ester ILs (**17** and **19**) and the 3-methoxypyridinium butyl ester IL (**22**) did not have high toxicity up to the maximum IL concentration limit, with IC₅₀/IC₈₀ values > 1000 μM. The 1-

methylimidazolium ethyl ester IL (**18**) inhibited *C. krusei* (CK1) at 500 μM after both 24 and 48 h, and *C. krusei* (CK2) at 1000 μM after both 24 and 48 h. Higher levels of fungal toxicity are usually observed as the length of the alkyl chain increases,⁷¹ so it is unexpected that the ethyl ester IL (**18**) presents here with the highest level of fungal toxicity. The only other ILs which showed fungal activity were the 1-methylimidazolium and pyridinium butyl ester ILs (**20** and **21**) which inhibited *C. tropicalis* at 2000 μM after 24 h. After 48 h ILs **20** and **21** no longer inhibited *C. tropicalis* up to the test concentration of 2000 μM , suggesting that the fungal strain was able to overcome the initial observed inhibition at 2000 μM after 24 h and recover. The overall findings are that none of the ILs demonstrated high toxicity towards the range of fungal strains that were screened against.

It is again necessary to compare the IC_{80} or IC_{50} values of the 1-methylimidazolium and pyridinium methyl and butyl ester ILs (**16**, **17**, **20** and **21**) (Table 2.7) to the previously published mandelic acid derived ILs with the same ester alkyl chain length and headgroup (**8–11**)¹⁸ (Figure 2.20, Appendix B2). It was found that only IL **16** had the same low level of inhibition as the previous ILs (**8–11**), with no high toxicity up to the maximum IL concentration limit ($\text{IC}_{50}/\text{IC}_{80} > 2000 \mu\text{M}$).^{19,68} IL **17** had a lower maximum concentration limit (1000 μM) and thus cannot be directly compared to the previous class of ILs. Of the previous ILs only IL **11** showed inhibition below the maximum IL concentration limit, with IC_{80} values of 2000 μM against *C. albicans* (CA1) and 2000 μM against *C. tropicalis* and *C. lusitaniae* after 24 h, which reduced to no toxicity up to the maximum IL concentration limit after 48 h ($\text{IC}_{80} > 2000 \mu\text{M}$). ILs **20** and **21** (which have the same butyl chain and pyridinium headgroup as IL **11**) only showed inhibition against *C. tropicalis* at 2000 μM after 24 h and $> 2000 \mu\text{M}$, the maximum IL concentration limit, after 48 h. No high toxicity was observed for IL **20** and **21** against all other fungal strains, up to the maximum IL concentration limit, with $\text{IC}_{50}/\text{IC}_{80}$ values $> 2000 \mu\text{M}$. When comparing ILs **11** and **21** the data suggests that this is a unique case, where the oxidation of the aromatic ring actually results in a slight increase in toxicity, albeit it to only two fungal strains.

2.4 Biodegradation

The aerobic biodegradability of the ten mandelate ILs **16–25** (Table 2.8) was evaluated using the Closed Bottle Test (CBT) (OECD 301D).⁷² The validity of the test run was

confirmed by the biodegradation of the reference substance sodium acetate being > 60 % within 14 days, and the concentration of oxygen in the bottles not falling below 0.5 mg L⁻¹ at any time. This work was carried out in collaboration with Dr Klaus Kümmerer from the Institute of Sustainable and Environmental Chemistry at Leuphana University Lüneburg in Germany.

Table 2.8 Percentage biodegradation for ILs **16–25** in the CBT after 28 days.

IL	Biodegradation (%)
16	5
17	8
18	20
19	16
20	27
21	21
22	22
23	31
24	0
25	1

The results show that none of the ILs reached > 60 % biodegradation in 28 days and thus cannot be classified as readily biodegradable by the CBT (Table 2.8). The 3-(ethoxycarbonyl)pyridinium butyl ester IL (**23**) had the highest level of biodegradation (31 % in 28 days) and the 1-methylimidazolium butyl amide IL (**24**) did not biodegrade under the test conditions (0 % in 28 days). The percentage biodegradation reached by each IL in the test can be rationalised as biodegradation of the ester/amide groups of the ILs. It is well known that ester groups show high levels of biodegradability and are often introduced into compounds to increase their levels of biodegradability.²⁶ IL **23** contains the largest percentage of ester groups per molecule, with both an ethyl and butyl ester, thus it is not surprising that it shows the highest level of biodegradation in the CBT. The CBT results also show, as expected, that the level of biodegradation increased as the ester chain length increased. This trend is observed for the 1-methylimidazolium ester ILs **16**, **18** and **20** (5, 20 and 27 % biodegradation in 28 days for methyl, ethyl and butyl esters respectively) and the pyridinium ILs **17**, **19** and **20** (8, 16 and 21 % biodegradation in 28 days for methyl, ethyl and butyl esters

respectively). Amide moieties have been shown in the literature to have poor levels of biodegradation, thus the low levels of biodegradation observed for the 1-methylimidazolium butyl amide IL (**24**) and the pyridinium butyl amide IL (**25**) in the CBT (0 and 1 % biodegradation in 28 days respectively) are expected.²⁶ When comparing the CBT results of the butyl ester ILs (**20–23**), the percentage biodegradation increased in the order pyridinium < 3-methoxypyridinium < 1-methylimidazolium < 3-(ethoxycarbonyl)pyridinium (21, 22, 27 and 31 % biodegradation in 28 days for ILs **21**, **22**, **20** and **23** respectively).

A percentage of theoretical ester/amide biodegradation can be calculated for a compound by assuming that all the ester/amide carbons in the molecule are broken down during biodegradation. The calculated theoretical ester/amide biodegradation values can then be compared to the experimental biodegradation values. If the values are similar it is reasonable to conclude that biodegradation of the compound is occurring at the ester/amide. Significantly lower theoretical values than the experimental values would suggest that other parts of the molecule are also likely to be biodegrading. Theoretical values that are significantly higher than the experimental values would suggest the ester/amide bond is likely not biodegrading, or only partially biodegrading. The theoretical ester/amide biodegradation calculations for ILs **16–25** were performed and the values compared to the experimental results obtained in the CBT (Table 2.9).

Table 2.9 Calculation of theoretical ester/amide biodegradation for ILs **16–25** with a comparison to the experimental results obtained in the CBT after 28 days.

IL	Total carbon number	Ester/amide carbon number	Theoretical biodegradation (%)	Experimental biodegradation (%)	Prediction accuracy (%)
16	13	1	8	5	+3
17	14	1	7	8	−1
18	14	2	14	20	−6
19	15	2	13	16	−3
20	16	4	25	27	−2
21	17	4	24	21	+3
22	18	4	22	22	+1
23	20	6	30	31	−1
24	16	4	25	0	+25
25	17	4	24	1	+22

The comparison of the theoretical ester/amide biodegradation values to the experimental values for the ILs **16–25** show a moderate to good prediction for the ester ILs **16–23**, with the most accurate prediction made for the pyridinium methyl ester IL (**17**), the 3-methoxypyridinium butyl ester IL (**22**) and the 3-(ethoxycarbonyl)pyridinium butyl ester IL (**23**). This analysis allows us to conclude that the biodegradation of the ester ILs is occurring only at the ester bonds. The theoretical ester/amide biodegradation calculation predicts a lower level of biodegradation (−6 %) than is observed experimentally for the 1-methylimidazolium ethyl ester IL (**18**), perhaps suggesting that an additional part of the molecule is biodegrading. However, the literature has shown that 1-methylimidazolium based ILs are often very poorly biodegradable.⁷³ Thus when taking into account the confidence levels of the test, it can be postulated that the extra 6 % biodegradation observed in the CBT over the prediction may likely not be significant enough to suggest that additional parts of the molecule (i.e. the 1-methylimidazolium ring) are breaking down.

The calculated theoretical biodegradation values for the 1-methylimidazolium butyl amide IL (**24**) and the pyridinium butyl amide IL (**25**) are much higher than the biodegradation results obtained experimentally (+25 and +22 % for ILs **24** and **25** respectively). The calculation is made assuming that biodegradation of the amide is occurring; however, from the experimental values it is clear that none of IL **24**

biodegraded under the conditions of the CBT in the 28 day period. IL **25** gave a very low level of biodegradation (1 %), again most likely not be significant enough to suggest that the amide is biodegrading as the literature shows that amides have poor levels of biodegradation.²⁶ Thus, the calculation overestimates the level of biodegradation expected for the amide ILs and it can be concluded that the amides did not biodegrade under the CBT conditions over 28 days.

2.4.1 Proposed Biodegradation Metabolites

A number of biodegradation metabolites are produced when a compound biodegrades.⁷⁴ The proposed biodegradation metabolites of ILs **16–25**, formed by ester/amide breakdown, are the carboxylic acid derivatives of the parent ILs (**38–41**) (Figure 2.20, Table 2.10). Metabolites can be detected after biodegradation studies by carrying out HPLC-MS, MS/MS, and/or NMR analysis on the biodegradation products.^{75,76} An analysis of the toxicity of the metabolites is also always recommended, as they may be more toxic than the parent compounds.⁷⁷ To analyse metabolite toxicity, synthesis of the individual metabolites needs to be carried out. With the same metabolites presenting for multiple ILs only a few metabolites would need to be synthesised to obtain toxicity/biodegradation data on the metabolites for multiple parent compounds.

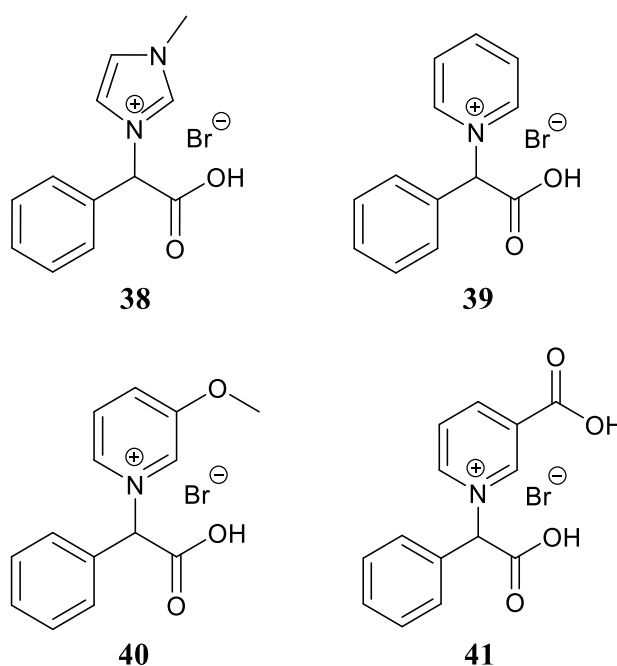


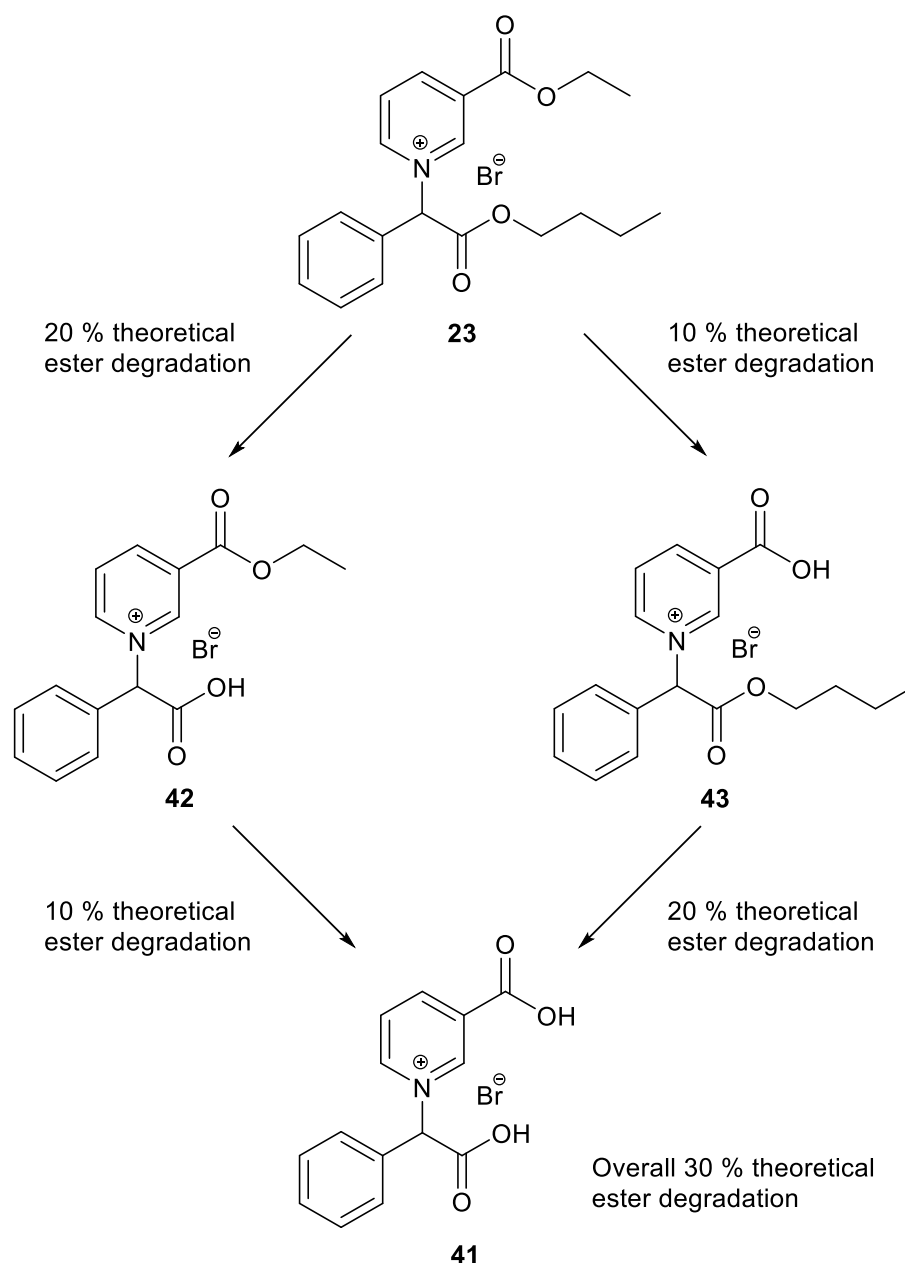
Figure 2.20 Proposed metabolites for ILs **16–25** (**38–41**).

Table 2.10 Proposed metabolites for ILs **16–25** (**38–41**).

Parent IL	Metabolite
16	38
17	39
18	38
19	39
20	38
21	39
22	40
23	41
24	— ^a
25	39

^aNo metabolite proposed; 0 % biodegradation in CBT.

The 3-(ethoxycarbonyl)pyridinium butyl ester IL (**23**) contains two ester groups which may have different rates of biodegradation in the CBT, leading to the production of two additional metabolites (**42** and **43**) (Scheme 2.9). A comparison of the theoretical ester/amide biodegradation of IL **23** to the experimental biodegradation (30 and 31 % respectively) shows that they are very similar. This suggests that the biodegradation of IL **23** did not stop at either of the mono ester metabolites (**42** and **43**) during the 28 day period of the CBT. Both biodegradation pathways may have the same rapid rate leading to the predominant metabolite **41** (Scheme 2.9) at the end of the CBT. If one of the mono ester biodegradation pathways was faster, it would most likely be the primary pathway. The rate of biodegradation would however still be slow when compared to the rate of biodegradation of the remaining ester group. Otherwise, the mono ester metabolite would predominate and an experimental biodegradation of 10–30 % would likely be observed in the CBT.



Scheme 2.9 Proposed biodegradation pathway for IL **23**.

2.5 Conclusion

A series of ten bromide ILs (**16–25**) derived from the renewable resource mandelic acid was synthesised with different structural moieties in a short and efficient synthesis in three stages: esterification/amidation of mandelic acid, halogenation of the α -position of the ester/amide and nucleophilic substitution reaction of the α -halo ester with an aromatic *N*-heterocycle. The ILs were produced in moderate to excellent yields (56–99 %) as solids with melting points in the range 48–169 °C. The different structural moieties in the ILs (various alkyl chain lengths, ester/amide moieties and various *N*-

heterocycle headgroups) allowed for the investigation of their effect on IL toxicity and biodegradation.

The results show that the majority of the ILs presented with low toxicity towards the Gram-positive bacterial strain, and the four Gram-negative bacterial strains they were screened against at high IL concentrations. IL toxicity across all bacterial strains increased as the alkyl chain length increased in the order methyl ester < ethyl ester < butyl ester/amide. None of the ILs demonstrated high toxicity to the the three CCM strains and the five clinical isolates they were screened against at low IL concentrations, with moderate toxicity observed for the 1-methylimidazolium ethyl ester (**18**) against several of the bacterial strains. Also, none of the ILs demonstrated high toxicity to the four ATCC strains and eight clinical isolates of yeasts they were screened against.

The biodegradation studies of the ILs in the CBT showed that the 3-(ethoxycarbonyl)pyridinium butyl ester IL (**23**) had the highest level of biodegradation (31 % in 28 days), with the 1-methylimidazolium butyl amide IL (**24**) showing no biodegradation under the test conditions (0 % in 28 days). The amide ILs **24** and **25** demonstrated zero to very poor levels of biodegradation in the CBT (0 and 1 % in 28 days respectively). Biodegradation of the butyl ester ILs increased in the headgroup order pyridinium < 3-methoxypyridinium < 1-methylimidazolium < 3-(ethoxycarbonyl)pyridinium. The biodegradation pathway proposed for the ILs is through ester alkyl chain biodegradation to a carboxylic acid derivative. This conclusion is based on previous results in the literature, and was reinforced by comparing the results of a predicted theoretical ester/amide biodegradation calculation to the results obtained in the CBT.

The dielectric properties of a selection of these ILs have also been evaluated (see chapter 4, section 4.2) to investigate their polarity for their potential use as solvents both with and without microwave heating.

2.6 Future Work

It is proposed that a study involving the detection of the biodegradation metabolites by LCMS/MS, and an evaluation of their toxicity, should follow on from this work.

Further synthesis and evaluation for aqueous stability, antimicrobial activity and biodegradability of the monofluoro mandelic acid IL (**37**), and future synthesised candidates, is anticipated.

It is also intended that these ILs will be used in relation to the overall theme of this work, which is targeted at the synthesis of low toxicity biodegradable ILs with applications in materials science.

2.7 References

1. C. A. Fewson, *FEMS Microbiol. Lett.*, 1988, **54**, 85.
2. D. J. D. Hockenhull, A. D. Walker, G. D. Wilkin and F. G. Winder, *Biochem. J.*, 1952, **50**, 605.
3. A. F. Landymore, N. J. Antia and G. H. N. Towers, *Phycologia*, 1978, **17**, 319.
4. J. W. Walker and V. K. Kriebel, *J. Chem. Soc., Trans.*, 1909, **95**, 1369.
5. E. Micklander, L. Brimer and S. B. Engelsens, *Appl. Spectrosc.*, 2002, **56**, 1139.
6. P. D. A. Singh, J. R. Jackson and S. P. James, *Biochem. Pharmacol.*, 1985, **34**, 2207.
7. M. J. R. Nout, G. Tuncel and L. Brimer, *Int J Food Microbiol*, 1995, **24**, 407.
8. K. Yamamoto, K. Oishi, I. Fujimatsu and K. Komatsu, *Appl. Environ. Microbiol.*, 1991, **57**, 3028.
9. Z. Sun, Y. Ning, L. Liu, Y. Liu, B. Sun, W. Jiang, C. Yang and S. Yang, *Microb. Cell Fact.*, 2011, **10**, 71.
10. E. N. Cook and H. A. Buchtel, *J. Am. Med. Assoc.*, 1936, **107**, 1799.
11. M. Poláková, Z. Krajčovicová, V. Melus, M. Stefkovicová and M. Sulcová, *Cent. Eur. J. Public Health*, 2012, **20**, 226.
12. K. Engström, H. Härkönen, P. Kalliokoski and J. Rantanen, *Scand. J. Work, Environ. Health*, 1976, **2**, 21.
13. S. I. T. Kennedy and C. A. Fewson, *J. Gen. Microbiol.*, 1968, **53**, 259.
14. S. G. Bhat and C. S. Vaidyanathan, *J. Bacteriol.*, 1976, **127**, 1108.
15. G. D. Hegeman, E. Y. Rosenberg and G. L. Kenyon, *Biochemistry*, 1970, **9**, 4029.
16. C. S. Harwood and R. E. Parales, *Annu. Rev. Microbiol.*, 1996, **50**, 553.
17. M. Jamaluddin, P. V. S. Rao and C. S. Vaidyanathan, *J. Bacteriol.*, 1970, **101**, 786.

18. S. P. M. Ventura, M. Gurbisz, M. Ghavre, F. M. M. Ferreira, F. Goncalves, I. Beadham, B. Quilty, J. A. P. Coutinho and N. Gathergood, *ACS Sustain. Chem. Eng.*, 2013, **1**, 393.
19. M. Ghavre, PhD Thesis, Dublin City University, 2012.
20. Z. Wang, in *Comprehensive Organic Name Reactions and Reagents*, John Wiley & Sons, Inc., New Jersey, 2010.
21. L. J. Gooßen, D. M. Ohlmann and P. P. Lange, *Synthesis*, 2009, **2009**, 160.
22. B. R. Kim, H.-G. Lee, S.-B. Kang, G. H. Sung, J.-J. Kim, J. K. Park, S.-G. Lee and Y.-J. Yoon, *Synthesis*, 2012, **44**, 42.
23. S.-Y. Han and Y.-A. Kim, *Tetrahedron*, 2004, **60**, 2447.
24. E. Valeur and M. Bradley, *Chem. Soc. Rev.*, 2009, **38**, 606.
25. G. C. Lloyd-Jones, P. D. Wall, J. L. Slaughter, A. J. Parker and D. P. Laffan, *Tetrahedron*, 2006, **62**, 11402.
26. S. Morrissey, B. Pegot, D. Coleman, M. T. Garcia, D. Ferguson, B. Quilty and N. Gathergood, *Green Chem.*, 2009, **11**, 475.
27. Z. Wang, in *Comprehensive Organic Name Reactions and Reagents*, John Wiley & Sons, Inc., New Jersey, 2010, ch. 426, pp. 1897-1900.
28. L. C. Bateman, M. G. Church, E. D. Hughes, C. K. Ingold and N. A. Taher, *J. Chem. Soc.*, 1940, 979.
29. C. Lim, S.-H. Kim, S.-D. Yoh, M. Fujio and Y. Tsuno, *Tetrahedron Lett.*, 1997, **38**, 3243.
30. S. D. Yoh, M. K. Lee, K. J. Son, D. Y. Cheong, I. S. Han and K. T. Shim, *Bull. Korean Chem. Soc.*, 1999, **20**, 466.
31. S.-D. Yoh, D.-Y. Cheong, C.-H. Lee, S.-H. Kim, J.-H. Park, M. Fujio and Y. Tsuno, *J. Phys. Org. Chem.*, 2001, **14**, 123.
32. H. S. Lee, D. Y. Cheong, S. D. Yoh, W. S. Kim, Y. W. Kwak, Y. T. Park and J. K. Lee, *Bull. Korean Chem. Soc.*, 2001, **22**, 633.
33. H. M. Yau, A. G. Howe, J. M. Hook, A. K. Croft and J. B. Harper, *Org. Biomol. Chem.*, 2009, **7**, 3572.
34. A. Kowalkowska and A. Jończyk, *Synth. Commun.*, 2011, **41**, 3308.
35. B. Riegel and H. Wittcoff, *J. Am. Chem. Soc.*, 1946, **68**, 1913.
36. C. Zhang, H. Ito, Y. Maeda, N. Shirai, S.-i. Ikeda and Y. Sato, *J. Org. Chem.*, 1999, **64**, 581.
37. Y. Su, L. Zhang and N. Jiao, *Org. Lett.*, 2011, **13**, 2168.

38. J. Clayden, N. Greeves and S. G. Warren, in *Organic Chemistry*, Oxford University Press, New York, 2000, ch. 11, pp. 243-277.
39. M. Balci, in *Basic ¹H- and ¹³C-NMR Spectroscopy*, Elsevier Science, Amsterdam, 2005, pp. 379-406.
40. J. J. Tindale and P. J. Ragoona, *Chem. Commun. (Cambridge, U. K.)*, 2009, 1831.
41. R. P. Swatloski, J. D. Holbrey and R. D. Rogers, *Green Chem.*, 2003, **5**, 361.
42. N. S. M. Vieira, P. M. Reis, K. Shimizu, O. A. Cortes, I. M. Marrucho, J. M. M. Araujo, J. M. S. S. Esperanca, J. N. C. Lopes, A. B. Pereiro and L. P. N. Rebelo, *RSC Adv.*, 2015, **5**, 65337.
43. O. Hollóczki, M. Macchiagodena, H. Weber, M. Thomas, M. Brehm, A. Stark, O. Russina, A. Triolo and B. Kirchner, *ChemPhysChem*, 2015, n/a.
44. C. M. S. S. Neves, K. A. Kurnia, K. Shimizu, I. M. Marrucho, L. P. N. Rebelo, J. A. P. Coutinho, M. G. Freire and J. N. Canongia Lopes, *Phys. Chem. Chem. Phys.*, 2014, **16**, 21340.
45. A. B. Pereiro, J. M. M. Araújo, S. Martinho, F. Alves, S. Nunes, A. Matias, C. M. M. Duarte, L. P. N. Rebelo and I. M. Marrucho, *ACS Sustain. Chem. Eng.*, 2013, **1**, 427.
46. K.-Y. Kim, B. C. Kim, H. B. Lee and H. Shin, *J. Org. Chem.*, 2008, **73**, 8106.
47. W. R. Dolbier, in *Guide to Fluorine NMR for Organic Chemists*, John Wiley & Sons, Inc, New Jersey, 2009, ch. 3, pp. 35-95.
48. W. R. Dolbier, in *Guide to Fluorine NMR for Organic Chemists*, John Wiley & Sons, Inc, New Jersey, 2009, ch. 2, pp. 9-34.
49. B. Modarai and E. Khoshdel, *J. Org. Chem.*, 1977, **42**, 3527.
50. K. Shibata, T. Kiyoura and Y. Hayashi, *J. Res. Inst. Catal., Hokkaido Univ.*, 1971, **19**, 29.
51. J. P. Adams, C. M. Alder, I. Andrews, A. M. Bullion, M. Campbell-Crawford, M. G. Darcy, J. D. Hayler, R. K. Henderson, C. A. Oare, I. Pendrak, A. M. Redman, L. E. Shuster, H. F. Sneddon and M. D. Walker, *Green Chem.*, 2013, **15**, 1542.
52. T. Krause, S. Baader, B. Erb and L. J. Gooszen, *Nat. Commun.*, 2016, **7**.
53. E. K. Woodman, J. G. K. Chaffey, P. A. Hopes, D. R. J. Hose and J. P. Gilday, *Org. Process Res. Dev.*, 2009, **13**, 106.
54. J. R. Dunetz, J. Magano and G. A. Weisenburger, *Org. Process Res. Dev.*, 2016, **20**, 140.

55. J. P. Taygerly, L. M. Miller, A. Yee and E. A. Peterson, *Green Chem.*, 2012, **14**, 3020.
56. R. K. Henderson, C. Jiménez-González, D. J. C. Constable, S. R. Alston, G. G. A. Inglis, G. Fisher, J. Sherwood, S. P. Binks and A. D. Curzons, *Green Chem.*, 2011, **13**, 854.
57. C. M. Alder, J. D. Hayler, R. K. Henderson, A. M. Redman, L. Shukla, L. E. Shuster and H. F. Sneddon, *Green Chem.*, 2016, **18**, 3879.
58. V. Pace, P. Hoyos, L. Castoldi, P. Domínguez de María and A. R. Alcántara, *ChemSusChem*, 2012, **5**, 1369.
59. T. Welton, *Proc. R. Soc. London, A*, 2015, **471**.
60. A. L'Heureux, F. Beaulieu, C. Bennett, D. R. Bill, S. Clayton, F. LaFlamme, M. Mirmehrabi, S. Tadayon, D. Tovell and M. Couturier, *J. Org. Chem.*, 2010, **75**, 3401.
61. I. D. Rae, *J. Chem. Educ.*, 2009, **86**, 689.
62. D. Suarez, G. Laval, S.-M. Tu, D. Jiang, C. L. Robinson, R. Scott and B. T. Golding, *Synthesis*, 2009, **2009**, 1807.
63. C. K. Tan and Y.-Y. Yeung, *Chem. Commun. (Cambridge, U. K.)*, 2013, **49**, 7985.
64. P. G. Jessop, *Green Chem.*, 2016, **18**, 2577.
65. X. F. Wang, C. A. Ohlin, Q. H. Lu, Z. F. Fei, J. Hu and P. J. Dyson, *Green Chem.*, 2007, **9**, 1191.
66. M. C. Bubalo, K. Radosevic, I. R. Redovnikovic, J. Halambek and V. G. Srcek, *Ecotoxicol. Environ. Saf.*, 2014, **99**, 1.
67. C.-W. Cho, Y.-C. Jeon, T. P. T. Pham, K. Vijayaraghavan and Y.-S. Yun, *Ecotoxicol. Environ. Saf.*, 2008, **71**, 166.
68. M. Gurbisz, PhD Thesis, Dublin City University, 2012.
69. M27-A3; Reference Method for Broth Dilution Antifungal Susceptibility Testing of Yeasts; Approved Standard Institute - Third Edition, Clinical and Laboratory Standards Institute, Wayne, PA, 2008.
70. M38-A2; Reference Method for Broth Dilution Antifungal Susceptibility Testing of Filamentous Fungi; Approved Standard Institute - Second Edition, Clinical and Laboratory Standards Institute, Wayne, PA, 2008.
71. J. Pernak, K. Sobaszekiewicz and I. Mirska, *Green Chem.*, 2003, **5**, 52.
72. Organization for Economic Cooperation and Development (OECD), *OECD Guideline for Testing of Chemicals; Ready Biodegradability*, Paris, July 1992.

- 73. S. Stolte, S. Abdulkarim, J. Arning, A. K. Blomeyer-Nienstedt, U. Bottin-Weber, M. Matzke, J. Ranke, B. Jastorff and J. Thoming, *Green Chem.*, 2008, **10**, 214.
- 74. S. Stolte, S. Steudte, A. Igartua and P. Stepnowski, *Curr. Org. Chem.*, 2011, **15**, 1946.
- 75. K. M. Docherty, M. V. Joyce, K. J. Kulacki and C. F. Kulpa, *Green Chem.*, 2010, **12**, 701.
- 76. Y. Deng, I. Beadham, M. Ghavre, M. F. Costa Gomes, N. Gathergood, P. Husson, B. Legeret, B. Quilty, M. Sancelme and P. Besse-Hoggan, *Green Chem.*, 2015, **17**, 1479.
- 77. A. B. A. Boxall, C. J. Sinclair, K. Fenner, D. Kolpin and S. J. Maud, *Environ. Sci. Technol.*, 2004, **38**, 368a.

3.0 Plasticisation of Poly(L-lactic acid) with 1-Methylimidazolium Ester ILs

3.1 Introduction

Poly(lactic acid) (PLA) is an aliphatic polyester consisting of lactic acid (2-hydroxypropionic acid) subunits.¹ Lactic acid is chiral and exists as the two optical isomers D-lactic (**44**) acid and L-lactic acid (**45**) (Figure 3.1). Synthesis of PLA from pure D-lactic acid (**44**) or L-lactic acid (**45**) produces poly(D-lactic acid) (PDLA) and poly(L-lactic acid) (PLLA) respectively. Synthesis of PLA from a mixture of the two enantiomers will result in poly(D,L-lactic acid) (PDLLA), where a different amount of each enantiomer will result in PLA with different material properties. This allows for the targeted synthesis of PLA with specific mechanical properties for a particular application.

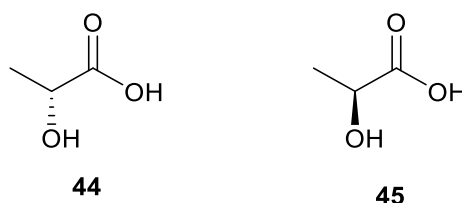


Figure 3.1 D-lactic acid (**44**) and L-lactic acid (**45**); the building blocks for poly(D-lactic acid) and poly(L-lactic acid) respectively.

The majority of lactic acid is produced by carbohydrate fermentation, but it can also be obtained by chemical synthesis.¹ High molecular weight PLA can be produced from lactic acid by azeotropic dehydrative condensation, direct condensation polymerisation and/or ring-opening polymerisation (ROP) of lactide.² Commercially available PLA consists of copolymers of PLLA and PDLLA, and is mainly produced using the ring-opening polymerisation of lactide monomers.³

PLA is a biodegradable (e.g. ASTM D5201 and D5209)⁴ and compostable (e.g. ISO 14855)^{5,6} biobased thermoplastic obtained from renewable biomass sources such as starch and sugar.² These properties have made PLA a very attractive alternative to petrochemical based polymers and also as a solution to the vast problem of excessive landfill when handled correctly. PLA is used heavily in the packaging industry for plastic bags and a variety of other food and drink containers.^{2,7} It is highly suitable for

this application due its low processing temperature, variable barrier properties, good printability and low toxicity.¹ PLA is also biocompatible and has found use in the medical industry for the construction of biomedical devices.⁸

3.1.1 Properties of PLA

PLA possesses the required mechanical and barrier properties desirable for a number of applications to compete with existing petrochemical thermoplastics. The structural, thermal, barrier and mechanical properties of PLA are considerably affected by its optical purity. In general, PLA can be amorphous or crystalline depending on the content of isomers. PLA with > 90 % L-isomer PLA tends to be crystalline, whilst a lower optical purity PLA will be amorphous.¹

The thermal behaviour of polymers is widely characterised using differential scanning calorimetry (DSC). A typical DSC plot of PLLA is illustrated in Figure 3.2. As can be seen, PLLA has a glass transition temperature (T_g) of ca 60 °C, a cold crystallisation temperature (T_c) of ca 100 °C and a melting temperature (T_m) of ca 175 °C. Moreover, the DSC trace shows a small pre-melt crystallisation peak at ca 160 °C, which is typical to many types of polyester.

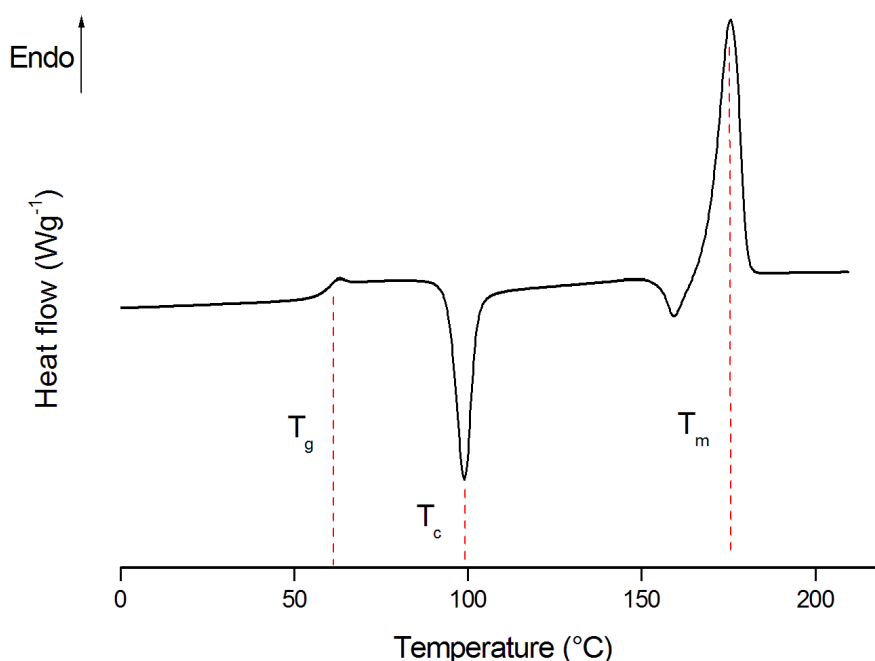


Figure 3.2 DSC trace of PLLA showing the glass transition temperature (T_g), the crystallisation temperature (T_c) and the melting temperature (T_m).

The T_g and T_m of PLA decrease with decreasing L-isomer content.¹ However, the T_g and T_m of PLA are high when compared with other thermoplastics such as polystyrene (PS), poly(ethylene terephthalate) (PET) and polypropylene (PP). The thermal history of the polymer is also known to affect the T_g of PLA.¹

PLLA is a slow crystallising polymer and its degree of crystallinity can be easily calculated from the DSC curve according to Equation 3.1.

$$\chi_c = \frac{\Delta H_m - \Delta H_c}{\Delta H_m^0} \times 100 \%$$

Equation 3.1 The degree of crystallinity (χ_c) of a polymer calculated from the DSC trace, where ΔH_m is the heat of fusion, ΔH_c is the enthalpy of cold-crystallisation and ΔH_m^0 is the enthalpy of fusion for a 100 % crystalline polymer. ΔH_m^0 is 93.1 J g⁻¹ for 100 % crystalline PLLA.¹

When optically pure PLA is quenched from the melt phase the resultant polymer will be quite amorphous, with the degree of crystallinity increasing as the cooling rate decreases.⁹

3.1.2 Mechanical Properties of Materials

The mechanical behaviour of materials can be evaluated by measuring the resulting deformations on specimens of the test material from an applied load. A static or dynamic tension test can be carried out, where the rate of loading applied to the specimen is either slow or fast respectively. Rapid loading in a dynamic tension test affects the properties of the materials; therefore, the rate of loading must also be measured. For both tests the results depend on the dimensions of the test specimen, which must also be measured.¹⁰

A material's mechanical properties can be defined by a variety of parameters, including:

- Tensile strength: the maximum stress that a material can withstand under loading in a tensile test before failure occurs, also known as ultimate strength.¹¹

- Elongation at break: a measure of how ductile a material is as determined by a tensile test.¹²
- Young's modulus: the rate of change of strain as a function of stress, also known as the modulus of elasticity in tension, and an indication of material stiffness.¹³

Stress and strain in a test specimen can be calculated from the tensile test with a sample of known diameter and length. Axial stress (σ) is then calculated by dividing the axial load (P) by the cross sectional area of the sample (A) (Equation 3.2).¹⁰

$$\sigma = \frac{P}{A}$$

Equation 3.2 Axial stress (σ) of test specimen, where P is the axial load and A is the cross sectional sample area.

Axial strain (ε) is calculated by dividing the measured elongation (δ) between the gauge marks by the gauge length (L), where the gauge length is the length of the test section (Equation 3.3).¹⁰ When a sample is in tension the strain is called the tensile strain, which is an elongation or stretching of the material.

$$\varepsilon = \frac{\delta}{L}$$

Equation 3.3 Axial strain (ε) of test specimen, where δ is the measured elongation and L is the gauge length.

Ductility of a material can be characterised by its elongation in area at the cross section where the fracture occurs. The percentage elongation at break is calculated by dividing the gauge length at fracture (L_f) minus the original gauge length (L_0), by the original gauge length (Equation 3.4).¹⁰

$$\text{Percentage elongation} = \frac{L_1 - L_0}{L_0} \times 100$$

Equation 3.4 Percentage elongation at break, where L_1 is the gauge length at fracture and L_0 the original gauge length.

Hooke's law is valid if the stress varies linearly with strain, and Young's modulus (E) can be calculated from the slope of the stress-strain curve or by dividing the stress (σ) by the strain (ϵ) (Equation 3.5).¹⁴

$$E = \frac{\sigma}{\epsilon}$$

Equation 3.5 Young's modulus (E) of test specimen, where σ is the axial stress and ϵ is the axial strain.

After performing the tensile test on a sample a stress-strain diagram is obtained which gives important information on the mechanical properties and the behaviour of the material. Polymers often have non-linear stress strain behaviour.¹⁴ A typical stress strain diagram for various polymers is given in Figure 3.3, where curve 1 represents a linear elastic and brittle material (e.g. PS), curve 2 represents a semi-ductile material (e.g. PMMA), curve 3 represents a ductile material (e.g. PET) and curve 4 represents a typical elastomer (e.g. polyurethane).¹⁵

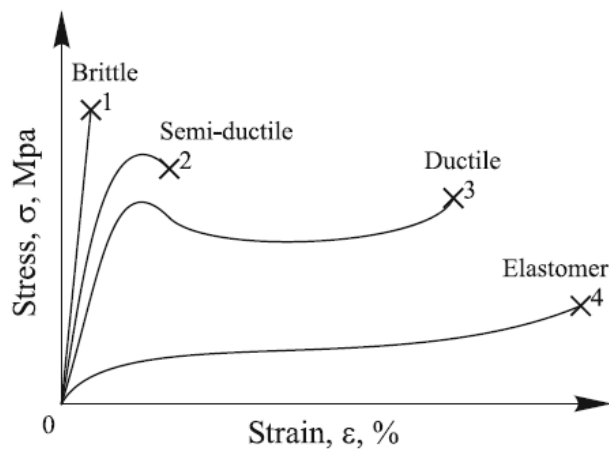


Figure 3.3 Typical stress-strain diagram for various polymer types.¹⁵

3.1.3 Modification of PLA

Mechanically, unoriented PLA is quite brittle with poor elongation at break, but possesses good strength and stiffness.¹ This is highlighted by comparing the mechanical properties of PLLA to PET, where PLLA is shown to have a tensile strength and Young's modulus comparable to PET, but a much lower elongation at break (Table 3.1). In order for PLA to be as versatile as possible, it is often necessary to modify the natural polymer through processing or the addition of specific additives. The additives are able to reduce the inherent brittleness of PLA by increasing the elongation at break. In this way, the crystallinity and processability of PLA can be modified, thus enabling it to be used in a much wider range of applications.

Table 3.1 Comparison of the mechanical properties of the thermoplastics PLLA and PET.¹⁶

Mechanical property	PLLA	PET
Tensile strength (MPa)	59	57
Elongation at break (%)	4–7	300
Young's modulus (GPa)	3.8	2.8–4.1

Methods based on melt processing are the main conversion method currently utilised for PLA. This involves heating the polymer above its melting point and shaping to the desired form, and subsequently cooling to stabilise its dimensions. Some of these methods are extrusion, injection moulding, injection stretch blow moulding, casting, film blowing, thermoforming, foaming, fibre spinning and compounding.¹ In order to optimise the conversion of PLA to moulded parts, films, foams and fibres, its unique material properties must be considered. It is also important to understand how these modifications affect the structural, thermal, physical, crystallisation and rheological properties of PLA.

Physical modification of PLA is often carried out through blending or plasticisation. PLA has been blended with various polymers such as thermoplastic starch,¹⁷ poly(ϵ -caprolactone)¹⁸ and PEG.¹⁹ In this way, the properties of the different polymers can be combined or new properties can arise due to the interaction of the materials. The addition of both biodegradable and non-biodegradable plasticisers to PLA is also employed to lower the T_g of the PLA and to increase its ductility and softness.²⁰

Plasticisation of PLA has been carried out by the addition of a variety of chemicals such as citrate esters,^{17,21,22,19} oligomeric lactic acid¹⁷ and glycerol.¹⁷ The limitations of currently evaluated PLLA plasticisers include leaching of the plasticiser during use, inadequate thermal stability, a greater plasticising effect required (increased ductility and material performance), problems with biocompatibility, high cost, high percentage loading required and the need for biobased plasticisers.²³

3.1.4 ILs as Plasticisers

ILs are effective plasticisers for polymeric materials because their chemical structures and molecular weights can easily be modified by structural changes to the IL cations and anions, directly affecting their ability to act as plasticisers. Currently the most heavily used plasticisers in industry are phthalates; however, they are now impacted by current REACH regulations²⁴ due to concerns over their toxicity, as they were found to migrate and leach from the polymer matrix.²⁵⁻²⁷ As a result, the use of phthalates has been banned or restricted in several applications.^{24,28} Thus, low toxicity and biodegradable ILs are an even more attractive alternative to current plasticisers.

Ammonium, imidazolium and phosphonium ILs have been used to plasticise poly(methyl methacrylate) (PMMA) and an increased flexibility and thermal stability of the material was demonstrated.²⁶ Further use of imidazolium ILs to plasticise PMMA showed a reduction in the T_g to near zero, and an improvement in the thermal stability of PMMA.²⁹ The use of ILs as plasticisers for biomedical grade polymers is deemed the most industrially relevant application, where the high cost of the IL is offset by the higher cost of the polymer. Phosphonium^{30,31} and pyridinium³¹ ILs have been successfully used to this effect with biomedical grade poly(vinyl chloride) (PVC). The antimicrobial activity of the ILs was also exploited to produce PVC films with antimicrobial and antibiofilm forming properties.³¹ Plasticisation of thermoplastic starch with [BMIM][Cl], as an alternative to glycerol, was able to increase the elongation at break by 300 %, coupled with a decrease in Young's modulus.³² DES were also shown to be effective plasticisers for starch.³³ The addition of ILs to polyether–polyamide block copolymer (Pebax®)³⁴ and poly(vinylidene fluoride) (PVDF)³⁵ has also been studied.

There are several reports on the plasticisation of PLA with ILs.³⁶⁻³⁹ Chen *et al.* showed that plasticising PLA with 1-methyl-3-pentylimidazolium hexafluorophosphate

([MPI][PF₆]) greatly improved PLA ductility, with elongation at break 25 times higher than neat PLA (62 % with 20 wt% IL).³⁶ The thermal stability of the material was also maintained. Park and Xanthos studied the degradation of PLA by phosphonium ILs with decanoate and [BF₄] anions and showed that the hydrolytic degradation of PLA was accelerated, with [BF₄] ILs additionally increasing the thermal stability of the PLA.³⁷ Gui. *et al.* investigated the use of 1-acetoxyethyl-3-methylimidazolium tetrafluoroborate ([AOEMIM][BF₄]) as a plasticiser for PLLA and showed compatibility, with a gradual decrease of the T_g with increasing IL content.³⁹ Plasticisation increased the impact strength and elongation at break (> 45 % and 200 % increase respectively at 4.8 wt% IL) of PLLA, with a slight decrease in tensile strength. However, the thermal stability of the plasticised PLLA was shown to decrease as the wt% of IL increased.

3.1.5 Physical Ageing of PLA

Rapid ageing of semi-crystalline PLLA has been observed to occur at ambient temperatures over the period of a few days.^{40,41} This is considered to be the cause of the brittleness of PLA, since ambient temperature is approximately 25 °C below the T_g.¹ Ageing is often been attributed to a reduction in free volume in the polymer,⁴² due to a rapid relaxation towards the equilibrium amorphous state.¹ The rate of physical ageing has been shown to increase with increasing temperature; however, above the T_g physical ageing has been evaluated to no longer be occurring.⁴⁰ The extent of ageing has also been determined to increase with decreasing PLA molecular weight, due to the increased number of chain terminals in the lower molecular weight PLA having greater motional freedom than the internal chain segments.⁴¹ Ageing below T_g is related entirely to the amorphous phase of the polymer, thus increasing the crystallinity of the polymer can reduce the ageing effect. The ageing of PLA is also affected by the temperature, pressure, cooling rate and cooling temperature when PLA is processed.¹

3.1.6 Selection of ILs for Plasticisation

To increase the ductility of PLLA and overcome the effect of physical ageing the plasticisation of PLLA with ILs was proposed. The aim of this study was to utilise 'green' ILs to overcome a number of the current PLLA plasticiser limitations by identifying plasticisers with increased thermal stability, a high plasticising effect and decreased leaching. This work was carried out as a proof of concept study where a number of prototype materials were synthesised. It is envisaged that this work will be

further progressed by utilising functionalised and task specific ILs as plasticisers, with the aim of creating plasticised materials targeted to specific applications.

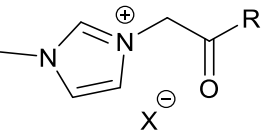
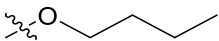
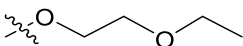
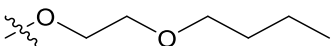
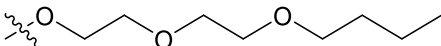
It was necessary that the chosen ILs fulfilled a number of specific criteria. These were:

1. Liquid at room temperature – preferable to assist polymer chain mobility.
2. Structural features present that promote low antimicrobial activity (e.g. ether) and increased biodegradability (e.g. ester) – desired to maintain biodegradability and material use in the medical and food packaging industries.
3. Ideally $> 300 \text{ g mol}^{-1}$ – a minimum molar volume is necessary to fill the free volume of the polymer.
4. Temperature resistant up to 200°C – to prevent material decomposition when melt processing with PLLA.
5. Low volatility – to prevent leaching from PLLA.
6. Containing polar functionalities in cation or/and anion to interact with the polar hydroxyl groups of PLLA (e.g. ester carbonyl group) – prevent material ageing and IL leaching.

A series of twelve target 1-methylimidazolium ester ILs (**46–57**) was selected for plasticisation with PLLA (Table 3.2). The ILs contained specific structural features that allowed for the investigation of their effect on the plasticisation of PLLA. These structural features included:

- Four alkyl chain lengths: butyl, 2-ethoxy ethyl, 2-butoxy ethyl, 2-(2-butoxyethoxy) ethyl
- Ester functional groups
- Three anions: bromide, bistriflimide, octyl sulfate

Table 3.2 1-Methylimidazolium ester ILs (**46–57**) with various alkyl/ether chain lengths and different anions.

			
R =	X =		
	Br	NTf ₂	OctSO ₄
	46	50	54
	47	51	55
	48	52	56
	49	53	57

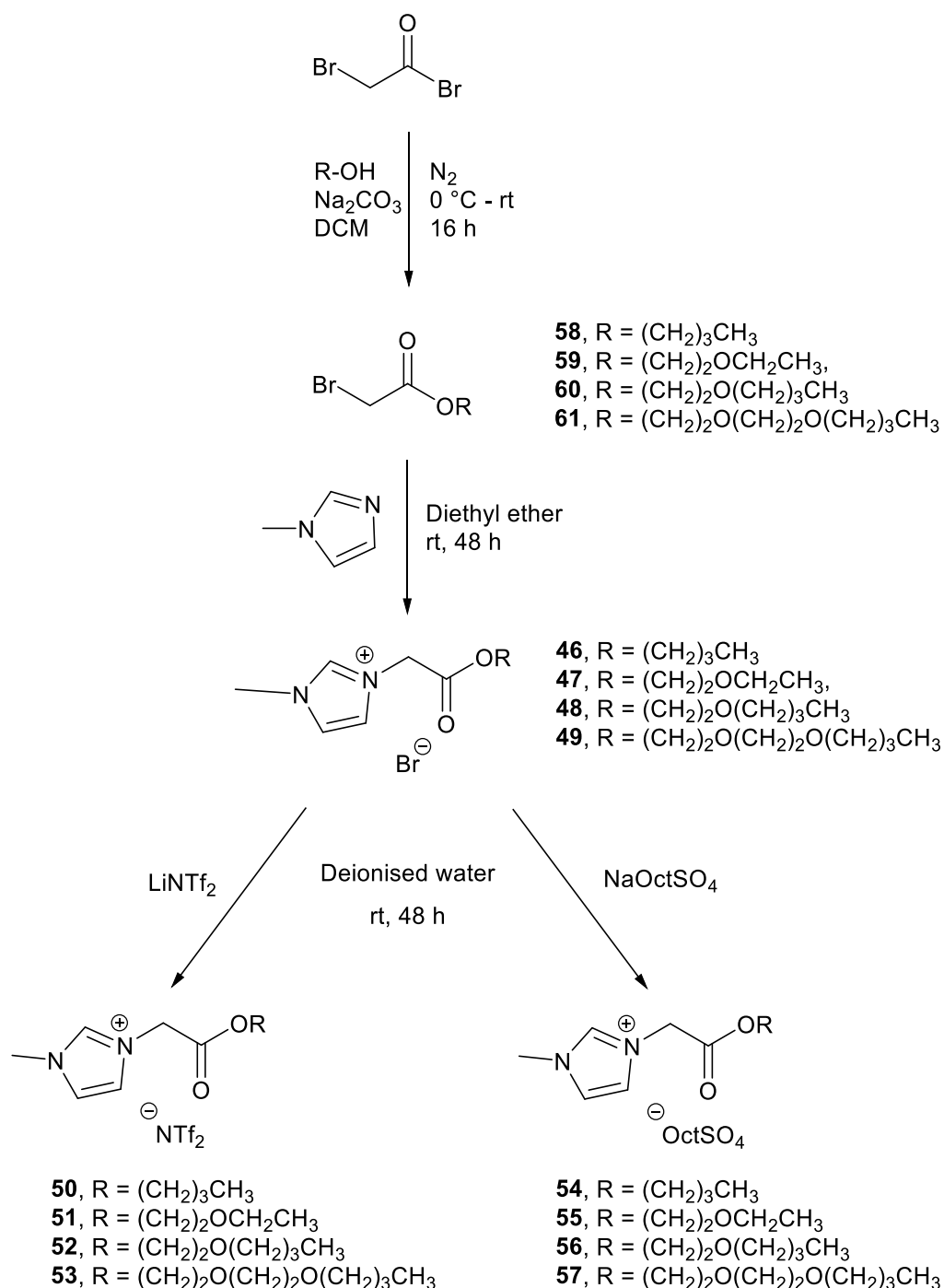
The antimicrobial activity of the 1-methylimidazolium ILs (**46–57**) has previously been reported, and low toxicity to a wide range of screened bacteria was demonstrated.⁴³ The biodegradability of the octyl sulfate ILs were evaluated by the CO₂ headspace test and showed that ILs **46–57** biodegraded 59–65 % during the 28 day test period, with ILs **56** and **57** classified as readily biodegradable with 61 and 65 % biodegradation respectively.⁴³

3.2 Synthesis of ILs for Plasticisation

The synthesis of the 1-methylimidazolium ester ILs consisted of three parts (Scheme 3.1):

1. Acylation of alcohol/glycol ether
2. Nucleophilic substitution reaction of the alkylating reagent with 1-methylimidazole
3. Anion metathesis with lithium bistriflimide or sodium octyl sulfate

Full procedural detail for the preparation of the 1-methylimidazolium ester ILs is provided in the experimental section of this work (chapter 6, section 6.3).



Scheme 3.1 General synthesis route to 1-methylimidazolium ester ILs (**46–57**).

3.2.1 Synthesis of Bromoester Alkylating Reagents

The four bromoester alkylating reagents (**58–60**) (Figure 3.4) were synthesised by acylation of the appropriate alcohol/glycol ether, according to a modified version of the procedure reported in the literature.⁴³ Bromoester alkylating reagent **61** (Figure 3.4) was available as a previously prepared sample, which was also synthesised according to a modified version of the literature procedure.⁴⁴

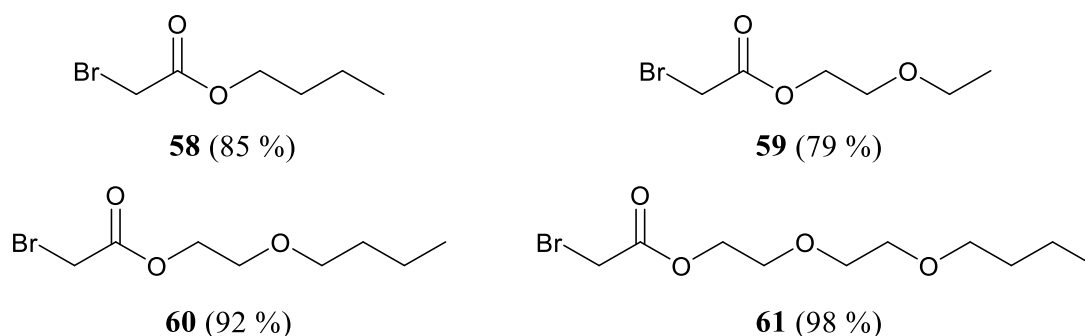


Figure 3.4 Percentage yields for bromoester alkylating reagents (**58–61**), synthesised from bromoacetyl bromide. Percentage yield for **61** reported from previous synthesis.⁴⁴

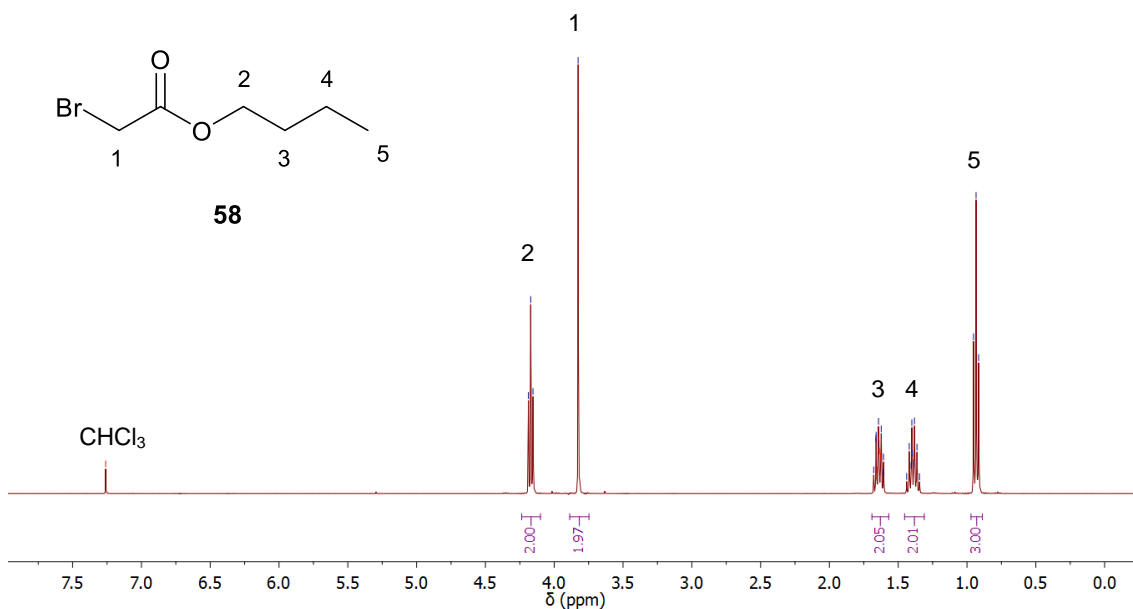
The literature procedure to synthesise **58–61** employed TEA as a homogeneous base, with purification of the product carried out by vacuum distillation.⁴³ However, the use of Na_2CO_3 as a heterogeneous base allowed simple filtration to be used to remove the base on reaction completion, and also negated the need for distillation to purify the product. Compound **61** was the only compound that required purification by column chromatography.⁴⁴ The addition of bromoacetyl bromide at $-78\text{ }^\circ\text{C}$ was also no longer necessary. In a typical reaction, bromoacetyl bromide (1.2 eq.) was added dropwise to the appropriate alcohol/glycol ether dissolved in DCM at $0\text{ }^\circ\text{C}$, with Na_2CO_3 (1.5 eq.). After 12–24 h TLC confirmed reaction completion and **58–61** were obtained as colourless to yellow liquids in good to excellent yields (79–98 %) (Figure 3.1). Products **58** and **61** were obtained as colourless liquids when using Na_2CO_3 , but had previously been obtained as coloured products, even after distillation, when TEA was used.⁴⁵ Percentage yields also increased from 60–75 % when TEA was used to 79–98 % when using Na_2CO_3 (Table 3.3). These reactions are nucleophilic substitution reactions which are proposed to occur mainly via an addition-elimination mechanism.⁴⁶

Table 3.3 Percentage yields for bromoester alkylating reagents (**58**–**61**).

Compound	Structure	Yield (%)	
		TEA ⁴³	Na ₂ CO ₃
58		68	85
59		60	79
60		75	92
61		72	98 ^a

^aPercentage yield for **61** reported from the literature.⁴⁴

The ¹H NMR of **58** in CDCl₃ shows a characteristic singlet at 3.83 ppm for the H1 protons (Figure 3.5). The CH₂ signal is shifted downfield due to the presence of the bromine and carbonyl group, which are both electron withdrawing. A deshielding of the neighbouring CH₂ protons occurs by negative induction (–I) through the sigma bonds, and through a negative mesomeric (–M) effect in the case of the ester group.

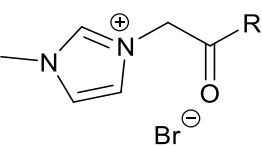
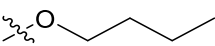
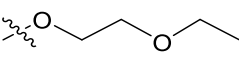
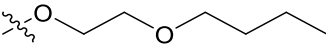
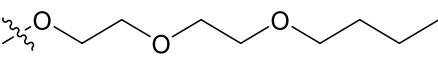
**Figure 3.5** ¹H NMR of alkylating reagent **58** in CDCl₃.

3.2.2 Synthesis of 1-Methylimidazolium Ester ILs

3.2.2.1 Synthesis of Bromide ILs

The four 1-methylimidazolium ester bromide ILs (**46–49**) (Table 3.4) were synthesised from the alkylating reagents **58–61** according to a modified version of the literature procedure.⁴³ The literature procedure states that the reactions were initiated at $-15\text{ }^{\circ}\text{C}$ and maintained for 3 h; however, this was deemed unnecessary for successful reaction completion. 1-Methylimidazole (1.02–1.1 eq.) was added dropwise to the bromoester alkylating reagent dissolved in diethyl ether. After 2 days of stirring under N_2 reaction completion was confirmed by TLC, with the desired IL precipitating during the course of the reaction. The ILs were purified by trituration with diethyl ether to give a viscous liquid (**46**), a brown solid (**47**) and a white solid (**48** and **49**) in excellent yields (96–99 %) (Table 3.4). The solid ILs had melting points significantly lower than $100\text{ }^{\circ}\text{C}$, in the range $36\text{--}70\text{ }^{\circ}\text{C}$ (Table 3.3). The melting points increase as the length of the alkyl chain and number of ether oxygens in the chain increases. This increase has been attributed to inter-chain hydrophobic packing affects and bilayer-type structure formation.⁴⁷

Table 3.4 Percentage yields and melting points for 1-methylimidazolium ester bromide ILs (**46–49**).

			
IL	R =	Yield (%)	mp ($^{\circ}\text{C}$)
46		99	n/a ^a
47		98	36–38
48		98	40–42
49		96	68–70

^aIL was liquid at rt.

The synthesis of ILs **46–49** is a nucleophilic substitution reaction, more specifically a Menshutkin reaction. Most often the reaction between 1-methylimidazole and an alkyl halide proceeds through a bimolecular S_N2 process.⁴⁸ However, the reaction mechanism can be influenced by the structure of the reactant and also the reaction conditions.⁴⁹

The ^1H NMR spectra of IL **46** in CDCl_3 shows a large downfield shift for the CH_2 singlet of the H5 protons, from 3.83 ppm for the corresponding peak in the alkylating reagent (**58**) (Figure 3.6), to 5.42 ppm (Figure 3.5). This downfield shift is due to a greater electron withdrawing effect from the imidazolium ring in IL **46**, by negative induction ($-I$), than from the bromine in compound **58**.

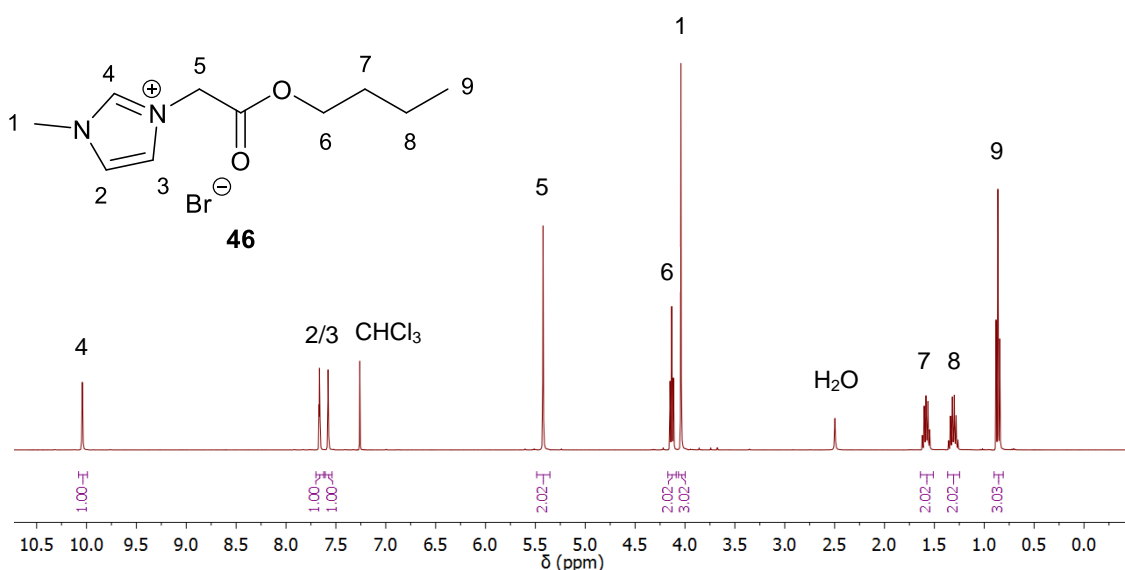


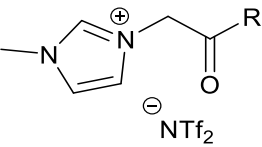

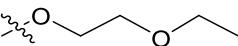
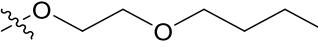
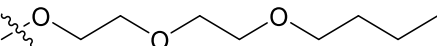
Figure 3.6 ^1H NMR of 1-methylimidazolium ester bromide IL **46** in CDCl_3 .

3.2.2.2 Synthesis of Bistriflimide ILs

The four 1-methylimidazolium ester bistriflimide (NTf_2) ILs (**50–53**) (Table 3.5) were synthesised from the corresponding bromide ILs **46–58**, according the literature procedure.⁴³ This reaction is an anion metathesis reaction, where the product is insoluble in the reaction solvent. In a typical reaction, LiNTf_2 (1.1 eq.) was added in one portion to the bromide IL dissolved in deionised water. The reaction was stirred for 2 days at rt, with the desired IL precipitating during the course of the reaction. The IL was purified by trituration with deionised water to give either a light yellow liquid (**50**) or a colourless liquid (**51–53**) in excellent yields (83–94 %) (Table 3.5). None of the ILs were solid at rt, as is often the case for NTf_2 ILs, as the anion is known to give RTILs with lower melting points and lower viscosities than the corresponding halide ILs.⁴⁷ The

low viscosity of the NTf₂ ILs can be attributed to the increase in asymmetry of the anion compared to the halide anions.⁴⁷ The low melting points of NTf₂ ILs are most often attributed to the ability of the NTf₂ anion to delocalise its negative charge, weakening its ability to hydrogen bond with the cation.^{47,50}

Table 3.5 Percentage yields and melting points for 1-methylimidazolium ester NTf₂ ILs (**50–53**).

		
IL	R =	Yield (%)
50		89
51		83
52		94
53		89

The ¹H NMR of IL **50** in CDCl₃ shows a characteristic upfield shift of the CH singlet for the H4 proton, from 10.04 ppm in the corresponding bromide IL (**46**) (Figure 3.6), to 8.74 ppm (Figure 3.7). This is caused by a slight shielding of the proton by the NTf₂ anion, due to it having a much more delocalised negative charge than the bromide anion.⁴⁴ In the ¹³C NMR spectra of **50** in CDCl₃, the presence of the NTf₂ anion is confirmed by the appearance of a quartet at 119.79 ppm with ¹J_{C-F} = 320.9 Hz (Figure 3.8).⁵¹ This quartet is formed by each of the CF₃ carbons (C11) coupling to the three neighbouring fluorine atoms through one bond coupling. The ¹⁹F NMR of IL **65** also gives a singlet at -79.22 ppm, which is a characteristic fluorine NMR chemical shift for CF₃ containing compounds.⁵¹

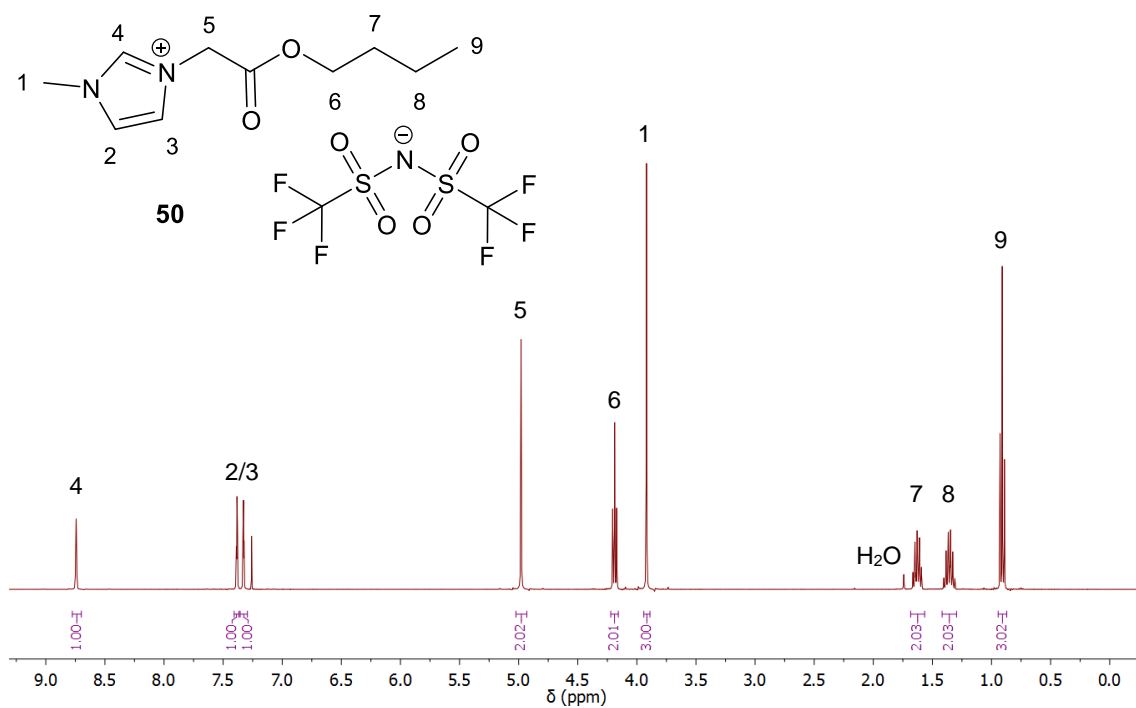


Figure 3.7 ^1H NMR of 1-methylimidazolium ester bistriflimide IL **50** in CDCl_3 .

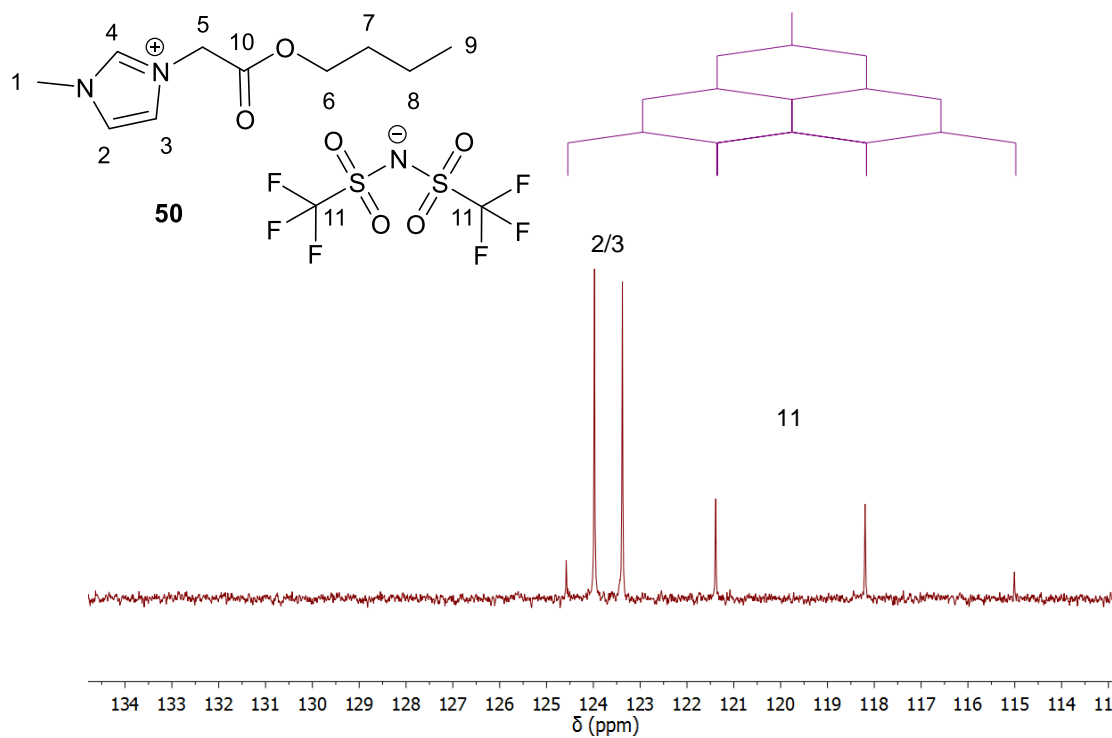
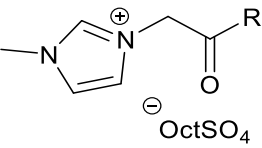
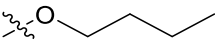
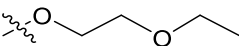
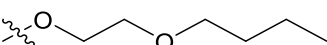
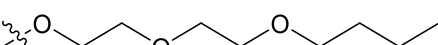


Figure 3.8 ^{13}C NMR of 1-methylimidazolium ester bistriflimide IL **50**, showing the quartet formed by C-F coupling of the CF_3 groups in the NTf_2 anion in CDCl_3 .

3.2.2.3 Synthesis of Octyl Sulfate ILs

The four 1-methylimidazolium ester octyl sulfate (OctSO₄) ILs (**54–57**) (Table 3.6) were synthesised from the corresponding bromide ILs **46–49**, according to a modified version of the literature procedure.⁴³ The literature states that the reaction was maintained at 60 °C for 2 h; however, heating was deemed unnecessary for reaction completion. This reaction is an anion metathesis reaction, where the product is insoluble in the reaction solvent. In a typical reaction, NaOctSO₄ (1.05 eq.) was added in one portion to the bromide IL dissolved in deionised water. The reaction was stirred overnight and after work-up the desired IL was isolated as either a colourless grease (**54**), a light yellow grease (**55**), a colourless liquid (**56**) or a light yellow gel (**57**) in good to excellent yields (75–99 %) (Table 3.6). The ILs were very hygroscopic and required extensive drying under high vacuum for 2 days at 50 °C.

Table 3.6 Percentage yields and melting points for 1-methylimidazolium ester OctSO₄ ILs (**54–57**).

		
IL	R =	Yield (%)
54		92
55		84
56		75
57		99

The ¹H NMR of IL **54** in CDCl₃ shows the acidic proton on the 1-methylimidazolium ring (H4) as a singlet at 9.37 ppm (Figure 3.9). This indicates that the octyl sulfate anion is shielding compared to the bromide anion, but not as shielding as the NTf₂ anion, with chemical shifts of 10.04 ppm and 8.74 ppm for the corresponding H4 proton in the bromide and NTf₂ ILs respectively.

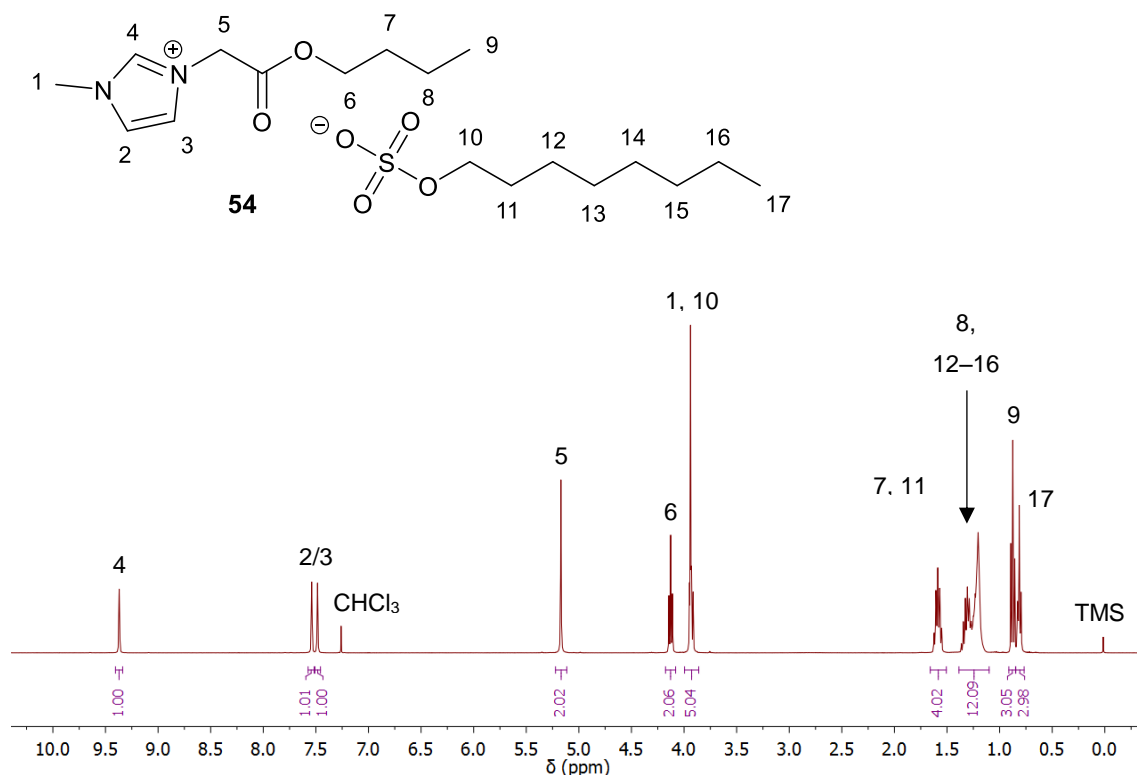


Figure 3.9 ^1H NMR of 1-methylimidazolium ester octyl sulfate IL **54** in CDCl_3 .

3.3 Thermogravimetric Analysis of ILs

The ILs needed to be stable in the melt extruder up to the temperature that the PLLA and IL were processed at during mixing. PLLA has a melting temperature of $176.3\text{ }^\circ\text{C}$ (identified by DSC); therefore, to reach the molten state of PLLA and facilitate homogeneous mixing with the IL, the temperature of the extruder was maintained at $200\text{ }^\circ\text{C}$. Thus, evaluation of each IL decomposition temperature was necessary. With this information, the ILs suitable for plasticisation with PLLA could be identified. The thermal decomposition data for each IL was used as an indication of the thermal stability of the IL when mixed with PLLA in the extruder, as the decomposition of the IL would likely be affected on mixing with PLLA.

The thermal stabilities of the 1-methylimidazolium ester ILs (**46–57**) were analysed by thermogravimetric analysis (TGA). The TGA curve for IL **53**, characteristic for ILs **46–57**, displays how the decomposition start temperature (T_{start}) and onset temperature (T_{onset}) of the ILs were detected (Figure 3.10). The TGA graphs for ILs **46–57** are provided in Appendix C.

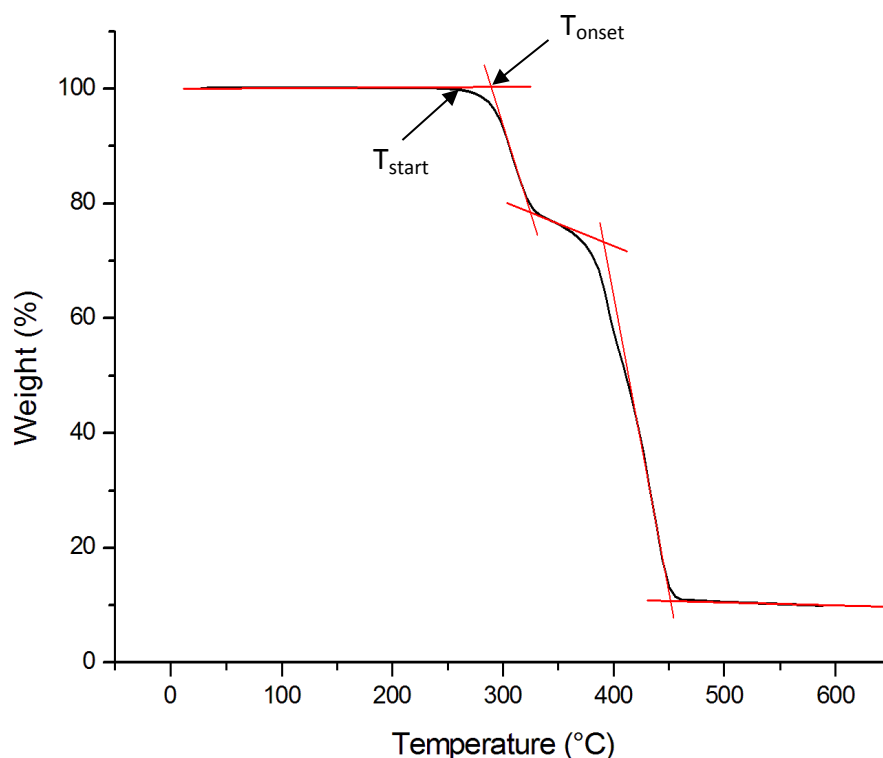


Figure 3.10 TGA curve for IL **53** showing how the start (T_{start}) and onset (T_{onset}) decomposition temperatures were detected.

The TGA curve for IL **53** (Figure 3.10) shows two prominent areas of decomposition. The first decomposition ($T_{\text{onset}} = 290\text{ }^{\circ}\text{C}$) is proposed breakdown of the ester moiety and the second decomposition ($T_{\text{onset}} = 390\text{ }^{\circ}\text{C}$) is proposed breakdown of the 1-methylimidazolium ring.^{39,52} The decomposition of the 1-methylimidazolium ring for all other 1-methylimidazolium ILs cannot be detected as clearly as seen in IL **53**. This is most likely due to decomposition of other areas of the IL (e.g. ether breakdown) masking the sharp transition that is expected for the 1-methylimidazolium breakdown. As the lowest temperature of IL decomposition will determine its use in the extruder at $200\text{ }^{\circ}\text{C}$, the T_{onset} and T_{start} decomposition temperatures for the first transition (most likely ester breakdown) were used to evaluate the thermal stability of the 1-methylimidazolium ILs (**46–57**) (Table 3.7).

Table 3.7 TGA data for ILs **46–57**, where T_{start} is the start temperature of decomposition and T_{onset} is the onset temperature of decomposition.

IL	Anion	T_{start} (°C)	T_{onset} (°C)
46	Br	161	207
47		157	213
48		162	208
49		155	207
50	NTf ₂	284	332
51		273	329
52		279	327
53		253	289
54	OctSO ₄	159	278
55		157	199
56		182	217
57		159	276

When comparing the T_{start} and T_{onset} of ILs **46–57** (Table 3.6) it is observed that the anion has a large impact on the decomposition temperatures of the ILs. IL thermal stability increased in the order Br < OctSO₄ < NTf₂. An average T_{onset} of 209, 242 and 319 °C was observed for the Br, OctSO₄ and NTf₂ ILs respectively. This was expected as the literature shows that NTf₂ ILs have higher decomposition temperatures than bromide ILs, with the reduced thermal stability of the halide ILs attributed to a high nucleophilicity and basic character.⁵³ The decomposition of the octyl sulfate IL [BMIM][OctSO₄] at 341 °C⁵⁴ is also between that of [BMIM][NTf₂] and [BMIM][Br], which have decomposition temperatures of 409 and 273 °C respectively.⁵³ The decomposition temperatures of ILs **46–57** are lower than would be expected for the equivalent alkyl ILs (no ester group), as the thermal stability of ILs has been shown to decrease with the addition of ester groups³⁹ and ether groups⁵⁵ (e.g. T_{onset} = 207 and 273 °C for IL **46** and [BMIM][Br] respectively).

The T_{onset} of the bromide ILs (**46–49**) at 201–213 °C (Table 3.6) was only a few degrees higher than the 200 °C temperature required to process PLLA and IL in the extruder. The T_{start} between 155–162 °C for ILs **46–49** was also much lower than the processing temperature. For this reason, the bromide ILs were deemed unsuitable for processing in

the extruder at 200 °C; therefore, the plasticisation of PLLA with ILs **46–49** was not carried out. However, not being able to use the bromide ILs **47–48** as plasticisers was acceptable as they were solid at rt, which is not an ideal quality for a plasticiser. ILs **46–49** were also key intermediates in the synthesis of ILs **50–53**, thus their thermal stability was assessed alongside ILs **50–53** to see if they could also be investigated as plasticisers.

The T_{onset} of the NTf₂ ILs (**50–53**) at 289–332 °C (Table 3.6) was much higher than the 200 °C temperature required to process PLLA and IL in the extruder. The T_{start} between 253–284 °C for ILs **50–53** was also much higher than the processing temperature. Thus, all the NTf₂ ILs had a suitable thermal stability for melt processing with PLLA.

The T_{onset} of the OctSO₄ ILs (**54–57**), at 199–278 °C (Table 3.6), was between the 200 °C temperature required to process the PLLA and IL in the extruder. The T_{start} of ILs **54–57**, 157–182 °C, was also lower than the processing temperature. However, the thermal stability of the IL would likely be affected by mixing with PLLA and also needed to be considered. The ILs (**54–57**) would also only be in the extruder at 200 °C for 7 minutes during the melt processing with PLLA. Consequently, it was decided to investigate ILs **54–57** as plasticisers for PLLA, taking into account the thermal decomposition temperatures of the ILs. The TGA curve of the OctSO₄ IL **57** (Appendix C, Figure C12) shows a large initial decomposition, with a T_{start} of 79 °C and a T_{onset} of 107 °C. As a result, the IL was not plasticised with PLLA due to its observed very low initial decomposition temperature. However, on subsequent analysis of the TGA curve it was deduced that this decomposition was highly likely to be due to the loss of water, despite the OctSO₄ ILs being extensively dried before TGA due to their hygroscopic nature. The initial IL decomposition, due to the ester breakdown, was subsequently calculated with a T_{start} and T_{onset} of 159 and 276 °C respectively, only 1 °C different to the OctSO₄ IL **54** (Table 3.6).

3.4 Plasticisation of PLLA with ILs

PLLA (> 99 % L-isomer) was used for this work as it was desired to work with semi-crystalline PLA for the plasticisation. It is also known that lactic acid from biological sources consists mostly of L-lactic acid, thus a greater amount of PLLA can be derived from renewable resources.¹ This work was carried out in collaboration with the Polymer Technology Group in the Department of Materials at ETH Zürich, Switzerland.

3.4.1 PLLA and PLLA/IL Film Formation

PLLA was plasticised with each IL (**50–56**) at 10, 20 and 30 wt% IL. Mixing was performed in a co-rotating twin-screw extruder (Figure 3.11) at 200 °C for 7 minutes. Films of approximately 0.5 mm in thickness were produced using a compression moulding technique. Firstly, the extrudate was compressed at 200 °C (above the PLLA melting point) in a hot press, followed by quenching to room temperature in a cold press. Neat PLLA films (i.e. without any IL) were produced for baseline measurements. Full procedural detail for the preparation of the PLLA/IL films is provided in the experimental section of this work (chapter 6, section 6.4).

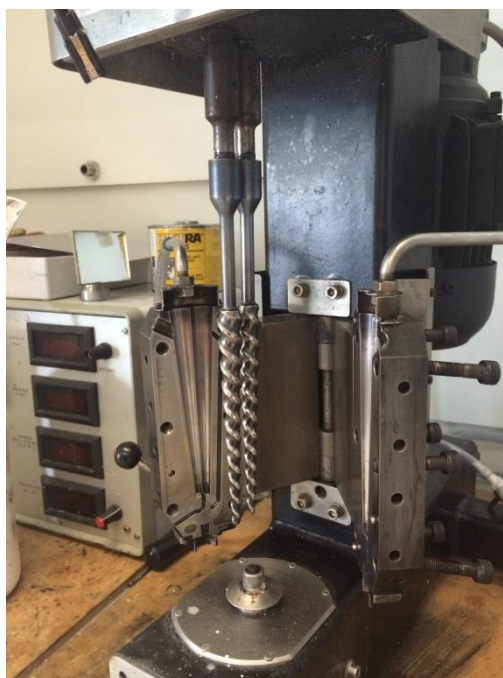
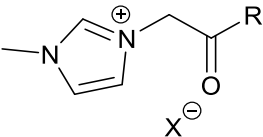
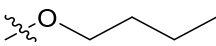
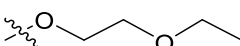
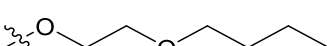
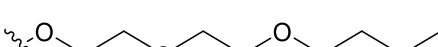
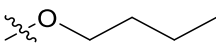
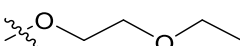
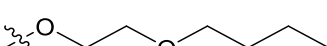


Figure 3.11 Laboratory scale co-rotating twin-screw extruder used for mixing of PLLA and ILs **50–56**.

A key to the structure of each IL (**50–56**) and the resultant PLLA/IL films (PLLA/IL**50–56**) formed after plasticisation is provided in Table 3.8.

Table 3.8 Key to the structures of the 1-methylimidazolium ester ILs (**50–56**) used for the synthesis of the corresponding PLLA/IL films (PLLA/IL**50–56**).

			
IL	R =	X =	Film
50		NTf ₂	PLLA/IL 50
51		NTf ₂	PLLA/IL 51
52		NTf ₂	PLLA/IL 52
53		NTf ₂	PLLA/IL 53
54		OctSO ₄	PLLA/IL 54
55		OctSO ₄	PLLA/IL 55
56		OctSO ₄	PLLA/IL 56

The visual characteristics of the resultant PLLA/IL films are displayed in Table 3.9. PLLA plasticised with the NTf₂ ILs (**50–53**) at 10, 20 and 30 wt% formed homogenous transparent to mostly transparent films (Table 3.9). Transparency of plasticised films is usually a good indication of compatibility and total miscibility of the plasticiser with the polymer.³⁰ Thus, the NTf₂ ILs appeared to be compatible with the PLLA. However, PLLA plasticised with the OctSO₄ ILs (**54–56**) formed hazy films at 10 wt% IL, with opaque films formed at 20 and 30 wt% IL, which also had a greasy texture. It was also difficult to obtain a film without bubbles for PLLA plasticised with the OctSO₄ ILs (**54–56**). All these visual signs are an indicator of possible incompatibility of the OctSO₄ ILs with PLLA. The greasy texture of PLLA/IL**55–56** with 20 and 30 wt% IL may be an

indication of leaching of the IL from the film. The PLLA/IL films containing 30 wt% NTf₂ or OctSO₄ IL were very flexible, which was in stark contrast to the PLLA/IL films containing 10 wt% NTf₂ ILs (**50–53**) or OctSO₄ ILs (**54–56**), which appeared to be very brittle. PLLA/IL films with 20 wt% IL appeared moderately flexible and not brittle.

Table 3.9 Visual appearance of PLLA/IL films with 10, 20 and 30 wt% IL.

Anion	IL	IL content (wt%)		
		10	20	30
NTf ₂	50	Transparent	Transparent	Transparent
	51	Transparent	Mostly Transparent	Mostly Transparent
	52	Transparent	Transparent	Transparent
	53	Transparent	Transparent	Transparent
OctSO ₄	54	Hazy film	Opaque	Opaque
	55	Hazy film	Opaque greasy film	Opaque greasy film
	56	Hazy film	Opaque greasy film	Hazy, greasy film

3.4.2 Mechanical Properties

The mechanical properties of neat PLLA and PLLA/IL films containing 10, 20 and 30 wt% of ILs **50–56** were analysed. The elongation at break, Young's modulus and tensile strength were obtained from the stress-strain curves of the measured films. A uniaxial tension test at constant rate of strain was carried out on the PLLA and PLLA/IL films, which had been cut into dumbbell-shaped specimens with a gauge length of 12 mm (Figure 3.12). For each sample a minimum of three specimens were tested, with the mean average of the values reported herein. Full procedural detail for the tensile testing of neat PLLA and PLLA/IL films is given in the experimental section of this work (chapter 6, section 6.1.9).

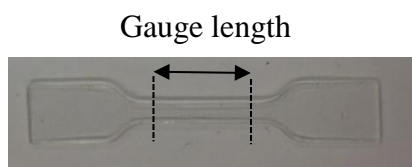


Figure 3.12 Dumbbell-shaped specimen used for tensile testing of the PLLA/IL films, with a gauge length of 12.7 mm.

The initial tensile testing of the PLLA and PLLA/IL**50–56** films was carried out on the same day as the melt extrusion and film formation were undertaken (day 0). The tensile testing results for the neat PLLA film, without any IL (0 wt% IL), on day 0 show that a relatively ductile material (> 300 % elongation at break), with a high Young's modulus (1514.30 MPa) and high tensile strength (55.62 MPa) were obtained (Table 3.10). However, the mechanical properties of PLLA films are greatly affected by physical ageing, which causes embrittlement of the films.⁴⁰ Ageing was confirmed by evaluation of the mechanical properties of the neat PLLA film four days after initial film formation (day 4), which showed a vast reduction in the elongation at break from 373.53 % on day 0 to 8.93 % on day 4 (Table 3.10). The Young's modulus and tensile strength of the neat PLLA increased slightly during the 4 day ageing period, indicating an increase in both the stiffness and strength.

Table 3.10 Effect of physical aging on the mechanical properties of neat PLLA films.

Day	Elongation at break (%)	Young's modulus (MPa)	Tensile strength (MPa)
0	373.53	1514.30	55.6
4	8.93	1630.57	62.8

The tensile testing results for the PLLA/IL**50–56** with 10 wt% IL showed a significant change in the elongation at break for the testing of subsequent samples (Table 3.11). All the initial samples tested (sample 1) had a high to moderate elongation at break (157–470 and 103–236 % for NTf₂ and OctSO₄ ILs respectively). However, the elongation at break drastically reduced in all subsequent samples for each PLLA/IL film, with only the PLLA/IL**53** film with 10 wt% IL giving an elongation at break higher than that of the 4 day aged PLLA (Table 3.10 and 3.11). The PLLA/IL**50–53** and PLLA/IL**54–56** with 10 wt% IL all had an elongation at break less than 7 %, which was less than for 4 day aged PLLA (8.93 %). The ILs **50–54** are initially acting as plasticisers with 10 wt% IL (Sample 1) as the elongation at break is higher than neat PLLA. However, overall ILs **50–54** can be said to be acting as antiplasticisers as they caused the PLLA to age and become brittle much faster than the neat PLLA film.³⁰

Table 3.11 Elongation at break for PLLA/IL**50–56** plasticised with 10 wt% NTf₂ and OctSO₄ ILs on day 0, for four consecutively tested samples.

Anion	IL	Elongation at break (%)			
		Sample 1	Sample 2	Sample 3	Sample 4
NTf ₂	50	470.31	6.89	6.38	6.63
	51	372.74	27.67	15.35	6.86
	52	156.82	5.78	6.62	6.00
	53	414.34	159.03	22.79	22.8
OctSO ₄	54	102.66	25.32	19.13	4.13
	55	236.13	28.75	18.19	7.83
	56	219.29	14.82	10.82	5.01

The comparison of the stress-strain curves for neat PLLA, aged for four days, and PLLA plasticised with 10 wt% IL **50**, last of four samples tested, is illustrated in Figure 3.13.

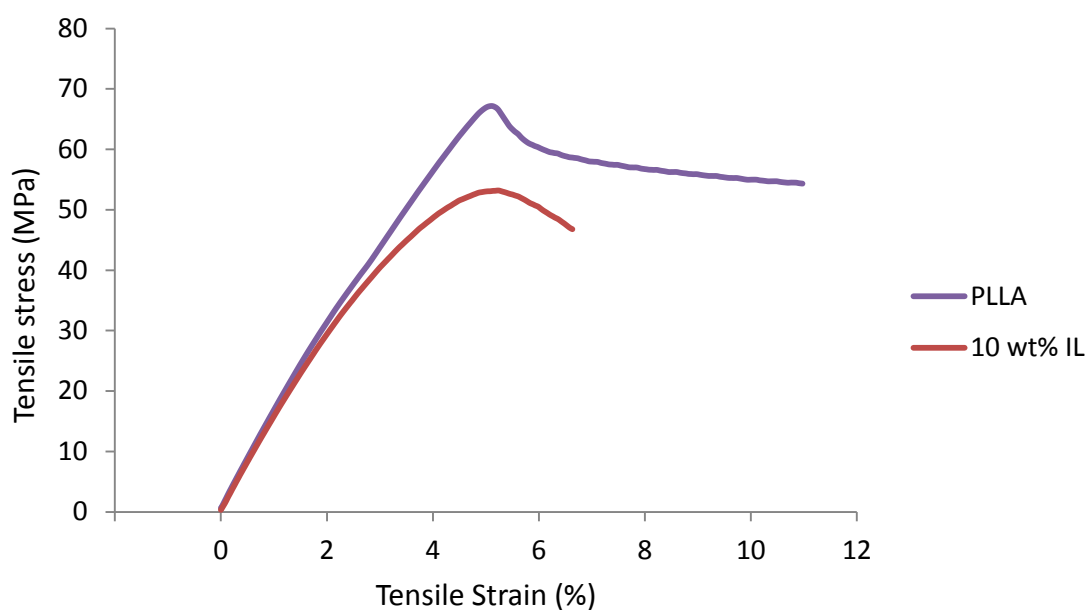


Figure 3.13 Stress-strain curves of neat PLLA (4 days aged) and PLLA/IL**50** with 10 wt% IL (last of four samples tested).

The tensile testing results for PLLA/IL**50–53** with 20 and 30 wt% NTf₂ ILs show a vast increase in the elongation at break, compared to neat PLLA, on addition of the ILs **50–53** (Table 3.12). The elongation at break also increased as the wt% of plasticiser in the

film is increased. The IL plasticiser increased the mobility of the PLLA chains, to a greater extent at higher wt% of IL, and the PLLA/IL films had much greater ductility as a result. The elongation at break was on average 56 times higher with 20 wt% IL **50–53**, and more than 80 times higher with 30 wt% IL **50–53**. The highest increase in the elongation at break was observed for PLLA/IL**50** with 30 wt% IL, with an elongation at break almost 90 times higher than neat PLLA. The greatest increase with 20 wt% IL was observed for PLLA/IL**53**, with an elongation at break 66 times higher than neat PLLA. These results show a much greater increase in the elongation at break than is observed in the literature for plasticising PLA with ILs, where 20 wt% [MPI][PF₆] gave a 25 times increase in the elongation at break.³⁶ As previously discussed (Table 3.11) the PLLA/IL**50–53** films with 10 wt% ILs showed poor elongation at break.

Table 3.12 Tensile testing results for neat PLLA, aged for 4 days, and PLLA/IL**50–53** with 10, 20 and 30 wt% NTf₂ IL.

Sample	IL content (wt%)	Elongation at break (%) ^a	Young's Modulus (MPa)	Tensile strength (MPa)
PLLA	0	8.93	1630.57	62.82
	10	6.63	1531.05	50.29
	20	510.82	1091.23	29.86
PLLA/IL 50	30	798.43	241.31	25.68
	10	6.86	1331.12	49.65
	20	502.39	1102.68	31.67
PLLA/IL 51	30	702.28	53.68	17.88
	10	6.00	1551.35	51.56
	20	403.07	860.97	22.74
PLLA/IL 52	30	714.77	252.44	25.65
	10	22.8	1510.32	47.80
	20	589.99	902.47	26.14
PLLA/IL 53	30	727.19	175.07	17.46

^aFor 10 wt% ILs the values are given for the last of 4 samples tested.

The Young's modulus of PLLA/IL**50–53** with 20 and 30 wt% NTf₂ IL decreased as the wt% of IL increased (Table 3.12). This result corresponds with the literature data for

PLLA plasticised with ILs.³⁶ The Young's modulus was on average 1481, 989 and 181 MPa for 10, 20 and 30 wt% IL respectively. The greatest decrease in the Young's modulus was observed for PLLA/IL**51** with 30 wt% IL, which decreased from 1630.57 MPa in neat PLLA to 53.68 MPa. This shows that the stiffness of the PLLA significantly reduced on plasticisation with the PLLA, which corresponds to the increased elongation at break observed for this material. For PLLA/IL**50** with 30 wt%, the material with the highest elongation at break, the Young's modulus was reduced from 1630.57 MPa in neat PLLA to 241.31 MPa. For PLLA/IL**53** with 20 wt%, the material with the highest elongation at break with 20 wt% IL, the Young's modulus was decreased from 1630.57 MPa to 902.47 MPa. The Young's modulus decreased in PLLA/IL**50–53** with 10 wt% IL despite the decrease in the elongation at break compared to neat PLLA.

The tensile strength of PLLA/IL**50–53** with 10, 20 and 30 wt% NTf₂ IL decreased as the wt% of IL increased (Table 3.12). This result corresponds with the literature data for PLLA plasticised with ILs.^{36,39} The tensile strength was on average 50, 28 and 22 MPa for 10, 20 and 30 wt% IL respectively. The greatest decrease in the tensile strength was observed for PLLA/IL**53** with 30 wt% IL, which decreased from 62.82 MPa in neat PLLA to 17.46 MPa. For PLLA/IL**50** with 30 wt%, the material with the highest elongation at break, the tensile strength was reduced from 62.82 MPa in neat PLLA to 25.68 MPa. For PLLA/IL**53** with 20 wt%, the material with the highest elongation at break with 20 wt% IL, the tensile strength was decreased from 62.82 MPa to 26.14 MPa.

These results show that the NTf₂ ILs **50–53** at 20 and 30 wt% were able to successfully plasticise PLLA and prevent embrittlement, with a large increase in the elongation compared to neat PLLA. Due to the decrease in the tensile strength with increasing wt% of IL, PLLA plasticisation with 20 wt% IL **50–53** gave the most promising results. The PLLA/IL**51** with 20 wt% IL gave a high elongation at break (502.39 %), with a moderate decrease in the Young's modulus and tensile strength of 1102.68 and 31.67 MPa respectively. In all cases the mechanical properties of PLLA plasticised with 20 wt% IL **50–53** were superior to the literature, which reported that the addition of 20 wt% [MPI][PF₆] to PLA gave an elongation of break of 61.6 % with a tensile strength of only 20.6 MPa.³⁶

The difference in the stress-strain curves of PLLA/IL**50** with 20 and 30 wt% IL is illustrated in Figure 3.14. Noticeably, PLLA/IL**50** with 20 wt% IL yields at higher stress and shows strain softening followed by strain hardening. On the other hand, PLLA/IL**50** with 30 wt% shows characteristic stress-strain behaviour of a rubber like material.

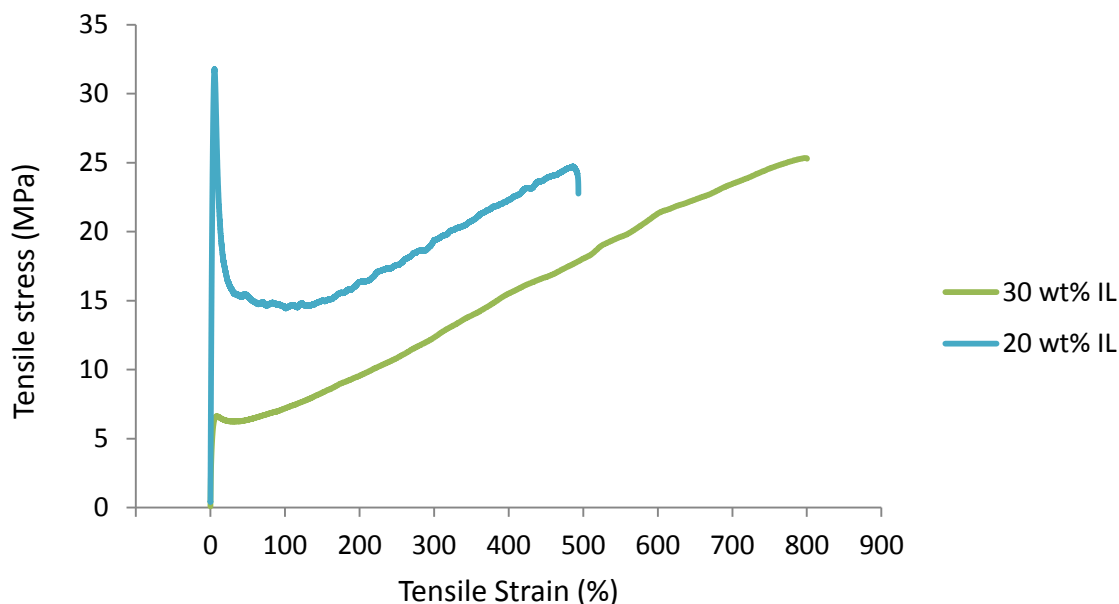


Figure 3.14 Stress-strain curves for PLLA/IL**50** with 20 and 30 wt% IL.

The tensile testing results for PLLA/IL**54–56** with 10, 20 and 30 wt% OctSO₄ ILs show that there was an increase in the elongation at break for PLLA/IL**54** and PLLA/IL**55** on increasing the wt% of the IL from 10 to 20 % (Table 3.13). The tensile properties of PLLA/IL**56** with 20 and 30 wt% IL could not be measured as the films were too brittle to allow an intact sample to be cut for testing. This result demonstrates the incompatibility of the OctSO₄ ILs **54–56** with the PLLA, as it has been previously shown that the introduction of an incompatible component into the PLLA matrix can cause a dramatic loss of the PLLA mechanical properties.¹⁷ For PLLA/IL**54** the elongation at break decreased from 18.41 % to 3.21 % with 30 wt% IL. For PLLA/IL**55** with 30 wt% IL the elongation at break increased to 76.34 %, the highest elongation measured for the OctSO₄ ILs (**54–56**). However, this elongation at break is only 8.5 times higher than the elongation at break measured for neat PLLA, with the corresponding NTf₂ IL (PLLA/IL**51** at 30 wt% IL) giving a much higher elongation of break at 702.28 % (Table 3.12). The tensile strength is also lower than was measured for the most promising result for PLLA plasticised with an NTf₂ IL (PLLA/IL**51** with

20 wt% IL). The Young's modulus and tensile strength decreased as the wt% of plasticiser increased for the PLLA/IL**54–55** films, with the exception of PLLA/IL**51** with 30 wt% IL where the Young's modulus increased between 20 and 30 wt% IL.

Table 3.13 Tensile testing results for 4 day aged PLLA and PLLA/IL**50–53** with 10, 20 and 30 wt% OctSO₄ IL.

Sample	IL content (wt%)	Elongation at break (%) ^a	Young's Modulus (MPa)	Tensile strength (MPa)
PLLA	0	8.93	1630.57	62.82
PLLA/IL 54	10	4.13	1349.59	40.78
	20	18.41	1243.42	33.22
	30	3.21	1283.37	29.96
PLLA/IL 55	10	7.83	1394.18	37.47
	20	10.40	1231.17	24.28
	30	76.34	1217.59	26.28
PLLA/IL 56 ^b	10	5.01	1485.91	46.42
	20	–	–	–
	30	–	–	–

^aFor 10 wt% ILs the values are given for the last of 4 samples tested.

^bSamples PLLA/IL**56** with 20 and 30 wt% IL were too brittle to be tested.

3.4.3 Physical Ageing Study

To understand how the properties of the PLLA/IL films change over time, a physical ageing study was carried out on PLLA/IL**50–53** with 20 and 30 wt% NTf₂ IL. These PLLA/IL films showed a successful plasticising effect on PLLA during testing on day 0. The PLLA/IL**50–53** with 20 and 30 wt% IL were stored in polyethylene sample bags at ambient conditions and mechanical properties were measured on day 1, 10 and 100. All the ageing study results for PLLA/IL**50–53** with 20 and 30 wt% IL are presented as graphs in Appendix D.

Ageing was observed in all PLLA/IL**50–53** films. Moreover, it occurred faster in films with a higher wt% of IL. In particular, the elongation at break of PLLA/IL**50–53** reduced faster and to a greater extent with 30 wt% IL than with 20 wt% IL (Table 3.14).

During the physical aging the ability of the PLLA/IL film to dissipate energy through molecular motion decreases,⁴⁰ and the films become increasingly brittle and the elongation at break is reduced as a result. The smallest reduction in the elongation at break is observed for PLLA/IL**51** with 20 wt% IL, where there was a loss of only 144 % in the elongation at break, to 358.74 %, after 100 days of aging (Table 3.14). None of the PLLA/IL**50–53** films showed an elongation at break lower than aged neat PLLA (8.93%), with PLLA/IL**51** with 30 wt% the closest at 33.92 % elongation at break after 100 days. In almost all cases the rate of ageing significantly decreased as the time from initial sample preparation (day 0) increased. This trend has also been observed in the literature.⁴⁰ PLLA/IL**51** with 20 wt% IL was an exception to this, where ageing did not seem to be occurring between day 1 and day 10.

Table 3.14 Effect of physical aging on the elongation at break of PLLA/IL**51–53** with 20 and 30 wt% NTf₂ IL.

Sample	IL content (wt%)	Elongation at break (%)			
		Day 0	Day 1	Day 10	Day 100
PLLA/IL 50	20	510.82	480.92	419.48	349.33
	30	798.43	679.70	622.46	152.08
PLLA/IL 51	20	502.39	437.11	506.23	358.74
	30	702.28	650.78	58.74	33.92
PLLA/IL 52	20	403.07	385.1	295.28	130.55
	30	714.77	677.55	462.57	120.92
PLLA/IL 53	20	589.99	523.28	467.61	228.01
	30	727.19	648.68	400.48	151.40

Physical ageing of PLLA has been attributed to a molecular rearrangement of the polymer chains that drive the thermodynamic variables (e.g. enthalpy) closer to equilibrium values.⁴¹ This is due to the polymer forming a non-equilibrium glassy state when it is quenched from the melt. Thus, it is unsurprising that PLLA/IL**52** at both 20 and 30 wt% IL have similar elongations at break after 100 days of ageing (131 and 121 % respectively) (Table 3.14). This could indicate that an equilibrium state is indeed being reached after 100 days of ageing, with PLLA having a certain free volume that can be occupied by the IL.

In general, the Young's modulus of PLLA/IL**50–53** with 20 wt% IL decreased as the films aged over the 100 day period of the test (Table 3.15). Exceptions were noted for PLLA/IL**51** with 20 wt% IL (day 0 to day 10) and PLLA/IL**52** with 20 wt% (day 10 to day 100), where an increase in the Young's modulus was observed. There was in general an increase in the Young's modulus from day 0 to day 100 for PLLA/IL**50–53** with 30 wt% IL, with exceptions noted for PLLA/IL**50** with 30 wt% IL (day 0 to day 10) and PLLA/IL**52** with 20 wt% (day 0 to day 10). The change in Young's modulus during ageing supports the idea that the films were ageing to an equilibrium state. At day 100 the Young's modulus for the PLLA/IL films with the same IL had similar values at 20 and 30 wt% IL, especially PLLA/IL**51** which had a Young's modulus of 457 and 478 MPa for 20 and 30 wt% IL respectively. This conclusion is highlighted when viewing the graphs of the ageing results for the tensile modulus of PLLA/IL**50–53** with 20 and 30 wt% IL, which are provided in Appendix D, Figures D5–D8.

Table 3.15 Effect of physical aging on the Young's modulus of PLLA/IL**51–53** with 20 and 30 wt% NTf₂ IL.

Sample	IL content (wt%)	Young's modulus (MPa)			
		Day 0	Day 1	Day 10	Day 100
PLLA/IL 50	20	1091.23	1071.72	1023.73	527.43
	30	241.31	225.33	255.88	390.13
PLLA/IL 51	20	1102.68	1184.27	860.14	456.80
	30	53.68	193.05	337.47	478.25
PLLA/IL 52	20	860.97	742.78	465.43	645.44
	30	252.44	242.59	293.64	444.36
PLLA/IL 53	20	902.47	832.12	755.24	598.64
	30	175.07	231.78	452.77	548.26

For the majority of the PLLA/IL**50–53** with 20 and 30 wt% IL the tensile strength initially increased during the ageing of the sample, and then decreased again to reach a lower tensile strength on day 100 than measured on day 1 (Table 3.16). PLLA/IL**52** with 20 wt% IL is an exception to this trend where the tensile strength initially decreased from day 0 to day 10, and subsequently increased from day 10 to day 100. In all cases it appears that the tensile strength of the PLLA/IL**50–53** films are ageing to an equilibrium state, with similar values in tensile strength observed for PLLA/IL**50–53**

with the same wt% of IL on day 100. The PLLA/IL**50–53** films had a tensile strength of ca 21 and ca 14 MPa for 20 and 30 wt% IL respectively on day 100. The smallest aging effects were observed for PLLA/IL**50–53** with 20 wt% IL, with a reduction of 1.26 MPa in tensile strength observed over the 100 days for PLLA/IL**52** with 20 wt% IL. PLLA/IL**51–53** with 20 wt% IL all had a higher tensile strength after 100 days of ageing than was measured in the literature for the least brittle sample of non-aged PLLA plasticised with 20 wt% [MPI][PF₆], which had a tensile strength of 20.6 MPa.

Table 3.16 Effect of physical aging on the tensile strength of PLLA/IL**51–53** with 20 and 30 wt% NTf₂ IL.

Sample	IL content (wt%)	Tensile strength (MPa)			
		Day 0	Day 1	Day 10	Day 100
PLLA/IL 50	20	29.86	31.83	34.34	20.58
	30	25.68	27.04	28.21	12.50
PLLA/IL 51	20	31.67	35.86	26.66	21.67
	30	17.88	25.38	21.18	14.95
PLLA/IL 52	20	22.74	21.07	16.82	21.48
	30	25.65	29.74	24.74	13.45
PLLA/IL 53	20	26.14	26.33	29.04	21.29
	30	17.46	28.43	23.76	16.32

3.4.4 Differential Scanning Calorimetry Analysis of PLLA/IL Films

Differential scanning calorimetry (DSC) was carried out on neat PLLA and the PLLA/IL**50–53** films with 10, 20 and 30 wt% IL, to estimate the efficiency of plasticisation by analysing the T_g, T_c, T_m and degree of crystallinity of the PLLA/IL films (Table 3.17). The DSC traces for neat PLLA and PLLA/IL**50–53** with 10, 20 and 30 wt% IL are provided in Appendix E.

Table 3.17 Effect of plasticisation with 10, 20 and 30 wt% NTf₂ IL **50–53** on the thermal properties and degree of crystallinity of PLLA.

Sample	IL content (wt%)	T _g (°C)	T _c (°C)	T _m (°C)	Crystallinity (%)
PLLA	0	60.2	94.0	176.3	21.1
PLLA/IL 50	10	47.8	84.7	173.5	24.3
	20	36.5	75.8	171.9	25.1
	30	14.5	63.8	168.9	27.0
PLLA/IL 51	10	44.5	81.7	174.0	25.2
	20	34.9	72.2	171.7	25.7
	30	—*	73.1	168.7	38.6
PLLA/IL 52	10	47.7	83.6	173.7	22.8
	20	35.9	73.0	171.2	25.7
	30	—*	73.5	168.6	35.67
PLLA/IL 53	10	43.6	80.9	170.2	24.4
	20	33.0	69.3	172.6	26.9
	30	—*	73.3	170.2	34.6

*Exact T_g value unable to be determined by DSC software.

The results show that for all the PLLA/IL**50–53** samples there is a significant depression of the T_g compared to that of neat PLLA, indicating that all the ILs have a substantial plasticising effect on PLLA (Table 3.17). T_g was shown to decrease with increasing plasticiser content (ca 15 and ca 25 °C depression of T_g for 10 and 20 wt% IL respectively). The greatest drop in the T_g (45 °C) is observed for PLLA/IL**50** where a T_g of 14.5 °C was measured. In the case of PLLA/IL**51–53** with 30 wt% IL, rather broad glass transitions were detected at a temperature range of 0–40°C. Unfortunately, the software could not extract a single T_g value from the DSC curves; however, they are believed to give a comparable T_g depression to PLLA/IL**50** with 30 wt% IL (below room temperature) as they all have similar DSC traces (Appendix E). Furthermore, no additional T_g was detected when analysing PLLA/IL**52** with 30 wt% IL with cryogenic DSC (–50 °C to 200 °C), confirming there was no phase separation between the PLA and the IL. The decrease in the T_g on the addition of ILs has been attributed to weakening of the interactions of PLLA chains, caused by the IL acting as a diluent of the PLLA chains and increasing chain mobility.³⁹

There is a significant increase in the crystallinity of the PLLA/IL**50–53** films as the percentage of plasticiser increases (Table 3.17). The greatest increase in the crystallinity, 38.6 %, is observed for PLLA/IL**51** with 30 wt% IL, which is about 18 % higher than the crystallinity of neat PLLA. The increase in the crystallinity is due to the plasticiser promoting the crystallinity of the material due to enhanced PLLA chain mobility.¹⁷

There is a significant decrease in the T_c of the PLLA/IL**50–53** as the wt% of plasticiser increases from neat PLLA to 10 and 20 wt% IL (Table 3.17). This is caused by the greater ease of PLLA crystallising at lower temperatures at higher plasticiser content, due to an increase in the chain mobility of the PLLA.¹⁷ The T_c appears to decrease linearly with increasing IL content, with a shift of ca 10 °C. The same ca 10 °C decrease in T_c is also observed for PLLA/IL**50** when the wt% of plasticiser increases from 20 wt% IL to 30 wt% IL. However, for PLLA/IL**51–53** there is a slight increase in the T_c of ca 2 % observed when the wt% of plasticiser increases from 20 wt% IL to 30 wt% IL.

There is a very slight decrease in the T_m as the plasticiser content increases, with only a deviation from this trend seen for PLLA/IL**53** with 30% IL (Table 3.17). This may indicate that the IL predominantly affects the amorphous phase without changing the crystal structure of the PLLA.

3.4.5 Thermal Stability of PLLA/IL Films

TGA of neat PLLA and PLLA/IL**52** with 30 wt% IL was carried out to assess the effect of the IL on the thermal stability of PLLA (Figure 3.15). (TGA curves are also provided in Appendix C for PLLA and PLLA/IL**52**, in Figure C13 and C14 respectively.)

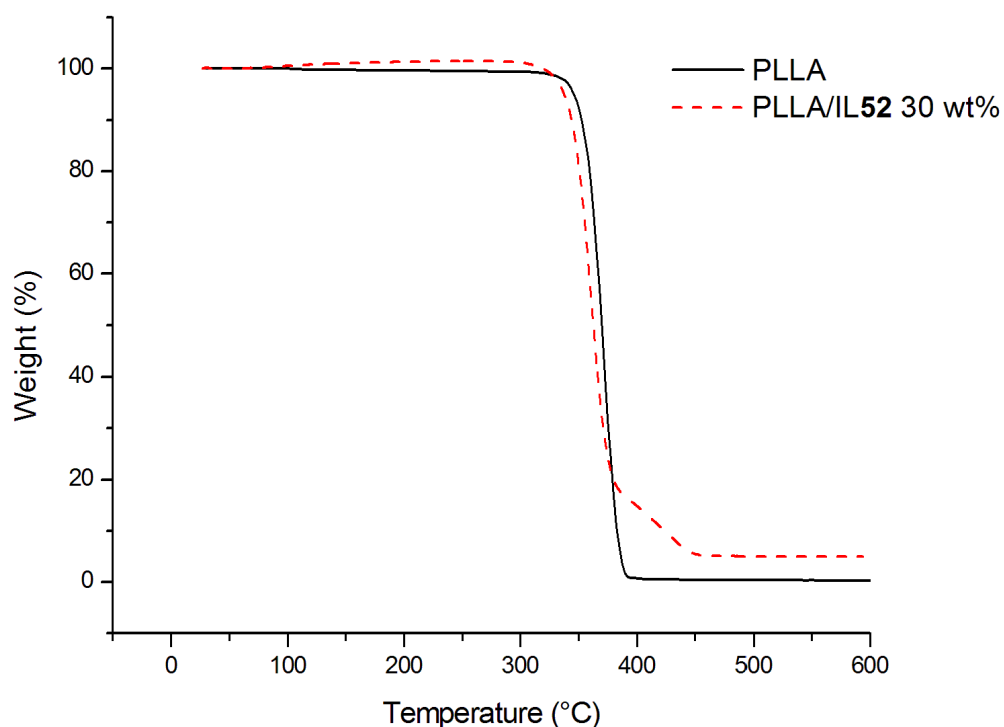


Figure 3.15 TGA curves of neat PLLA and PLLA/IL**52** with 30 wt% IL.

When comparing the T_{start} and T_{onset} of degradation for PLLA to PLLA/IL**52** with 30 wt% IL (Table 3.18), it can be seen that the addition of the IL has a minimal effect on the thermal stability of the PLLA. For the PLLA/IL**52** with 30 wt% IL the T_{start} decreased by 28 °C and the T_{onset} decreased by 12 °C, compared to neat PLLA. The decrease of T_{onset} by 12 °C is less than the decrease measured by Gui *et al.* (24 °C) for PLLA plasticised with 0.99 wt% [AOEMIM][BF₄].³⁹ Furthermore, PLLA plasticised with 8.3 wt% [AOEMIM][BF₄], the maximum IL content studied by Gui *et al.*, showed a decrease in T_{onset} of 52 °C compared to neat PLLA. Thus, PLLA/IL**53** shows a higher thermal stability at much higher levels of plasticisation (30 wt% IL); illustrating the minimal impact that plasticisation with 30 wt% IL **52** has on the thermal stability of PLLA.

Table 3.18 TGA data for PLLA and PLLA/IL**52** with 30 wt% IL.

Sample	IL content (wt%)	T_{start} (°C)	T_{onset} (°C)
PLLA	—	315	355
IL 52	—	279	327
PLLA/IL 52	30	287	343

3.5 Conclusions

In this proof of concept study a successful number of IL plasticised PLLA prototype materials were synthesised. It can be concluded that the NTf₂ ILs **50–53** have a significant plasticising effect on PLLA at 20 and 30 wt%, with the elongation at break increased by > 400 and > 700 % with 20 and 30 wt% IL respectively. The most promising result was observed for PLLA plasticised with 20 wt% IL **51** which had an elongation at break of more than 500 %, a Young's modulus of 1103 MPa and a tensile strength of 32 MPa. A significant depression of the T_g for PLLA/IL**50–53** was observed, on average 15, 20 and 45 °C at 10, 20 and 30 wt% IL respectively. However, 10 wt% NTf₂ ILs **50–53** appeared to have an antiplasticising effect on PLLA, with a decrease in the elongation at break observed compared to neat PLLA.

The OctSO₄ ILs **54–56** appeared to be incompatible with PLLA, initially from the appearance of the PLLA/IL**54–56** films, and subsequently from the tensile testing results where an antiplasticising effect on PLLA was observed for PLLA/IL**54** with 20 and 30 wt% IL, PLLA/IL**55** with 10 wt% IL and PLLA/IL**56** with 10, 20 and 30 wt% IL. Any plasticising effects observed with the OctSO₄ ILs **54–56** were minimal compared to those observed for the NTf₂ ILs.

The ageing results show that the plasticisation of PLLA with NTf₂ ILs **50–53** can in all cases significantly reduce the ageing rate of PLLA, with several ILs showing a very minimal ageing effect over 100 days, especially PLLA/IL**50** and PLLA/IL**51** with 20 wt% IL. During ageing the Young's modulus appeared to be ageing to an equilibrium state for each IL (**50–53**), and the tensile strength appeared to be ageing to an equilibrium state for each wt% of IL (**50–53**).

The thermal stability of PLLA/IL**52** with 30 wt% IL show that IL **52** had very little effect on the thermal stability of PLLA, with only a 12 °C decrease in T_{onset} observed for PLLA/IL**52** with 30 wt% IL compared to neat PLLA. This is a very promising result that shows that the NTf₂ ILs **50, 51** and **53** at 20 and 30 wt% also have the potential to minimally effect the thermal stability of PLLA.

Overall, plasticisation of PLLA with 1-methylimidazolium NTf₂ ILs (**50–53**) successfully overcame several of the limitations of currently reported PLLA plasticisers

by utilising plasticisers with high thermal stabilities, preventing plasticiser leaching, demonstrating high plasticiser compatibility and increasing the ductility of PLLA to a greater extent than the previously published work.³⁹

3.6 Future Work

The morphology of the PLLA/IL films could be studied using microscopy, more specifically field emission scanning electron microscopy (FESEM). With this technique a comparison of the morphology of the neat PLLA film to that of the plasticised PLLA films could be carried out. Also, by comparing FESEM micrographs of PLLA plasticised with OctOSO₄ ILs and with NTf₂ ILs, the effect of IL miscibility on film morphology could be examined. Any phase separation in the PLLA/IL films containing OctOSO₄ ILs could be identified. Any defects due to the plasticisation would also be detected. By comparing aged and non-aged PLLA/IL films, changes in the morphology of the films during ageing could be studied.

Literature data shows that the plasticisation of PLA with ILs can increase the hydrolytic degradation of PLA.³⁷ Thus, it would be very interesting to investigate to what extent the ILs studied herein affect the biodegradation of PLLA.

From this work it is clear that the level of plasticisation is greatly dependent on the anion of the IL. It would be of great interest to investigate the use of the dicyanamide (DCA) anion, with the same series of cations employed herein, as ILs for plasticisation of PLLA. Literature data shows that these ILs would be liquid at room temperature,⁴³ with the potential to have low viscosity⁵⁶ and a thermal stability above 200 °C.^{57,58} They have also been shown to have low antimicrobial activity.⁴³ If the 1-methylimidazolium DCA ILs have suitable thermal properties to allow for plasticisation with PLLA, it is hoped that they would give promising results as plasticisers, as they would be an attractive alternative to the NTf₂ ILs as they do not contain any fluorine. In addition, when comparing the cost of the starting materials used to synthesise the ILs, sodium dicyanamide is cheaper than lithium bistriflimide, which will result in a cheaper synthesis for the DCA ILs making them more attractive to industry.

It is envisaged that this work will be further progressed by utilising functionalised and task specific ILs as plasticisers, with the aim of creating plasticised materials targeted to specific applications.

3.7 References

1. L. T. Lim, R. Auras and M. Rubino, *Prog. Polym. Sci.*, 2008, **33**, 820.
2. D. Garlotta, *J. Polym. Environ.*, 2001, **9**, 63.
3. K. Madhavan Nampoothiri, N. R. Nair and R. P. John, *Bioresour. Technol.*, 2010, **101**, 8493.
4. M. Itavaara, S. Karjomaa and J. F. Selin, *Chemosphere*, 2002, **46**, 879.
5. M. Funabashi, F. Ninomiya and M. Kunioka, *J. Polym. Environ.*, 2007, **15**, 245.
6. M. Funabashi, F. Ninomiya and M. Kunioka, *Int. J. Mol. Sci.*, 2009, **10**, 3635.
7. R. G. Sinclair, *J. Macromol. Sci., Part A: Pure Appl. Chem.*, 1996, **33**, 585.
8. A. J. R. Lasprilla, G. A. R. Martinez, B. H. Lunelli, A. L. Jardini and R. M. Filho, *Biotechnol. Adv.*, 2012, **30**, 321.
9. J. R. Sarasua, A. L. Arraiza, P. Balerdi and I. Maiza, *Polym. Eng. Sci.*, 2005, **45**, 745.
10. J. Gere and B. Goodno, in *Mechanics of materials*, Nelson Education, Canada, 2012, ch. 1, pp. 5-87.
11. Instron Glossary of Materials Testing Terms, <http://www.instron.com/en-gb/our-company/library/glossary/t/tensile-strength>, Accessed October 2015.
12. Instron Glossary of Materials Testing Terms, <http://www.instron.com/en-gb/our-company/library/glossary/e/elongation> Accessed October 2015.
13. Instron Glossary of Materials Testing Terms, <http://www.instron.com/en-gb/our-company/library/glossary/m/modulus-of-elasticity>, Accessed October 2015.
14. H. F. Brinson and L. C. Brinson, in *Polymer Engineering Science and Viscoelasticity*, Springer New York, 2008, ch. 2, pp. 15-54.
15. H. F. Brinson and L. C. Brinson, in *Polymer Engineering Science and Viscoelasticity*, Springer New York, 2008, ch. 3, pp. 55-97.
16. K. S. Anderson, K. M. Schreck and M. A. Hillmyer, *Polym. Rev. (Philadelphia, PA, U. S.)*, 2008, **48**, 85.
17. O. Martin and L. Avérous, *Polymer*, 2001, **42**, 6209.
18. T. Patrício and P. Bártolo, *Procedia Engineering*, 2013, **59**, 292.
19. K. Sungsanit, N. Kao and S. N. Bhattacharya, *Polym. Eng. Sci.*, 2012, **52**, 108.
20. L. Xiao, B. Wang, G. Yang and M. Gauthier, in *Biomedical Science, Engineering and Technology*, ed. D. N. Ghista, InTech, Croatia, 2012, ch. 11, pp. 255-256.
21. N. Ljungberg and B. Wesslén, *Biomacromolecules*, 2005, **6**, 1789.

22. M. A. Shirai, M. V. E. Grossmann, S. Mali, F. Yamashita, P. S. Garcia and C. M. O. Müller, *Carbohydr. Polym.*, 2013, **92**, 19.
23. T. Mekonnen, P. Mussone, H. Khalil and D. Bressler, *J. Mater. Chem. A*, 2013, **1**, 13379.
24. J. Rank, *TES*, 2005, **4**, 1.
25. G. Latini, M. Ferri and F. Chiellini, *Curr. Med. Chem.*, 2010, **17**, 2979.
26. M. Rahman and C. S. Brazel, *Polym. Degrad. Stab.*, 2006, **91**, 3371.
27. D. Y. Bang, M. Kyung, M. J. Kim, B. Y. Jung, M. C. Cho, S. M. Choi, Y. W. Kim, S. K. Lim, D. S. Lim, A. J. Won, S. J. Kwack, Y. Lee, H. S. Kim and B. M. Lee, *Compr. Rev. Food Sci. Food Saf.*, 2012, **11**, 453.
28. K. Christen, *Environ. Sci. Technol.*, 2000, **34**, 11A.
29. M. P. Scott, M. Rahman and C. S. Brazel, *Eur. Polym. J.*, 2003, **39**, 1947.
30. A. M. A. Dias, S. Marceneiro, M. E. M. Braga, J. F. J. Coelho, A. G. M. Ferreira, P. N. Simoes, H. I. M. Veiga, L. C. Tome, I. M. Marrucho, J. M. S. S. Esperanca, A. A. Matias, C. M. M. Duarte, L. P. N. Rebelo and H. C. de Sousa, *Acta Biomater.*, 2012, **8**, 1366.
31. S. Y. Choi, H. Rodriguez, A. Mirjafari, D. F. Gilpin, S. McGrath, K. R. Malcolm, M. M. Tunney, R. D. Rogers and T. McNally, *Green Chem.*, 2011, **13**, 1527.
32. A. Sankri, A. Arhaliass, I. Dez, A. C. Gaumont, Y. Grohens, D. Lourdin, I. Pillin, A. Rolland-Sabaté and E. Leroy, *Carbohydr. Polym.*, 2010, **82**, 256.
33. E. Leroy, P. Jacquet, G. Coativy, A. I. Reguerre and D. Lourdin, *Carbohydr. Polym.*, 2012, **89**, 955.
34. P. Bernardo, J. C. Jansen, F. Bazzarelli, F. Tasselli, A. Fuoco, K. Friess, P. Izák, V. Jarmarová, M. Kačírková and G. Clarizia, *Sep. Purif. Technol.*, 2012, **97**, 73.
35. L. Guo, Y. Liu, C. Zhang and J. Chen, *J. Membr. Sci.*, 2011, **372**, 314.
36. B.-K. Chen, T.-Y. Wu, Y.-M. Chang and A. F. Chen, *Chem. Eng. J. (Lausanne, Switz.)*, 2013, **215–216**, 886.
37. K. I. Park and M. Xanthos, *Polym. Degrad. Stab.*, 2009, **94**, 834.
38. K. Park, J. U. Ha and M. Xanthos, *Polym. Eng. Sci.*, 2010, **50**, 1105.
39. H. Gui, Y. Li, S. Chen, P. Xu, B. Zheng and Y. Ding, *Macromol. Res.*, 2014, **22**, 583.
40. H. Cai, V. Dave, R. A. Gross and S. P. McCarthy, *J. Polym. Sci., Part B: Polym. Phys.*, 1996, **34**, 2701.
41. A. Celli and M. Scandola, *Polymer*, 1992, **33**, 2699.

42. R. Acioli-Moura and X. S. Sun, *Polym. Eng. Sci.*, 2008, **48**, 829.
43. S. Morrissey, B. Pegot, D. Coleman, M. T. Garcia, D. Ferguson, B. Quilty and N. Gathergood, *Green Chem.*, 2009, **11**, 475.
44. M. Ghavre, PhD Thesis, Dublin City University, 2012.
45. S. Morrissey, PhD Thesis, Dublin City University, 2008.
46. M. L. Bender, *Chem. Rev. (Washington, DC, U. S.)*, 1960, **60**, 53.
47. J. G. Huddleston, A. E. Visser, W. M. Reichert, H. D. Willauer, G. A. Broker and R. D. Rogers, *Green Chem.*, 2001, **3**, 156.
48. X. Zhu, D. Zhang and C. Liu, *J. Mol. Model.*, 2011, **17**, 2099.
49. Z. Wang, in *Comprehensive Organic Name Reactions and Reagents*, John Wiley & Sons, Inc., New Jersey, 2010, ch. 426, pp. 1897-1900.
50. P. Bonhôte, A.-P. Dias, N. Papageorgiou, K. Kalyanasundaram and M. Grätzel, *Inorg. Chem.*, 1996, **35**, 1168.
51. W. R. Dolbier, in *Guide to Fluorine NMR for Organic Chemists*, John Wiley & Sons, Inc, New Jersey, 2009, ch. 5, pp. 137-175.
52. H. L. Ngo, K. LeCompte, L. Hargens and A. B. McEwen, *Thermochim. Acta*, 2000, **357**, 97.
53. C. Maton, N. De Vos and C. V. Stevens, *Chem. Soc. Rev.*, 2013, **42**, 5963.
54. P. Wasserscheid, R. v. Hal and A. Bosmann, *Green Chem.*, 2002, **4**, 400.
55. H.-B. Han, K. Liu, S.-W. Feng, S.-S. Zhou, W.-F. Feng, J. Nie, H. Li, X.-J. Huang, H. Matsumoto, M. Armand and Z.-B. Zhou, *Electrochim. Acta*, 2010, **55**, 7134.
56. D. R. MacFarlane, J. Golding, S. Forsyth, M. Forsyth and G. B. Deacon, *Chem. Commun. (Cambridge, U. K.)*, 2001, 1430.
57. D. R. MacFarlane, S. A. Forsyth, J. Golding and G. B. Deacon, *Green Chem.*, 2002, **4**, 444.
58. C. P. Fredlake, J. M. Crosthwaite, D. G. Hert, S. N. V. K. Aki and J. F. Brennecke, *J. Chem. Eng. Data*, 2004, **49**, 954.

4.0 The Dielectric Properties of ILs

4.1 Introduction

Microwaves are electromagnetic waves that consist of an electric field and a magnetic field which oscillate perpendicularly to each other at a frequency between 300 MHz to 300 GHz.¹ Molecules can be heated by the electric field of microwaves through both dipole rotation and ionic conduction, thus only polar materials are heated based on their dielectric constant.¹ Understanding solvent polarity is very important in determining the potential use of a solvent in a given application. A measure of solvent polarity is given by its dielectric constant (relative permittivity), where a high dielectric constant indicates a high susceptibility to heating by microwaves.¹ Solvent behaviour is also often modelled using dielectric constants as many approaches to do so use dielectric continuum models.²

Microwaves have been extensively applied in synthetic chemistry and have been shown to shorten reaction times, prevent side product formation, increase percentage yields and simplify multi-step reactions.³ ILs are very susceptible to heating by microwaves due to their ionic nature (through ionic conduction), which has led to their simultaneous use with microwaves in areas such as polymer synthesis,⁴ organic synthesis,^{3,5} catalysis,⁵ extractions⁶⁻⁸ and dissolution.⁹ Properties of a low vapour pressure and high thermal stability have also made ILs highly attractive for use in microwave chemistry.⁵ ILs with high dielectric properties have also been investigated for use in energy storage applications, such as replacements for current electrolytes in lithium-ion batteries, as ILs can offer the potential to increase the thermal and electrochemical stability of the devices.¹⁰⁻¹²

When a dielectric material is placed in an external electric field dielectric polarisation occurs, resulting in a separation of positive and negative charges and dipole formation.¹³ The three mechanisms which describe dielectric polarisation include:

- 1) Electronic polarisation – displacement of electrons relative to the nucleus.¹⁴
- 2) Atomic polarisation – displacement of atomic position in a molecule or lattice (ionic polarisation) relative to each other.¹³

3) **Orientational polarisation** – orientation of the dipole of polar molecules with the electric field, resulting in a net polarisation in the direction of the applied field.¹³ This is also known as **dipolar polarisation**.

The mechanisms of polarisation are depicted in Figure 4.1.

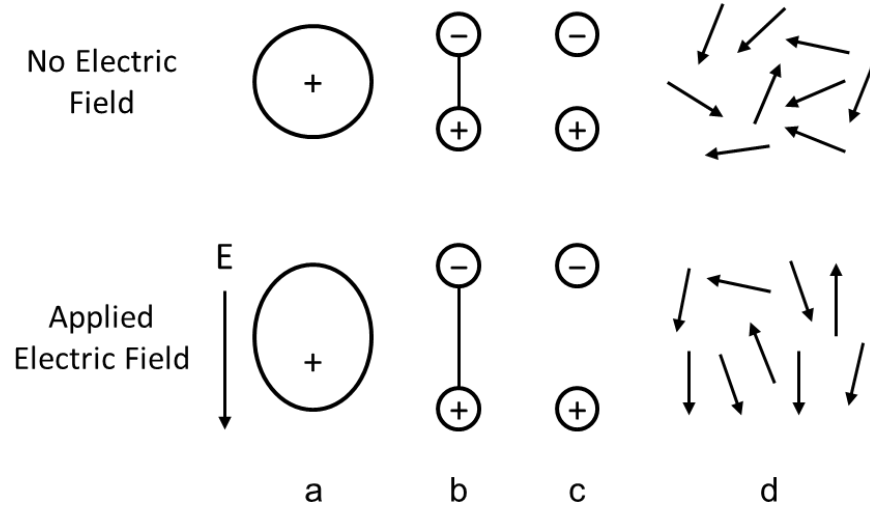


Figure 4.1 Mechanisms of polarisation in an applied electric field (E); a) electronic; b) atomic; c) ionic; d) orientational (dipolar).

The absolute complex permittivity (ϵ) of a material describes its interaction with an electromagnetic field¹⁵ and is usually expressed in terms of the relative complex permittivity (ϵ_r) and the permittivity of free space (ϵ_0) ($8.854 \times 10^{-12} \text{ F m}^{-1}$) (Equation 4.1).¹⁶

$$\epsilon = \epsilon_r \epsilon_0$$

Equation 4.1 Absolute permittivity (ϵ) of a material, where ϵ_r is the relative permittivity and ϵ_0 is the permittivity of free space ($8.854 \times 10^{-12} \text{ F m}^{-1}$).¹⁶

Thus, the relative permittivity of a material can be obtained using equation 4.2.

$$\epsilon_r = \frac{\epsilon}{\epsilon_0}$$

Equation 4.2 Relative permittivity (ϵ_r) of a material expressed as a ratio of absolute complex permittivity (ϵ) to the permittivity of free space (ϵ_0) ($8.854 \times 10^{-12} \text{ F m}^{-1}$).

Relative permittivity (ϵ_r) varies with both temperature and frequency¹⁷ and contains both real and imaginary parts (Equation 4.3).¹⁶ The real part of permittivity (ϵ'), also called the dielectric constant, is a measure of how much energy from an external field is stored in a material.¹⁷ The imaginary part of permittivity (ϵ'') is the dielectric loss factor and is a measure of how dissipative a material is in the presence of an external electric field¹⁷ and also represents the ability of a material to convert stored electromagnetic energy to heat.¹⁸

$$\epsilon_r = \epsilon' - j\epsilon''$$

Equation 4.3 Relative permittivity (ϵ_r) of a material expressed in terms of the dielectric constant (ϵ') and the dielectric loss factor (ϵ''), where j is an imaginary unit.¹⁶

Permanent polarisation occurs in the presence of a static electric field. However, in an alternating electric field the polarisation oscillates with the electric field.¹⁴ The modes of polarisation contributing to the overall dielectric constant of the material depend on the frequency of the applied field.¹⁴ When a dielectric material is placed in an alternating electric field a relaxation is observed, which can be described as a ‘lag’ observed in the system which is trying to reach an equilibrium state.¹³ Dielectric relaxation is described as the exponential decay with time of the dielectric polarisation on the removal of the external electric field.¹³ Dielectric relaxation consists of dipole relaxation and ionic relaxation and is most usually observed between 10^2 – 10^{10} Hz, as depicted in the dielectric resonance spectra given in Figure 4.2.¹³ Atomic and electronic transitions are much faster than dielectric relaxation mechanisms and usually occur at frequencies greater than 10^{12} Hz (Figure 4.2).

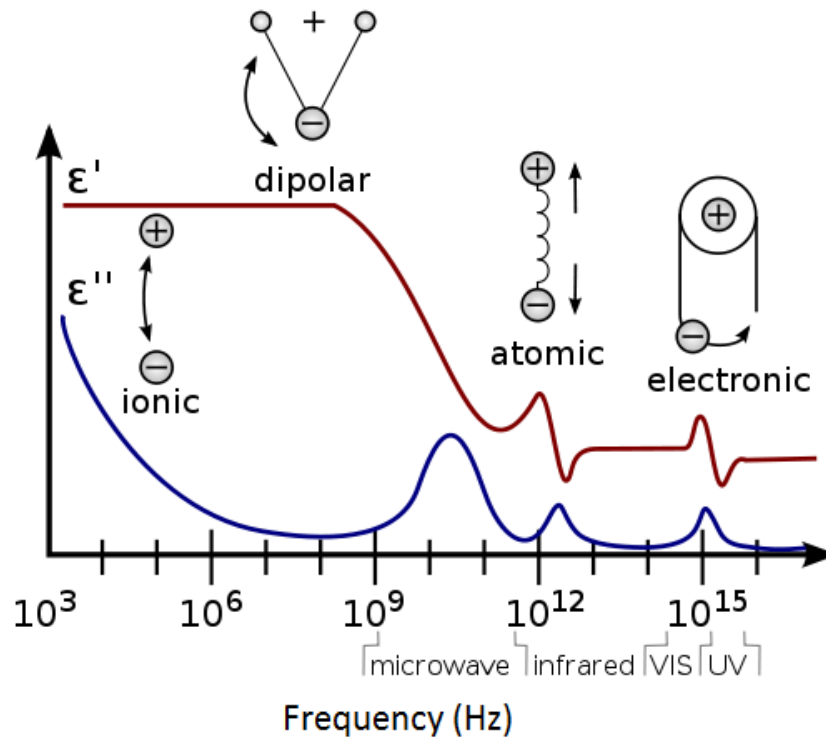


Figure 4.2 Frequency response of dielectric mechanisms as shown by the dielectric resonance spectra for the real (ϵ') and imaginary (ϵ'') parts of permittivity, where dielectric relaxation occurs up to 10^{10} Hz.¹³ Figure adapted by author from M. Huang, PhD Thesis, Ruhr University Bochum, 2011.

A measure of the relative “lossiness” of a material is given by the dielectric loss tangent ($\tan \delta$) and is the ratio of the energy lost to the energy stored.¹⁷ It also quantifies the extent to which a material absorbs microwave energy.¹⁸ The loss tangent is calculated by dividing the dielectric loss factor (ϵ'') by the dielectric constant (ϵ') (Equation 4.4).¹⁶

$$\tan \delta = \frac{\epsilon''}{\epsilon'}$$

Equation 4.4 Dielectric loss tangent ($\tan \delta$), where ϵ' is the dielectric constant and ϵ'' is the dielectric loss factor of the material.¹⁶

The loss tangent ($\tan \delta$) can be described schematically as depicted in Figure 4.3.

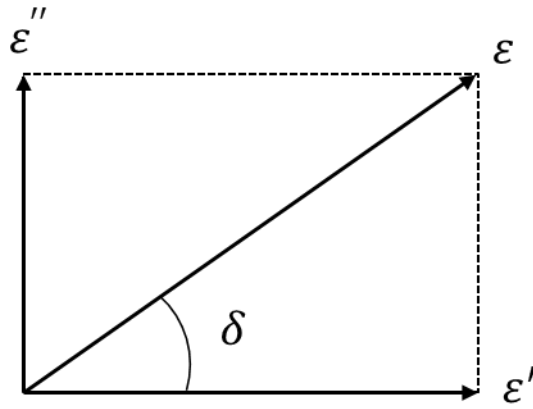


Figure 4.3 Schematic representation of the loss tangent ($\tan \delta$).

4.1.1 Dielectric Measurement Techniques

To make an informed decision about the technique that should be selected for measuring the dielectric properties of a material, a number of factors need to be considered, which include:¹⁷

- Frequency of interest
- Cost of technique
- Expected dielectric constant
- Required measurement accuracy
- Ease of sample preparation and measurement
- Required measurement speed
- Material properties
- Material form
- Available sample size
- Destructive or non-destructive technique
- Contacting or non-contacting technique
- Temperature

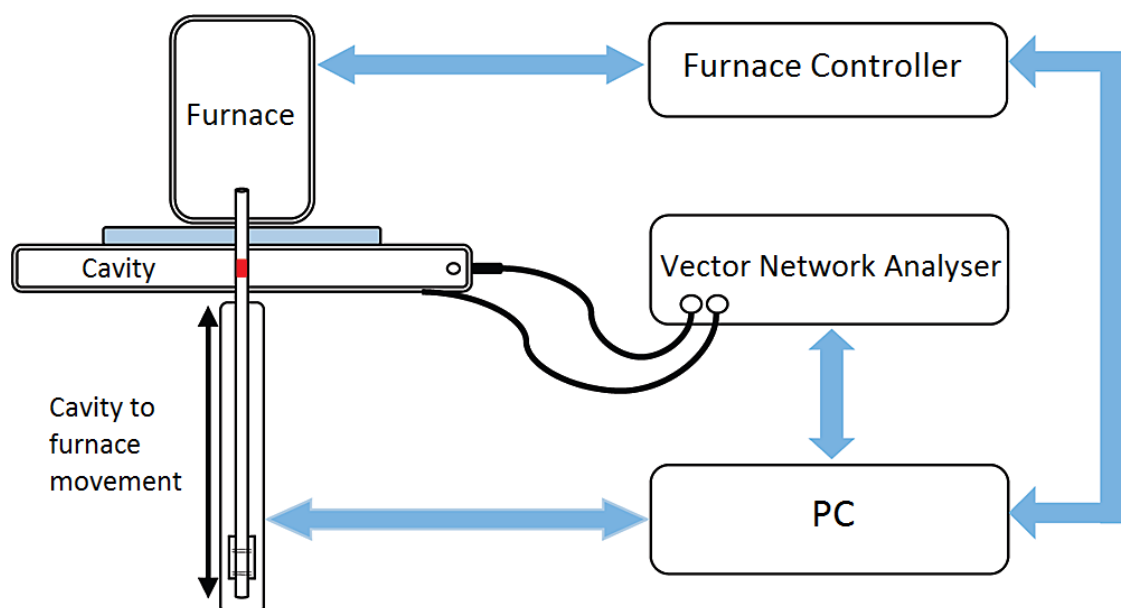
A variety of techniques exist for measuring the dielectric properties of materials, which include the coaxial probe, free space, resonant cavity, transmission line and parallel plate methods.¹⁵ A technique can be either resonant or non-resonant, where resonant techniques take measurements at a single frequency or at discrete frequency points.¹⁵ Due to the high electrical conductance of ILs, their dielectric properties cannot be measured using traditional capacitance methods,¹⁹ so the coaxial probe and cavity perturbation techniques are often used. For materials with high dielectric constants the

coaxial probe is the preferred technique, which can be used for semi-solids and liquids with simple sample preparation and high accuracy for high loss materials.¹⁵ However, this technique requires a large amount of sample material.¹⁵ The cavity perturbation technique (also known as resonant cavity) is suitable for both solid and liquid samples, and is able to give high accuracy for low permittivity materials with only small sample sizes required.¹⁵

4.1.1.1 The Cavity Perturbation Technique

The most accurate methods currently used to measure the dielectric permittivity of materials are the resonant measurement methods which are usually limited to the microwave frequency range (300 MHz and 300 GHz).²⁰ A common resonant method used for measuring microwave permittivity of materials is the cavity perturbation technique, which consists of a resonant cavity connected to a vector network analyser (VNA). (Figure 4.4)

Figure 4.4 Schematic of the cavity perturbation apparatus.¹⁸ Reprinted with permission



from A. D. Smith, E. H. Lester, K. J. Thurecht, S. W. Kingman, J. El Harfi, G. Dimitrakis, J. P. Robinson and D. J. Irvine, *Ind. Eng. Chem. Res.*, 2010, **49**, 3011. Copyright 2010 American Chemical Society.

A sample is introduced into the centre of the empty resonant cavity where the electric field has the maximum value, to allow for maximum interaction with the sample. This causes the resonant frequency of the cavity (f_c) to decrease to that of the resonant

frequency of the cavity containing the sample (f_s). The shift in the resonant frequency is related to the dielectric constant (ϵ') of the specimen, and results in a decrease in the quality factor (Q), due to dielectric loss (ϵ''). The VNA detects the frequency shift and resultant quality factor (Q) (using Equation 4.5 and 4.6) and calculates the dielectric constant (ϵ') and dielectric loss factor (ϵ'') using Equations 4.7 and 4.8.²¹

$$Q_c = \frac{f_c}{\Delta f_c}$$

Equation 4.5 Quality factor of the empty cavity (Q_c), where f_c is the resonant frequency of the empty cavity and Δf_c is the bandwidth at half power of the empty cavity.²¹

$$Q_s = \frac{f_s}{\Delta f_s}$$

Equation 4.6 Quality factor of the cavity containing the sample (Q_s), where f_s is the resonant frequency of the cavity containing the sample and Δf_s is the bandwidth at half power of the cavity containing the sample.²¹

$$\epsilon' = \frac{V_c(f_c - f_s)}{2V_s f_s}$$

Equation 4.7 Dielectric constant (ϵ'), where V_c is the volume of the empty cavity, V_s is the volume of the sample, f_c is the resonant frequency of the empty cavity and f_s is the resonant frequency of the cavity containing the sample.²¹

$$\epsilon'' = \frac{V_c}{4V_s} \left(\frac{1}{Q_s} - \frac{1}{Q_c} \right)$$

Equation 4.8 Dielectric loss factor (ϵ''), where V_c is the volume of the empty cavity, V_s is the volume of the sample, Q_s is the quality factor of the cavity containing the sample and Q_c is the quality factor of the empty cavity.²¹

A furnace is situated above the cavity (Figure 4.1) and allows high temperature measurements to be carried out. During a high temperature experiment, the sample

resides in the furnace and is moved into the cavity using a step-motor for the measurement to be taken. Minimal time is spent outside the furnace and in the cavity during the measurement, thus the heat loss is considered negligible.

4.1.2 Static Dielectric Constants of ILs

Static dielectric constants (ϵ) (zero frequency) of ILs can be determined by zero frequency extrapolation of the frequency dependent dielectric constants.^{2,19,22-24} Huang *et al.* studied the dielectric properties of 42 ILs using a coaxial method and showed the ILs were tuneable over a wide range by variation of the cation and anion.¹⁹ Low dielectric constants were observed for aprotic ILs with high symmetry ($\epsilon = 10\text{--}16$), with an increase observed when oxoanions were employed. Protic ILs exhibited higher dielectric constants than aprotic ILs ($\epsilon = 20\text{--}30$ for monoalkylammonium ILs). Hydroxyl functionalised alkylammonium ILs had the highest dielectric constants, with 2-hydroxyethyl ammonium lactate, prepared from DL-lactic acid, (Figure 4.5) giving the highest dielectric constant of $\epsilon = 85.6$.¹⁹

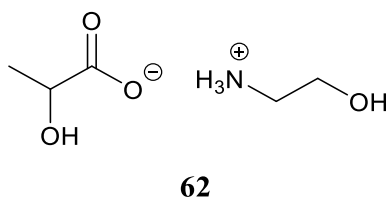


Figure 4.5 2-Hydroxyethyl ammonium lactate with static dielectric constant $\epsilon = 85.6$, as determined using the coaxial probe method.¹⁹

A material's dielectric constant changes with both temperature and frequency and is most often seen to decrease as frequency increases, which in turn increases the dielectric loss factor.¹⁵ As the temperature of a material increases, the dielectric constant also increases for low permittivity materials, but this relation has also been seen to inverse in high permittivity materials.¹⁵ Due to the complex way in which dielectric properties of components change over a range of frequencies and temperatures, it is necessary to study these changes to understand how materials will respond under a wide range of conditions. The temperature, physical state and chemical composition of components in a reaction will also change as it progresses, thus it is necessary to understand how these changes affect the dielectric properties of the components. This information will enable microwaves to be successfully employed to enhance reaction rates, improve solvation and enhance the extraction of a variety of components.

4.1.3 Selection of ILs for Dielectric Property Measurements

Seven mandelic acid ILs **18–20** and **22–25** (Figure 4.6) and three 1-methylimidazolium ILs **49**, **50** and **51** (Figure 4.7) were chosen to investigate the dielectric properties of ILs using the cavity perturbation technique. The different structural features and different states (solid and liquid) of the ILs allowed for an investigation into how the structures and physical states of the ILs relate to their dielectric properties. It is desired that by analysing the dielectric properties at high temperatures and different frequencies, information can be gathered on how both these factors affect the dielectric properties of the ILs.

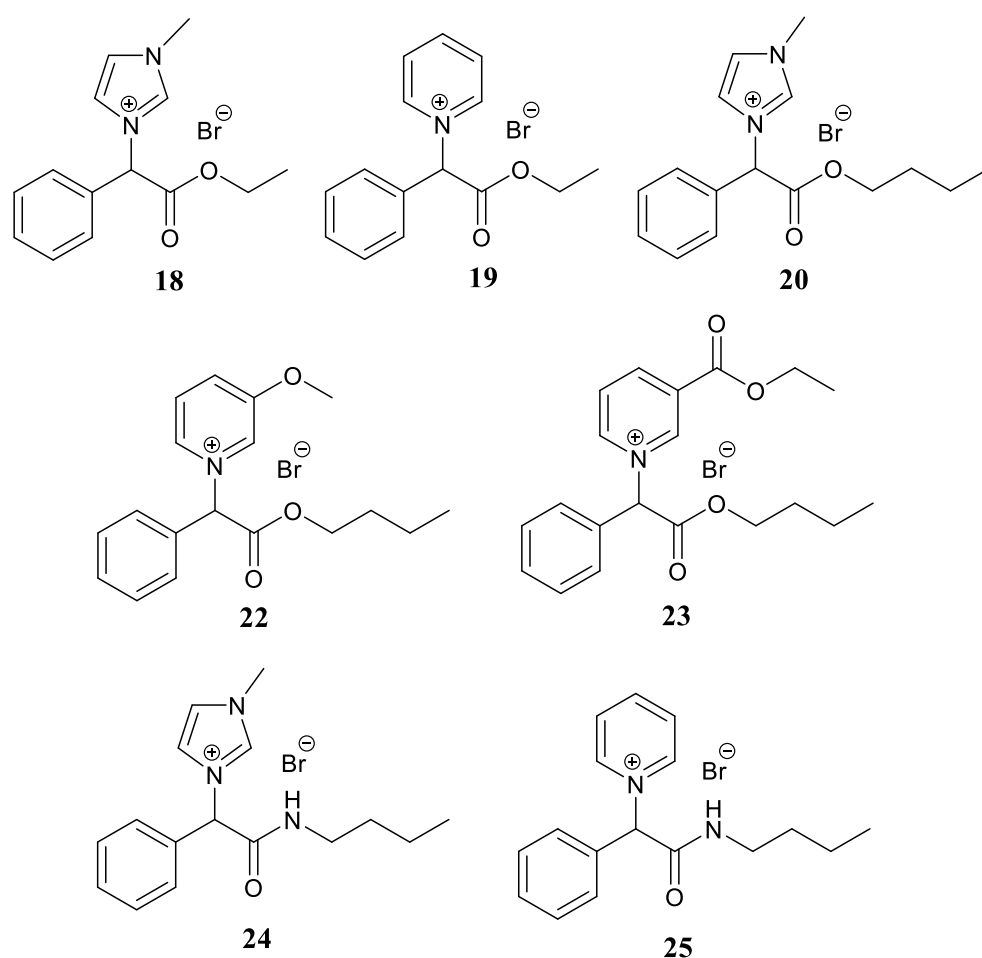


Figure 4.6 Mandelic acid ILs **18–20** and **22–25** selected to investigate the dielectric properties of ILs using the cavity perturbation technique.

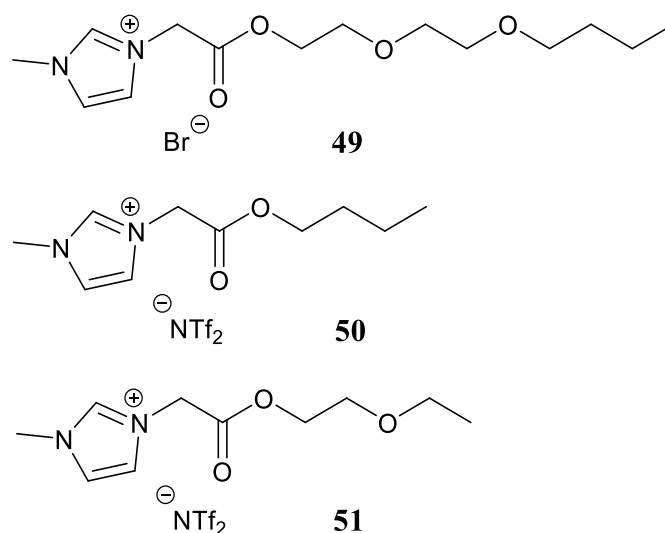


Figure 4.7 1-Methylimidazolium ILs **49–51** selected to investigate the dielectric properties of ILs using the cavity perturbation technique.

4.2 Results and Discussion

Dielectric properties of the mandelic acid ILs **18–20** and **22–25** (Figure 4.6) and 1-methylimidazolium ester ILs **49–51** (Figure 4.7) were measured using a cavity perturbation technique.

Full experimental details of this technique are provided in chapter 6, section 6.1.11. Two frequencies, 910 and 2470 MHz, were used to measure the dielectric properties, as these frequencies are similar to those used for microwave heating in industry.²⁵ The study herein does not discuss the static dielectric constants of the ILs, only the frequency dependent dielectric constants, hence the results are not directly comparable to previously published results on the static dielectric constants of ILs.¹⁹ Frequency dependent dielectric constants of the ILs were measured over a wide temperature range, and provide a direct insight into the use of the ILs in microwave reactions carried out at the measured temperatures and frequencies, as the dielectric properties are known to change with frequency and temperature.¹⁷ This work was undertaken in collaboration with Dr Derek Irvine from the Department of Chemical and Environmental Engineering at The University of Nottingham, UK.

4.2.1 Mandelic Acid ILs

Room temperature dielectric properties of the mandelic acid ILs **18–20** and **22–25** were initially measured at 910 and 2470 MHz. The results show that the dielectric constants

(ϵ') of the ILs fall between 1.48–2.26 and 1.49–2.30 for 910 and 2470 MHz respectively (Table 4.1 and 4.2). The ϵ' of the ILs are very similar at both frequencies, with a very slight increase in ϵ' observed at 2470 MHz (maximum 0.1 MHz increase measured between 910 and 2470 MHz observed for IL **18**).

Table 4.1 Dielectric properties of mandelic acid ILs **18–20** and **22–25** measured at room temperature and 910 MHz, where ϵ' is the dielectric constant, ϵ'' is the dielectric loss and $\tan \delta$ is the loss tangent.

IL	ϵ'	ϵ''	$\tan \delta$
18	1.70	0.00	0.00
19	1.91	0.00	0.00
20	2.25	0.00	0.00
22	2.24	0.00	0.00
23	2.26	0.00	0.00
24	2.08	0.00	0.00
25	1.48	0.00	0.00

ILs **20**, **22** and **23**, which contain a butyl ester chain, had the highest ϵ' with very similar values of 2.25, 2.24 and 2.26 at 910 MHz measured respectively (Table 4.1). As the ester alkyl chain length increased in the 1-methylimidazolium ILs from ethyl (**18**) to butyl (**20**) the ϵ' increased from 1.70 to 2.25 at 910 MHz respectively. This increase in ϵ' with increasing alkyl chain length for imidazolium ILs with a common anion has previously been observed in the literature.¹⁹

Table 4.2 Dielectric properties of mandelic acid ILs **18–20** and **22–25** measured at room temperature and 2470 MHz, where ϵ' is the dielectric constant, ϵ'' is the dielectric loss and $\tan \delta$ is the loss tangent.

IL	ϵ'	ϵ''	$\tan \delta$
18	1.80	0.00	0.00
19	1.96	0.00	0.00
20	2.28	0.00	0.00
22	2.26	0.00	0.00
23	2.30	0.00	0.00
24	2.11	0.00	0.00
25	1.49	0.00	0.00

The dielectric loss (ϵ'') and loss tangent ($\tan \delta$) of the mandelic acid ILs **18–20** and **22–25** at both 910 and 2470 MHz are all zero (Table 4.1 and 4.2). ILs **18–20** and **22–25** are solid at room temperature. When subjected to an alternating electric field the dipoles of the IL will attempt to align with the field, causing intra- and intermolecular motion.¹⁸ This molecular motion is restricted in a solid, where strong intermolecular forces prevent the dipoles from significantly aligning with the very fast alternating electric field at microwave frequencies. Orientational motion of dipoles causes internal friction in materials and results in dielectric energy losses.²⁶ Thus, due to the restriction of molecular motion in solids, zero $\tan \delta$ and ϵ'' are measured for ILs **18–20** and **22–25**.

4.2.2 1-Methylimidazolium Ester ILs

The dielectric properties of the 1-methylimidazolium ester ILs **49–51** were initially measured at room temperature at 910 and 2470 MHz. The results show that the ϵ' of the ILs fall between 3.15–5.79 and 3.13–3.57 for 910 and 2470 MHz respectively (Table 4.3 and 4.4). Very similar ϵ' of IL **49** were measured at both frequencies, with 3.15 and 3.13 at 910 and 2470 MHz respectively. However, there was a lower ϵ' observed at a higher frequency for ILs **50** and **51**, which is an observation that has also been described in the literature for RTILs.¹⁹ The highest ϵ' of 5.79 is observed for IL **50** at 910 MHz, with a higher ϵ' observed for the NTf₂ ILs **50** and **51** compared to the bromide IL **49**. NTf₂ ILs are known to have lower viscosities than halide ILs,²⁷ thus the decrease in IL viscosity and subsequent reduction in intermolecular interactions would result in an increased interaction of the ILs electronic structure with the applied electric field²⁵ and

decreased relaxation times,¹³ which may be the reason for the increase in dielectric constant observed. However, ILs **50** and **51** have a different cation than IL **49**, so these ILs cannot be directly compared because the decrease in ϵ' may be due to the decrease in cation size, which has shown to lead to a decrease in IL ϵ' .¹³ In the NTf₂ ILs as the ester alkyl chain is changed from a butyl (**50**) to a polyether chain (**51**) there is a decrease in ϵ' at 910 MHz but an increase at 2470 MHz, demonstrating the complex nature of the dielectric properties of materials at different frequencies.

Table 4.3 Dielectric properties of 1-methylimidazolium ester ILs **49–51** measured at room temperature and 910 MHz, where ϵ' is the dielectric constant, ϵ'' is the dielectric loss and $\tan \delta$ is the loss tangent.

IL	ϵ'	ϵ''	$\tan \delta$
49	3.15	0.31	0.10
50	5.79	1.72	0.30
51	5.76	1.47	0.26

Table 4.4 Dielectric properties of 1-methylimidazolium ester ILs **49–51** measured at room temperature and 2470 MHz, where ϵ' is the dielectric constant, ϵ'' is the dielectric loss and $\tan \delta$ is the loss tangent.

IL	ϵ'	ϵ''	$\tan \delta$
49	3.13	0.23	0.07
50	5.42	1.23	0.22
51	5.57	1.15	0.21

The ϵ'' of the 1-methylimidazolium ILs **49–51** are 0.31–1.72 and 0.23–1.23 at 910 and 2470 MHz respectively (Table 4.1 and 4.2). Non-zero $\tan \delta$ for **49–51** ILs at 910 and 2470 MHz tells us that the ILs are permeable to the microwaves and they are able to absorb the microwaves to an appreciable degree, with $\tan \delta$ of 0.10–0.30 and 0.07–0.21 at 910 and 2470 MHz respectively. At room temperature ILs **49–51** are liquid, thus there are less restrictions on its molecular motions than in a solid IL (e.g. mandelic acid ILs **18–20** and **22–25**) so the dipoles are able to align with the alternating electric field, causing molecular rotation¹⁸ and non-zero $\tan \delta$ values are measured as a result.

4.2.3 High Temperature Experiments

The dielectric properties of the mandelic acid ILs **20** and **23** and the 1-methylimidazolium IL **50** (Figure 4.8) were studied between 20 and 120 °C at 910 and 2470 MHz to investigate how the dielectric properties of the IL vary with temperature at the two different frequencies. Measurements were taken every 5 °C. The exact values for ϵ' , ϵ'' and $\tan \delta$ for each high temperature experiment are given in Appendix F.

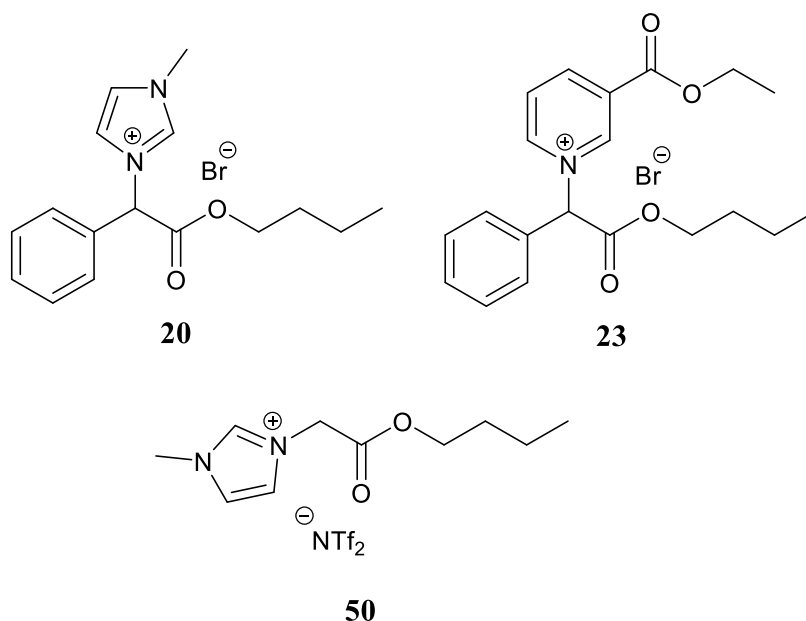


Figure 4.8 Mandelic acid ILs **20** and **23** and 1-methylimidazolium IL **50** utilised in the high temperature studies on the dielectric properties of ILs.

4.2.3.1 Mandelic Acid ILs

It can be seen that as the temperature increases from 20 to 120 °C the ϵ' of IL **20** increases (Figure 4.9). The dielectric constant is also observed to be higher for the lower frequency of 910 MHz, with a maximum value of 4.15 at 115 °C recorded. This increase in ϵ' is caused by a decrease in the amount/strength of the intermolecular interactions of the IL as the temperature increases.²⁵ This causes an increase in the interaction of the ILs electronic structure with the electric field, as restrictions on the IL molecular motion are reduced, resulting in the increase observed in the ϵ' . There is a sharp increase in the dielectric constant observed between 80 °C and 85 °C, where the dielectric constant increases from 3.12 to 3.67. This observation was initially deduced to be most likely due to a change in the state of the IL when passing through its melting point transition, which would significantly reduce the restrictions on the IL molecular

motion. However, the melting point of IL **20** was measured to be 99–101 °C and was thus unable to confirm this hypothesis. A sudden break in the constant increase in ϵ' with increasing temperature has previously been observed in the literature for ILs and was attributed to be caused by a sudden change in IL structure or the physicochemical interactions between the ions.¹² There is a slight decrease in ϵ' for IL **20** between 115 and 120 °C at 910 and 2470 MHz. This is potentially due to a change in the relaxation characteristics of the IL as the temperature increases, as respective relaxation times are temperature dependent.²⁵

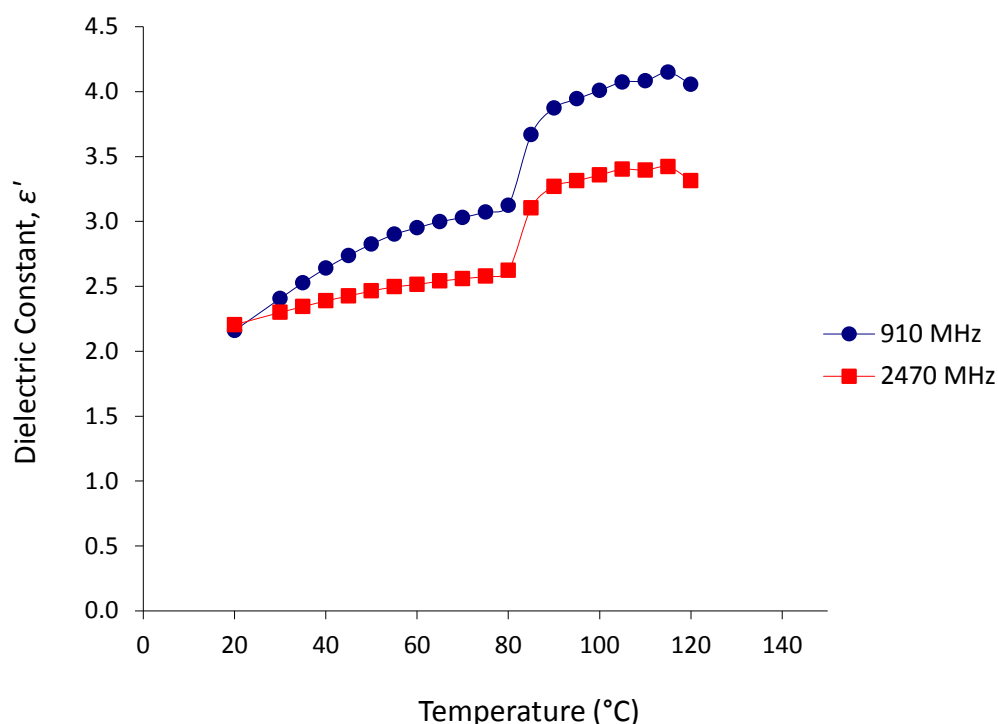


Figure 4.9 Variation in ϵ' of IL **20** at 910 and 2470 MHz over the temperature range 20–120 °C using the cavity perturbation technique.

The ϵ'' of IL **20** remains constant until 80 °C where it increases at both 910 and 2470 MHz (Figure 4.10). This increase was once again postulated to be due to sudden change in IL structure or the physicochemical interactions between the ions,¹² resulting in an increased capacity of the IL to turn stored energy to heat. The highest ϵ'' measured is 0.75 at 120 °C and 910 MHz.

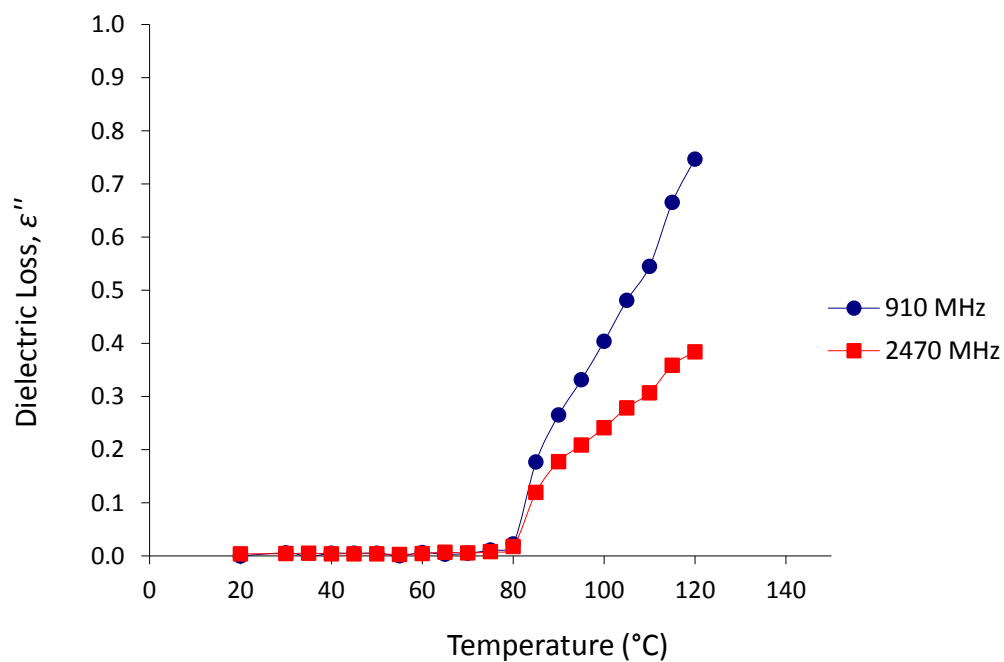


Figure 4.10 Variation in ϵ'' of IL **20** at 910 and 2470 MHz over the temperature range 20–120 °C using the cavity perturbation technique.

The $\tan \delta$ of IL **20** remains constant until 80 °C where it increases at both 910 and 2470 MHz (Figure 4.11). This increase was once again postulated to be due to sudden change in IL structure or the physicochemical interactions between the ions.¹² The highest $\tan \delta$ measured is 0.18 at 120 °C and 910 MHz.

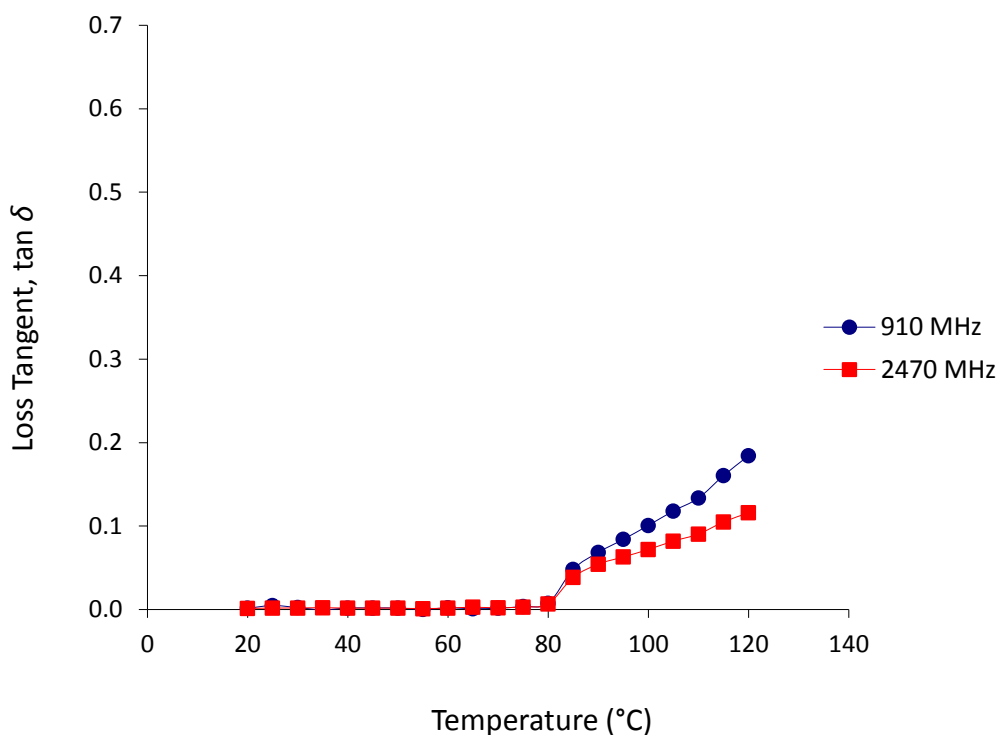


Figure 4.11 Variation in $\tan \delta$ of IL **20** at 910 and 2470 MHz over the temperature range 20–120 °C using the cavity perturbation technique.

The high temperature dielectric measurements for IL **23** were undertaken between 20 °C and 105 °C. It can be seen that as the temperature increases from 20 to 105 °C the ϵ' of IL **20** decreases, more significantly at 910 MHz (Figure 4.12). This is the opposite behaviour to that which was observed for IL **20**, where ϵ' was seen to increase with increasing temperature. However, ϵ' has been shown to decrease with temperature in solvents with high dielectric constants (e.g. water, acetonitrile, ethanol etc.).²⁸ There was an increase in the ϵ' observed at 90 °C, which decreased rapidly at 95 °C and increased again at 100 °C at 910 and 2470 MHz. This was postulated to be due to a breakdown of the IL during the measurements. However, with the melting point of IL **20** being above this temperature at 112–113 °C this was deemed unlikely. Sudden changes in the IL structure or the physicochemical interactions between the ions under microwave irradiation at this temperature may again be the reason for this observation.¹² Further analysis to obtain thermal degradation data on IL **23** (TGA) would help to aid an understanding of this result.

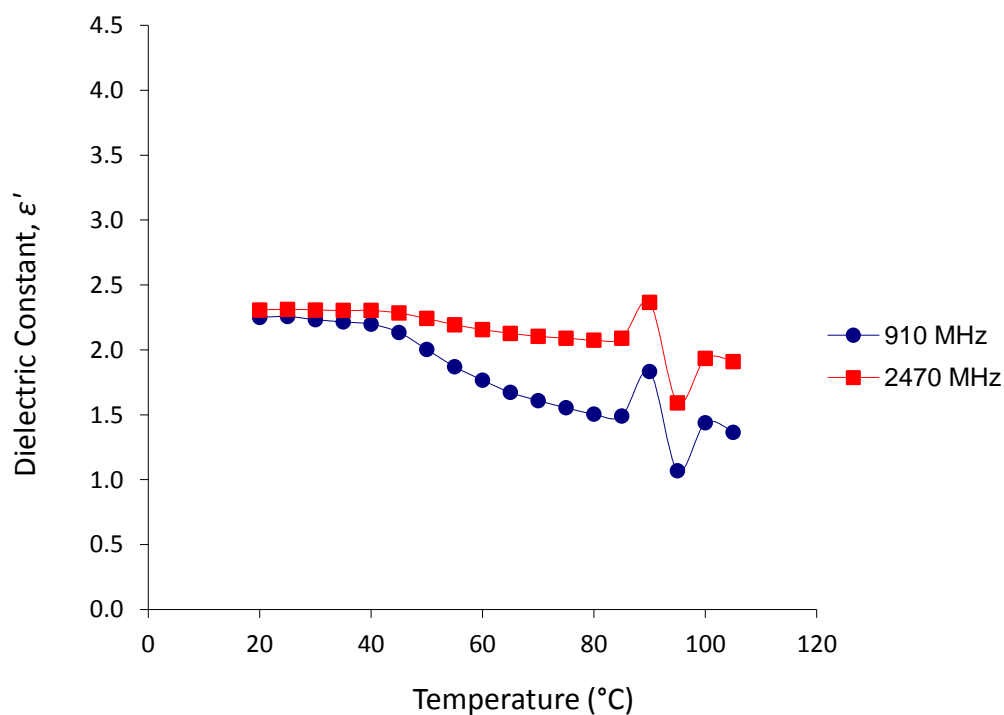


Figure 4.12 Variation in ϵ' of IL **23** at 910 and 2470 MHz over the temperature range 20–105 °C using the cavity perturbation technique.

The ϵ'' of IL **23** remains constant and zero until 80 °C where it increases at both 910 and 2470 MHz (Figure 4.13). This is the same change at the same temperature as was observed for IL **20**, and is once again postulated to be due to sudden change in IL structure or the physicochemical interactions between the ions,¹² resulting in an increased capacity of the IL to turn stored energy to heat. The ϵ'' are lower than were measured for IL **20** with the highest ϵ'' measured being 0.37 at 100 °C and 910 MHz.

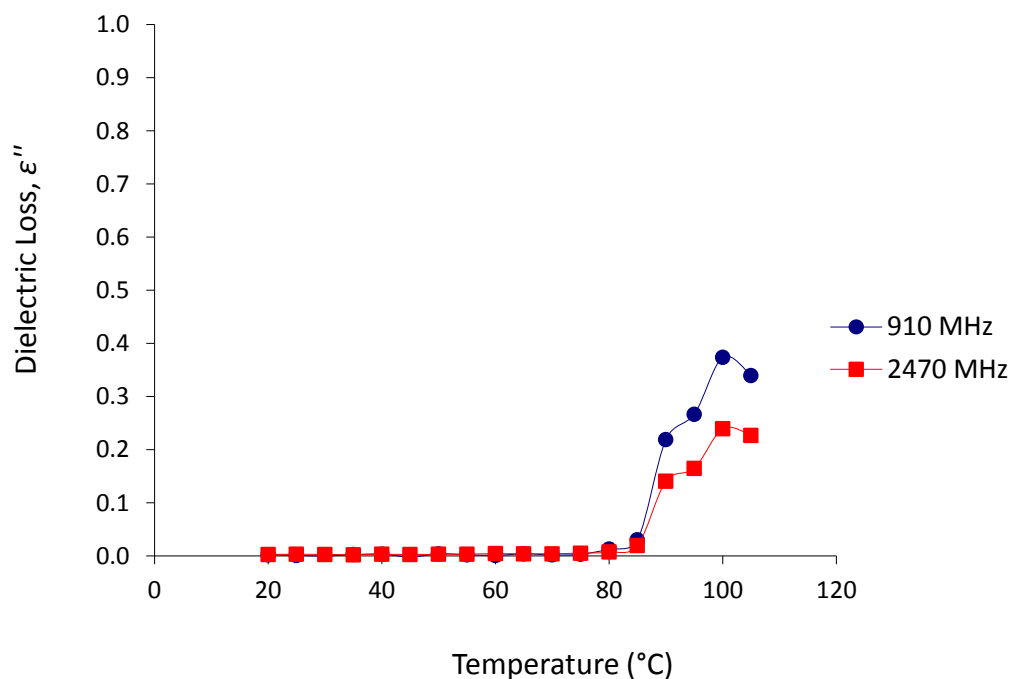


Figure 4.13 Variation in ϵ'' of IL **23** at 910 and 2470 MHz over the temperature range 20–105 °C using the cavity perturbation technique.

The $\tan \delta$ of IL **23** remains constant until 80 °C where it increases at both 910 and 2470 MHz (Figure 4.14). This increase was once again postulated to be due to sudden change in IL structure or the physicochemical interactions between the ions.¹² There is a slight decrease in $\tan \delta$ at 105 °C. This may be due to a decrease in the resistance to molecular movement, caused by a reduction in the IL viscosity as the temperature increases, meaning less energy is dissipated as heat.¹⁸ The highest $\tan \delta$ measured is 0.26 at 100 °C and 910 MHz.

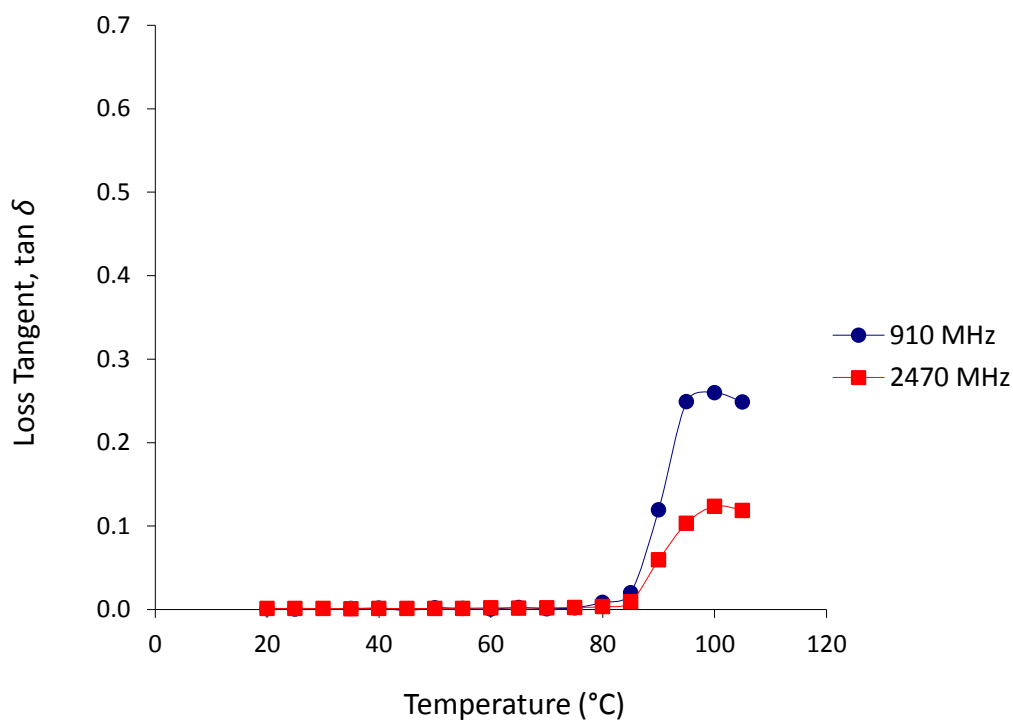


Figure 4.14 Variation in $\tan \delta$ of IL **23** at 910 and 2470 MHz over the temperature range 20–105 °C using the cavity perturbation technique.

It is interesting to note that the sudden changes in IL dielectric properties are observed at 80 °C for both mandelic acid ILs **20** and **33**. One suggestion is that a specific structural change that is taking place at 80 °C for both the ILs that is specifically related to the change in the dielectric properties. A more detailed study would be required to investigate this observation further.

4.2.3.2 1-Methylimidazolium Ester ILs

For the 1-methylimidazolium IL **50** the ϵ' increases as the temperature increases from 20 to 120 ° for both 910 and 2740 MHz (Figure 4.15). A maximum ϵ' of 15.64 and 11.55 at 120 °C are recorded at 910 and 2470 MHz respectively. This increase is caused by a decrease in the amount/strength of the intermolecular interactions of the IL at higher temperatures.²⁵ This causes an increase in the interaction of the ILs electronic structure with the electric field, causing the increase observed in the ϵ' .

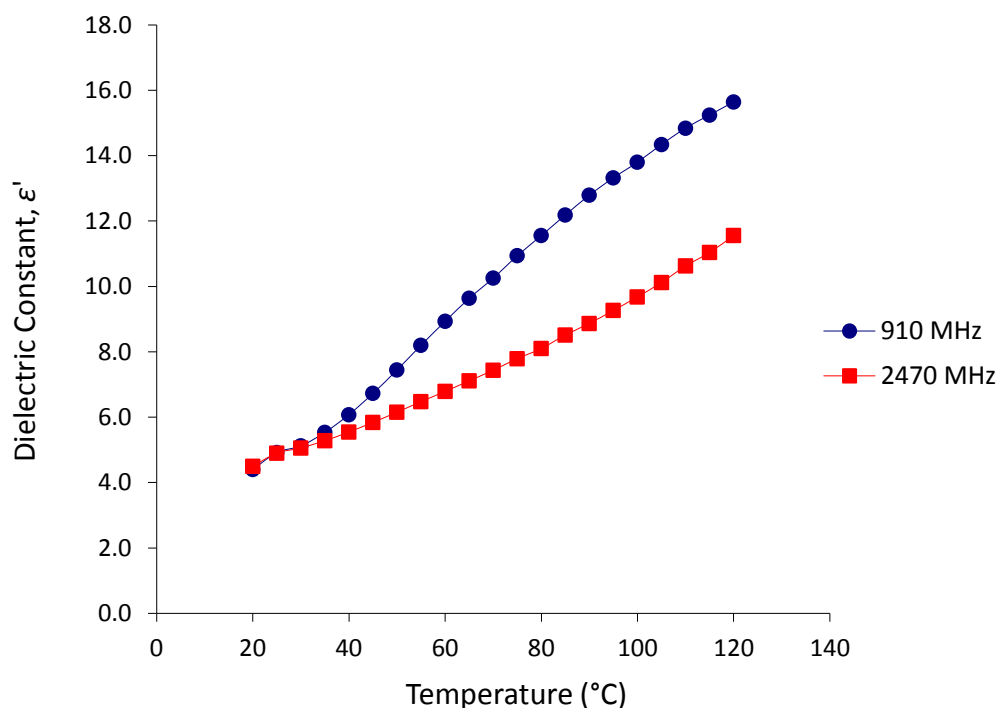


Figure 4.15 Variation in ϵ' of IL **50** at 910 and 2470 MHz over the temperature range 20–120 °C using the cavity perturbation technique.

For IL **50** at both 910 and 2740 MHz the ϵ'' increases initially as the temperature increases (Figure 4.16). This increase is consistent at 2470 MHz and continues to reach a maximum ϵ'' of 6.51 at 120 °C. However, at 910 MHz there is a decrease in ϵ'' at 90 °C which continues to decrease until 120 °C. This is postulated to be caused by a decrease in the viscosity/density of the IL as the temperature increases above 85 °C at 910 MHz, which causes a decrease in the intermolecular interactions of the IL.²⁵ Consequently, less energy is dissipated as heat and the ϵ'' decreases as a result.¹⁸

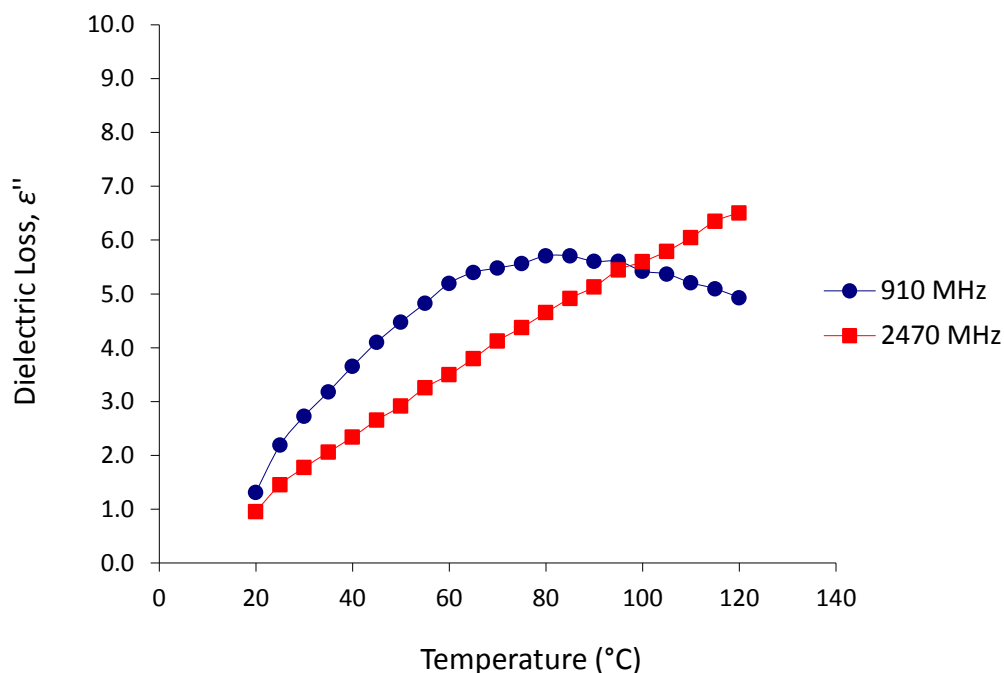


Figure 4.16 Variation in ϵ'' of IL 50 at 910 and 2470 MHz over the temperature range 20–120 °C using the cavity perturbation technique.

There were differing observations for the $\tan \delta$ of IL **50** at 910 and 2470 MHz (Figure 4.17). Initially, at both frequencies the $\tan \delta$ increases; however, it appears to reach a plateau at 80 °C at 2470 MHz with an approximate $\tan \delta$ of 0.58. This is not observed at 910 MHz where $\tan \delta$ reaches a maximum of 0.61 at 45 °C and continues to decrease after this point to 0.32 at 120 °C. This decrease is likely due to a decrease in the resistance to molecular movement caused by a reduction in the IL viscosity as the temperature increases, meaning less energy is dissipated as heat.¹⁸ The decomposition of IL **50** is much higher than the temperature of the observed decrease in $\tan \delta$ ($T_{\text{start}} = 284$ °C) thus it is not likely that the decrease observed is due to mass loss caused by IL breakdown.

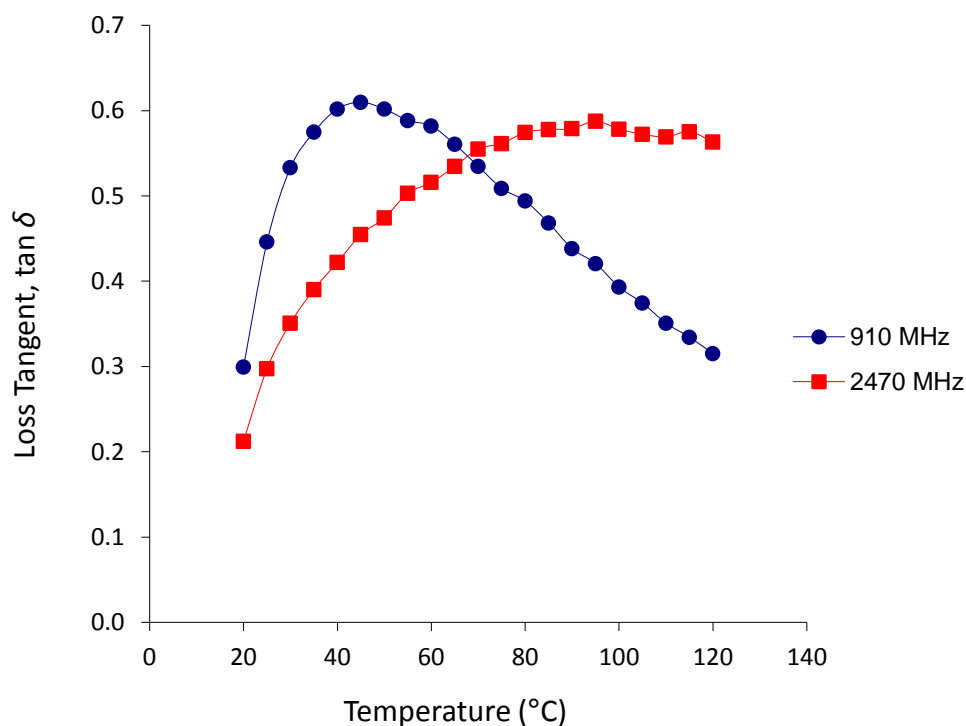


Figure 4.17 Variation in $\tan \delta$ of IL **50** at 910 and 2470 MHz over the temperature range 20–120 °C using the cavity perturbation technique.

4.3 Conclusion

The highest ϵ' for the mandelic acid ILs **18–20** and **22–25** at room temperature were recorded for IL **23** with dielectric constants of 2.26 and 2.30 at 910 and 2470 MHz respectively. The ϵ' of the ILs were very similar at both frequencies and increased as the length of the ester alkyl chain increased from ethyl to butyl. All the mandelic acid ILs had zero ϵ'' and $\tan \delta$ at room temperature as all the ILs are in a solid state and have restricted molecular motion.. At higher temperatures the mandelic acid ILs **20** and **23** are able to absorb microwave energy and ϵ'' and $\tan \delta$ increases as a result. A maximum $\tan \delta$ was measured for IL **20** of 0.18 at 910 MHz.

The 1-methylimidazolium ester ILs **49–51** have very promising dielectric properties with high dielectric properties observed at room temperature, with a maximum ϵ'' observed for IL **50** of 5.79 at 910 MHz and for IL **51** of 5.57 at 2470 MHz. The 1-methylimidazolium ester ILs **49–51** are liquid at room temperature and thus are able to absorb microwave energy to an appreciable degree at room temperature, with non-zero ϵ'' and $\tan \delta$ measured as a result. During the high temperature experiment of IL **50** ϵ'

increased as the temperature increased to reach a maximum of 15.64 at 120 °C and 910 MHz. The maximum $\tan \delta$ of 0.61 for IL **50** was reached at 45 °C at 910 MHz.

Despite this work not reporting on the static dielectric constants of the ILs, and thus not being directly comparable to previous studies,¹⁹ the results obtained herein provide a clear insight into the complex relationship between the dielectric properties of the ILs and both frequency and temperature. Necessary preliminary data has been collected to enable further informed studies on dielectric properties of ILs to be carried out using the cavity perturbation technique. A greater understanding of how IL structures influence their dielectric properties can thus be obtained, facilitating the targeted design of high polarity ILs for applications in extractions, dissolution and synthetic chemistry both with and without microwave irradiation.

4.4 Future Work

It would be of great interest to further investigate the dielectric properties of the mandelic acid ILs **18–20** and **22–25**. To try and exploit the maximum dielectric potential of the ILs, it is proposed that examples of mandelic acid ILs with DCA and NTf₂ anions should be investigated. DCA and NTf₂ examples of the mandelic acid ILs (**63–66**) would likely have lower melting points, with the potential to be liquid at room temperature, as it is widely known that DCA and NTf₂ ILs often have lower melting points than the corresponding halide ILs.²⁹ The reduction in IL melting point would ideally give a much larger window for the dielectric properties of the ILs to be measured, thus enabling higher dielectric properties at lower temperatures to be recorded. This would increase the potential of the mandelic acid ILs to be used as reaction solvents both with and without microwaves. Reactions with the ILs could be carried out at lower temperatures to achieve the same dielectric constant, making them applicable to a wider range of reactions (e.g. temperature sensitive reactions).

Before further dielectric measurements are carried out, it would be beneficial to investigate into the thermal decomposition temperatures of the mandelic acid ILs **18–20** and **22–25**. With this information the high temperature experiments could be carried out to the maximum possible temperature. This would enable the highest amount of dielectric data for the processing range of the ILs to be obtained. It would be highly undesirable for the IL to break down during the temperature ramp and whilst in the cavity as the ILs pyrolysis products may contaminate the cavity.

4.5 References

1. A. Baiano, *Molecules*, 2014, **19**, 14821.
2. C. Wakai, A. Oleinikova, M. Ott and H. Weingärtner, *J. Phys. Chem. B*, 2005, **109**, 17028.
3. R. Martinez-Palou, *J. Mex. Chem. Soc.*, 2007, **51**, 252.
4. N. Tarasova, A. Zanin, K. Burdakov and P. Sobolev, *Polym. Adv. Technol.*, 2015, **26**, 687.
5. N. E. Leadbeater, H. M. Torenus and H. Tye, *Comb. Chem. High Throughput Screening*, 2004, **7**, 511.
6. X. Liu, Y. Wang, J. Kong, C. Nie and X. Lin, *Analytical Methods*, 2012, **4**, 1012.
7. H. Guolin, S. Jeffrey, Z. Kai and H. Xiaolan, *J. Anal. Methods Chem.*, 2012, **2012**, 1.
8. A. Delazar, L. Nahar, S. Hamedeyazdan and S. Sarker, in *Natural Products Isolation*, ed. S. D. Sarker and L. Nahar, Humana Press, New Jersey, 2012, vol. 864, ch. 5, pp. 89-115.
9. R. P. Swatloski, S. K. Spear, J. D. Holbrey and R. D. Rogers, *J. Am. Chem. Soc.*, 2002, **124**, 4974.
10. M. Smiglak, J. M. Pringle, X. Lu, L. Han, S. Zhang, H. Gao, D. R. MacFarlane and R. D. Rogers, *Chem. Commun. (Cambridge, U. K.)*, 2014, **50**, 9228.
11. D. Rochefort, in *Functional Materials: For Energy, Sustainable Development and Biomedical Sciences*, eds. M. Leclerc and R. Gauvin, Walter de Gruyter GmbH, 2014, ch. 9, pp. 189–206, DOI: 10.1515/9783110307825.189
12. C. Petra, G. Attila, B. Katalin and G. László, in *Ionic Liquids - Classes and Properties*, ed. S. Handy, InTech, Croatia, 2012, ch. 9, pp. 187-208.
13. M. Huang, PhD Thesis, Ruhr University Bochum, 2011.
14. Z. Ahmad, in *Dielectric Material*, ed. M. A. Silaghi, InTech, 2012, ch. 1, pp. 3-26, DOI: 10.5772/50638
15. M. T. Jilani, M. Z. u. Rehman, A. M. Khan, M. T. Khan and S. M. Ali, *Int. J. Inf. Technol. Electr. Eng.*, 2012, **1**, 1.
16. R. Sorrentino and G. Bianchi, in *Microwave and RF engineering*, John Wiley & Sons, Inc, Singapore, 2010, vol. 1, ch. 2, pp. 9-38.
17. O. Tereshchenko, F. Buesink and F. Leferink, presented in part at the XXXth URSI General Assembly and Scientific Symposium, Istanbul August, 2011.

18. A. D. Smith, E. H. Lester, K. J. Thurecht, S. W. Kingman, J. El Harfi, G. Dimitrakis, J. P. Robinson and D. J. Irvine, *Ind. Eng. Chem. Res.*, 2010, **49**, 3011.
19. M.-M. Huang, Y. Jiang, P. Sasisanker, G. W. Driver and H. Weingärtner, *J. Chem. Eng. Data*, 2011, **56**, 1494.
20. R. Sorrentino and G. Bianchi, in *Microwave and RF engineering*, John Wiley & Sons, Inc, Singapore, 2010, vol. 1, ch. 1, pp. 1-8.
21. B. Schumacher, H.-G. Bach, P. Spitzer and J. Obrzut, in *Springer Handbook of Materials Measurement Methods*, ed. H. Czichos, T. Saito and L. Smith, Springer-Verlag, Berlin, 2006, ch. 9, pp. 431-484.
22. H. Weingärtner, A. Knocks, W. Schrader and U. Kaatze, *J. Phys. Chem. A*, 2001, **105**, 8646.
23. H. Weingärtner, *Z. Phys. Chem.*, 2006, **220**, 1395.
24. C. Daguenet, P. J. Dyson, I. Krossing, A. Oleinikova, J. Slattery, C. Wakai and H. Weingärtner, *J. Phys. Chem. B*, 2006, **110**, 12682.
25. M. J. Kamaruddin, N. T. Nguyen, G. A. Dimitrakis, J. El Harfi, E. R. Binner, S. W. Kingman, E. Lester, J. P. Robinson and D. J. Irvine, *RSC Adv.*, 2014, **4**, 5709.
26. A. Delgado, M. F. García-Sánchez, J.-C. M'Peko, A. R. Ruiz-Salvador, G. Rodríguez-Gattorno, Y. Echevarría and F. Fernández-Gutierrez, *J. Chem. Educ.*, 2003, **80**, 1062.
27. J. G. Huddleston, A. E. Visser, W. M. Reichert, H. D. Willauer, G. A. Broker and R. D. Rogers, *Green Chem.*, 2001, **3**, 156.
28. P. Lidstrom, J. Tierney, B. Wathey and J. Westman, *Tetrahedron*, 2001, **57**, 9225.
29. C. P. Fredlake, J. M. Crosthwaite, D. G. Hert, S. N. V. K. Aki and J. F. Brennecke, *J. Chem. Eng. Data*, 2004, **49**, 954.

5.0 Conclusion and Future Work

5.1 Conclusion

A series of ten bromide ILs (**16–25**) derived from mandelic acid was synthesised with different structural moieties (various alkyl chain lengths, ester/amide moieties and various *N*-heterocycle headgroups) to facilitate an investigation into their effect on IL toxicity and biodegradation. The results showed that the majority of the ILs have low toxicity towards the Gram-positive bacterial strain and four Gram-negative bacterial strains screened at high IL concentrations. IL toxicity was shown to increase with increasing alkyl chain length, with methyl ester < ethyl ester < butyl ester/amide. None of the ILs demonstrated high toxicity to the three CCM strains and the five clinical isolates screened at low IL concentrations. Moderate toxicity was observed for the 1-methylimidazolium ethyl ester IL (**18**) against several bacterial strains screened. Also, none of the ILs demonstrated high toxicity to the four ATCC strains and eight clinical isolates of yeasts screened.

Biodegradation studies of the mandelic acid ILs (**16–25**) in the CBT showed that the 3-(ethoxycarbonyl)pyridinium butyl ester IL (**23**) had the highest level of biodegradation, with the 1-methylimidazolium butyl amide IL (**24**) showing no biodegradation under the test conditions. The amide ILs **24** and **25** showed none to very poor levels of biodegradation in the CBT. The butyl ester ILs had an increased biodegradation in the headgroup order pyridinium < 3-methoxypyridinium < 1-methylimidazolium < 3-(ethoxycarbonyl)pyridinium. Biodegradation of the ILs was proposed to proceed through ester alkyl chain biodegradation to a carboxylic acid derivative. This conclusion is based on previous results found in the literature, and was reinforced by carrying out a comparison of a predicted theoretical ester/amide biodegradation calculation to the results obtained in the CBT.

Plasticisation of PLLA with 1-methylimidazolium ester ILs with NTf₂ (**50–53**) and OctSO₄ (**54–56**) anions was undertaken to increase the ductility of PLLA and overcome the effect of physical ageing. The results showed that NTf₂ ILs **50–53** have a significant plasticising effect on PLLA at 20 and 30 wt%, with the elongation at break increased by two orders of magnitude. PLLA plasticised with 20 wt% IL **51** gave the most promising results with an elongation at break of more than 500 %, a Young's modulus of 1103 MPa and a tensile strength of 32 MPa. A significant depression of the T_g for

PLLA/IL**50–53** was observed. However, plasticisation of PLLA with 10 wt% NTf₂ ILs **50–53** appeared to have an antiplasticising effect, with a decrease in the elongation at break observed compared to neat PLLA. The OctSO₄ ILs **54–56** appeared to be incompatible with PLLA, where an antiplasticising effect was observed for PLLA/IL**54** with 20 and 30 wt% IL, PLLA/IL**55** with 10 wt% IL and PLLA/IL**56** with 10, 20 and 30 wt% IL. Any plasticising effects observed with the OctSO₄ ILs **54–56** were minimal compared to those observed for the NTf₂ ILs.

Plasticisation of PLLA with NTf₂ ILs **50–53** was shown in all cases to significantly reduce the ageing rate of PLLA, with several ILs showing a very minimal ageing effect over 100 days, especially PLLA/IL**50** and PLLA/IL**51** with 20 wt% IL. During ageing the Young's modulus appeared to be ageing to an equilibrium state for each IL (**50–53**), and the tensile strength appeared to be ageing to an equilibrium state for each wt% of IL (**50–53**). The thermal stability of PLLA/IL**52** with 30 wt% IL showed that IL **52** had very little effect on the thermal stability of PLLA.

Dielectric properties of the mandelic acid ILs **18–20** and **22–25** and 1-methylimidazolium ester ILs **49–51** were measured using a cavity perturbation technique at 910 and 2470 MHz. At room temperature the mandelic acid ILs **18–20** and **22–25** are all in a solid state and have restricted molecular motion and consequently have zero ϵ'' and $\tan \delta$ values. Mandelic acid IL **23** gave the highest ϵ' values at room temperature, of 2.26 and 2.30 at 910 and 2470 MHz respectively. Very similar ϵ' at both frequencies were recorded for ILs **18–20** and **22–25**, which increased as the length of the ester alkyl chain increased from ethyl to butyl. During the high temperature experiments the mandelic acid ILs **20** and **23** were able to absorb microwave energy and thus had non-zero ϵ'' and $\tan \delta$. A maximum $\tan \delta$ was measured for IL **20** of 0.18 at 910 MHz.

The dielectric properties of the 1-methylimidazolium ester ILs **49–51** at room temperature were very promising, with a maximum ϵ'' observed for IL **50** of 5.79 at 910 MHz and for IL **51** of 5.57 at 2470 MHz. At room temperature the ILs were able to absorb microwave energy to an appreciable degree due to being in a liquid state. During the high temperature experiment of IL **50** ϵ' increased as the temperature increased to reach a maximum of 15.64 at 120 °C and 910 MHz. The maximum $\tan \delta$ of 0.61 for IL **50** was reached at 45 °C at 910 MHz.

A clear insight into the complex relationship between the dielectric properties of the ILs and both frequency and temperature have been gained through this work. Preliminary data on the dielectric properties of the mandelic acid ILs **18–20** and **22–25** and 1-methylimidazolium ester ILs **49–51** was collected and will allow further informed studies on dielectric properties of ILs to be carried out using the cavity perturbation technique.

In conclusion, a series of ten bromide ILs (**16–25**) derived from mandelic acid was synthesised and demonstrated low toxicity to the bacterial strains screened, with all ILs showing no high toxicity to the fungal strains screened. This work successfully satisfied the 7th principle of green chemistry (use of renewable feedstocks) by utilising mandelic acid for the synthesis of the ILs (**16–25**). The 4th principle of green chemistry (designing safer chemicals) was also successfully fulfilled as all the ILs (**16–25**) presented with low bacterial toxicity and no high fungal toxicity to all the strains screened against. Biodegradation of the ILs in the CBT was concluded to proceed through ester alkyl chain biodegradation to a carboxylic acid derivative, and has highlighted the relevance of considering biodegradation breakdown products (metabolites) in future studies. Despite designing the synthesis of the ILs with the aim of achieving high biodegradation, and thus satisfying the 10th principle of green chemistry, none of the ILs reached the threshold of > 60 % biodegradation in 28 days in the CBT and thus cannot be classed as readily biodegradable. Plasticisation of PLLA with 1-methylimidazolium NTf₂ ILs (**50–53**) showed a significant plasticising effect on PLLA and in all cases significantly reduced the ageing rate compared to pure PLLA. Investigation into the dielectric properties of the mandelic acid ILs **18–20** and **22–25** and 1-methylimidazolium ester ILs **49–51** demonstrated the complex relationship between dielectric properties and both frequency and temperature, paving the way for future in-depth studies in this area.

5.2 Future Work

Further work on the mandelic acid bromide ILs (**16–25**) will involve a study targeted at the detection of the biodegradation metabolites by LCMS/MS, and an evaluation of their toxicity. Structural modification of the ILs could be undertaken with the aim of increasing the biodegradability of the ILs to fully satisfy the 10th principle of green chemistry (designing for degradation). Further synthesis and evaluation for aqueous stability, antimicrobial activity and biodegradation of the monofluoro mandelic acid IL

(37), and future synthesised candidates, is also anticipated. It is proposed that the mandelic acid ILs (16–25) will be used in relation to the overarching theme of this work, which is towards synthesis of low toxicity biodegradable ILs with applications in materials science.

To further investigate the plasticising effect of the 1-methylimidazolium ester ILs (50–56) on PLLA, the morphology of the PLLA/IL films could be studied using field emission scanning electron microscopy (FESEM). With this technique, a comparison of the morphology of the neat PLLA film to the plasticised PLLA films could be carried out. Also by comparing FESEM micrographs of PLLA plasticised with OctOSO₄ ILs to PLLA plasticised with NTf₂ ILs the effect of IL miscibility on film morphology could be examined. Any phase separation in the PLLA/IL films containing OctOSO₄ ILs could be identified, and any defects caused by the plasticisation would also be detected. By comparing aged and non-aged PLLA/IL films, changes in the morphology of the films during ageing could be studied. Literature data shows that the plasticisation of PLA with ILs can increase the hydrolytic degradation of PLA.¹ Thus, it would be very interesting to investigate to what extent the ILs studied herein affect the biodegradation of PLLA.

It is clear from the work carried out on the plasticisation of PLLA with ILs (50–56) that the level of plasticisation is greatly dependent on the IL anion. Thus, investigation into the use of the dicyanamide (DCA) anion with the same series of cations employed herein, as ILs for plasticisation of PLLA, is proposed. Literature data shows that these ILs would be liquid at room temperature² with the potential to have low viscosity³ and a thermal stability above 200 °C.^{4,5} They also demonstrated low antimicrobial activity.² If the proposed 1-methylimidazolium DCA ILs have suitable thermal stability to withstand the PLLA plasticisation process, it is hoped that they would give promising results as plasticisers as they would be an attractive alternative to the NTf₂ ILs as they do not contain any fluorine. Also, when comparing the cost of the starting materials used to synthesise the ILs, sodium dicyanamide is cheaper than lithium bistriflimide, which will result in a cheaper synthesis for the DCA ILs making them more attractive to industry.

It would be of great interest to further investigate the dielectric properties of the mandelic acid ILs 18–20 and 22–25. With the aim of exploiting the maximum dielectric

potential of the ILs, it is proposed that examples of mandelic acid ILs with DCA and NTf₂ anions should be investigated. Four mandelic acid ILs have been suggested for this purpose (Figure 5.1).

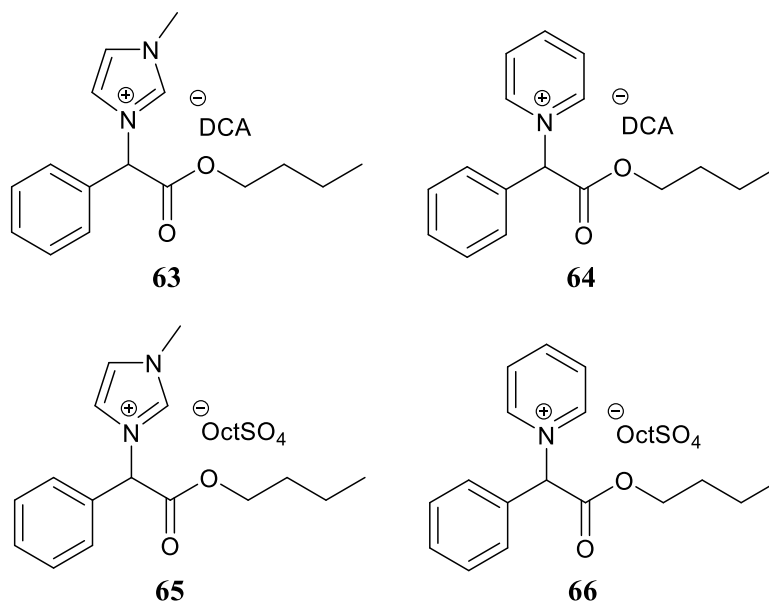


Figure 5.1 Suggested mandelic acid ILs (**63–66**) with DCA and OctSO₄ anions for further investigation into the dielectric properties of ILs.

DCA and NTf₂ examples of the mandelic acid ILs **63–66** would be likely to have lower melting points, with the potential to be liquid at room temperature, as it is widely known that DCA and NTf₂ ILs often have lower melting points than the corresponding halide ILs.⁵ The reduction in IL melting point would ideally give a much larger window for the dielectric properties of the ILs to be measured, thus enabling higher dielectric properties at lower temperatures to be recorded. This would increase the potential of the mandelic acid ILs to be used as reaction solvents both with and without microwaves. The desired dielectric constants could be reached at lower temperatures, making them applicable to a wider range of reactions (e.g. temperature sensitive reactions). Using these ILs would also satisfy the 6th principle of green chemistry (design for energy efficiency) as reactions could be undertaken at lower temperatures. Mandelic acid ILs that are liquid at RT would also be of interest to investigate for the plasticisation of PLLA (see chapter 2).

Before further dielectric measurements are undertaken, an investigation into the thermal decomposition temperatures of the mandelic acid ILs **18–20** and **22–25** would be beneficial. The high temperature experiments could then be carried out to the maximum

possible temperature. This would enable the highest amount of dielectric data for the processing range of the ILs to be obtained. It would be highly undesirable for the IL to break down during the temperature ramp and whilst in the cavity, as the ILs pyrolysis products may contaminate the cavity.

5.3 References

1. K. I. Park and M. Xanthos, *Polym. Degrad. Stab.*, 2009, **94**, 834.
2. S. Morrissey, B. Pegot, D. Coleman, M. T. Garcia, D. Ferguson, B. Quilty and N. Gathergood, *Green Chem.*, 2009, **11**, 475.
3. D. R. MacFarlane, J. Golding, S. Forsyth, M. Forsyth and G. B. Deacon, *Chem. Commun. (Cambridge, U. K.)*, 2001, 1430.
4. D. R. MacFarlane, S. A. Forsyth, J. Golding and G. B. Deacon, *Green Chem.*, 2002, **4**, 444.
5. C. P. Fredlake, J. M. Crosthwaite, D. G. Hert, S. N. V. K. Aki and J. F. Brennecke, *J. Chem. Eng. Data*, 2004, **49**, 954.

6.0 Experimental

6.1 Introduction

6.1.1 Chemicals

The majority of chemicals were purchased from Sigma Aldrich, with the exception of lithium bis(trifluoromethanesulfonyl) imide (LiNTf_2) which was purchased from Solvionic and sodium octyl sulfate (NaOctSO_4) which was purchased from Alfa Aesar. Pyridine (99.8 %), bromoacetyl bromide (≥ 98 %), thionyl chloride (≥ 99 %) and thionyl bromide (97 %) were used without further purification. 1-methylimidazole (99 %) was distilled before use. Methanol and ethanol were pre-dried with magnesium sulphate and subsequently 3 Å molecular sieves. *n*-Butanol was dried over molecular sieves and used without further purification. THF was dried over sodium/benzophenone ketyl and was distilled before use. DCM was dried over calcium hydride, and distilled before use. Sodium carbonate (Na_2CO_3) and magnesium sulphate heptahydrate ($\text{MgSO}_4 \cdot 7\text{H}_2\text{O}$) were obtained from Riedel de Haën and Fluka respectively. Riedel de Haën silica gel was used for flash and thin layer chromatography. Commercial grade PLLA 1010 (> 99% L-isomer) was supplied by Synbra Technology in pellet form. Weight-average molecular weight and polydispersity were $127400 \text{ g mol}^{-1}$ and 1.83 respectively, as determined by GPC using polystyrene standards. The glass transition, crystallisation and melting temperature were 58, 100 and 175 °C respectively, as measured by DSC. Compound **61** was available within the group from stock.

6.1.2 NMR Analysis

All the NMR analysis was undertaken using a Bruker AC 400 MHz spectrometer operating at 400 MHz for ^1H NMR and 101 MHz for ^{13}C NMR, in deuterated chloroform (99.8 % D) or DMSO- d_6 (99.8 % D). Chemical shifts are reported in parts per million (ppm) relative to the internal standard (TMS) and coupling constants (J) are reported in Hertz (Hz). When stating peak multiplicity the following abbreviations are used; s – singlet, bs – broad singlet, d – doublet, t – triplet, q – quartet, dd – doublet of doublets, dt – doublet of triplets, dq – doublet of quartets, tt – triplet of triplets, tq – triplet of quartets, ddd – doublet of doublet of doublets, ddt – doublet of doublet of triplets, dtd – doublet of triplet of doublets and m – multiplet. NMR assignment was assisted by 2D NMR spectroscopy (^1H - ^1H COSY, ^1H - ^{13}C HMQC and ^1H - ^{13}C HMBC).

6.1.3 IR Analysis

All IR analysis was carried out on a Perkin Elmer 100 FT-IR spectrum GX spectrometer with a Thermo Scientific iD5 Diamond ATR attachment.

6.1.4 Melting Points

All melting points (uncorrected) were obtained using a Stuart SMP40 Melting Point Apparatus and the values are expressed in degrees Celsius (°C).

6.1.5 Mass Spectrometry

High resolution mass spectrometry (HRMS) was obtained in the ABCRF Mass Spectrometry Laboratory in University College Cork (UCC) using a Waters Micromass LCT Premier mass spectrometer (KD 160). The analysis was performed in ESI+ mode with an external reference standard of leucine enkephalin. A sulfadimethoxine concentration test was performed to ensure peak accuracy in the ion count range 1×10^3 to 1×10^6 .

6.1.6 Thermogravimetric Analysis

Thermogravimetric analysis (TGA) was obtained in ETH Zurich using a Mettler Toledo TGA/SDTA 851e instrument (Mettler Toledo, Switzerland). TGA thermograms were recorded under N₂ at a heating rate of 10 K min⁻¹, with an average sample weight of ca 10 mg. Alumina pans were used for all TGA carried out.

6.1.7 Melt Extrusion

Melt extrusion was carried out in ETH Zurich using a co-rotating twin-screw extruder (Eindhoven University of Technology, Netherlands) under N₂ at 200 °C and 100 rpm for approximately 10 min. Films with a thickness of 0.5 ± 0.05 mm were prepared by melt-compressing the compounded PLLA/IL blends of various ratios at 200 °C, under ca 5 kN force in a hot-press (Rondol Technology), followed by quenching to room temperature in a cold press (Rondol Technology). To ensure consistency in the film thickness, a rectangular steel spacer was used.

6.1.8 Film Casting

Films were made in ETH Zurich using a hot press (Rondol Technology) and a cold press. (Rondol Technology).

6.1.9 Tensile Testing

Mechanical characteristics were investigated using an Instron 5864 Mechanical Testing Equipment. The measurements were performed using the compression moulded films cut into dumbbell-shaped specimens with a gauge length of 12.7 mm, at an extension rate of 5 mm min⁻¹ or 0.007 s⁻¹. Samples were initially tested on the same day as melt extrusion and film formation (day 0). Samples were stored in polyethylene bags at rt between the ageing tests, which were carried out on day 4 for the PLLA films and on day 1, 10 and 100 for the PLLA/IL films. For each sample a minimum of three specimens were tested with the mean average of the values reported herein.

6.1.10 Differential Scanning Calorimetry

Differential scanning calorimetry (DSC) measurements were carried out in ETH Zurich using a DSC822e instrument (Mettler Toledo, Switzerland). DSC calorigrams were recorded under N₂ purge at standard heating and cooling rates of 10 K min⁻¹, with a sample weight of 5–10 mg. Aluminium pans were used for all DSC carried out.

6.1.11 Cavity Perturbation Apparatus^{1,2}

Dielectric property measurements were carried out in The University of Nottingham using an in house built cavity perturbation apparatus. The system consists of a cylindrical copper cavity (diameter 570 mm and height 50 mm) connected to a Hewlett Packard 8753B vector network analyser (VNA). Samples of approximately 15 mm were encased in a quartz tube of approximately 3 mm internal diameter (diameter to length ratio of 0.2–0.3) and introduced into the centre of the resonant cavity, resonating in TM_{0n0} mode. The frequency shift and change in quality factor were measured by the VNA at a resonant frequency of 910 MHz and 2470 MHz. Perturbation theory was subsequently used to determine the dielectric properties of the sample. A linear stage driven by a step motor and a furnace enabled high temperature measurements to be carried out. The temperature of the furnace was increased by 1 °C per minute, with measurements recorded every 5 °C. The sample resided in the furnace above the cavity

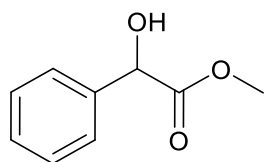
until the test temperature was reached. The sample was maintained at the test temperature for 10 min to allow the sample to equilibrate, after which the step-motor rapidly moved the sample into the cavity for testing. During the measurement the sample spent ca 3 s outside the furnace in the cavity, thus the heat loss was considered negligible. The high temperature experiments were carried out between 20–120 °C. For rt measurements the results recorded herein are an average of a minimum of four measurements.

6.2 Experimental Preparations for Mandelate ILs

6.2.1 Mandelate Esters

General Procedure A: Preparation of Mandelate Ester (26–28)

Methyl 2-hydroxy-2-phenylacetate (26)³



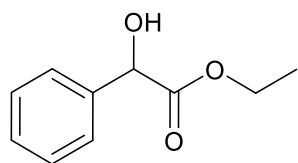
A flask was charged with mandelic acid (10.10 g, 66.38 mmol) and methanol (50 mL), under N₂. Whilst stirring and cooling in an ice bath (0 °C), thionyl chloride (2.40 mL, 33.1 mmol) was added dropwise and the reaction was stirred for 4 h at rt. TLC confirmed reaction completion. N₂ was bubbled through the reaction for 1 h. The solvent was removed, deionised water (25 mL) was added and the product extracted with ethyl acetate (3 × 25 mL). The combined organic extracts were washed with saturated aqueous sodium bicarbonate (20 mL), dried over MgSO₄, filtered and the solvent removed. The organic phase was dried under reduced pressure to give the title compound (**26**) as a white waxy solid (10.20 g, 61.38 mmol), 92 % yield.

Chemical formula: C₉H₁₀O₃; Molecular weight: 166.18 g mol⁻¹

¹H NMR (400 MHz, CDCl₃) δ 7.45–7.30 (m, 5H), 5.18 (d, *J* = 5.1 Hz, 1H), 3.77 (s, 3H), 3.44 (d, *J* = 5.1 Hz, 1H). ¹³C NMR (101 MHz, CDCl₃) δ 174.28, 138.34, 128.77, 128.67, 126.73, 73.01, 53.22.

¹H and ¹³C NMR data are in agreement with the literature.³

Ethyl 2-hydroxy-2-phenylacetate (27)⁴



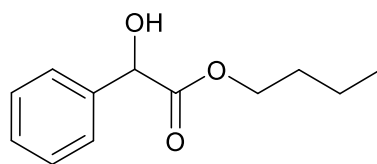
The title compound (**27**) was synthesised from mandelic acid (10.03 g, 65.92 mmol), ethanol (50 mL) and thionyl chloride (2.40 mL, 33.1 mmol) according to the general procedure A to give a colourless liquid (10.90 g, 60.49 mmol), 92 % yield.

Chemical formula: C₁₀H₁₂O₃; Molecular weight: 180.20 g mol⁻¹

¹H NMR (400 MHz, CDCl₃) δ 7.46–7.29 (m, 5H), 5.16 (d, *J* = 5.8 Hz, 1H), 4.27 (dq, *J* = 10.8, 7.1 Hz, 1H), 4.17 (dq, *J* = 10.8, 7.1 Hz, 1H), 3.51 (d, *J* = 5.8 Hz, 1H), 1.23 (t, *J* = 7.1 Hz, 3H). ¹³C NMR (101 MHz, CDCl₃) δ 173.79, 138.52, 128.67, 128.50, 126.63, 72.98, 62.36, 14.14.

¹H and ¹³C NMR data are in agreement with the literature.⁴

Butyl 2-hydroxy-2-phenylacetate (28)⁵



The title compound (**28**) was synthesised from mandelic acid (50.01 g, 328.7 mmol), *n*-butanol (250 mL) and thionyl chloride (12.0 mL, 165 mmol) according to the general procedure A to give a yellow liquid (66.68 g, 320.2 mmol), 97 % yield.

Chemical formula: C₁₂H₁₆O₃; Molecular weight: 208.26 g mol⁻¹

¹H NMR (400 MHz, CDCl₃) δ 7.46–7.39 (m, 2H), 7.39–7.28 (m, 3H), 5.16 (d, *J* = 5.8 Hz, 1H), 4.22–4.09 (m, 2H), 3.59 (bs, 1H), 1.61–1.50 (m, 2H), 1.30–1.19 (m, 2H), 0.85 (t, *J* = 7.4 Hz, 3H). ¹³C NMR (101 MHz, CDCl₃) δ 173.88, 138.55, 128.61, 128.46, 126.58, 72.94, 66.12, 30.48, 18.94, 13.65.

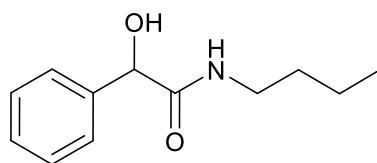
¹H and ¹³C NMR data are in agreement with the literature.⁵

6.2.2 Mandelate Amide

Preparation of Mandelate Amide (29)

N-Butyl-2-hydroxy-2-phenylacetamide (29)⁶

Coupling Procedure



A flask was charged with mandelic acid (2.08 g, 13.7 mmol) and DCM (20 mL), under N₂. Whilst stirring and cooling in an ice bath (0 °C), HOSu (1.74 g, 15.1 mmol) and EDC (2.34 g, 15.1 mmol) were added simultaneously. The reaction was stirred at 0 °C for 30 min. *n*-Butylamine (1.35 mL, 13.7 mmol) was added and the reaction was stirred for a further 15 min at 0 °C, and subsequently for 2 days at rt. TLC confirmed reaction completion. The organic phase was washed with deionised water (2 × 15 mL) and saturated aqueous ammonium chloride (20 mL). Next, the organic phase was dried over MgSO₄, filtered and the solvent removed. The crude product was purified by column chromatography (SiO₂,

EtOAc:hexane, 60:40) and dried under reduced pressure to give the title compound (**29**) as a white crystalline solid (1.29 g, 6.22 mmol), 45 % yield.

Acetyl Chloride Procedure

A flask was charged with mandelic acid (50.19 g, 329.9 mmol) and methanol (300 mL), under N₂. Whilst stirring and cooling in an ice bath (0 °C), acetyl chloride (24.0 mL, 336 mmol) was added dropwise and the reaction was stirred overnight at rt. TLC confirmed reaction completion. The solvent was removed and methanol (150 mL) was added. Whilst stirring and cooling in an ice bath (0 °C), *n*-butylamine (130 mL, 1.32 mol) was added dropwise and the reaction was left in the fridge (< 5 °C) overnight. TLC confirmed reaction completion. The solvent was removed, DCM (250 mL) was added, and the organic phase was washed with water (3 × 100 mL) and saturated aqueous ammonium chloride (100 mL). The organic phase was dried over MgSO₄, filtered and the solvent removed. The product was dried under reduced pressure to give the title compound (**29**) as a white crystalline solid (61.05 g, 294.5 mmol), 89 % yield.

Chemical formula: C₁₂H₁₇NO₂; Molecular weight: 207.27 g mol⁻¹

¹H NMR (400 MHz, CDCl₃) δ 7.41–7.29 (m, 5H), 6.12 (bs, 1H), 4.98 (s, 1H), 3.77 (bs, 1H), 3.31–3.17 (m, 2H), 1.48–1.38 (m, 2H), 1.33–1.21 (m, 2H), 0.88 (t, *J* = 7.3 Hz, 3H).

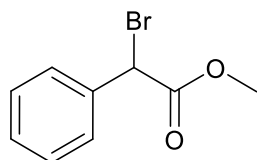
¹³C NMR (101 MHz, CDCl₃) δ 172.09, 139.66, 129.05, 128.82, 127.01, 74.25, 39.54, 31.63, 20.06, 13.83.

¹H and ¹³C NMR data are in agreement with the literature.⁶

6.2.3 Mandelate Alkylating Reagents

General Procedure B: Preparation of Mandelate Alkylating Reagent (30–33)

Methyl 2-bromo-2-phenylacetate (**30**)⁷



A flask was charged with methyl 2-hydroxy-2-phenylacetate (**26**) (18.08 g, 108.8 mmol) and dry DCM (100 mL), under N₂. Whilst stirring, triethylamine (22.8 mL, 163 mmol) was added. The reaction was cooled in an ice bath (0 °C), thionyl bromide (10.0 mL, 129 mmol) was added dropwise and the reaction was stirred overnight at rt. TLC confirmed reaction completion and N₂ was bubbled through the reaction for 1 h. The organic phase was washed with deionised water (3 × 50 mL) and the combined aqueous phase was subsequently washed with DCM (20 mL). The combined organic phase was dried over MgSO₄, filtered and the solvent removed. The crude product was

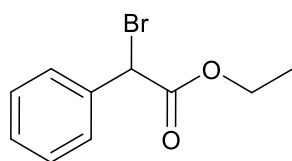
purified by column chromatography (SiO₂, hexane to EtOAc:hexane, 20:80): and dried under reduced pressure to give the title compound (**30**) as a yellow liquid (16.68 g, 72.82 mmol), 67 % yield.

Chemical formula: C₉H₉BrO₂; Molecular weight: 229.07 g mol⁻¹

¹H NMR (400 MHz, CDCl₃) δ 7.58–7.50 (m, 2H), 7.41–7.31 (m, 3H), 5.37 (s, 1H), 3.79 (s, 3H). ¹³C NMR (101 MHz, CDCl₃) δ 168.94, 135.85, 129.46, 128.99, 128.78, 53.55, 46.67.

¹H and ¹³C NMR data are in agreement with the literature.⁷

Ethyl 2-bromo-2-phenylacetate (**31**)⁸



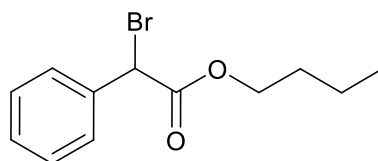
The title compound (**31**) was synthesised from ethyl 2-hydroxy-2-phenylacetate (**27**) (15.00 g, 83.24 mmol), dry DCM (100 mL), triethylamine (17.5 mL, 125 mmol) and thionyl bromide (7.7 mL, 99 mmol), according to the general procedure B. The crude product was purified by column chromatography (SiO₂, EtOAc:hexane, 20:80) to give a yellow liquid (11.32 g, 46.57 mmol), 56 % yield.

Chemical formula: C₁₀H₁₁BrO₂; Molecular weight: 243.10 g mol⁻¹

¹H NMR (400 MHz, CDCl₃) δ 7.59–7.52 (m, 2H), 7.41–7.31 (m, 3H), 5.35 (s, 1H), 4.32–4.16 (m, 2H), 1.28 (t, *J* = 7.1 Hz, 3H). ¹³C NMR (101 MHz, CDCl₃) δ 168.42, 135.98, 129.38, 128.94, 128.78, 62.66, 46.99, 14.07.

¹H and ¹³C NMR data are in agreement with the literature.⁸

Butyl 2-bromo-2-phenylacetate (**32**)



The title compound (**32**) was synthesised from butyl 2-hydroxy-2-phenylacetate (**28**) (30.07 g, 144.4 mmol), dry DCM (250 mL), triethylamine (30.0 mL, 215 mmol) and thionyl bromide (13.5 mL, 174 mmol), according to the general procedure B. The organic phase was washed with deionised water (3 × 150 mL), and the crude product was purified by column chromatography (SiO₂, EtOAc:hexane, 40:60) to give a yellow liquid (19.85 g, 73.21 mmol), 51 % yield.

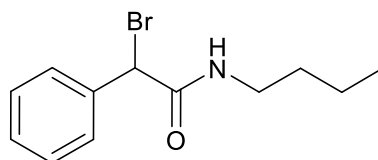
Chemical formula: C₁₂H₁₅BrO₂; Molecular weight: 271.15 g mol⁻¹

¹H NMR (400 MHz, CDCl₃) δ 7.59–7.51 (m, 2H), 7.41–7.31 (m, 3H), 5.35 (s, 1H), 4.25–4.12 (m, 2H), 1.68–1.58 (m, 2H), 1.44–1.27 (m, 2H), 0.91 (t, *J* = 7.4 Hz, 3H). ¹³C NMR (101 MHz, CDCl₃) δ 168.46, 135.98, 129.33, 128.88, 128.75, 66.43, 47.03, 30.47, 19.06, 13.74.

IR (neat) 2960, 2874, 1744, 1455, 1251, 1138, 693 cm^{-1} .

HRMS (ESI^+ , m/z) Calculated for $[\text{M}+\text{H}]^+ \text{C}_{12}\text{H}_{16}^{79}\text{BrO}_2^+$, requires 271.0328 found 271.0329.

2-Bromo-*N*-butyl-2-phenylacetamide (**33**)



The title compound (**33**) was synthesised from *n*-butyl-2-hydroxy-2-phenylacetamide (**29**) (20.05 g, 96.73 mmol), dry DCM (110 mL), triethylamine (20.0 mL, 143 mmol) and thionyl bromide (9.0 mL,

0.12 mol), according to the general procedure B. The crude product was purified by column chromatography (SiO_2 , EtOAc:hexane, 20:80) to give a light yellow crystalline solid (13.64 g, 50.49 mmol), 52 % yield.

Chemical formula: $\text{C}_{12}\text{H}_{16}\text{BrNO}$; Molecular weight: 270.17 g mol^{-1}

^1H NMR (400 MHz, CDCl_3) δ 7.47–7.40 (m, 2H), 7.40–7.28 (m, 3H), 6.67 (bs, 1H), 5.43 (s, 1H), 3.32 (dt, $J = 6.8, 6.8$ Hz, 2H), 1.60–1.50 (m, 2H), 1.43–1.31 (m, 2H), 0.94 (t, $J = 7.3$ Hz, 3H). ^{13}C NMR (101 MHz, CDCl_3) δ 166.95, 137.74, 129.21, 129.11, 128.40, 52.02, 40.35, 31.49, 20.17, 13.88.

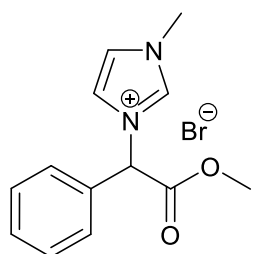
IR (neat) 3295, 2931, 1657, 1545, 1231, 1168, 692 cm^{-1} .

HRMS (ESI^+ , m/z) Calculated for $[\text{M}+\text{H}]^+ \text{C}_{12}\text{H}_{17}^{79}\text{BrNO}^+$, requires 270.0488 found 270.0485.

6.2.4 Mandelate Bromide ILs

General Procedure C: Preparation of Mandelate Bromide ILs (16–25)

3-(2-Methoxy-2-oxo-1-phenylethyl)-1-methyl-1H-imidazol-3-ium bromide (**16**)



A flask was charged with methyl 2-bromo-2-phenylacetate (**30**) (5.04 g, 22.0 mmol) and diethyl ether (20 mL), under N_2 . Whilst stirring 1-methylimidazole (1.72 mL, 21.6 mmol) was added and the reaction was stirred overnight at rt. TLC confirmed reaction completion. Diethyl ether was decanted and the product was washed with diethyl ether (5×25 mL). The volatiles were removed via rotary evaporation and the product was dried under reduced pressure to give the title compound (**16**) as a white solid (6.37 g, 20.5 mmol), 95 % yield.

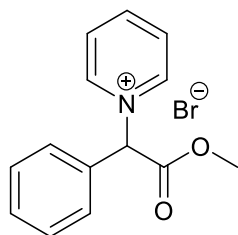
Chemical formula: $\text{C}_{13}\text{H}_{15}\text{BrN}_2\text{O}_2$; Molecular weight: 311.18 g mol^{-1} ; mp: 61–63 $^\circ\text{C}$

^1H NMR (400 MHz, CDCl_3) δ 10.67 (bs, 1H), 7.62–7.55 (m, 2H), 7.48–7.41 (m, 4H), 7.41 (s, 1H), 7.34 (dd, $J = 1.9, 1.9$ Hz, 1H), 4.04 (s, 3H), 3.82 (s, 3H). ^{13}C NMR (101 MHz, CDCl_3) δ 168.24, 138.13, 132.13, 130.61, 129.96, 128.80, 122.57, 121.91, 64.04, 53.92, 36.96.

IR (neat) 3042, 2954, 1744, 1552, 1437, 1278, 1216, 1160, 986, 733 cm^{-1} .

HRMS (ESI^+ , m/z) Calculated for $[\text{M}-\text{Br}]^+ \text{C}_{13}\text{H}_{15}\text{N}_2\text{O}_2^+$, requires 231.1128, found 231.1125.

1-(2-Methoxy-2-oxo-1-phenylethyl)pyridin-1-ium bromide (17)



The title compound (**17**) was synthesised from methyl 2-bromo-2-phenylacetate (**30**) (5.02 g, 21.9 mmol), diethyl ether (5 mL) and pyridine (1.73 mL, 21.5 mmol), according to the general procedure C to give a white solid (5.66 g, 18.4 mmol), 86 % yield.

Chemical formula: $\text{C}_{14}\text{H}_{14}\text{BrNO}_2$;

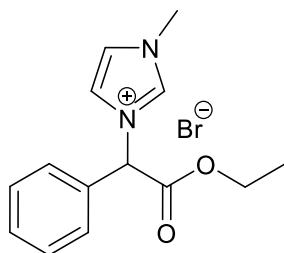
Molecular weight: 308.18 g mol^{-1} ; mp: 140–142 $^\circ\text{C}$

^1H NMR (400 MHz, CDCl_3) δ 9.63–9.56 (m, 2H), 8.56 (tt, $J = 7.8, 1.4$ Hz, 1H), 8.51 (s, 1H), 8.11–8.03 (m, 2H), 7.77–7.68 (m, 2H), 7.54–7.42 (m, 3H), 3.87 (s, 3H). ^{13}C NMR (101 MHz, CDCl_3) δ 167.98, 146.51, 145.30, 131.27, 131.13, 130.23, 129.88, 127.92, 73.25, 54.35.

IR (neat) 3021, 2959, 1743, 1628, 1482, 1279, 1218, 1159, 993, 748 cm^{-1} .

HRMS (ESI^+ , m/z) Calculated for $[\text{M}-\text{Br}]^+ \text{C}_{14}\text{H}_{14}\text{NO}_2^+$, requires 228.1019 found 228.1022.

3-(2-Ethoxy-2-oxo-1-phenylethyl)-1-methyl-1H-imidazol-3-ium bromide (18)



The title compound (**18**) was synthesised from ethyl 2-bromo-2-phenylacetate (**31**) (5.01 g, 20.6 mmol), diethyl ether (20 mL) and 1-methylimidazole (1.61 mL, 20.2 mmol), according to the general procedure C. The reaction was stirred for 2 days to give a white solid (6.15 g, 18.9 mmol), 94 % yield.

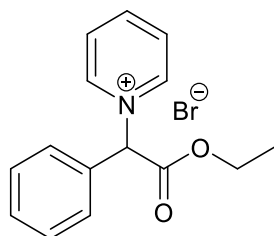
Chemical formula: $\text{C}_{14}\text{H}_{17}\text{BrN}_2\text{O}_2$; Molecular weight: 325.21 g mol^{-1} ; mp: 101–102 $^\circ\text{C}$

^1H NMR (400 MHz, CDCl_3) δ 10.87 (bs, 1H), 7.63–7.56 (m, 2H), 7.48–7.42 (m, 3H), 7.40 (dd, $J = 1.8, 1.8$ Hz, 1H), 7.30 (s, 1H), 7.18 (dd, $J = 1.8, 1.8$ Hz, 1H), 4.308 (q, $J = 7.1$ Hz, 1H), 4.305 (q, $J = 7.1$ Hz, 1H), 4.03 (s, 3H), 1.27 (t, $J = 7.1$ Hz, 3H). ^{13}C NMR (101 MHz, CDCl_3) δ 167.61, 137.87, 132.27, 130.49, 129.88, 128.71, 122.82, 121.90, 64.11, 63.44, 36.94, 14.04.

IR (neat) 3070, 3016, 1746, 1576, 1280, 1209, 1170, 1010, 735 cm^{-1} .

HRMS (ESI^+ , m/z) Calculated for $[\text{M}-\text{Br}]^+ \text{C}_{14}\text{H}_{17}\text{N}_2\text{O}_2^+$, requires 245.1285, found 245.1277.

1-(2-Ethoxy-2-oxo-1-phenylethyl)pyridin-1-ium bromide (**19**)⁹



A flask was charged with ethyl 2-bromo-2-phenylacetate (**31**) (5.00 g, 20.6 mmol) under N_2 . With no stirring, pyridine (1.62 mL, 20.1 mmol) was added and the reaction was left for 2 days at rt. TLC confirmed reaction completion. The product was washed with diethyl ether (5×25 mL). The volatiles were

removed via rotary evaporation, and the product was dried under reduced pressure to give the title compound (**19**) as a white solid (6.35 g, 19.7 mmol), 98 % yield.

Chemical formula: $\text{C}_{15}\text{H}_{16}\text{BrNO}_2$; Molecular weight: $322.20 \text{ g mol}^{-1}$; mp: $161\text{--}162^\circ\text{C}$

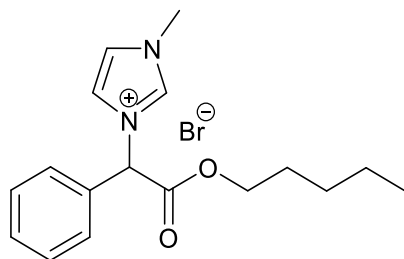
^1H NMR (400 MHz, CDCl_3) δ 9.61–9.56 (m, 2H), 8.53 (tt, $J = 7.8, 1.3$ Hz, 1H), 8.41 (s, 1H), 8.08–8.01 (m, 2H), 7.79–7.70 (m, 2H), 7.53–7.44 (m, 3H), 4.43–4.35 (m, 1H), 4.35–4.28 (m, 1H), 1.30 (t, $J = 7.1$ Hz, 3H). ^{13}C NMR (101 MHz, CDCl_3) δ 167.52, 146.30, 145.38, 131.24, 131.24, 130.21, 129.92, 127.77, 73.41, 64.11, 14.08.

IR (neat) 3029, 2949, 1747, 1629, 1486, 1216, 1160, 1012, 706 cm^{-1} .

HRMS (ESI^+ , m/z) Calculated for $[\text{M}-\text{Br}]^+ \text{C}_{15}\text{H}_{16}\text{NO}_2^+$, requires 242.1176, found 242.1170.

^1H and ^{13}C NMR data are in agreement with the literature.⁹

3-(2-Butoxy-2-oxo-1-phenylethyl)-1-methyl-1H-imidazol-3-ium bromide (**20**)



The title compound (**20**) was synthesised from butyl 2-bromo-2-phenylacetate (**32**) (7.04 g, 26.0 mmol), diethyl ether (20 mL) and 1-methylimidazole (2.03 mL, 25.5 mmol), according to the general procedure C. The reaction was stirred for 5 days to give a white solid (7.55 g, 21.4 mmol), 84 % yield.

Chemical formula: $\text{C}_{16}\text{H}_{21}\text{BrN}_2\text{O}_2$; Molecular weight: $353.26 \text{ g mol}^{-1}$; mp: $99\text{--}101^\circ\text{C}$

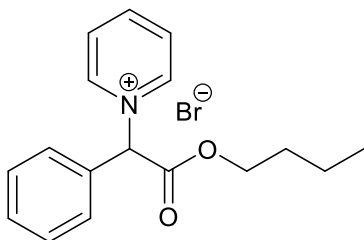
^1H NMR (400 MHz, CDCl_3) δ 10.52 (bs, 1H), 7.59–7.51 (m, 2H), 7.49 (dd, $J = 1.9, 1.9$ Hz, 1H), 7.45 (dd, $J = 1.9, 1.9$ Hz, 1H), 7.43–7.35 (m, 3H), 7.23 (s, 1H), 4.23 (dt, $J = 10.7, 6.8$ Hz, 1H), 4.16 (dt, $J = 10.7, 6.7$ Hz, 1H), 4.03 (s, 3H), 1.64–1.48 (m, 2H), 1.21 (tq, $J = 7.4, 7.4$ Hz, 2H), 0.81 (t, $J = 7.4$ Hz, 3H). ^{13}C NMR (101 MHz, CDCl_3) δ

167.64, 137.68, 132.28, 130.44, 129.80, 128.65, 122.99, 121.87, 67.12, 64.10, 36.93, 30.23, 18.87, 13.58.

IR (neat) 3060, 2958, 1742, 1549, 1280, 1210, 1192, 1158, 794, 729 cm^{-1} .

HRMS (ESI^+ , m/z) Calculated for $[\text{M}-\text{Br}]^+ \text{C}_{16}\text{H}_{21}\text{N}_2\text{O}_2^+$, requires 273.1598, found 273.1601.

1-(2-Butoxy-2-oxo-1-phenylethyl)pyridin-1-ium bromide (21)



The title compound (**21**) was synthesised from butyl 2-bromo-2-phenylacetate (**32**) (7.03 g, 25.9 mmol), diethyl ether (7 mL) and pyridine (2.04 mL, 25.3 mmol), according to the general procedure C. The reaction was stirred for 5 days to give a brown solid (4.94 g, 14.1 mmol), 56 % yield.

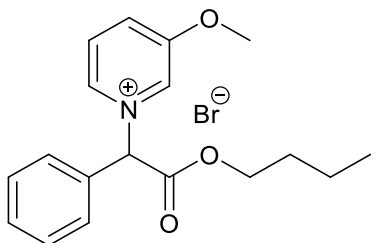
Chemical formula: $\text{C}_{17}\text{H}_{20}\text{BrNO}_2$; Molecular weight: $350.26 \text{ g mol}^{-1}$; mp: 48–50 °C

^1H NMR (400 MHz, CDCl_3) δ 9.59–9.53 (m, 2H), 8.54 (tt, $J = 7.7, 1.4 \text{ Hz}$, 1H), 8.37 (s, 1H), 8.09–8.01 (m, 2H), 7.78–7.69 (m, 2H), 7.53–7.43 (m, 3H), 4.34 (dt, $J = 10.7, 6.7 \text{ Hz}$, 1H), 4.23 (dt, $J = 10.7, 6.7 \text{ Hz}$, 1H), 1.71–1.53 (m, 2H), 1.28 (tq, $J = 7.5, 7.4 \text{ Hz}$, 2H), 0.85 (t, $J = 7.4 \text{ Hz}$, 3H). ^{13}C NMR (101 MHz, CDCl_3) δ 167.42, 146.60, 145.19, 131.20, 131.17, 130.11, 129.84, 127.93, 73.46, 67.76, 30.22, 18.91, 13.59.

IR (neat) 3036, 2958, 2871, 1739, 1628, 1480, 1279, 1212, 1159, 748 cm^{-1} .

HRMS (ESI^+ , m/z) Calculated for $[\text{M}-\text{Br}]^+ \text{C}_{17}\text{H}_{20}\text{NO}_2^+$, requires 270.1489, found 270.1482.

1-(2-Butoxy-2-oxo-1-phenylethyl)-3-methoxypyridin-1-ium bromide (22)



The title compound (**22**) was synthesised from butyl 2-bromo-2-phenylacetate (**32**) (5.00 g, 18.4 mmol), diethyl ether (25 mL) and 3-methoxypyridine (1.77 mL, 17.6 mmol), according to the general procedure C. The reaction was stirred for 5 days to give a white solid (4.95 g, 13.0 mmol), 74 % yield.

Chemical formula: $\text{C}_{18}\text{H}_{22}\text{BrNO}_3$; Molecular weight: $380.28 \text{ g mol}^{-1}$; mp: 127–128 °C

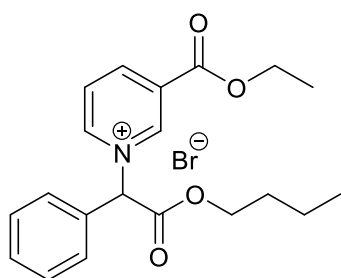
^1H NMR (400 MHz, CDCl_3) δ 9.81 (dd, $J = 2.6, 1.3 \text{ Hz}$, 1H), 8.63 (ddd, $J = 6.0, 1.3, 1.1 \text{ Hz}$, 1H), 8.38 (s, 1H), 7.99 (ddd, $J = 8.8, 2.6, 1.1 \text{ Hz}$, 1H), 7.87 (dd, $J = 8.8, 6.0 \text{ Hz}$, 1H), 7.74–7.68 (m, 2H), 7.50–7.41 (m, 3H), 4.32 (dt, $J = 10.7, 6.8 \text{ Hz}$, 1H), 4.20 (dt, $J = 10.7, 6.8 \text{ Hz}$, 1H), 4.16 (s, 3H), 1.61 (ddt, $J = 13.8, 11.6, 6.8 \text{ Hz}$, 2H), 1.26 (tq, $J = 7.5,$

7.4 Hz, 2H), 0.83 (t, $J = 7.4$ Hz, 3H). ^{13}C NMR (101 MHz, CDCl_3) δ 167.46, 158.50, 136.80, 132.63, 132.62, 131.42, 131.06, 129.99, 129.86, 127.69, 73.44, 67.66, 58.80, 30.21, 18.91, 13.60.

IR (neat) 3034, 2956, 1741, 1624, 1519, 1294, 1284, 1209, 1153, 744 cm^{-1} .

HRMS (ESI^+ , m/z) Calculated for $[\text{M}-\text{Br}]^+ \text{C}_{18}\text{H}_{22}\text{NO}_3^+$, requires 300.1594, found 300.1592.

1-(2-Butoxy-2-oxo-1-phenylethyl)-3-(ethoxycarbonyl)pyridin-1-ium bromide (23)



The title compound (**23**) was synthesised from butyl 2-bromo-2-phenylacetate (**32**) (5.03 g, 18.2 mmol), diethyl ether (5 mL) and ethyl nicotinate (2.49 mL, 18.2 mmol), according to the general procedure C. The reaction was stirred for 5 days give a light pink solid (4.80 g, 11.4 mmol), 63 % yield.

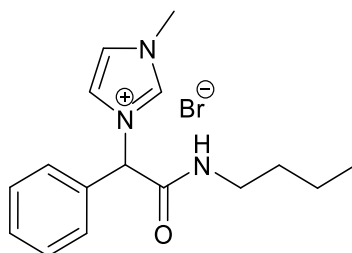
Chemical formula: $\text{C}_{20}\text{H}_{24}\text{BrNO}_4$; Molecular weight: 422.32 g mol^{-1} ; mp: 112–113 $^\circ\text{C}$

^1H NMR (400 MHz, CDCl_3) δ 10.41 (ddd, $J = 6.3, 1.4, 1.4$ Hz, 1H), 9.43 (bs, 1H), 8.96 (ddd, $J = 8.0, 1.4, 1.4$ Hz, 1H), 8.59 (s, 1H), 8.23 (dd, $J = 8.0, 6.3$ Hz, 1H), 7.85–7.76 (m, 2H), 7.56–7.48 (m, 3H), 4.47 (q, $J = 7.1$ Hz, 2H), 4.36 (dt, $J = 10.7, 6.8$ Hz, 1H), 4.25 (dt, $J = 10.7, 6.8$ Hz, 1H), 1.64 (ddt, $J = 13.8, 12.0, 6.8$ Hz, 2H), 1.42 (t, $J = 7.1$ Hz, 3H), 1.28 (tq, $J = 7.4, 7.4$ Hz, 2H), 0.87 (t, $J = 7.4$ Hz, 3H). ^{13}C NMR (101 MHz, CDCl_3) δ 167.58, 160.84, 149.43, 146.07, 145.23, 131.50, 130.65, 130.51, 130.29, 130.11, 128.05, 73.91, 68.05, 63.81, 30.26, 18.96, 14.23, 13.64.

IR (neat) 3045, 2961, 1737, 1721, 1635, 1456, 1297, 1280, 1177, 706 cm^{-1} .

HRMS (ESI^+ , m/z) Calculated for $[\text{M}-\text{Br}]^+ \text{C}_{20}\text{H}_{24}\text{NO}_4^+$, requires 342.1700, found 342.1692.

3-(2-(Butylamino)-2-oxo-1-phenylethyl)-1-methyl-1H-imidazol-3-ium bromide (24)



The title compound (**24**) was synthesised from 2-bromo-*N*-butyl-2-phenylacetamide (**33**) (5.00 g, 18.5 mmol), diethyl ether (20 mL) and 1-methylimidazole (1.40 mL, 17.6 mmol), according to the general procedure C. The reaction was stirred for 2 days to give a white solid (6.12 g, 17.4 mmol), 99 % yield.

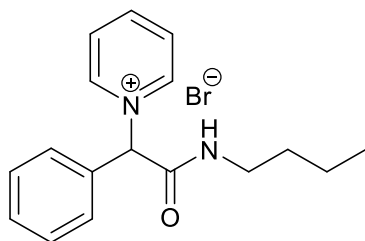
Chemical formula: $\text{C}_{16}\text{H}_{22}\text{BrN}_3\text{O}$; Molecular weight: 352.28 g mol^{-1} ; mp: 143–145 $^\circ\text{C}$

^1H NMR (400 MHz, CDCl_3) δ 9.76 (bs, 1H), 8.29 (t, $J = 5.3$ Hz, 1H), 7.79 (s, 1H), 7.75 (dd, $J = 1.8, 1.8$ Hz, 1H), 7.67–7.60 (m, 2H), 7.42–7.34 (m, 3H), 7.19 (dd, $J = 1.9, 1.9$ Hz, 1H), 3.98 (s, 3H), 3.34–3.25 (m, 1H), 3.25–3.16 (m, 1H), 1.53 (dtd, $J = 8.8, 7.4, 5.8$ Hz, 2H), 1.38–1.23 (m, 2H), 0.86 (t, $J = 7.3$ Hz, 3H). ^{13}C NMR (101 MHz, CDCl_3) δ 166.17, 136.32, 133.49, 129.96, 129.48, 128.44, 123.00, 122.30, 63.89, 39.94, 36.91, 31.09, 20.25, 13.79.

IR (neat) 3158, 3022, 2929, 1675, 1554, 1227, 1164, 742 cm^{-1} .

HRMS (ESI^+ , m/z) Calculated for $[\text{M}-\text{Br}]^+ \text{C}_{16}\text{H}_{22}\text{N}_3\text{O}^+$, requires 272.1757, found 272.1757.

1-(2-(Butylamino)-2-oxo-1-phenylethyl)pyridin-1-ium bromide (25)



The title compound (**25**) was synthesised from 2-bromo-*N*-butyl-2-phenylacetamide (**33**) (5.00 g, 18.5 mmol), diethyl ether (5 mL) and pyridine (1.42 mL, 17.6 mmol), according to the general procedure C. The reaction was stirred for 2 days to give a white solid (5.26 g, 15.1 mmol), 86 % yield.

Chemical formula: $\text{C}_{17}\text{H}_{21}\text{BrN}_2\text{O}$; Molecular weight: 349.27 g mol^{-1} ; mp: 167–169 $^\circ\text{C}$

^1H NMR (400 MHz, CDCl_3) δ 9.60–9.53 (m, 2H), 8.72 (bs, 1H), 8.68 (s, 1H), 8.43 (tt, $J = 7.8, 1.4$ Hz, 1H), 8.01–7.92 (m, 2H), 7.69–7.62 (m, 2H), 7.51–7.41 (m, 3H), 3.43–3.31 (m, 1H), 3.31–3.21 (m, 1H), 1.65–1.52 (m, 2H), 1.35 (tq, $J = 7.4, 7.3$ Hz, 2H), 0.89 (t, $J = 7.3$ Hz, 3H). ^{13}C NMR (101 MHz, CDCl_3) δ 164.93, 145.47, 144.92, 132.40, 130.82, 129.94, 129.39, 127.63, 72.58, 40.25, 31.05, 20.29, 13.80.

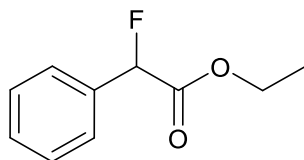
IR (neat) 3126, 3014, 2958, 1674, 1626, 1553, 1481, 1226, 1157, 708 cm^{-1} .

HRMS (ESI^+ , m/z) Calculated for $[\text{M}-\text{Br}]^+ \text{C}_{17}\text{H}_{21}\text{N}_2\text{O}^+$, requires 269.1648, found 269.1644.

6.2.4.3 Monofluoro Mandate Bromide IL

Preparation of α -Fluoroester of Mandelic Acid (35)

Ethyl 2-fluoro-2-phenylacetate (**35**)⁹



A flask was charged with ethyl 2-hydroxy-2-phenylacetate (**27**) (1.08 g, 5.99 mmol) and dry DCM (15 mL), under N_2 . Whilst stirring and cooling in an ice bath (0 $^\circ\text{C}$), DAST

(1.42 mL, 10.7 mmol) was added dropwise and the reaction was stirred for 1 day at rt. TLC confirmed reaction completion. The reaction was quenched by the slow dropwise addition of saturated aqueous sodium bicarbonate (15 mL), and the product was subsequently extracted with DCM (2 × 15 mL). The combined organic extracts were washed with 0.5 N HCl solution (2 × 15 mL) and dried over MgSO₄. After filtering, the solvent was removed. The crude product was purified by column chromatography (SiO₂, EtOAc:hexane, 10:90) and dried under reduced pressure to give the title compound (**35**) as a yellow oil (0.703 g, 3.86 mmol), 64 % yield.

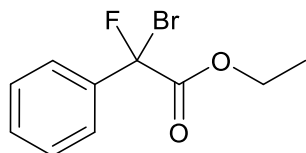
Chemical formula: C₁₀H₁₁FO₂; Molecular weight: 182.19 g mol⁻¹

¹H NMR (400 MHz, CDCl₃) δ 7.52–7.43 (m, 2H), 7.43–7.35 (m, 3H), 5.78 (d, *J*_{H-F} = 47.8 Hz, 1H), 4.34–4.14 (m, 2H), 1.26 (t, *J* = 7.1 Hz, 3H). ¹³C NMR (101 MHz, CDCl₃) δ 168.66 (d, ²*J*_{C-F} = 27.4 Hz), 134.36 (d, ²*J*_{C-F} = 20.4 Hz), 129.68 (d, ⁵*J*_{C-F} = 2.3 Hz), 128.86, 126.74 (d, ³*J*_{C-F} = 6.0 Hz), 89.45 (d, ¹*J*_{C-F} = 185.3 Hz), 61.94, 14.13. ¹⁹F NMR (376 MHz, CDCl₃) δ -179.77 (d, ²*J*_{H-F} = 47.9 Hz).

¹H, ¹³C and ¹⁹F NMR data are in agreement with the literature.¹⁰

Preparation of α-Bromo-α-fluoroester of Mandelic Acid (**36**)

Ethyl 2-bromo-2-fluoro-2-phenylacetate (**36**)



A flask was charged with ethyl 2-fluoro-2-phenylacetate (**35**) (0.500 g, 2.74 mmol) and dry CCl₄ (10 mL). NBS (0.488 g, 2.74 mmol) was added in one portion and the reaction was refluxed whilst under illumination from a 300 W mercury lamp. After 1 h the reaction turned orange and subsequently yellow after 19 h. TLC confirmed reaction completion. After filtering the solvent was removed. The crude product was purified by column chromatography (SiO₂, EtOAc:hexane, 5:95) and dried under reduced pressure, to give the title compound (**36**) as a colourless viscous liquid (0.608 g, 2.33 mmol), 85 % yield.

Chemical formula: C₁₀H₁₀BrFO₂; Molecular weight: 261.09 g mol⁻¹

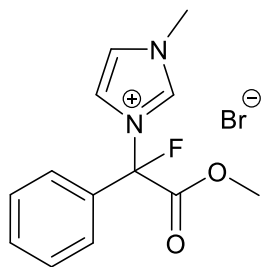
¹H NMR (400 MHz, CDCl₃) δ 7.77–7.67 (m, 2H), 7.47–7.37 (m, 3H), 4.40–4.27 (m, 2H), 1.33 (t, *J* = 7.1 Hz, 3H). ¹³C NMR (101 MHz, CDCl₃) δ 165.71 (d, ²*J*_{C-F} = 28.5 Hz), 136.89 (d, ²*J*_{C-F} = 21.6 Hz), 130.37 (d, ⁵*J*_{C-F} = 1.2 Hz), 128.51 (d, ⁴*J*_{C-F} = 1.3 Hz), 126.12 (d, ³*J*_{C-F} = 7.9 Hz), 96.77 (d, ¹*J*_{C-F} = 264.0 Hz), 63.73, 13.91. ¹⁹F NMR (376 MHz, CDCl₃) δ -114.41 (d, ⁴*J*_{F-H} = 8.2 Hz).

IR (neat) 2985, 1752, 1450, 1252, 1221, 1094, 1069, 1018, 859, 738, 691 cm⁻¹.

HRMS (ESI⁺, m/z) Calculated for [M+H]⁺ C₁₀H₁₁⁷⁹BrFO₂⁺, requires 260.9921, found 260.9938.

Preparation of Monofluoro Mandelate Bromide IL (37)

3-(1-Fluoro-2-methoxy-2-oxo-1-phenylethyl)-1-methyl-1H-imidazol-3-ium bromide (37)



A flask was charged with ethyl 2-bromo-2-fluoro-2-phenylacetate (**36**) (0.251 g, 0.961 mmol) under N₂. Whilst stirring 1-methylimidazole (77 μ L, 0.96 mmol) was added and the reaction was stirred for 2 days at rt. TLC confirmed reaction completion. The product was washed with diethyl ether (5 \times 5 mL). The volatiles were removed via rotary evaporation and the crude product was purified by column chromatography (SiO₂, DCM to MeOH:DCM, 1:9), where transesterification to the methyl ester occurred. The product was dried under reduced pressure to give the title compound (**37**) as an off-white solid (53 mg, 0.16 mmol), 17 % yield.

Chemical formula: C₁₃H₁₄BrFN₂O₂; Molecular weight: 329.17 g mol⁻¹; mp: 174–175 °C

¹H NMR (400 MHz, DMSO-d₆) δ 9.44 (bs, 1H), 7.72 (dd, J = 1.9, 1.9 Hz, 1H), 7.64 (dd, J = 1.9, 1.9 Hz, 1H), 7.52–7.41 (m, 5H), 3.87 (s, 3H), 3.35 (s, 3H). ¹³C NMR (151 MHz, DMSO-d₆) δ 162.12 (d, ² J_{C-F} = 22.1 Hz), 137.24, 136.36 (d, ² J_{C-F} = 25.7 Hz), 129.58, 128.38, 125.83 (³ J_{C-F} , J = 6.8 Hz), 123.46, 121.15, 100.23 (d, ¹ J_{C-F} = 223.2 Hz), 40.06, 35.97. ¹⁹F NMR (376 MHz, DMSO-d₆) δ -115.39.

IR (neat) 3072, 3036, 1665, 1578, 1537, 1350, 1272, 1233, 1162, 1052, 1043, 749 cm⁻¹.

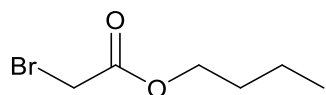
HRMS (ESI⁺, m/z) Calculated for [M-Br]⁺ C₁₃H₁₄FN₂O₂⁺, requires 249.1034, found 249.1048.

6.3 Experimental Preparations for 1-Methylimidazolium Ester ILs

6.3.1 Alkylating Regents

General Procedure D: Preparation of α -Bromoesters (58–60)

Butyl 2-bromoacetate (58)¹¹



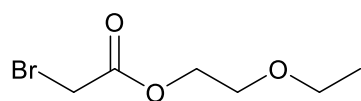
A flask was charged with *n*-butanol (6.02 g, 81.2 mmol), Na₂CO₃ (12.91 g, 121.8 mmol) and dry DCM (30 mL), under N₂. Whilst stirring and cooling in an ice bath (0 °C) bromoacetyl bromide (8.5 mL, 98 mmol) was added dropwise and the reaction was stirred overnight at rt. TLC confirmed reaction completion. The Na₂CO₃ was removed by vacuum filtration and the organic phase was washed with saturated aqueous sodium bicarbonate (2 × 20 mL) and deionised water (2 × 25 mL). The organic phase was dried over MgSO₄, filtered and the solvent removed via rotary evaporation. The product was dried under reduced pressure to give the title compound (**58**) as a colourless liquid (13.5 g, 69.2 mmol), 85 % yield.

Chemical formula: C₆H₁₁BrO₂; Molecular weight: 195.06 g mol⁻¹

¹H NMR (400 MHz, CDCl₃) δ 4.17 (t, *J* = 6.6 Hz, 2H), 3.83 (s, 2H), 1.70–1.58 (m, 2H), 1.46–1.32 (m, 2H), 0.93 (t, *J* = 7.4 Hz, 3H). ¹³C NMR (101 MHz, CDCl₃) δ 167.47, 66.30, 30.54, 26.12, 19.12, 13.79.

¹H and ¹³C NMR data are in agreement with the literature.¹¹

2-Ethoxyethyl 2-bromoacetate (59)



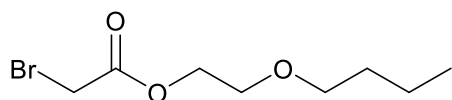
The title compound (**59**) was synthesised from 2-ethoxyethanol (8.02 g, 89.0 mmol), Na₂CO₃ (14.15 g, 133.5 mmol), dry DCM (50 mL) and bromoacetyl bromide (9.3 mL, 0.11 mol), according to the general procedure D to give a yellow liquid (14.8 g, 70.1 mmol), 79 % yield.

Chemical formula: C₆H₁₁BrO₃; Molecular weight: 211.06 g mol⁻¹

¹H NMR (400 MHz, CDCl₃) δ 4.36–4.29 (m, 2H), 3.88 (s, 2H), 3.70–3.62 (m, 2H), 3.54 (q, *J* = 7.0 Hz, 2H), 1.22 (t, *J* = 7.0 Hz, 3H). ¹³C NMR (101 MHz, CDCl₃) δ 167.45, 68.08, 66.87, 65.60, 26.03, 15.23.

¹H and ¹³C NMR data are in agreement with the literature.¹¹

2-Butoxyethyl 2-bromoacetate (**60**)¹¹



The title compound (**60**) was synthesised from 2-butoxyethanol (10.02 g, 84.79 mmol), Na₂CO₃ (13.48 g, 127.2 mmol), dry DCM (50 mL) and bromoacetyl bromide (8.9 mL, 0.10 mol), according to the general procedure D to give a yellow liquid (18.7 g, 78.2 mmol), 92 % yield.

Chemical formula: C₈H₁₅BrO₃; Molecular weight: 239.11 g mol⁻¹

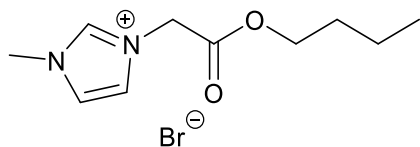
¹H NMR (400 MHz, CDCl₃) δ 4.36–4.28 (m, 2H), 3.88 (s, 2H), 3.69–3.61 (m, 2H), 3.47 (t, *J* = 6.7 Hz, 2H), 1.61–1.51 (m, 2H), 1.43–1.31 (m, 2H), 0.92 (t, *J* = 7.4 Hz, 3H). ¹³C NMR (101 MHz, CDCl₃) δ 167.44, 71.38, 68.28, 65.58, 31.75, 26.02, 19.37, 14.05.

¹H and ¹³C NMR data are in agreement with the literature.¹¹

6.3.2 Bromide ILs

General Procedure E: Preparation of Bromide ILs (**46–49**)

3-(2-Butoxy-2-oxoethyl)-1-methyl-1*H*-imidazol-3-ium bromide (**46**)¹¹



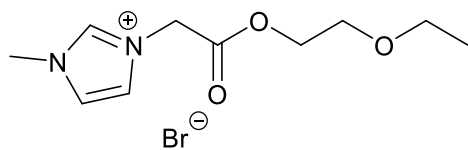
A flask was charged with butyl 2-bromoacetate (**58**) (13.00 g, 66.65 mmol) and diethyl ether (30 mL), under N₂. Whilst stirring 1-methylimidazole (4.85 mL, 60.8 mmol) was added dropwise and the reaction was stirred for 2 days at rt. TLC confirmed reaction completion. Diethyl ether was decanted and the product was washed with diethyl ether (5 × 25 mL). Residual volatiles were removed via rotary evaporation and the product was dried under reduced pressure to give the title compound (**46**) as a colourless viscous liquid (16.73 g, 60.36 mmol), 99 % yield.

Chemical formula: C₁₀H₁₇BrN₂O₂; Molecular weight: 277.16 g mol⁻¹; T_{dec}: 161 °C

¹H NMR (400 MHz, CDCl₃) δ 10.04 (bs, 1H), 7.66 (dd, *J* = 1.8, 1.8 Hz, 1H), 7.58 (dd, *J* = 1.8, 1.8 Hz, 1H), 5.42 (s, 2H), 4.13 (t, *J* = 6.8 Hz, 2H), 4.04 (s, 3H), 1.64 – 1.51 (m, 2H), 1.37 – 1.25 (m, 2H), 0.86 (t, *J* = 7.4 Hz, 3H). ¹³C NMR (101 MHz, CDCl₃) δ 166.22, 138.62, 123.84, 122.98, 66.91, 50.38, 37.00, 30.42, 19.06, 13.75.

¹H and ¹³C NMR data are in agreement with the literature.¹¹

3-[2-(2-Ethoxyethoxy)-2-oxoethyl]-1-methyl-1*H*-imidazol-3-ium bromide (**47**)¹¹



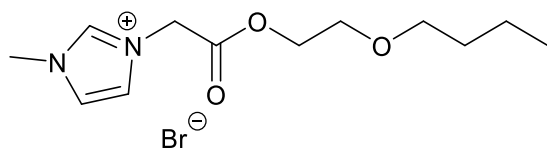
The title compound (**47**) was synthesised from 2-ethoxyethyl 2-bromoacetate (**59**) (10.51 g, 49.80 mmol), diethyl ether (20 mL) and 1-methylimidazole (3.65 mL, 45.8 mmol), according to the general procedure E to give a brown solid (13.19 g, 44.99 mmol), 98 % yield.

Chemical formula: C₁₀H₁₇BrN₂O₃; Molecular weight: 293.16 g mol⁻¹; mp: 36–38 °C; T_{dec}: 157 °C

¹H NMR (400 MHz, CDCl₃) δ 10.16 (bs, 1H), 7.61 (dd, *J* = 1.8, 1.8 Hz, 1H), 7.48 (dd, *J* = 1.8, 1.8 Hz, 1H), 5.51 (s, 2H), 4.37–4.30 (m, 2H), 4.07 (s, 3H), 3.69–3.61 (m, 2H), 3.52 (q, *J* = 7.0 Hz, 2H), 1.19 (t, *J* = 7.0 Hz, 3H). ¹³C NMR (101 MHz, CDCl₃) δ 166.26, 138.99, 123.74, 122.78, 67.83, 66.87, 66.00, 50.42, 37.03, 15.23.

¹H and ¹³C NMR data are in agreement with the literature.¹¹

3-[2-(2-Butoxyethoxy)-2-oxoethyl]-1-methyl-1*H*-imidazol-3-ium bromide (**48**)¹¹



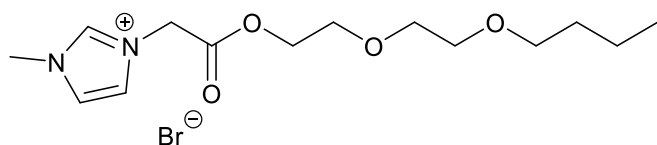
The title compound (**48**) was synthesised from 2-butoxyethyl 2-bromoacetate (**60**) (12.98 g, 54.28 mmol), diethyl ether (30 mL) and 1-methylimidazole (3.95 mL, 49.5 mmol), according to the general procedure E to give a white solid (15.62 g, 48.63 mmol), 98 % yield.

Chemical formula: C₁₂H₂₁BrN₂O₃; Molecular weight: 321.22 g mol⁻¹; mp: 40–42 °C; T_{dec}: 162 °C

¹H NMR (400 MHz, CDCl₃) δ 10.11 (bs, 1H), 7.63 (dd, *J* = 1.8, 1.8 Hz, 1H), 7.55 (dd, *J* = 1.8, 1.8 Hz, 1H), 5.47 (s, 2H), 4.33–4.27 (m, 2H), 4.06 (s, 3H), 3.64–3.58 (m, 2H), 3.42 (t, *J* = 6.7 Hz, 2H), 1.55–1.45 (m, 2H), 1.37–1.25 (m, 2H), 0.87 (t, *J* = 7.3 Hz, 3H). ¹³C NMR (101 MHz, CDCl₃) δ 166.29, 138.49, 123.84, 123.08, 71.30, 68.01, 65.85, 50.37, 37.02, 31.64, 19.29, 14.01.

¹H and ¹³C NMR data are in agreement with the literature.¹¹

3-[2-[2-(2-Butoxyethoxy)ethoxy]-2-oxoethyl]-1-methyl-1*H*-imidazol-3-ium bromide (49)



The title compound (49) was synthesised from 2-(2-butoxyethoxy)ethyl 2-bromoacetate

(61) (19.01 g, 67.14 mmol), diethyl ether (35 mL) and 1-methylimidazole (5.24 mL, 65.8 mmol) according to the general procedure E to give a white solid (23.13 g, 63.32 mmol), 96 % yield.

Chemical Formula: C₁₄H₂₅BrN₂O₄ Molecular Weight: 365.27 g mol⁻¹ mp: 68–70 °C
T_{dec}: 155 °C

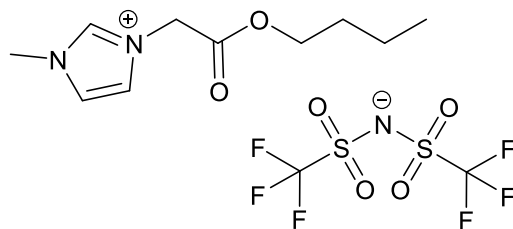
¹H NMR (400 MHz, CDCl₃) δ 10.12 (bs, 1H), 7.65 (dd, *J* = 1.8, 1.8 Hz, 1H), 7.48 (dd, *J* = 1.8, 1.8 Hz, 1H), 5.50 (s, 2H), 4.38–4.30 (m, 2H), 4.06 (s, 3H), 3.75–3.68 (m, 2H), 3.65–3.59 (m, 2H), 3.59–3.53 (m, 2H), 3.42 (t, *J* = 6.8 Hz, 2H), 1.58–1.46 (m, 2H), 1.39–1.25 (m, 2H), 0.88 (t, *J* = 7.3 Hz, 3H). ¹³C NMR (101 MHz, CDCl₃) δ 166.29, 138.50, 124.00, 122.98, 71.29, 70.69, 70.03, 68.62, 65.74, 50.33, 36.99, 31.71, 19.33, 14.03.

¹H and ¹³C NMR data are in agreement with the literature.¹¹

6.3.3 Bistriflimide ILs

General Procedure F: Preparation of Bistriflimide ILs (50–53)

3-(2-Butoxy-2-oxoethyl)-1-methyl-1*H*-imidazol-3-ium bis(trifluoromethylsulfonyl)imide (50)¹¹



A flask was charged with 3-(2-butoxy-2-oxoethyl) -1-methyl-1*H*-imidazol-3-ium bromide (46) (49.68 g, 179.2 mmol) and deionised water (100 mL). Whilst stirring LiNTf₂ (56.56 g, 197.0 mmol) was added in

one portion and the reaction was stirred for 2 days at rt. The water was decanted and the product was washed with deionised water (5 × 50 mL). The volatiles were removed via rotary evaporation and the product was dried under reduced pressure to give the title compound (50) as a light yellow liquid (76.28 g, 159.8 mmol), 89 % yield.

Chemical formula: C₁₂H₁₇F₆N₃O₆S₂; Molecular weight: 477.39 g mol⁻¹; T_{dec}: 284 °C

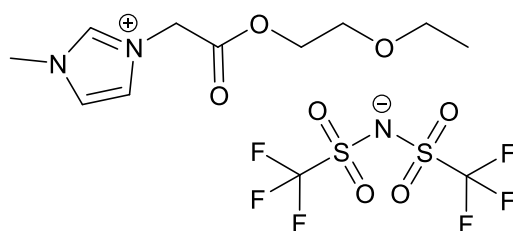
^1H NMR (400 MHz, CDCl_3) δ 8.74 (bs, 1H), 7.38 (dd, $J = 1.8, 1.8$ Hz, 1H), 7.33 (dd, $J = 1.8, 1.8$ Hz, 1H), 4.98 (s, 2H), 4.19 (t, $J = 6.7$ Hz, 2H), 3.92 (s, 3H), 1.68–1.57 (m, 2H), 1.42–1.30 (m, 2H), 0.91 (t, $J = 7.4$ Hz, 3H).

^{13}C NMR (101 MHz, CDCl_3) δ 165.89, 137.53, 123.98, 123.38, 119.79 (q, $^1J_{\text{C-F}} = 320.9$ Hz), 66.95, 49.94, 36.53, 30.30, 18.94, 13.61.

^{19}F NMR (376 MHz, CDCl_3) δ -79.22.

^1H and ^{13}C NMR data are in agreement with the literature.¹¹

3-[2-(2-Ethoxyethoxy)-2-oxoethyl]-1-methyl-1*H*-imidazol-3-ium bis(trifluoromethylsulfonyl)imide (**51**)¹¹



The title compound (**51**) was synthesised from 3-[2-(2-ethoxyethoxy)-2-oxoethyl]-1-methyl-1*H*-imidazol-3-ium bromide (**47**) (5.87 g, 20.0 mmol), deionised water (20 mL) and LiNTf_2 (6.32 g, 22.0 mmol), according

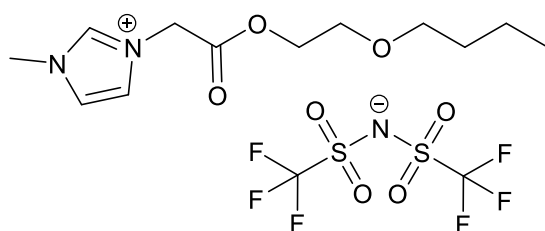
to the general procedure F. Trituration was carried out with deionised water (5×10 mL) to give a colourless liquid (8.19 g, 16.6 mmol), 83 % yield.

Chemical formula: $\text{C}_{12}\text{H}_{17}\text{F}_6\text{N}_3\text{O}_7\text{S}_2$; Molecular weight: $493.39 \text{ g mol}^{-1}$; T_{dec} : 273°C

^1H NMR (400 MHz, CDCl_3) δ 8.81 (bs, 1H), 7.36 (dd, $J = 1.8, 1.8$ Hz, 1H), 7.31 (dd, $J = 1.8, 1.8$ Hz, 1H), 5.04 (s, 2H), 4.39–4.33 (m, 2H), 3.95 (s, 3H), 3.70–3.61 (m, 2H), 3.53 (q, $J = 7.0$ Hz, 2H), 1.20 (t, $J = 7.0$ Hz, 3H). ^{13}C NMR (101 MHz, CDCl_3) δ 165.88, 137.78, 123.90, 123.34, 119.81 (q, $^1J_{\text{C-F}} = 320.9$ Hz), 67.74, 66.80, 66.09, 50.05, 36.69, 15.13. ^{19}F NMR (376 MHz, CDCl_3) δ -79.08.

^1H and ^{13}C NMR data are in agreement with the literature.¹¹

3-[2-(2-Butoxyethoxy)-2-oxoethyl]-1-methyl-1*H*-imidazol-3-ium bis(trifluoromethylsulfonyl)imide (**52**)¹¹



The title compound (**52**) was synthesised from 3-[2-(2-butoxyethoxy)-2-oxoethyl]-1-methyl-1*H*-imidazol-3-ium bromide (**48**) (6.52 g, 20.3 mmol), deionised water (20 mL) and LiNTf_2 (6.41 g, 22.3 mmol),

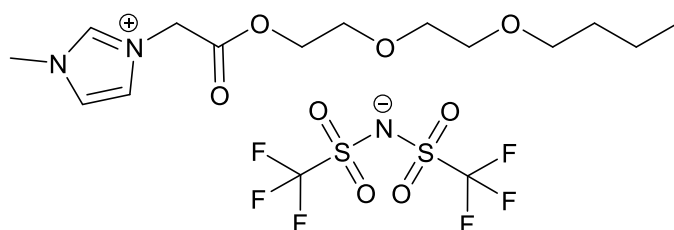
according to the general procedure F. Trituration was carried out with deionised water (5×10 mL) to give a colourless liquid (9.89 g, 19.0 mmol), 94 % yield.

Chemical formula: $\text{C}_{14}\text{H}_{21}\text{F}_6\text{N}_3\text{O}_7\text{S}_2$; Molecular weight: $521.45 \text{ g mol}^{-1}$; T_{dec} : 279°C

^1H NMR (400 MHz, CDCl_3) δ 8.81 (bs, 1H), 7.36 (dd, $J = 1.8, 1.8$ Hz, 1H), 7.32 (dd, $J = 1.8, 1.8$ Hz, 1H), 5.03 (s, 2H), 4.39–4.32 (m, 2H), 3.95 (s, 3H), 3.69–3.61 (m, 2H), 3.46 (t, $J = 6.7$ Hz, 2H), 1.60–1.49 (m, 2H), 1.42–1.29 (m, 2H), 0.91 (t, $J = 7.4$ Hz, 3H). ^{13}C NMR (101 MHz, CDCl_3) δ 165.83, 137.75, 123.89, 123.37, 119.81 (q, $^1J_{\text{C-F}} = 321.0$ Hz), 71.31, 67.94, 66.06, 50.04, 36.68, 31.67, 19.30, 13.98. ^{19}F NMR (376 MHz, CDCl_3) δ -79.08.

^1H and ^{13}C NMR data are in agreement with the literature.¹¹

3-{2-[2-(2-Butoxyethoxy)ethoxy]-2-oxoethyl}-1-methyl-1*H*-imidazol-3-ium bis(trifluoromethylsulfonyl)imide (53)¹¹



The title compound (**53**) was synthesised from 3-{2-[2-(2-butoxy-ethoxy)ethoxy]-2-oxoethyl} -1-methyl-1*H*-imidazol-3-ium bromide (**49**) (6.56 g,

18.0 mmol), deionised water (20 mL) and LiNTf_2 (5.69 g, 19.8 mmol), according to the general procedure F. Trituration was carried out with deionised water (5×10 mL) to give a colourless liquid (9.05 g, 16.0 mmol), 89 % yield.

Chemical formula: $\text{C}_{16}\text{H}_{25}\text{F}_6\text{N}_3\text{O}_8\text{S}_2$; Molecular weight: $565.50 \text{ g mol}^{-1}$; T_{dec} : 253°C

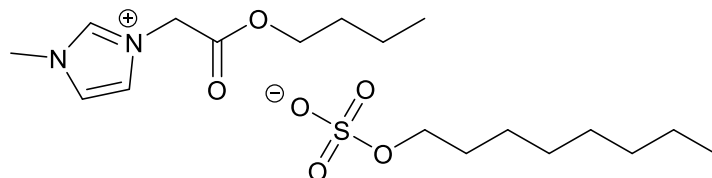
^1H NMR (400 MHz, CDCl_3) δ 8.89 (bs, 1H), 7.37 (dd, $J = 1.8, 1.8$ Hz, 1H), 7.29 (dd, $J = 1.8, 1.8$ Hz, 1H), 5.06 (s, 2H), 4.41–4.35 (m, 2H), 3.98 (s, 3H), 3.77–3.71 (m, 2H), 3.66–3.62 (m, 2H), 3.61–3.56 (m, 2H), 3.45 (t, $J = 6.8$ Hz, 2H), 1.60–1.50 (m, 2H), 1.41–1.29 (m, 2H), 0.91 (t, $J = 7.4$ Hz, 3H). ^{13}C NMR (151 MHz, CDCl_3) δ 165.76, 138.25, 123.86, 123.11, 119.86 (q, $^1J_{\text{C-F}} = 321.4$ Hz), 77.37, 70.76, 70.10, 68.55, 66.08, 50.22, 36.86, 31.80, 19.39, 14.05. ^{19}F NMR (376 MHz, CDCl_3) δ -79.00.

^1H and ^{13}C NMR data are in agreement with the literature.¹¹

6.3.4 Octyl Sulfate ILs

General Procedure G: Preparation of Octyl Sulfate ILs (54–57)

3-(2-Butoxy-2-oxoethyl)-1-methyl-1*H*-imidazol-3-ium octyl sulfate (54)¹¹



A flask was charged with 3-(2-butoxy-2-oxoethyl)-1-methyl-1*H*-imidazol-3-ium bromide (**46**) (7.68 g,

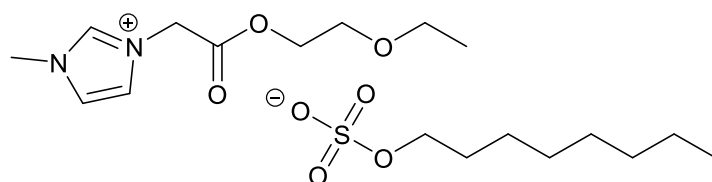
27.7 mmol) and deionised water (20 mL). Whilst stirring NaOctSO₄ (6.68 g, 29.1 mmol) was added in one portion and the reaction was stirred overnight at rt. The water was removed via rotary evaporation and the IL was dissolved in DCM (20 mL) and washed with deionised water (3 × 5 mL). The volatiles were removed via rotary evaporation and the product was dried under reduced pressure at 50 °C for 2 days to give the title compound (**54**) as a colourless grease (10.31 g, 25.36 mmol), 92 % yield.

Chemical formula: C₁₈H₃₄N₂O₆S; Molecular weight: 406.54 g mol⁻¹; T_{dec}: 159 °C

¹H NMR (400 MHz, CDCl₃) δ 9.37 (bs, 1H), 7.54 (dd, *J* = 1.7, 1.7 Hz, 1H), 7.48 (dd, *J* = 1.7, 1.7 Hz, 1H), 5.17 (s, 2H), 4.13 (t, *J* = 6.8 Hz, 2H), 4.00 – 3.86 (m, 5H), 1.66–1.51 (m, 4H), 1.39–1.10 (m, 12H), 0.87 (t, *J* = 7.4 Hz, 3H), 0.81 (t, *J* = 6.8 Hz, 3H). ¹³C NMR (101 MHz, CDCl₃) δ 166.39, 139.62, 123.51, 122.80, 68.01, 66.94, 50.12, 36.79, 31.96, 30.47, 29.65, 29.50, 29.40, 26.01, 22.80, 19.10, 14.26, 13.78.

¹H and ¹³C NMR data are in agreement with the literature.¹¹

3-[2-(2-Ethoxyethoxy)-2-oxoethyl]-1-methyl-1*H*-imidazol-3-ium octyl sulfate (55)¹¹



The title compound (**55**) was synthesised from 3-[2-(2-ethoxyethoxy)-2-oxoethyl]-1-methyl-1*H*-imidazol-3-ium

bromide (**47**) (7.07 g, 24.1 mmol), deionised water (20 mL) and NaOctSO₄ (5.88 g, 25.3 mmol), according to the general procedure G to give a light yellow grease (8.58 g, 20.3 mmol), 84 % yield.

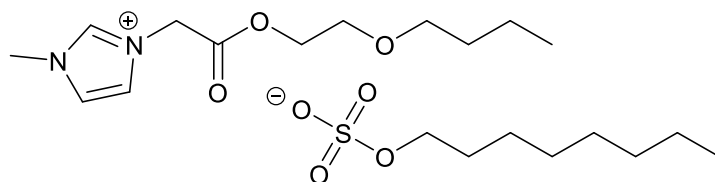
Chemical formula: C₁₈H₃₄N₂O₇S; Molecular weight: 422.54 g mol⁻¹; T_{dec}: 157 °C

¹H NMR (400 MHz, CDCl₃) δ 9.49 (bs, 1H), 7.49 (dd, *J* = 1.8, 1.8 Hz, 1H), 7.40 (dd, *J* = 1.8, 1.8 Hz, 1H), 5.25 (s, 2H), 4.37–4.30 (m, 2H), 3.99 (s, 3H), 3.99 (t, *J* = 6.9 Hz, 2H), 3.68–3.63 (m, 2H), 3.52 (q, *J* = 7.0 Hz, 2H), 1.70–1.57 (m, 2H), 1.40–1.21 (m,

10H), 1.19 (t, $J = 7.0$ Hz, 3H), 0.85 (t, $J = 6.7$ Hz, 3H). ^{13}C NMR (101 MHz, CDCl_3) δ 166.56, 138.97, 123.84, 123.14, 67.97, 67.85, 66.79, 65.82, 50.04, 36.71, 31.93, 29.61, 29.47, 29.37, 25.98, 22.77, 15.20, 14.23.

^1H and ^{13}C NMR data are in agreement with the literature.¹¹

3-[2-(2-Butoxyethoxy)-2-oxoethyl]-1-methyl-1*H*-imidazol-3-ium octyl sulfate (**56**)¹¹



The title compound (**56**) was synthesised from 3-[2-(2-butoxyethoxy)-2-oxoethyl]-1-methyl-1*H*-imidazol-3-ium

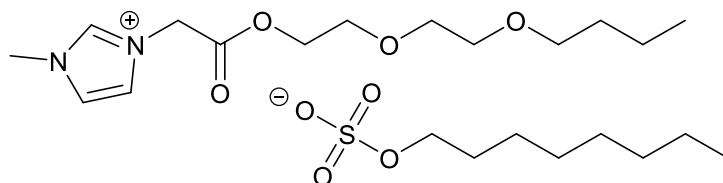
octyl bromide (**48**) (7.48 g, 23.3 mmol), deionised water (20 mL) and NaOctSO_4 (5.68 g, 24.5 mmol), according to the general procedure G to give a colourless liquid (7.82 g, 17.4 mmol), 75 % yield.

Chemical formula: $\text{C}_{20}\text{H}_{38}\text{N}_2\text{O}_7\text{S}$; Molecular weight: $450.59 \text{ g mol}^{-1}$; T_{dec} : 182°C

^1H NMR (400 MHz, CDCl_3) δ 9.65 (bs, 1H), 7.38 (dd, $J = 1.8, 1.8$ Hz, 1H), 7.29 (dd, $J = 1.8, 1.8$ Hz, 1H), 5.24 (s, 2H), 4.39–4.31 (m, 2H), 4.02 (t, $J = 6.9$ Hz, 2H), 4.01 (s, 3H), 3.69–3.62 (m, 2H), 3.46 (t, $J = 6.7$ Hz, 2H), 1.71–1.61 (m, 2H), 1.60–1.51 (m, 2H), 1.43–1.17 (m, 12H), 0.92 (t, $J = 7.4$ Hz, 3H), 0.87 (t, $J = 6.7$ Hz, 3H). ^{13}C NMR (101 MHz, CDCl_3) δ 166.39, 139.57, 123.57, 122.87, 71.38, 68.05, 68.00, 65.93, 50.10, 36.79, 31.96, 31.73, 29.65, 29.50, 29.40, 26.01, 22.80, 19.37, 14.26, 14.06.

^1H and ^{13}C NMR data are in agreement with the literature.¹¹

3-{2-[2-(2-Butoxyethoxy)ethoxy]-2-oxoethyl}-1-methyl-1*H*-imidazol-3-ium octyl sulfate (**57**)¹¹



The title compound (**57**) was synthesised from 3{2-[2-(2-butoxyethoxy)ethoxy]-2-oxoethyl}-1-methyl -1*H* -

imidazol-3-ium bromide (**49**) (7.54 g, 20.6 mmol), deionised water (20 mL) and LiNTf_2 (5.04 g, 21.7 mmol), according to the general procedure G. The reaction was stirred for 2 days to give a light yellow gel (10.08 g, 20.38 mmol), 99 % yield.

Chemical formula: $\text{C}_{22}\text{H}_{42}\text{N}_2\text{O}_8\text{S}$; Molecular weight: $494.64 \text{ g mol}^{-1}$; T_{dec} : 159°C

^1H NMR (400 MHz, CDCl_3) δ 9.64 (bs, 1H), 7.48 (dd, $J = 1.8, 1.8$ Hz, 1H), 7.33 (dd, $J = 1.8, 1.8$ Hz, 1H), 5.27 (s, 2H), 4.39–4.33 (m, 2H), 4.04–3.98 (m, 5H), 3.76–3.70 (m, 2H), 3.67–3.61 (m, 2H), 3.61–3.55 (m, 2H), 3.45 (t, $J = 6.8$ Hz, 2H), 1.70–1.60 (m, 2H),

1.60–1.50 (m, 2H), 1.42–1.15 (m, 12H), 0.90 (t, $J = 7.4$ Hz, 3H), 0.86 (t, $J = 6.7$ Hz, 3H). ^{13}C NMR (101 MHz, CDCl_3) δ 166.53, 138.75, 123.97, 123.17, 71.30, 70.65, 70.02, 68.65, 67.99, 65.64, 49.99, 36.69, 31.90, 31.70, 29.57, 29.43, 29.35, 25.95, 22.74, 19.33, 14.21, 14.03.

^1H and ^{13}C NMR data are in agreement with the literature.¹¹

6.4 Experimental Preparations for PLLA and PLLA/IL Films

PLLA was mixed with IL (0, 10, 20 and 30 wt%) (Table 5.1) in a laboratory scale co-rotating twin-screw extruder under N_2 at 200 °C and 100 rpm for approximately 7 min. Films with a thickness of 0.5 ± 0.05 mm were prepared by melt compressing the extruded PLLA/IL blends of various weight ratios at 200 °C, under ca 5 kN force in a hot press followed by quenching to room temperature in a cold press. To ensure consistency in the film thickness a rectangular steel spacer (0.5 mm) was used.

Table 6.1 Mass of IL and PLLA used to synthesis PLLA/IL films with 0, 10, 20 and 30 wt% IL.

IL (wt%)	Mass (g)	
	PLLA	IL
0	8.0	0.0
10	7.2	0.8
20	6.4	1.6
30	5.6	2.4

6.5 Antimicrobial Screening Test Procedures

6.5.1 Antibacterial Activity – DCU

Mueller-Hinton broth was purchased from Oxoid. Five bacterial strains were used in this study: the Gram-positive bacterium *Bacillus subtilis* DSMZ 10 (*B. subtilis*) and the Gram-negative bacteria *Escherichia coli* DSMZ 498 (*E. coli*), *Pseudomonas fluorescens* DSMZ 270 50090 (*P. fluorescens*), *Pseudomonas putida* CP1 (*P. putida* CP1) and *Pseudomonas putida* KT2440 (*P. putida* KT2440). All strains were purchased at DSMZ (German Collection of Microorganisms and Cell Cultures).

IC₅₀ values for the compounds were determined using a modification of the broth microdilution method described by Amsterdam.¹² Strains were grown in nutrient broth overnight, washed with 0.01 M sodium phosphate buffer (pH 7) and the cell number adjusted to give an optical density reading of 0.07 at 660 nm. The antimicrobial activity of the ILs was tested in 96 well round bottom microplates. 180 µL of Mueller-Hinton broth was pipetted into column 1 of the wells and 100 µL into the other wells. 20 µL of the chemical solution was transferred into column 1 giving a maximum concentration of 200 mM. 100 µL of the solution from column 1 was then transferred to the next column and mixed. The procedure was repeated to give a series of two-fold dilutions. Each well was inoculated with 5 µL of bacterial culture. Wells containing medium only were used as blanks and wells containing medium and culture only were used as positive controls. All the toxicity tests were carried out in triplicate. The microplates were incubated overnight at 30 °C. The presence or absence of growth was determined by measuring the optical density of the wells at a wavelength of 405 nm using a plate reader. The IC₅₀ values were determined as the concentration or range of concentrations that caused a 50 % reduction in growth.

6.5.2 Antibacterial Activity – Charles University

In vitro antibacterial activities of the compounds were evaluated on a panel of three ATCC strains (*Staphylococcus aureus* ATTC 6538, *Escherichia coli* ATTC 8739, *Pseudomonas aeruginosa* ATTC 9027) and five clinical isolates (*Staphylococcus aureus* MRSA HK5996/08, *Staphylococcus epidermidis* HK6966/08, *Enterococcus sp.* HK14365/08, *Klebsiella pneumoniae* HK11750/08, *Klebsiella pneumoniae* ESBL HK14368/08) from the collection of bacterial strains deposited at the Department of Biological and Medical Sciences, Faculty of Pharmacy, Charles University, Hradec Králové, Czech Republic. The abovementioned ATCC strains also served as the quality control strains. All the isolates were maintained on Mueller-Hinton dextrose agar prior to being tested.

Dimethyl sulfoxide (100 %) served as a diluent for all compounds; the final concentration did not exceed 2 %. Mueller-Hinton agar (MH, HiMedia, Čadarský-Envitek, Czech Republic) buffered to pH 7.4 (±0.2) was used as the test medium. The wells of the microdilution tray contained 200 µL of the Mueller-Hinton medium with 2-fold serial dilutions of the compounds (2000 or 1000 to 0.24 µmol L⁻¹) and 10 µL of inoculum suspension. Inoculum in MH medium was prepared to give a final

concentration of 0.5 McFarland scale (1.5×10^8 cfu mL⁻¹). The trays were incubated at 35 °C and MICs were read visually after 24 h and 48 h. The MICs were defined as 95 % inhibition (IC₉₅) of the control growth. MICs were determined twice and in duplicate. The deviations from the usually obtained values were no higher than the nearest concentration value up and down the dilution scale.

6.5.3 Antifungal Activity – Charles University

In vitro antifungal activities of the compounds were evaluated on a panel of four ATCC strains (*Candida albicans* ATCC 44859, *Candida albicans* ATCC 90028, *Candida parapsilosis* ATCC 22019, *Candida krusei* ATCC 6258) and eight clinical isolates of fungi; five yeasts (*Candida krusei* E28, *Candida tropicalis* 156, *Candida glabrata* 20/I, *Candida lusitanae* 2446/I, *Trichosporon asahii* 1188) and three filamentous fungi (*Aspergillus fumigatus* 231, *Absidia corymbifera* 272, *Trichophyton mentagrophytes* 445) from the collection of fungal strains deposited at the Department of Biological and Medical Sciences, Faculty of Pharmacy, Charles University, Hradec Králové, Czech Republic. Three of the above ATCC strains (*Candida albicans* ATCC 90028, *Candida parapsilosis* ATCC 22019, *Candida krusei* ATCC 6258) also served as the quality control strains. All the isolates were maintained on Sabouraud dextrose agar prior to being tested. Minimum inhibitory concentrations (MICs) were determined by modified CLSI standard of the microdilution format of the M27-A3 and M38-A2 documents for yeasts and filamentous fungi respectively.^{13,14}

Dimethyl sulfoxide (100 %) served as a diluent for all compounds; the final concentration did not exceed 2 %. RPMI 1640 (Sevapharma, Prague) medium supplemented with L-glutamine and buffered with 0.165 M morpholinepropanesulfonic acid (Serva) to pH 7.0 by 10 N NaOH was used as the test medium. The wells of the microdilution tray contained 200 µL of the RPMI 1640 medium with 2-fold serial dilutions of the compounds (2000 or 1000 to 0.24 µmol L⁻¹) and 10 µL of inoculum suspension. Fungal inoculum in RPMI 1640 was prepared to give a final concentration of $5 \times 10^3 \pm 0.2$ cfu mL⁻¹. The trays were incubated at 35 °C and MICs were read visually for filamentous fungi and photometrically for yeasts at an absorbance at 540 nm after 24 h and 48 h. The MIC values for the dermatophytic strain (*T. mentagrophytes*) were determined after 72 h and 120 h. For all other strains MIC values were evaluated after 24 and 48 h. The MICs were defined as 50 % inhibition (IC₅₀) of the control growth for yeasts or 80 % inhibition (IC₈₀) of the growth of control for

filamentous fungi. MICs were determined twice and in duplicate. The deviations from the usually obtained values were no higher than the nearest concentration value up and down the dilution scale.

6.6 Closed Bottle Biodegradation Test Procedure

The CBT measures aerobic biodegradability and is one of six test methods described in the OECD Guidelines for Testing of Chemicals¹⁵ used to evaluate readily biodegradability of organic compounds. The test was undertaken at 20 ± 1 °C in the dark in the laboratories of the Institute of Sustainable and Environmental Chemistry at Leuphana University Lüneburg as described in details elsewhere.¹⁶ It consisted of four different test series all run in duplicate. The blank series contained only mineral medium and inoculum. The test series contained additionally the IL as the only organic carbon available for the microorganisms during the test. The quality control contained, in addition to the blank, the readily biodegradable compound sodium acetate, which was used to monitor the activity of the microorganisms. The toxicity control contained both the IL and the sodium acetate in addition to the mineral medium and inoculum. The amount of IL and sodium acetate corresponded to a theoretical oxygen demand (ThOD) of 5 mgL^{-1} . The same mineral salt solution was used for all the test vessels with two drops of inoculum obtained from the effluent of the municipal sewage treatment plant in Lüneburg, Abwasser, Grünund Lüneburger Service GmbH, Germany.

According to the guidelines, for the test to be valid the reference compound sodium acetate needs to degrade by at least 60 % within 14 days. Toxicity towards the test microorganisms was evaluated by comparing the oxygen consumption of the toxicity control to the predicted level of oxygen consumption, calculated from the oxygen consumption of the quality control and the test control. A compound is labelled toxic if the difference between the predicted oxygen consumption and the measured oxygen consumption exceeds 25 %.¹⁵

The biochemical oxygen demand (BOD) was measured in accordance with international standard methods¹⁷ using sensor spots in the bottles and an oxygen electrode (Oxi 196 with EO 196-1.5 WTW Weilheim, Germany)¹⁸ at a day 0, 0 (after 3 h), 1, 7, 14, 21 and 28.

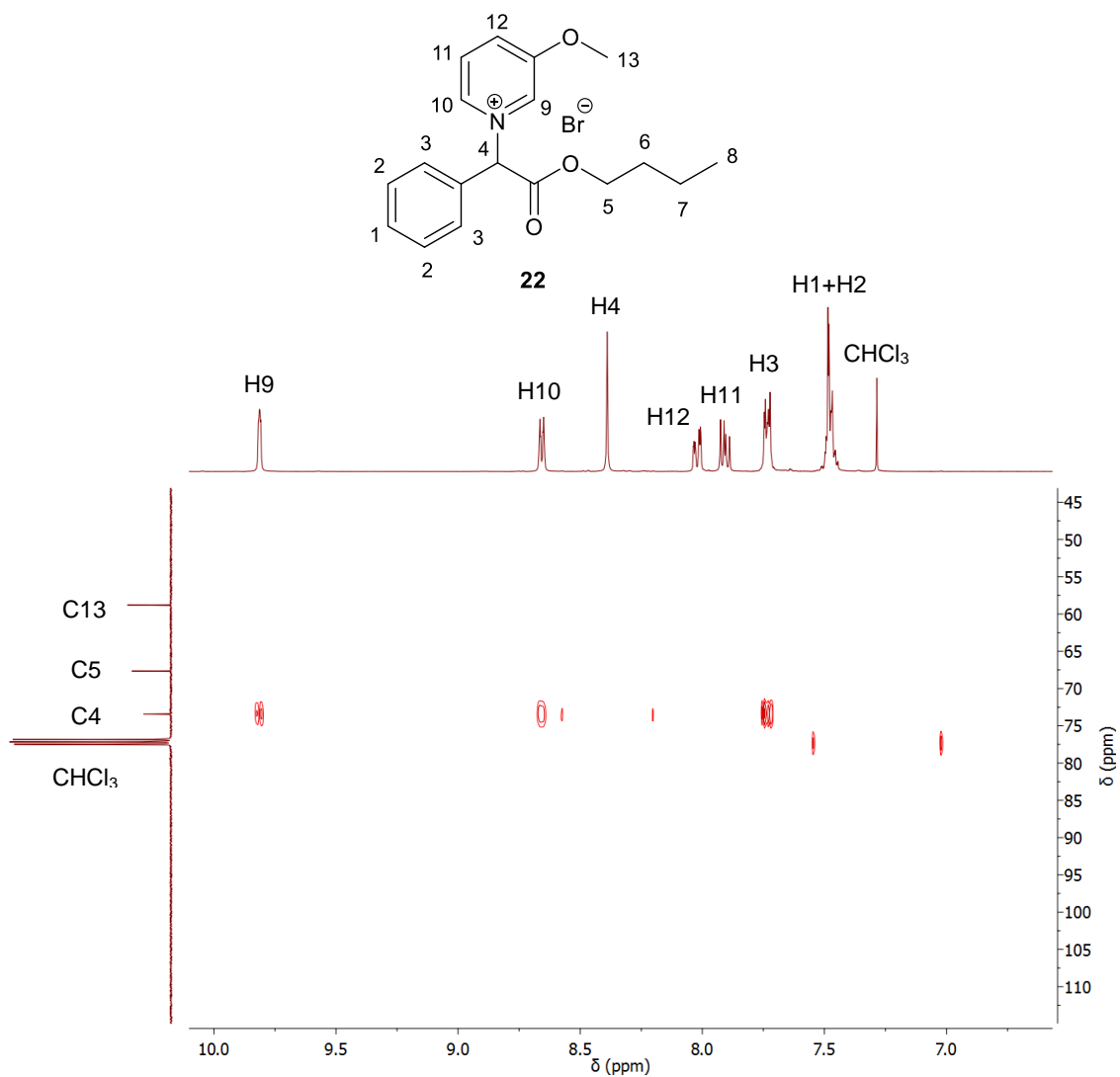
6.7 References

1. M. J. Kamaruddin, N. T. Nguyen, G. A. Dimitrakis, J. El Harfi, E. R. Binner, S. W. Kingman, E. Lester, J. P. Robinson and D. J. Irvine, *RSC Adv.*, 2014, **4**, 5709.
2. A. D. Smith, E. H. Lester, K. J. Thurecht, S. W. Kingman, J. El Harfi, G. Dimitrakis, J. P. Robinson and D. J. Irvine, *Ind. Eng. Chem. Res.*, 2010, **49**, 3011.
3. M. Sreenivasulu, K. Arun Kumar, K. Sateesh Reddy, K. Siva Kumar, P. Rajender Kumar, K. B. Chandrasekhar and M. Pal, *Tetrahedron Lett.*, 2011, **52**, 727.
4. C. S. Marques, M. Dindaroglu, H.-G. Schmalz and A. J. Burke, *RSC Adv.*, 2014, **4**, 6035.
5. S.-S. Weng, H.-C. Li and T.-M. Yang, *RSC Adv.*, 2013, **3**, 1976.
6. N. Kambe, T. Inoue, T. Takeda, S.-i. Fujiwara and N. Sonoda, *J. Am. Chem. Soc.*, 2006, **128**, 12650.
7. C. Dai, J. M. R. Narayanam and C. R. J. Stephenson, *Nature Chem.*, 2011, **3**, 140.
8. K. Ohno, Y. Ma, Y. Huang, C. Mori, Y. Yahata, Y. Tsujii, T. Maschmeyer, J. Moraes and S. Perrier, *Macromolecules*, 2011, **44**, 8944.
9. Y. Su, L. Zhang and N. Jiao, *Org. Lett.*, 2011, **13**, 2168.
10. Y.-M. Su, G.-S. Feng, Z.-Y. Wang, Q. Lan and X.-S. Wang, *Angew. Chem., Int. Ed.*, 2015, **54**, 6003.
11. S. Morrissey, B. Pegot, D. Coleman, M. T. Garcia, D. Ferguson, B. Quilty and N. Gathergood, *Green Chem.*, 2009, **11**, 475.
12. D. Amsterdam, in *Antibiotics in Laboratory Medicine*, ed. V. Lorian, Lippincott Williams & Wilkins, Philadelphia, 2005, ch. 3, pp. 61-143.
13. M27-A3; Reference Method for Broth Dilution Antifungal Susceptibility Testing of Yeasts; Approved Standard Institute - Third Edition, Clinical and Laboratory Standards Institute, Wayne, PA, 2008.
14. M38-A2; Reference Method for Broth Dilution Antifungal Susceptibility Testing of Filamentous Fungi; Approved Standard Institute - Second Edition, Clinical and Laboratory Standards Institute, Wayne, PA, 2008.
15. Organization for Economic Cooperation and Development (OECD), *OECD Guidelines for Testing of Chemicals; Ready Biodegradability*, Paris, July 1992.

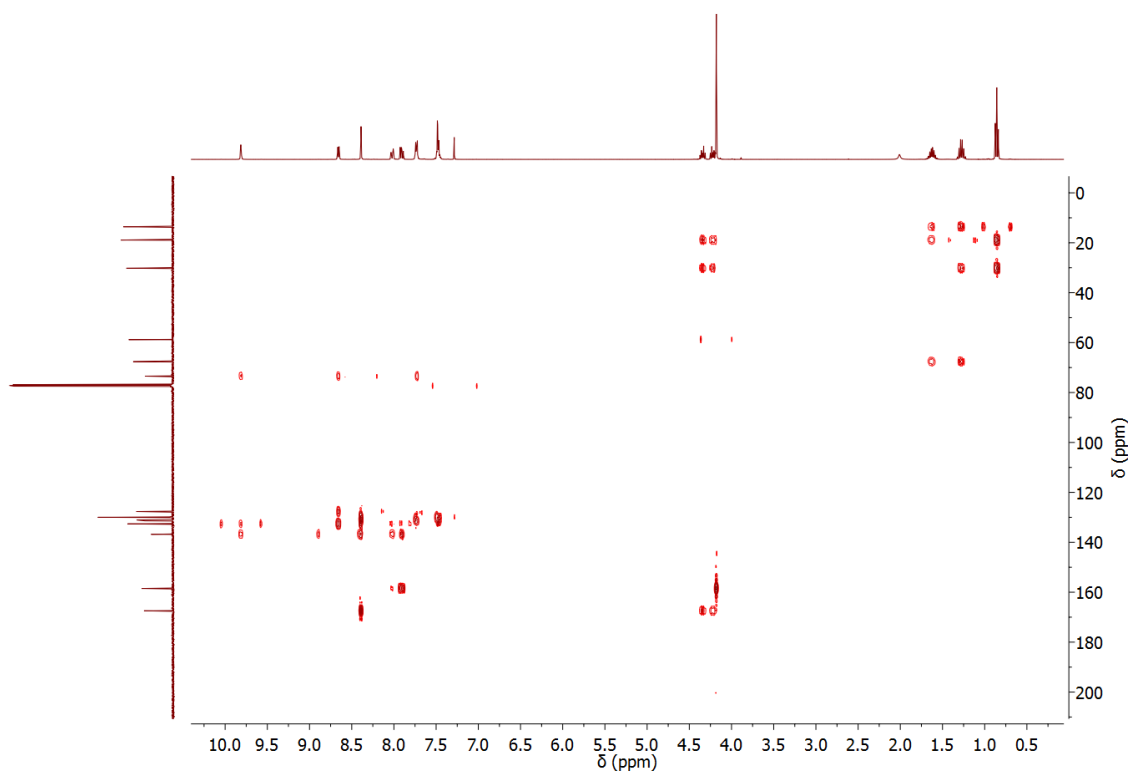
16. K. Kümmerer, A. Al-Ahmad and T. Steger-Hartmann, *Umweltmed. Forsch. Prax.*, 1996, **1**, 133.
17. International Organization for Standardization (ISO), ISO Standard 5814, Water quality - Determination of dissolved oxygen - Electrochemical probe method, Geneva, 2012.
18. J. Friedrich, A. Längin and K. Kümmerer, *CLEAN – Soil, Air, Water*, 2013, **41**, 251.

Appendices

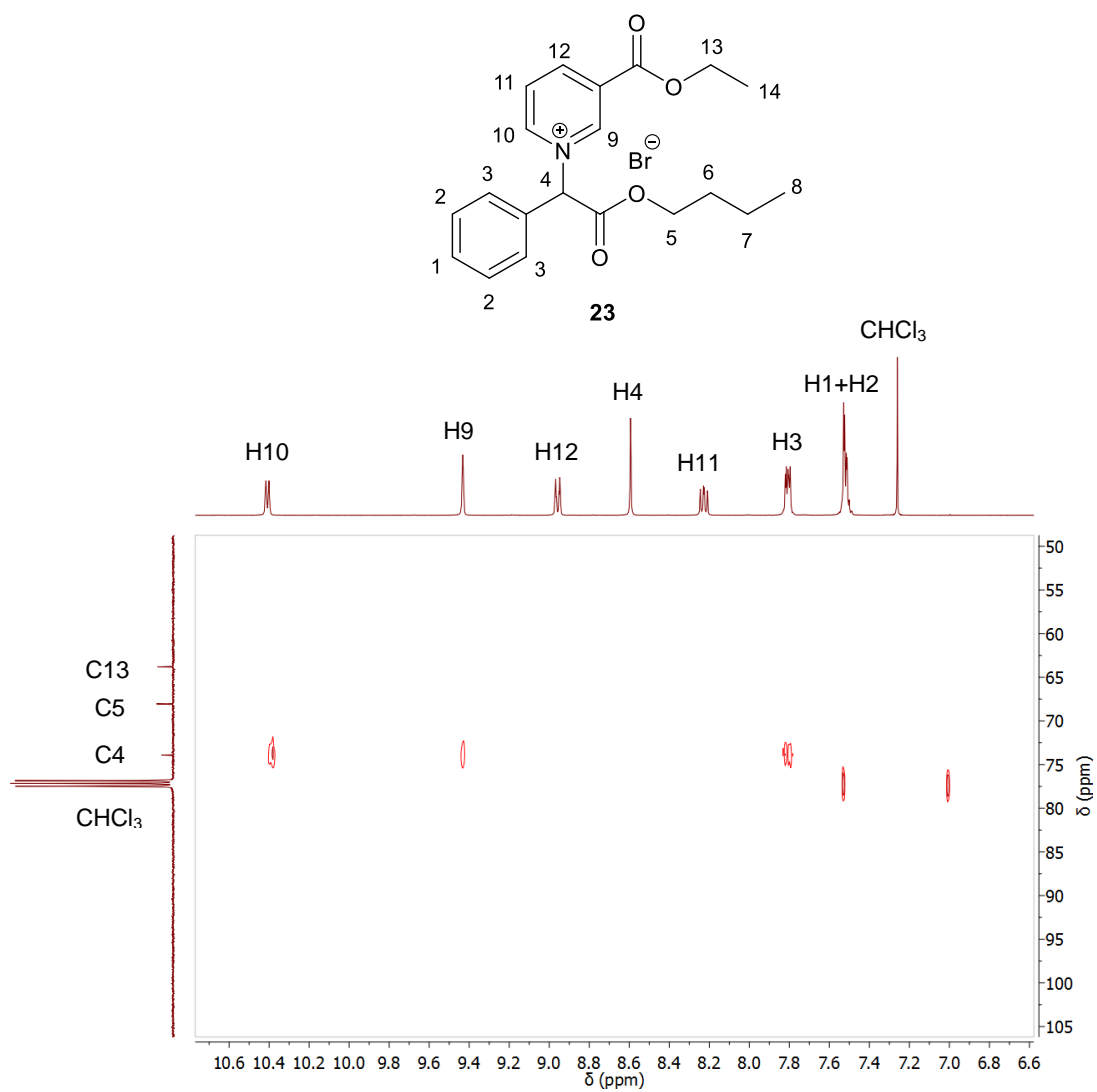
Appendix A – HMBC Spectra



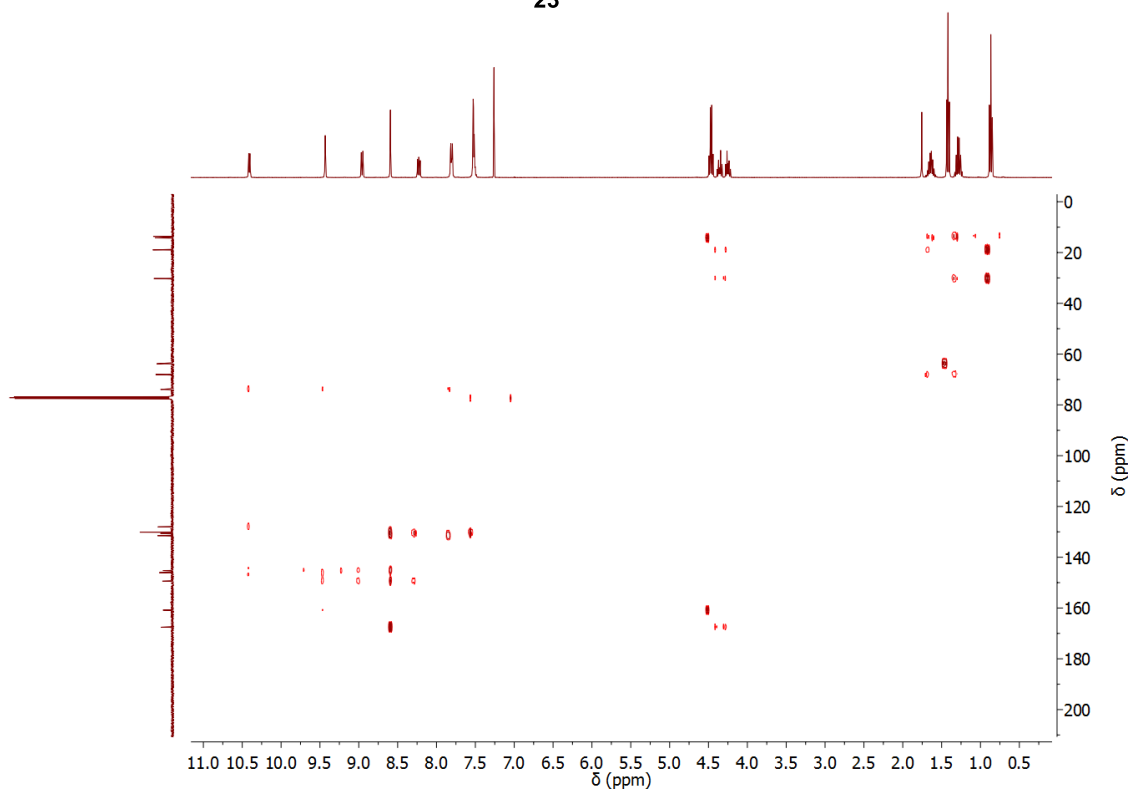
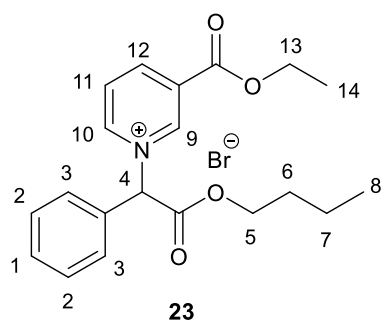
A1 HMBC spectrum of IL **22** in CDCl_3 showing the presence of the multiple bond correlation between H10 to C4, and the absence of the correlation between H12 and C4.



A-2



A3 HMBC spectrum of IL **23** in CDCl₃ showing the presence of the multiple bond correlation between H10 to C4, and the absence of the correlation between H12 and C4.



A4 Full HMBC spectrum of IL **23** in CDCl₃.

Appendix B – Antimicrobial Screening Data

B1 Antibacterial screening results for ILs **8–11** (MIC, IC₉₅).^{1,2}

Strain	Time (h)	IL MIC (μM)
		8–11
SA	24h	>2000
	48h	>2000
MRSA	24h	>2000
	48h	>2000
SE	24h	>2000
	48h	>2000
EF	24h	>2000
	48h	>2000
EC	24h	>2000
	48h	>2000
KP	24h	>2000
	48h	>2000
KP-E	24h	>2000
	48h	>2000
PA	24h	>2000
	48h	>2000

B2 Antifungal screening results for ILs **8–11** (MIC, IC₈₀ or IC₅₀).^{1,2}

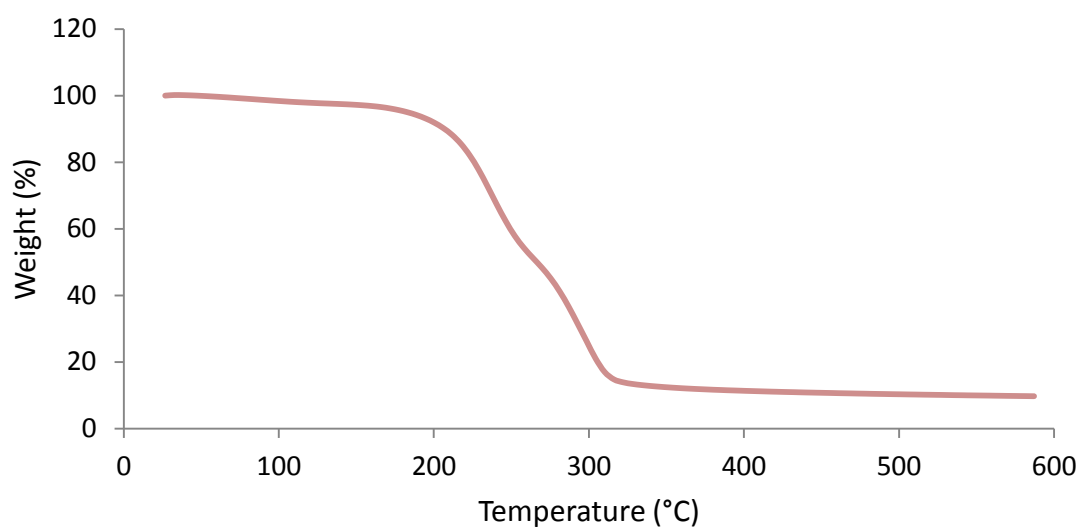
Strain	Time (h)	IL MIC (μM) ^a	
		8–10	11
CA1	24h	>2000	2000
	48h	>2000	2000
CA2	24h	>2000	>2000
	48h	>2000	>2000
CP	24h	>2000	>2000
	48h	>2000	>2000
CK1	24h	>2000	>2000
	48h	>2000	>2000
CK2	24h	>2000	>2000
	48h	>2000	>2000
CT	24h	>2000	2000
	48h	>2000	>2000
CG	24h	>2000	>2000
	48h	>2000	>2000
CL	24h	>2000	2000
	48h	>2000	>2000
TA	24h	>2000	>2000
	48h	>2000	>2000
AF	24h	>2000	>2000
	48h	>2000	>2000
AC	24h	>2000	>2000
	48h	>2000	>2000
TM	72h	>2000	>2000
	120h	>2000	>2000

^aIC₅₀ values were assessed for AF, AC and TM and IC₈₀ for all other strains.

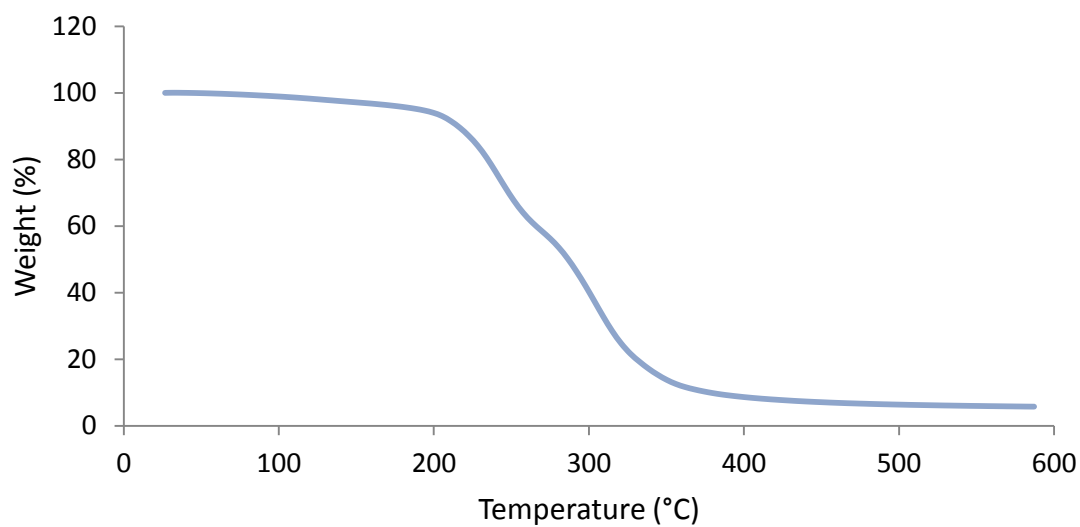
References

1. M. Ghavre, PhD Thesis, Dublin City University, 2012.
2. M. Gurbisz, PhD Thesis, Dublin City University, 2012.

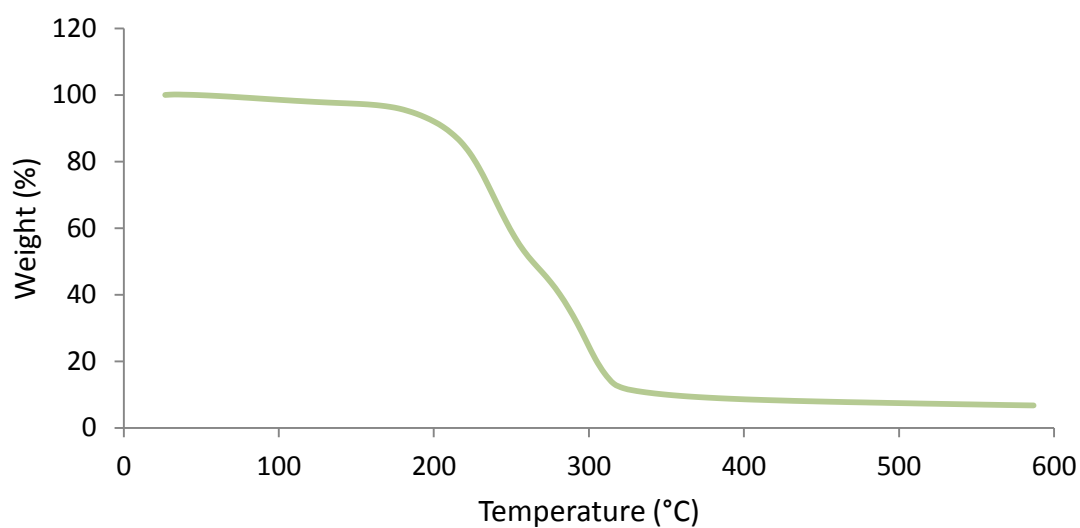
Appendix C – TGA Curves



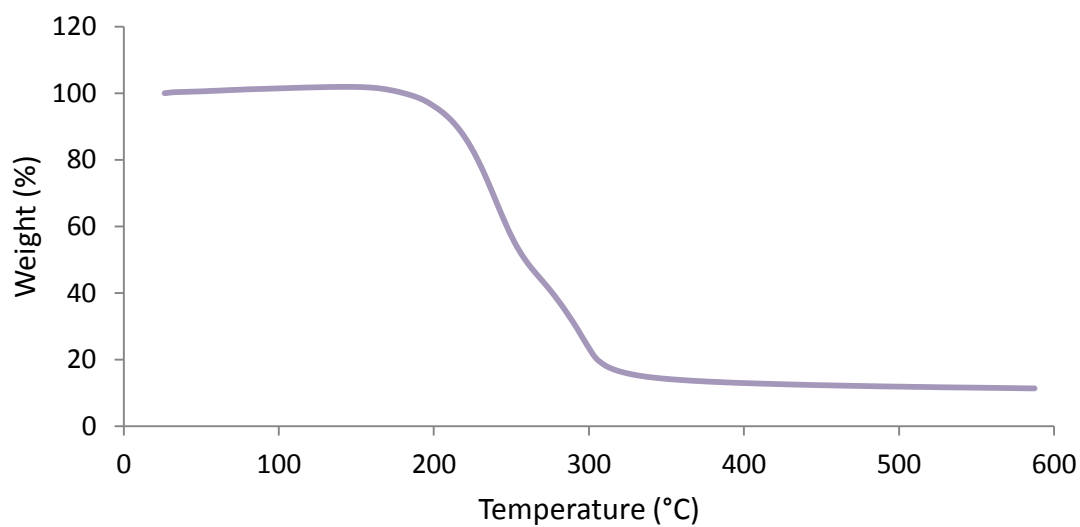
C1 TGA curve for IL **46**.



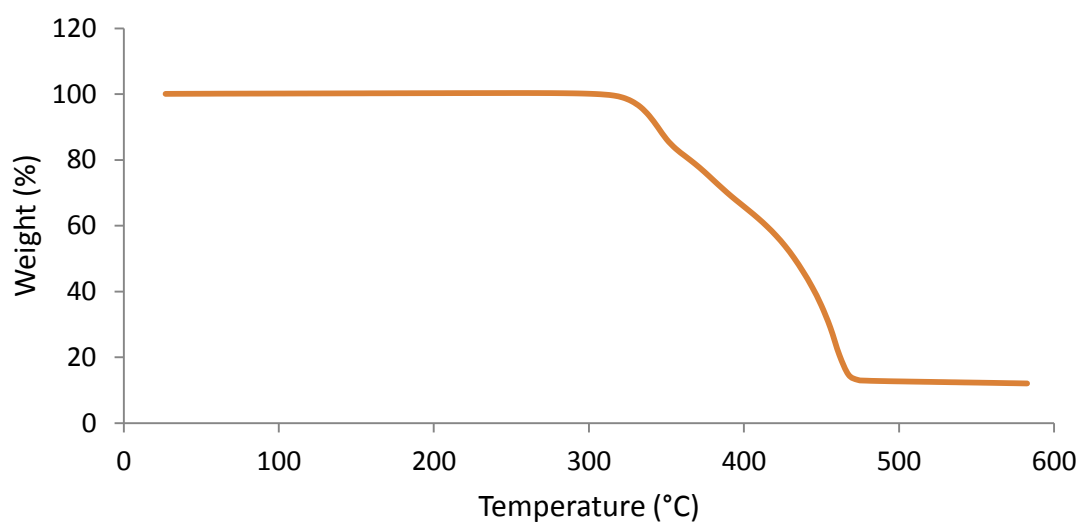
C2 TGA curve for IL **47**.



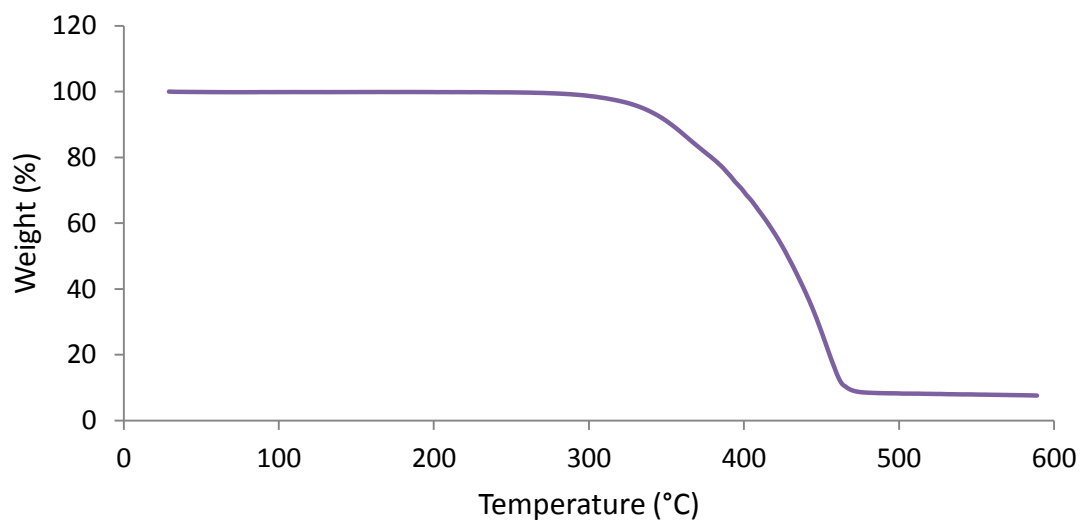
C3 TGA curve for IL **48**.



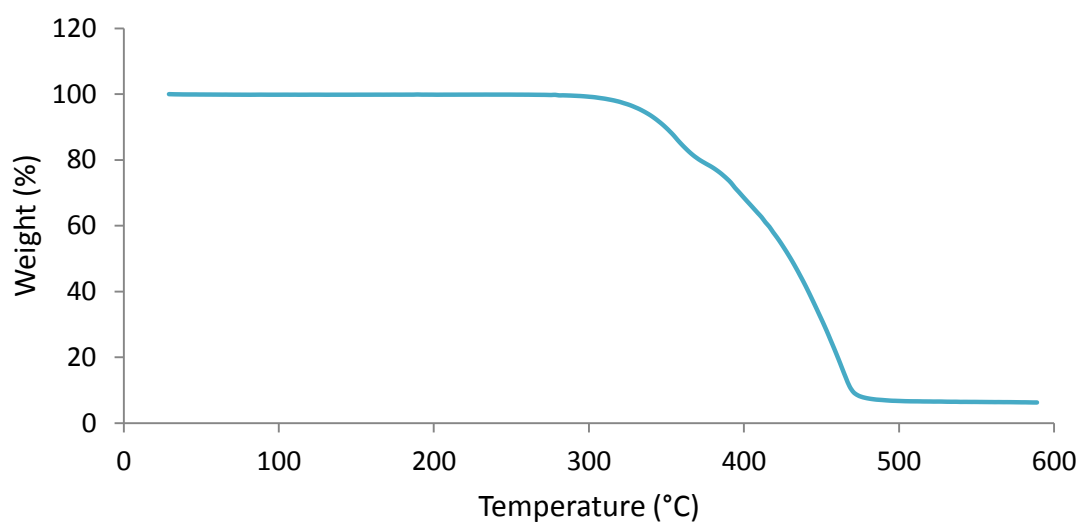
C4 TGA curve for IL **49**.



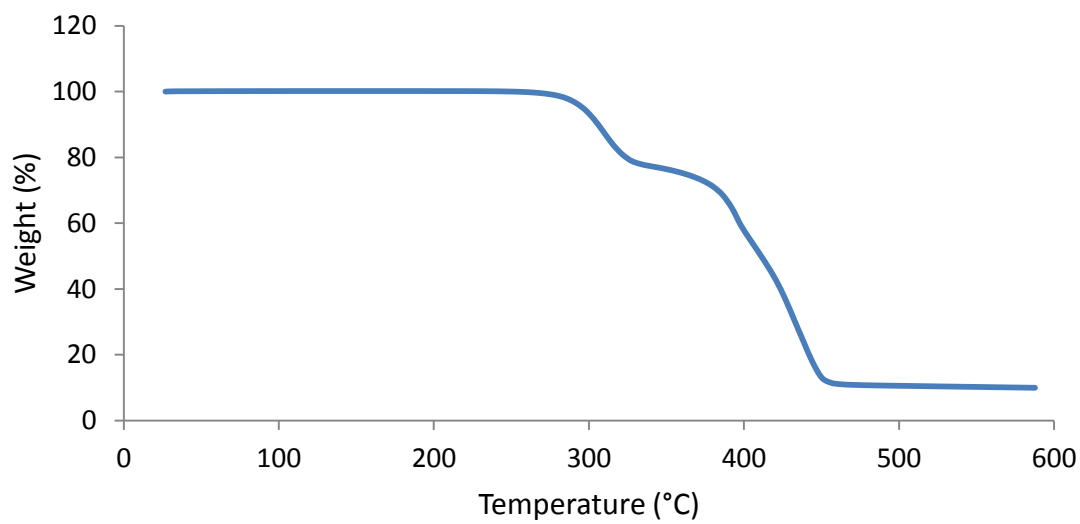
C5 TGA curve for IL **50**.



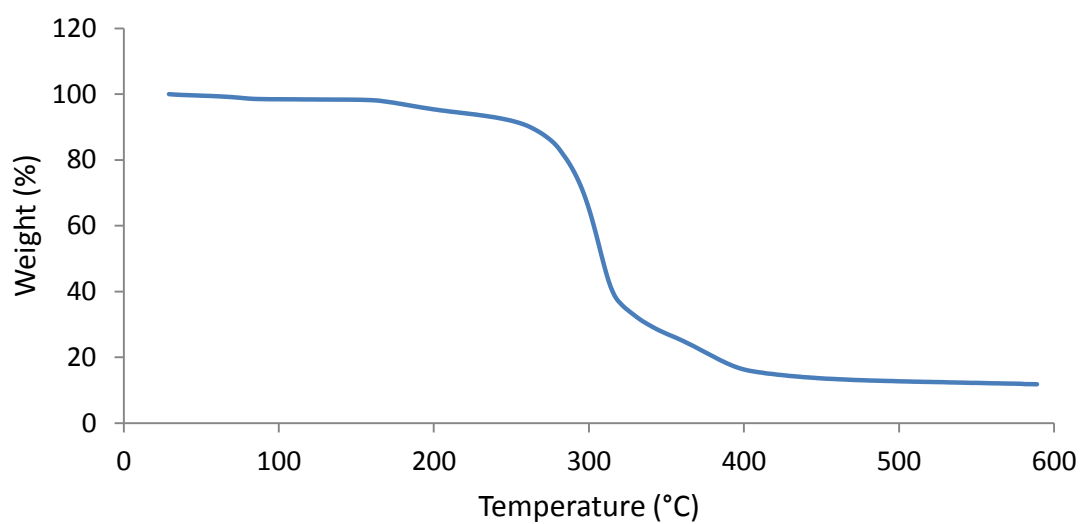
C6 TGA curve for IL **51**.



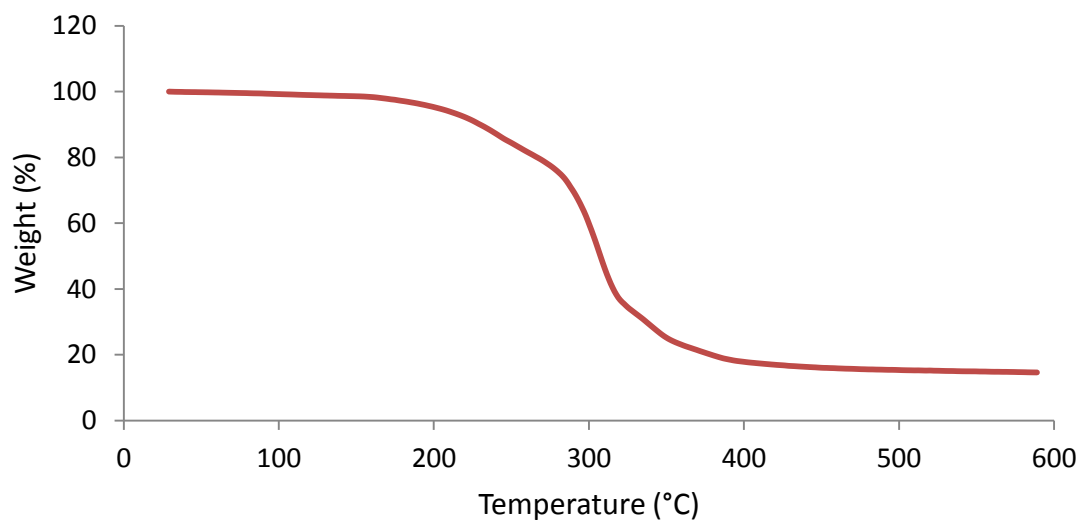
C7 TGA curve for IL **52**.



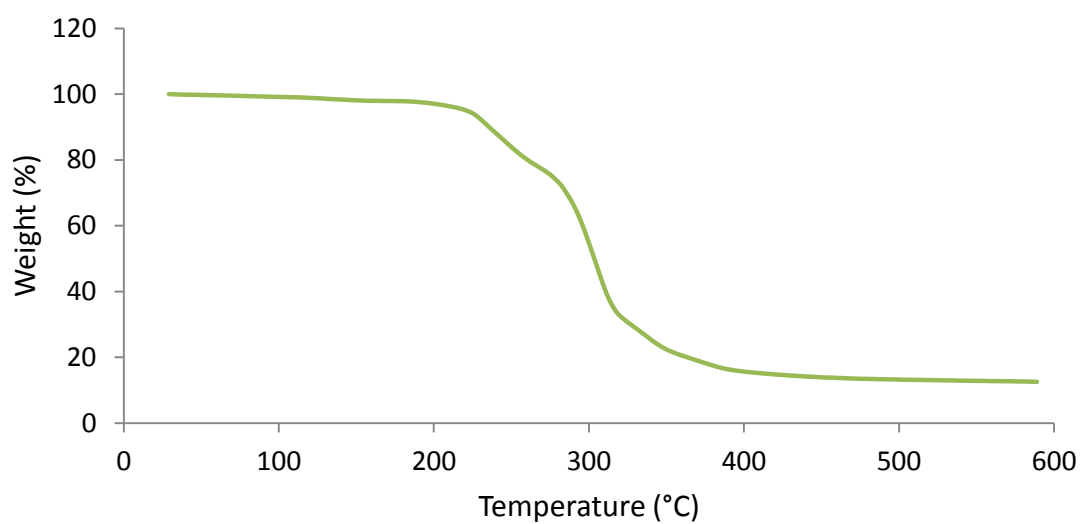
C8 TGA curve for IL **53**.



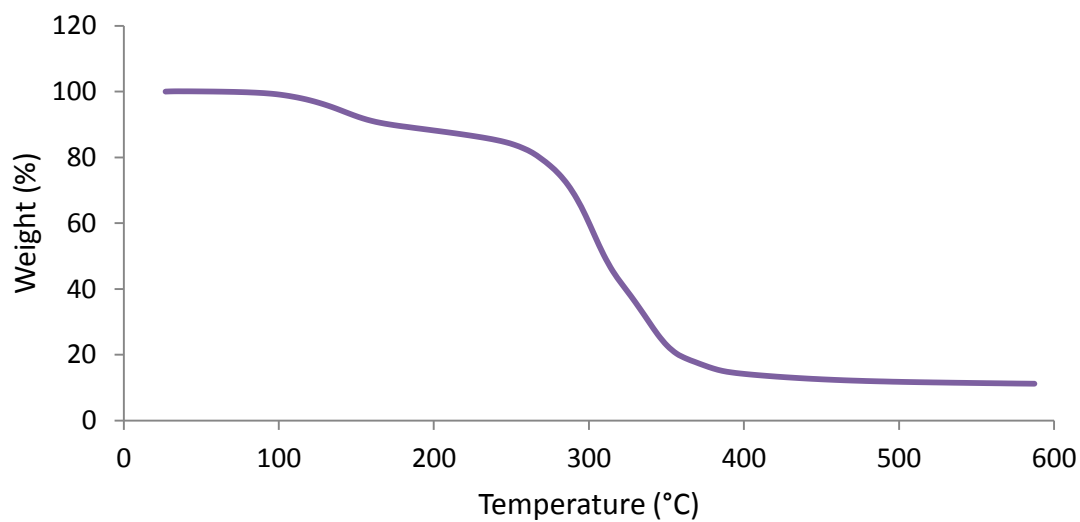
C9 TGA curve for IL **54**.



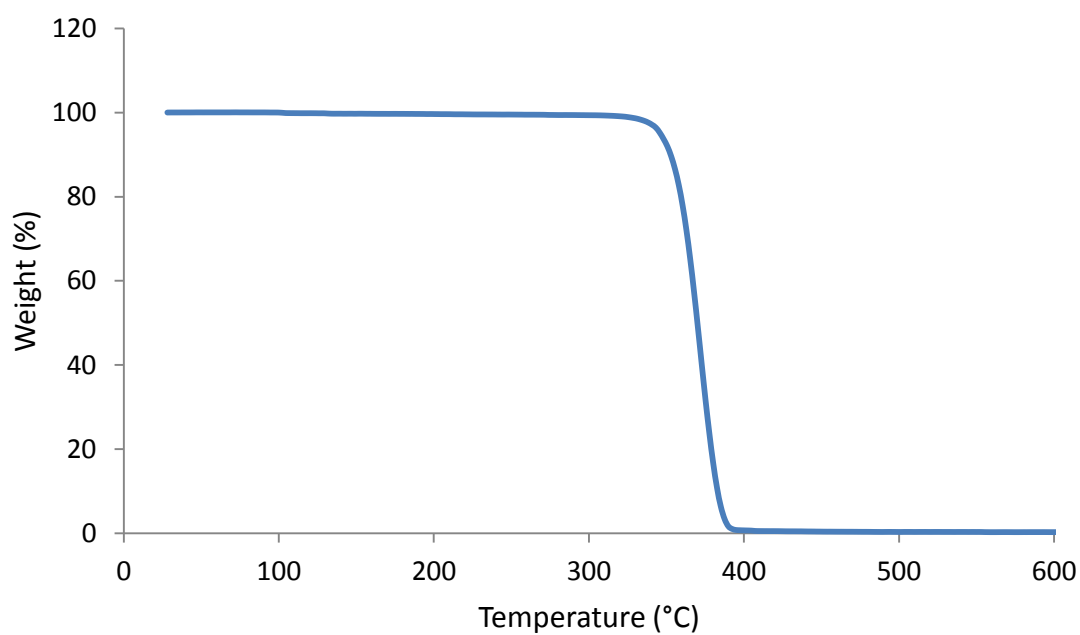
C10 TGA curve for IL **55**.



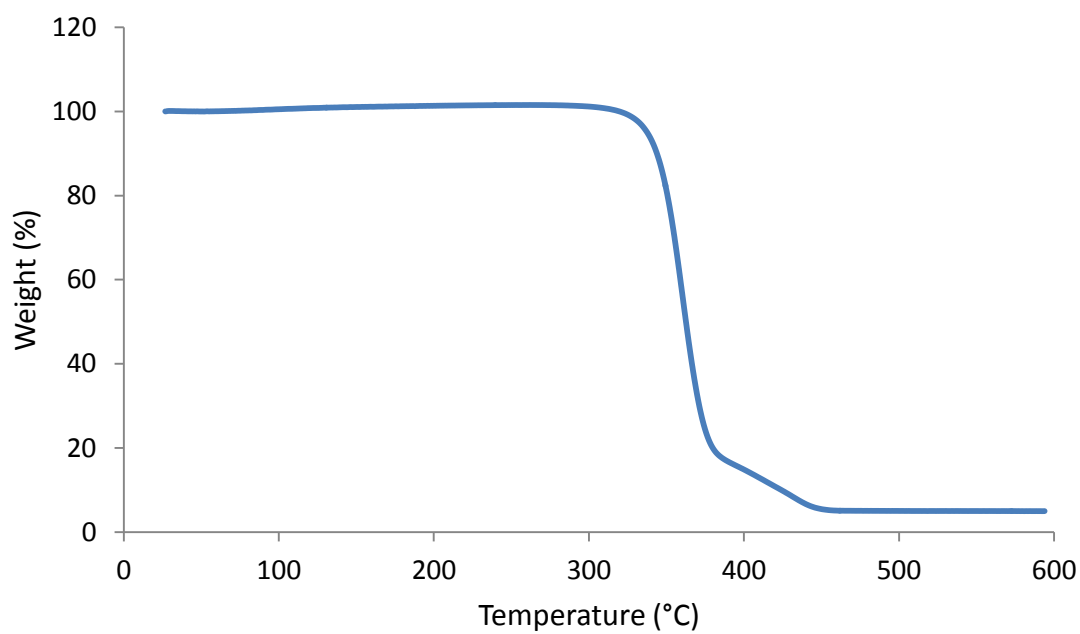
C11 TGA curve for IL **56**.



C12 TGA curve for IL **57**.

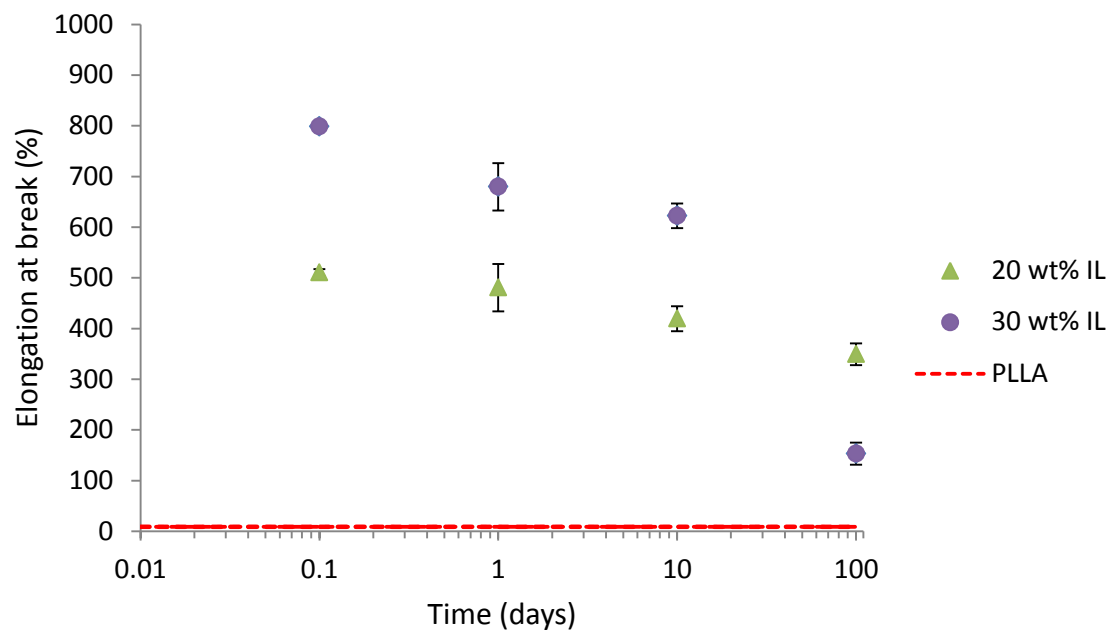


C13 TGA curve for PLLA.

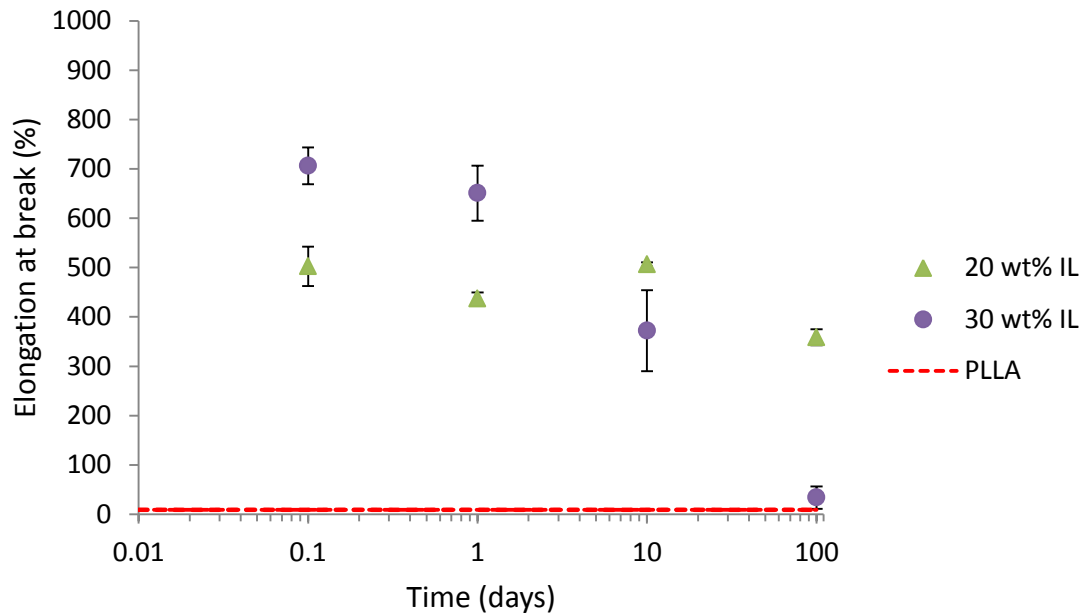


C14 TGA curve for PLLA/IL52 with 20 wt% IL.

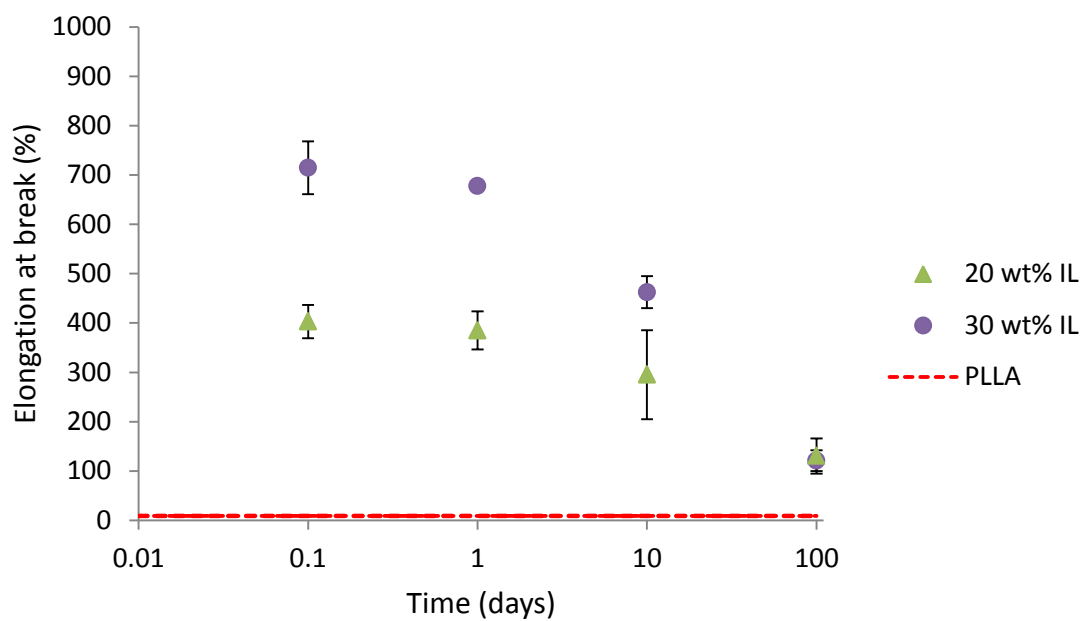
Appendix D – Tensile Testing Graphs



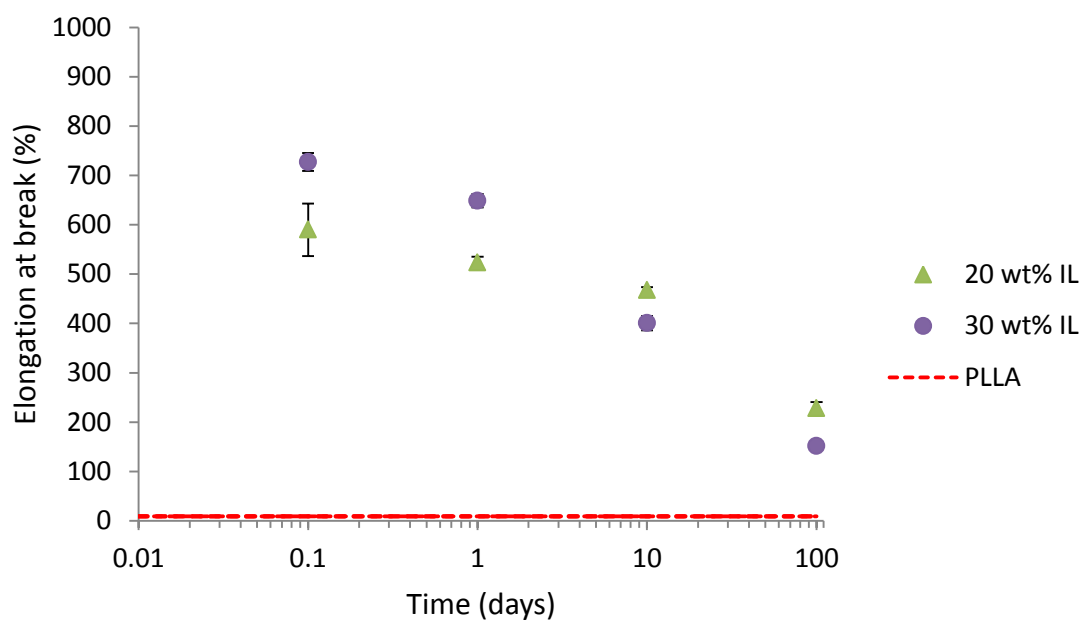
Appendix D1 Elongation at break for PLLA/IL50 with 20 and 30 wt% IL.



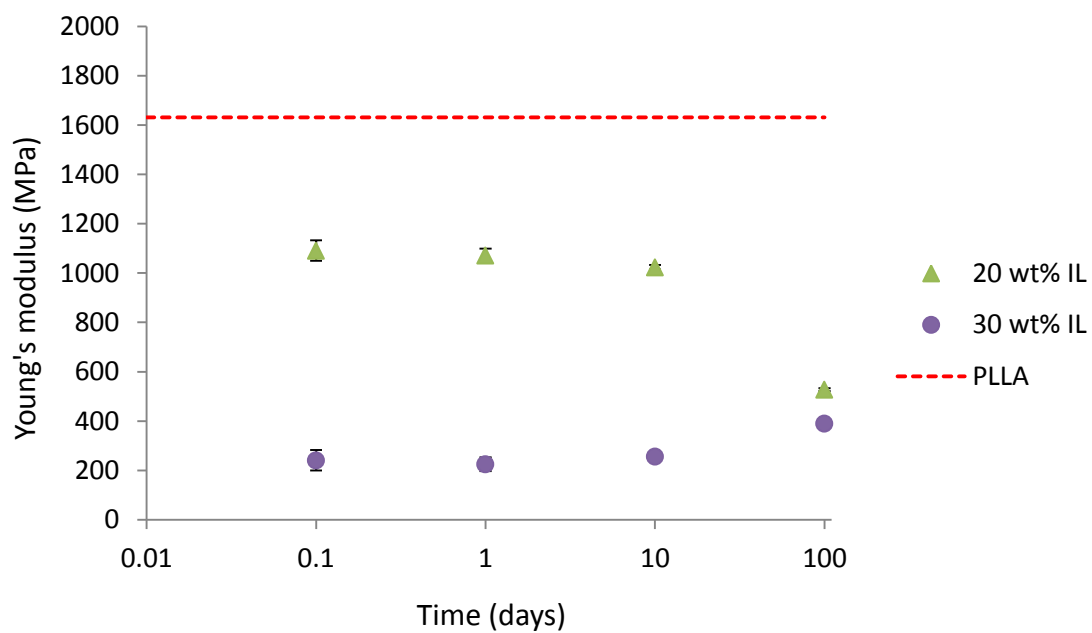
Appendix D2 Elongation at break for PLLA/IL51 with 20 and 30 wt% IL.



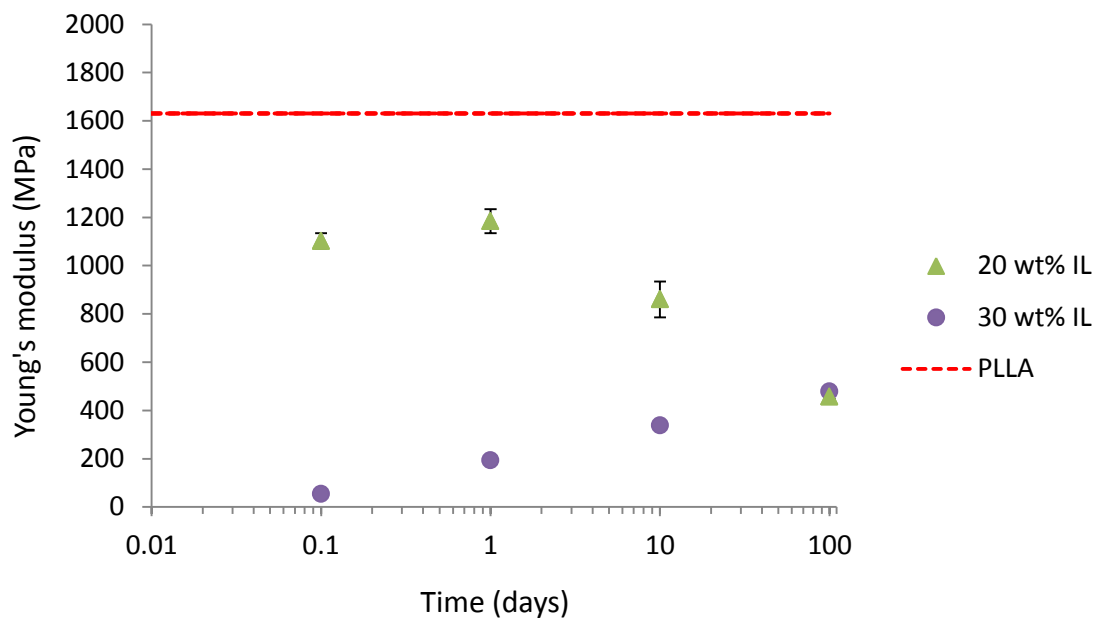
Appendix D3 Elongation at break for PLLA/IL52 with 20 and 30 wt% IL.



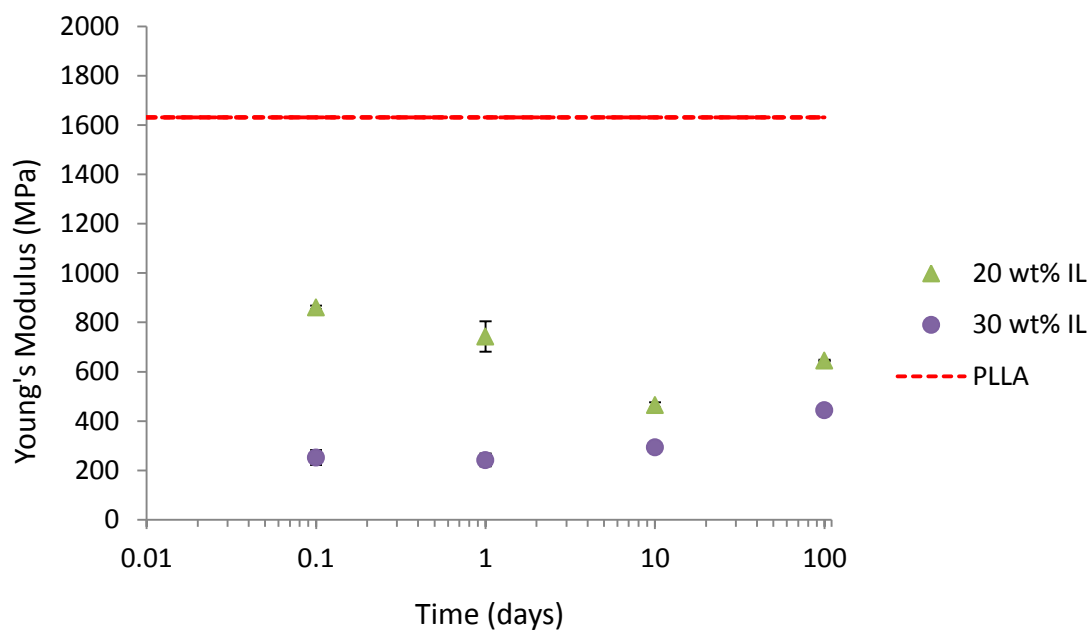
Appendix D4 Elongation at break for PLLA/IL53 with 20 and 30 wt% IL.



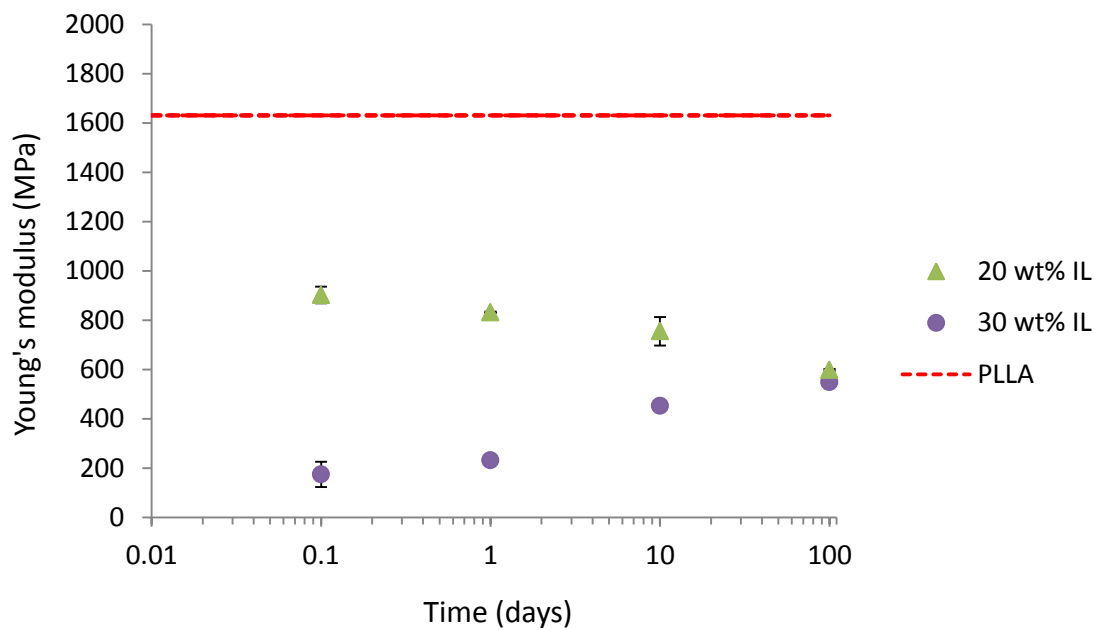
Appendix D5 Young's modulus for PLLA/IL50 with 20 and 30 wt% IL.



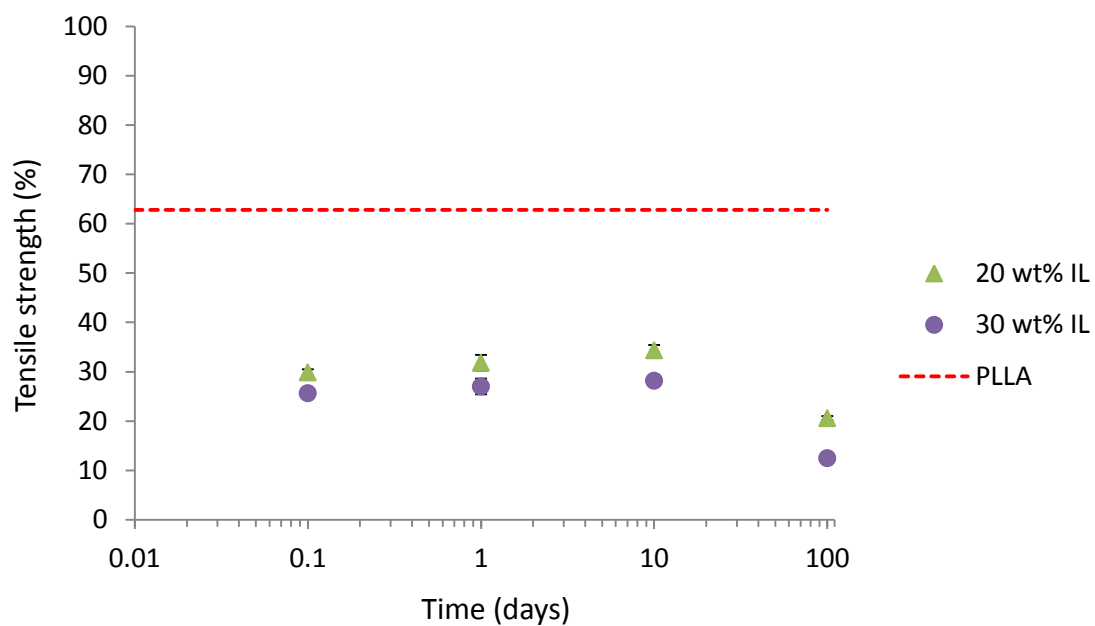
Appendix D6 Young's modulus for PLLA/IL51 with 20 and 30 wt% IL.



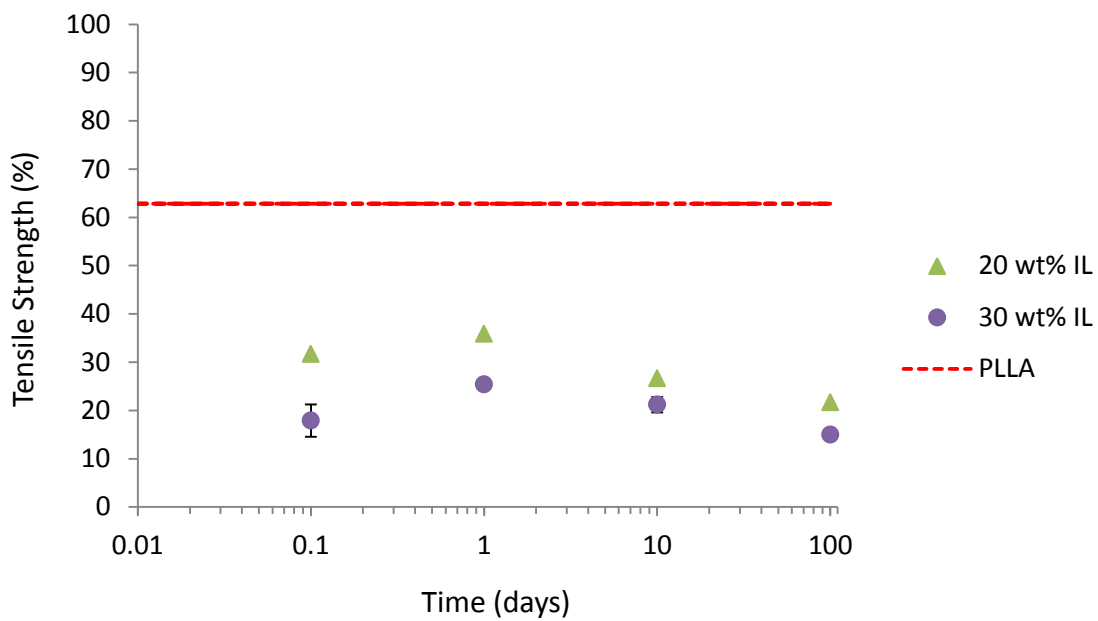
Appendix D7 Young's modulus for PLLA/IL52 with 20 and 30 wt% IL.



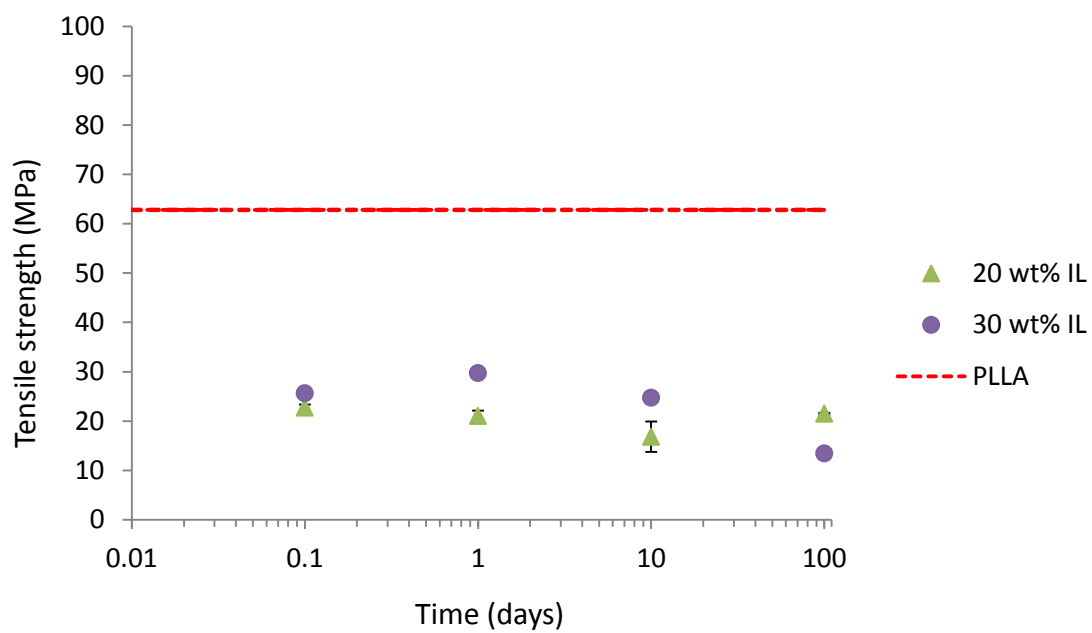
Appendix D8 Young's modulus for PLLA/IL53 with 20 and 30 wt% IL.



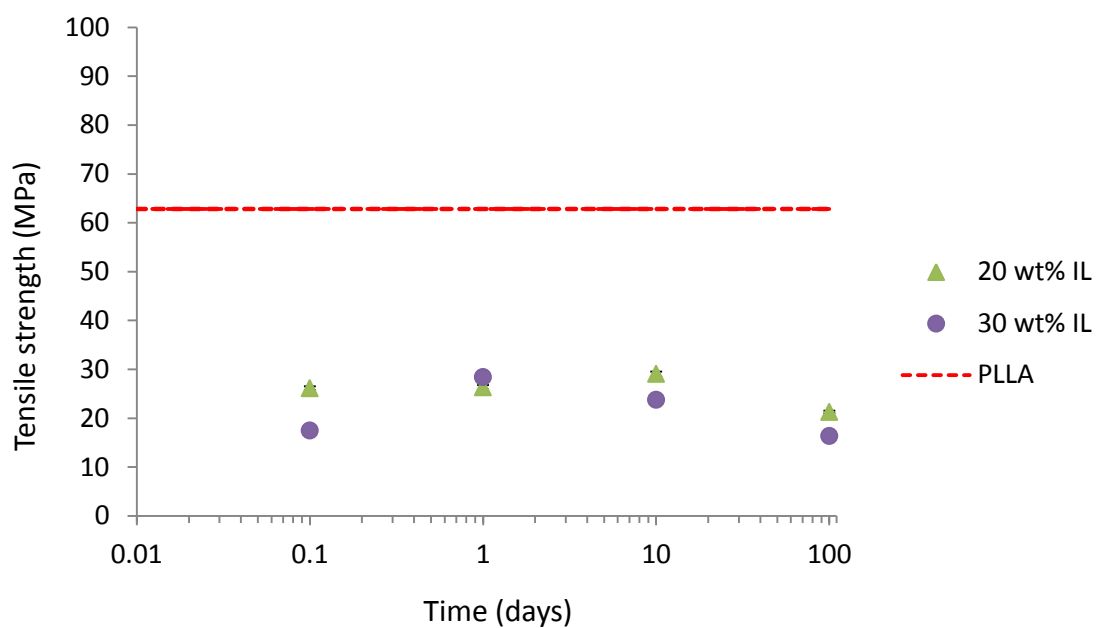
Appendix D9 Tensile strength for PLLA/IL50 with 20 and 30 wt% IL.



Appendix D10 Tensile strength for PLLA/IL51 with 20 and 30 wt% IL.

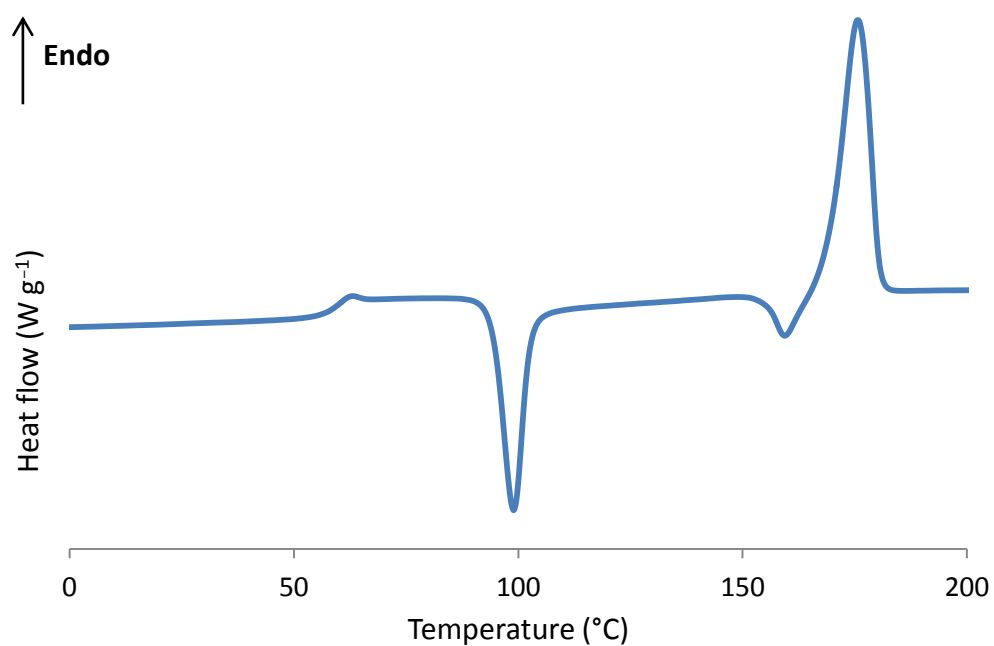


Appendix D11 Tensile strength for PLLA/IL52 with 20 and 30 wt% IL.

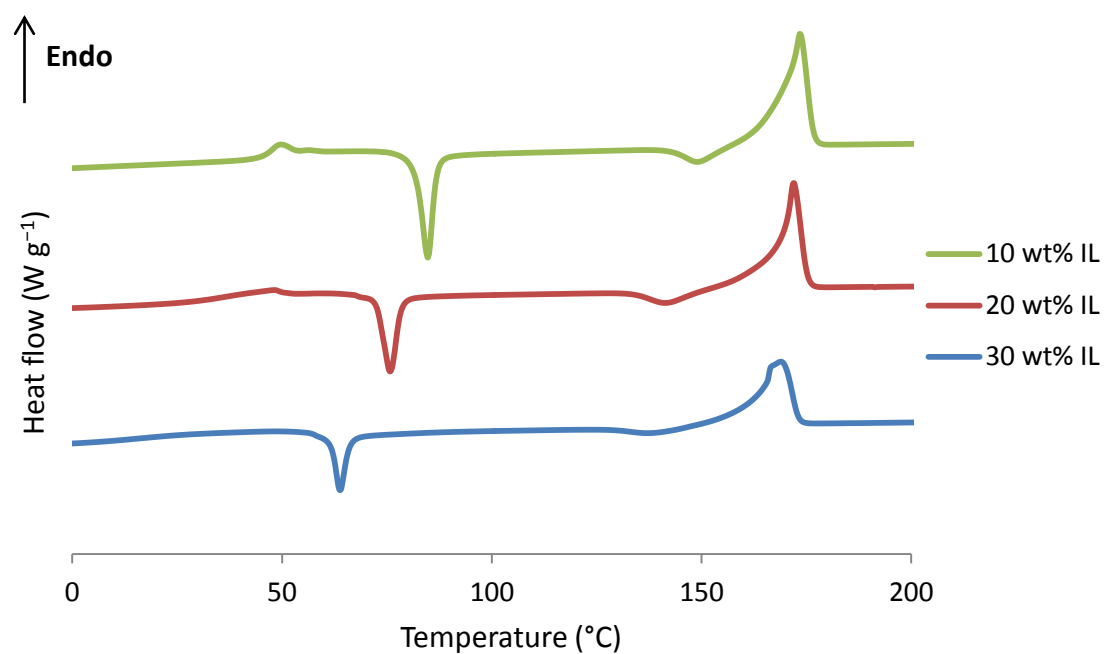


Appendix D12 Tensile strength for PLLA/IL53 with 20 and 30 wt% IL.

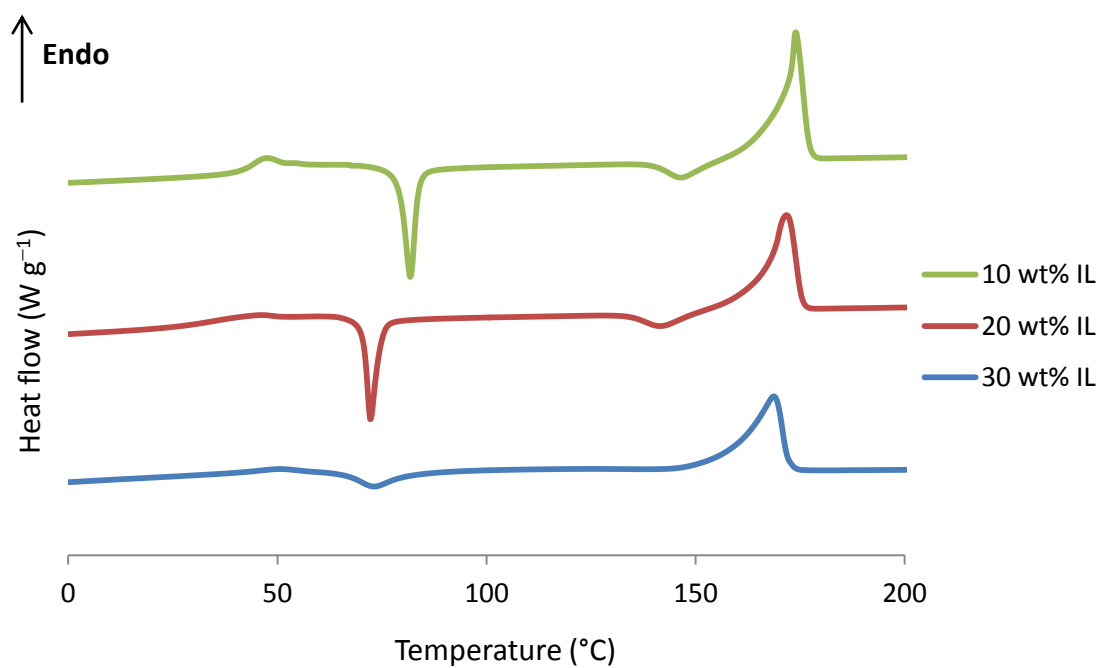
Appendix E – DSC Traces



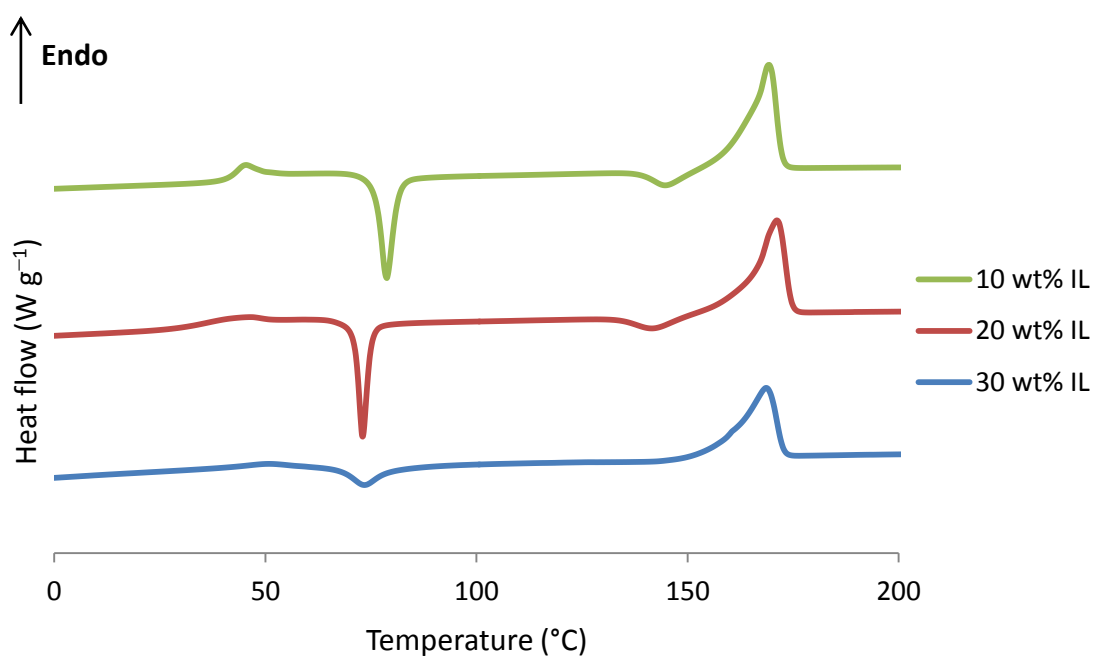
Appendix E1 DSC trace for PLLA.



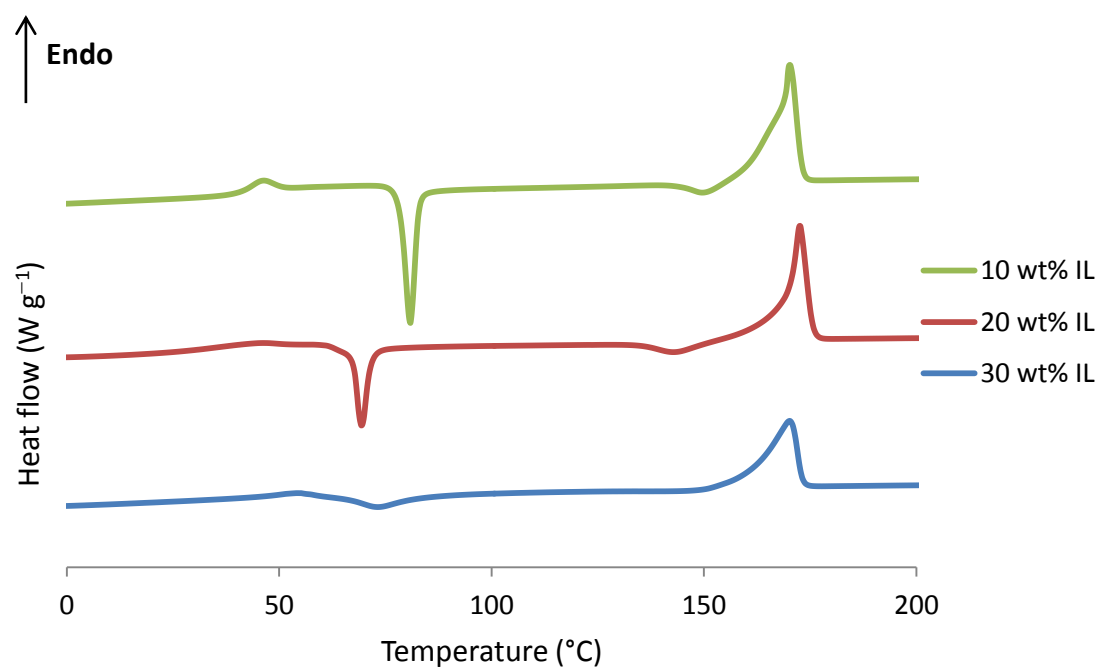
Appendix E2 DSC trace for PLLA/IL50.



Appendix E3 DSC trace for PLLA/IL51.



Appendix E4 DSC trace for PLLA/IL52.



Appendix E5 DSC trace for PLLA/IL53.

Appendix F – High Temperature Dielectric Data

Appendix F1 Dielectric properties of mandelic acid IL **20** measured at 20–120 °C and 910 MHz, where ϵ' is the dielectric constant, ϵ'' is the dielectric loss and $\tan \delta$ is the loss tangent.

Temperature (°C)	ϵ'	ϵ''	$\tan \delta$
20	2.16	0.00	0.00
30	2.41	0.01	0.00
35	2.53	0.00	0.00
40	2.64	0.00	0.00
45	2.74	0.00	0.00
50	2.83	0.01	0.00
55	2.90	0.00	0.00
60	2.95	0.01	0.00
65	3.00	0.00	0.00
70	3.03	0.00	0.00
75	3.07	0.01	0.00
80	3.12	0.02	0.01
85	3.67	0.18	0.05
90	3.87	0.27	0.07
95	3.94	0.33	0.08
100	4.01	0.40	0.10
105	4.07	0.48	0.12
110	4.08	0.55	0.13
115	4.15	0.67	0.16
120	4.05	0.75	0.18

Appendix F2 Dielectric properties of mandelic acid IL **20** measured at 20–120 °C and 2470 MHz, where ϵ' is the dielectric constant, ϵ'' is the dielectric loss and $\tan \delta$ is the loss tangent.

Temperature (°C)	ϵ'	ϵ''	$\tan \delta$
20	2.20	0.00	0.00
30	2.30	0.01	0.00
35	2.34	0.00	0.00
40	2.39	0.00	0.00
45	2.43	0.00	0.00
50	2.46	0.01	0.00
55	2.50	0.00	0.00
60	2.51	0.01	0.00
65	2.54	0.00	0.00
70	2.56	0.00	0.00
75	2.58	0.01	0.00
80	2.62	0.02	0.01
85	3.10	0.18	0.04
90	3.27	0.27	0.05
95	3.31	0.33	0.06
100	3.36	0.40	0.07
105	3.40	0.48	0.08
110	3.40	0.55	0.09
115	3.42	0.67	0.10
120	3.31	0.75	0.12

Appendix F3 Dielectric properties of mandelic acid IL **23** measured at 20–105 °C and 910 MHz, where ϵ' is the dielectric constant, ϵ'' is the dielectric loss and $\tan \delta$ is the loss tangent.

Temperature (°C)	ϵ'	ϵ''	$\tan \delta$
20	2.25	0.00	0.00
25	2.26	0.00	0.00
30	2.23	0.00	0.00
35	2.22	0.00	0.00
40	2.20	0.00	0.00
45	2.14	0.00	0.00
50	2.00	0.00	0.00
55	1.87	0.00	0.00
60	1.77	0.00	0.00
65	1.67	0.00	0.00
70	1.61	0.00	0.00
75	1.55	0.00	0.00
80	1.50	0.01	0.01
85	1.49	0.03	0.02
90	1.83	0.22	0.12
95	1.07	0.27	0.25
100	1.44	0.37	0.26
105	1.37	0.34	0.25

Appendix F4 Dielectric properties of mandelic acid IL **23** measured at 20–105 °C and 2470 MHz, where ϵ' is the dielectric constant, ϵ'' is the dielectric loss and $\tan \delta$ is the loss tangent.

Temperature (°C)	ϵ'	ϵ''	$\tan \delta$
20	2.31	0.00	0.00
25	2.31	0.00	0.00
30	2.31	0.00	0.00
35	2.30	0.00	0.00
40	2.30	0.00	0.00
45	2.28	0.00	0.00
50	2.24	0.00	0.00
55	2.19	0.00	0.00
60	2.16	0.00	0.00
65	2.13	0.00	0.00
70	2.10	0.00	0.00
75	2.09	0.01	0.00
80	2.08	0.01	0.00
85	2.09	0.02	0.01
90	2.36	0.14	0.06
95	1.59	0.16	0.10
100	1.93	0.24	0.12
105	1.91	0.23	0.12

Appendix F5 Dielectric properties of mandelic acid IL **50** measured at 20–120 °C and 910 MHz, where ϵ' is the dielectric constant, ϵ'' is the dielectric loss and $\tan \delta$ is the loss tangent.

Temperature (°C)	ϵ'	ϵ''	$\tan \delta$
20	4.40	1.32	0.30
25	4.92	2.19	0.45
30	5.12	2.73	0.53
35	5.53	3.18	0.57
40	6.08	3.66	0.60
45	6.73	4.10	0.61
50	7.44	4.48	0.60
55	8.20	4.83	0.59
60	8.93	5.20	0.58
65	9.63	5.40	0.56
70	10.25	5.48	0.53
75	10.94	5.57	0.51
80	11.55	5.71	0.49
85	12.18	5.71	0.47
90	12.79	5.60	0.44
95	13.32	5.61	0.42
100	13.80	5.43	0.39
105	14.34	5.37	0.37
110	14.84	5.21	0.35
115	15.24	5.10	0.33
120	15.64	4.93	0.32

Appendix F6 Dielectric properties of mandelic acid IL **50** measured at 20–120 °C and 2470 MHz, where ϵ' is the dielectric constant, ϵ'' is the dielectric loss and $\tan \delta$ is the loss tangent.

Temperature (°C)	ϵ'	ϵ''	$\tan \delta$
20	4.50	0.96	0.21
25	4.90	1.46	0.30
30	5.06	1.78	0.35
35	5.28	2.06	0.39
40	5.55	2.34	0.42
45	5.84	2.66	0.45
50	6.15	2.92	0.47
55	6.48	3.26	0.50
60	6.79	3.50	0.52
65	7.11	3.80	0.53
70	7.44	4.13	0.56
75	7.79	4.37	0.56
80	8.10	4.65	0.57
85	8.51	4.92	0.58
90	8.87	5.13	0.58
95	9.27	5.45	0.59
100	9.68	5.60	0.58
105	10.12	5.79	0.57
110	10.62	6.05	0.57
115	11.04	6.35	0.58
120	11.55	6.51	0.56